MSc. Thesis

Ice-structure interaction in the Baltic Sea: defining a feasibility map for monopiles

Florian van der Stap

WT WOOD THILSTED

TU Delft

ICE-STRUCTURE INTERACTION IN THE BALTIC SEA: DEFINING A FEASIBILITY MAP FOR MONOPILES

Thesis submitted to the Delft University of Technology in partial fulfillment of the requirements for the degree of

Master of Science in Offshore & Dredging Engineering

by

Florian van der Stap
4522990

August 2022

Supervisors:	Dr. Ir. Hayo Hendrikse	Delft University of Technology
	Dr. Ir. Martin Bjerre Nielsen	Wood Thilsted
	Ir. Cody Owen	Delft University of Technology
Graduation Committee:	Dr. Ir. Hayo Hendrikse	Delft University of Technology
	Dr. Ir. Martin Bjerre Nielsen	Wood Thilsted
	Dr. Ir. Pim van der Male	Delft University of Technology
	Ir. Jeroen Hoving	Delft University of Technology

Cover photo: Rampion Offshore Wind Farm located offshore UK in the English Channel
(https://unsplash.com/s/photos/rampion-offshore-wind-farm%2C-east-quay%2C-newhaven%2C-uk)

Florian van der Stap : *Ice-structure interaction in the Baltic Sea: Defining a Feasibility Map for Monopiles* (2022)

This report was made at Wood Thilsted, in close cooperation with:

Section Offshore Engineering
Faculty of Mechanical, Maritime & Materials Engineering
Delft University of Technology

ABSTRACT

The increasing popularity of offshore wind as a result of the demand for renewable energy, forces the industry to consider the development of wind farms in sub-arctic areas. One of these areas is the Baltic Sea, where the potential for wind energy is very large, but which is also prone to the occurrence of ice. For the design of offshore foundations it is paramount that ice-structure interaction is appropriately considered as ice-induced vibrations are known to significantly increase the loads. As a result, ice-mitigating measures may need to be included in the design. However, such measures will substantially increase the cost estimates required for competitive tenders. Hence it is valuable for developers to have early screening tools to assess this.

The aim of the research was to provide a 'feasibility map', which predicts the necessity for ice-mitigating measures in the entire Baltic region. Feasibility of monopiles was considered both technically and economically. The former by imposing design, installation & fabrication constraints and the latter was measured in terms of weight increase of monopiles. This research was conducted in three parts, an analysis of metocean conditions in the Baltic Sea, development of coupled ice and aero-elastic models, and the optimization of monopiles based on generated ice, wind & wave loading.

In Part I of the research, an analysis of metocean data was conducted for the Baltic Sea. Strong emphasis was put upon ice parameters, such as ice thickness, ridge properties and the ice crushing coefficient. Subsequently, based on the collected data, nine characteristic regions in the Baltic Sea were identified: the Danish Straits, the Baltic Proper South, the Baltic Proper North, the Gulf of Riga, the Gulf of Finland, the Archipelago Sea, the Bothnian Sea South, the Bothnian Sea North and the Bay of Bothnia. For each characteristic region representative metocean conditions were determined to aid in defining the 'feasibility map'. The extreme 50-year ice thickness was found in the range of 0.40–1.25 m, and the 1-year extreme ice crushing coefficient C_R in the range of 0.86–0.98 MPa.

In Part II, a novel integrated software for coupled simulations of offshore wind turbines in the time domain under ice, wind & wave loading was developed for this research. The TU Delft developed software VANILLA to assess ice crushing load was integrated in the Wood Thilsted in-house software MORPHEUS, which determines the response of the structure in the time domain. The integration was extensively verified versus the stand-alone VANILLA based on statistical measures of displacement, velocity and ice load. Subsequently, VANILLA was coupled to the aero-elastic simulation tool HAWC2, which is an DTU developed aero-elastic tool to determine wind turbine response. By setting up a TCP/IP link between Matlab and HAWC2 the two applications were able to run stand-alone, which allowed for minimal changes to the existing code.

In Part III a design assessment of offshore wind turbines across the Baltic Sea was conducted by optimizing foundation designs for the IEA 15 MW reference turbine, including and excluding ice loading. The applied method provided a screening to assess the significance of ice loads versus other actions as well as a screening for the necessity of costly ice-mitigating measures. Based on comparison of the designs, the following regions were deemed feasible for monopile design without ice-mitigating measures: the Danish Straits, the Baltic Proper South, the Baltic Proper North, the Gulf of Riga and the Archipelago Sea. The Bothnian Sea North and the Bay of Bothnia were deemed infeasible for design as a result of significant increase in weight due to additional required stiffness. For the Bothnian Sea South and the Gulf of Finland no conclusive answer was found, as more research into the cost competitiveness of alternative options is required. Investigation of the designs showed that the increase in fatigue as a result from ice loading were the main cause for weight increase of the designs.

The current study provided rough estimates for the cost increase due to an ice cone, however, a thorough analysis should be performed to determine the impact of such ice-mitigating measures on both hydrodynamic loading and project cost. Additionally, due to scarcity of measurements and data outside the Bay of Bothnia, ice conditions were often scaled or chosen conservatively. Further research into ice conditions in other regions could improve the findings of this research.

Keywords: Ice loading, feasibility map, monopiles, design optimization, offshore wind turbines, design load cases, fatigue limit state, ultimate limit state, ice-mitigating measures.

CONTENTS

NOMENCLATURE

Symbols

α	Power law exponent
α_f	Relative weight coefficient of forcing terms
α_k	WT stiffness parameter
α_m	Relative weight coefficient of inertia terms
ΔM_{eq}	Damage equivalent moment
δ	Critical deformation
ℓ	Latent heat of fusion of water
η	Surface elevation
γ_{e}	Effective buoyancy
$\mathbf{K}$	Stiffness matrix
$\mathbf{M}_*$	Modified mass matrix
$\mathbf{M}$	Mass matrix
μ_ϕ	Passive pressure coefficient
μ_{drift}	Ice drift factor
ω	Region specific empirical ice thickness coefficient
ϕ	Internal friction angle
ρ_{w}	Sea water density
ρ_{ice}	Ice density
c	Keel cohesion
C_1	VANILLA model parameter for linear dashpot
C_2	VANILLA model parameter for non-linear dashpot
C_{d}	Drag coefficient
C_{FDD}	Cumulative freezing degree days
C_{l}	Lift coefficient
C_{m}	Moment coefficient
C_{R}	Ice strength coefficient
d	Water depth
D_{fr}	Freeze delay
D_{ice}	Ice interaction days
e	Porosity
F_{ice}	Global ice load
f_{AR}	Rubble term for ice crushing
F_{c}	Consolidated layer action
F_{k}	Keel action
F_{r}	Ridge action
g	Gravitational acceleration
h	Ice thickness
h_{50}	50-year extreme ice thickness
h_{c}	Consolidated layer thickness
h_{k}	Keel depth
H_{s}	Significant wave height
K_1	VANILLA model parameter for linear spring
K_2	VANILLA model parameter for non-linear spring
k_{ice}	Thermal conductivity of ice
l_{ice}	Landfast-to-drift ice scale factor
L_{s}	Length of ice season
m	Empirical crushing coefficient
M_{F}	Mass of foundation
M_{MP}	Mass of monopile
M_{RNA}	Mass of RNA
M_{TP}	Mass of transition piece
N	Number of ice elements
n	Empirical crushing coefficient
p_{c}	Probability of ice occurrence at the coast
p_{G}	Global average ice pressure
p_{ice}	Ice state probability of occurrence
r_{max}	Maximum roughness of ice
t	Time
t	Tonne
T_{air}	Air temperature

T_{fr}	Freezing temperature	V_1	1-year extreme wind speed
T_{OWT}	Lifetime of offshore wind turbine	$V_{\text{cut-out}}$	Cut-out wind speed
T_{p}	Peak wave period	v_{ice}	Ice drift velocity
U	Wind speed	V_{rated}	Rated wind speed
u_{s}	Structural displacement	w	Width of structure
u_i	Ice element displacement	z	Height

ACKNOWLEDGEMENTS

After finally handing in this thesis, I get to take the time to thank everyone who helped me throughout this process. First of all, I'd like to express my gratitude to my daily supervisors, Cody, Hayo & Martin.

Martin, thank you for your extensive guidance, in the form of direct feedback or 20 minute mini-lectures on any given topic. I greatly benefitted from your knowledge about the entire sector and specifically foundation design.

Secondly, I like to thank Cody & Hayo. Our biweekly meetings were incredibly helpful. Whether it was extra sessions looking at our code or diving into papers on ridge actions, you were both always prepared to help. Simultaneously, you never let the aim of this thesis out of sight, which helped me with staying focused on the goal and working towards it.

Next, I would like to thank all of Wood Thilsted & specifically Team Malin. Not only was I made to feel part of the team from day one, every team member has shown to be incredibly knowledgeable and of great support during this project. I am really looking forward to start working with all of you, and everyone else at Wood Thilsted.

Two members of Team Malin deserve some individual praise, namely Eric & Niels Christian. Eric, thank you for your unwavering patience in guiding me through HAWC2. I really appreciate the head of the aero-elastic department taking so much time out of his schedule to help a student. Niels Christian, thank you for helping me through each step of my project, whether it was with Dropbox problems, showing me the inner secrets & mysteries of MORPHEUS or explaining when subscripts should or should not be italic.

Last but not least, I'd like to thank my girlfriend for supporting me during this adventure in Denmark. Even though it was sometimes difficult from afar, I have always felt your support throughout the entire process and for that I am incredibly grateful.

Florian van der Stap
Copenhagen, August 2022

1 INTRODUCTION

In recent decades offshore wind has become increasingly important as it provides clean, renewable energy and can aid with the worldwide commitment to combat climate change. Besides providing clean energy, offshore wind has additional benefits compared to onshore wind as there is more public support, the potential for increased capacity is very large and the overall environmental impact is smaller [Wu et al., 2019; Esteban et al., 2011]. As a result, unsurprisingly, the offshore wind energy production has accelerated greatly over the past decade as can be seen from Figure 1.1. This growth will surely continue as the EU alone has already committed to investing close to twenty billion euros in the wind sector by 2030, 60% of which in the offshore market [Wu et al., 2019].

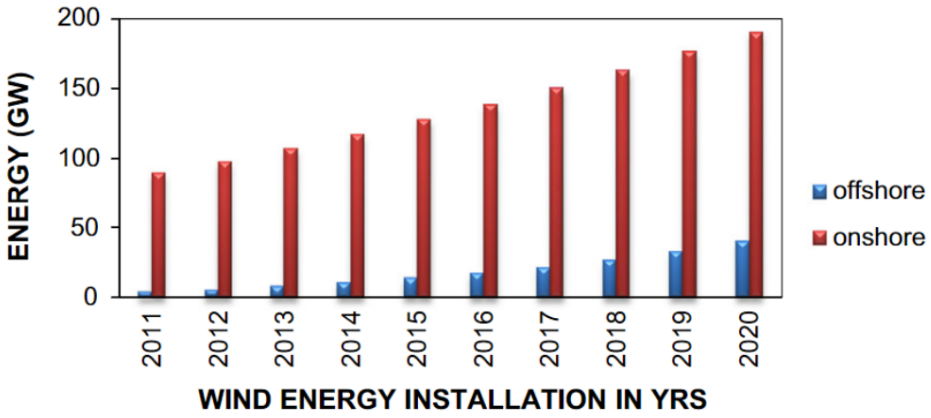

Figure 1.1: Offshore and onshore global installed capacity over the period 2011–2020 [Wu et al., 2019].

One potential area for significant growth of the offshore wind market is the Baltic Sea. At the end of 2020, an installed capacity of only 2 GW was reported, while the projected potential capacity is 93 GW [WindEurope, 2020]. The Baltic Sea, however, introduces a new challenge for designing an Offshore Wind Turbine (OWT), namely ice-structure interaction. The probability of ice occurrence varies greatly over the entire region, but even in the Southern regions the probability per season was at least 32% in the twentieth century [Jevrejeva et al., 2004]. Although a decreasing trend for this probability is observed in the Southern regions, ice loading is still far from negligible. Farther North in the region, no decreasing trend was observed, with some regions reporting a probability of ice occurrence of 100% [Jevrejeva et al., 2004], further emphasizing the necessity to include its effects in design.

A major advantage of the rapid growth of the offshore wind industry is the significant decrease in Levelized Cost of Energy (LCOE), which can be defined as *"the minimum price of electricity, above which a return on capital can be obtained"* [Bosch et al., 2019]. As a result of the expansion of offshore wind, the industry has matured substantially over the past decade and increased experience has led to more efficient wind farm design, improved reliability and lower operational & maintenance costs [The Crown Estate, 2017]. This — combined with a decrease in cost of capital — has aided in reducing the LCOE of the offshore wind industry [Finance, 2017]. In 2017 the LCOE of offshore wind energy was first reported to dive below £100 per MWh (€112 per MWh) in the United Kingdom, four years ahead of projections. For other wind energy strongholds such as Denmark and the Netherlands the reported LCOE is even lower, with prices reported around €63.90 per MWh and €54.50 per MWh, respectively [The Crown Estate, 2017].

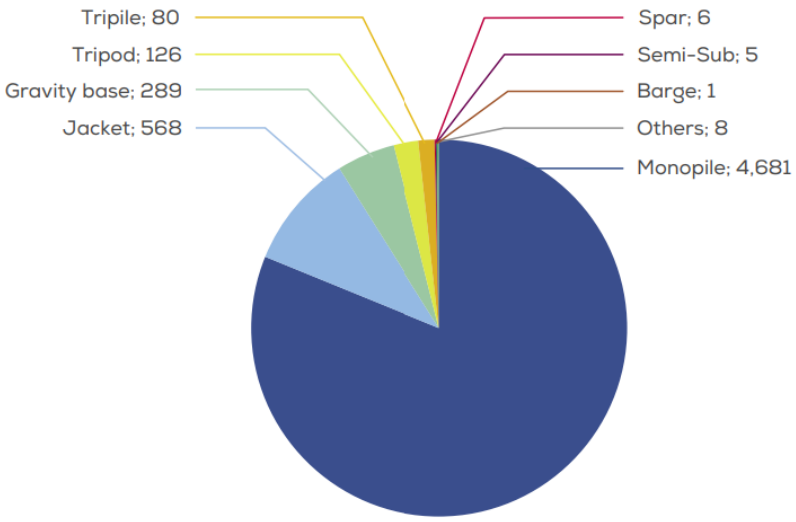

Figure 1.2: Total number of foundations installed in Europe per substructure type [WindEurope, 2020].

However, despite the great strides in terms of economic feasibility, offshore wind is still substantially more expensive than onshore wind. In a recent review on offshore foundations for wind turbines the investment per megawatt was estimated to be around 50% higher for offshore turbines. Moreover, for an offshore wind farm 20-30% of the total investment is used for the foundations [Wu et al., 2019]. In other words, an efficient foundation design is vital for a financially sound project.

1.1 ICE–STRUCTURE INTERACTION

From Figure 1.2 it is evident that the monopile is, by a substantial margin, the preferred option for an offshore wind support structure. This foundation type has matured relatively long and is often the simplest in both design and installation phase, resulting in the lowest LCOE [Wu et al., 2019; WindEurope, 2020].

However, vertically-sided structures, such as monopiles, can experience severe structural vibrations due to interaction with level ice. These ice-induced vibrations are dependent on flexibility of the structure and the velocity of the ice as illustrated by Figure 1.3. The occurring ice-induced vibrations, or interaction regimes, are Continuous Brittle Crushing (CBR), Intermittent Crushing (ICR), Frequency Lock-In (FLI) and — specific to OWTs — Multi-modal interaction I (MMI) and Multi-modal interaction II (MMII) [Hammer et al., 2022]. The ice loads associated with these interaction regimes vary greatly in magnitude and load effect, e.g. the peak loads associated with ICR can be up to 4 times higher than peak loads due to CBR [Singh et al., 1990]. Furthermore, FLI may cause significant damage due to structural fatigue [Hendrikse and Koot, 2019].

1.2 ICE–MITIGATING MEASURES

Since the entire Baltic Sea is prone to ice occurrence and the loads resulting from ice-structure interaction can be substantial, the effect of ice loading should be considered during the design process. In the Southern Baltic Sea, the loads as a result of ice are often not governing as the magnitude is relatively low [Gravesen and Kärnä, 2009]. However, given the severity of ice seasons in the Northern & Eastern regions of the Baltic Sea, and the amplifying effect of ice-induced vibrations, mitigating measures might be necessary once wind farm development expands into these areas.

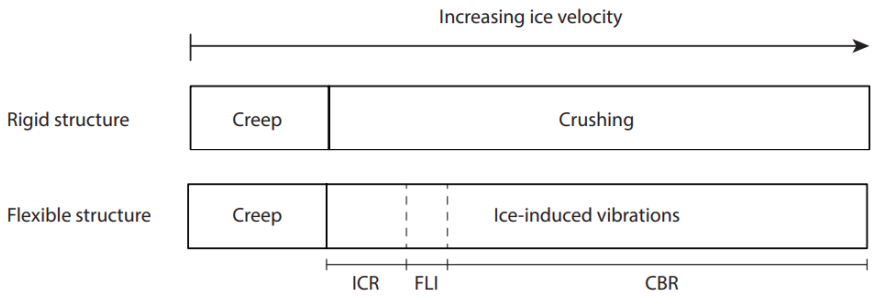

Figure 1.3: Overview of traditional interaction regimes for crushing between vertically-sided structure and level ice based on ice velocity and structural compliance [Hendrikse, 2017].

One common mitigating measure is the installation of ice cones at the ice action point, which causes the ice to fail in bending rather than crushing, which reduces the overall load on the structure. However, including ice cones in the design negatively affects the LCOE as they are 1) expensive to fabricate, 2) labour-intensive to assemble and 3) need to be post-installed offshore as a pile. Additionally, the ice cone is subject to significantly higher wave-loading when ice is not present due to the increased diameter at the waterline [Tang et al., 2021; Zhu et al., 2021]. Other mitigating options include the consideration of alternative substructures more aptly equipped against the effects of ice loading. One such a substructure is the Gravity Based Structure (GBS), which can easily be designed with an inclined ice-structure surface. A GBS is known to resist high ice loading and can be cost-competitive for shallow water positions [Anku-Vinyoh et al., 2021].

Since the effect of ice can greatly alter the design of an OWT foundation, both in LCOE and type of substructure, it is important to understand what the effect of ice loading is within a region. Specifically, it can be of great interest to know which regions *do* or *do not* require ice-mitigating measures for monopiles. There is currently no information available regarding such an 'ice-defined boundary' or 'feasibility map' for monopiles in the Baltic Sea. Hence this research will aim to answer the following question:

Where in the Baltic Sea is it feasible to install monopiles without ice-mitigating measures?

1.3 THESIS OBJECTIVE

The main objective of the thesis is to research the limit of the applicability of monopiles for OWT without ice-mitigating measures in the Baltic Sea. Moreover, the aim of the research is to present this limit in terms of a feasibility map for monopiles in the Baltic Sea, which visually presents the possibility of installing monopiles in a certain region. Both technical and economic feasibility are considered. The former by imposing design, fabrication and installation constraints, and the latter in terms in terms of weight of additional steel, which serves as proxy for economic feasibility.

This map provides insight into the future of offshore wind design, specifically the future of the monopile, within the entire Baltic Sea. It provides information on the LCOE of wind farm designs within the various regions, as the inclusion of ice-mitigating measures will most likely increase the LCOE. Inversely, if a region does not require any ice-mitigating measures, projects in this region might be more economically feasible, which could save both financial (€) and environmental costs (CO_2 emissions).

In order to investigate this limit, the ice load effect on the foundation design has to be evaluated in the entire Baltic Sea region. This introduces two secondary objectives to this thesis, namely 1) identifying characteristic regions in the Baltic Sea and their metocean conditions and 2) developing a model which can accurately run coupled ice-structure interaction and aero-elastic

simulations. The former provides a thorough analysis and comparison of the extremity of ice seasons in different regions of the Baltic Sea. The latter is a specific goal of Wood Thilsted (WT), as it provides them the opportunity to design OWTs in colder regions in the future.

1.4 THESIS OUTLINE

The framework of this thesis, as outlined by Figure 1.4, consists of three parts, each necessary for achieving the main objective of the research. The first two parts are aimed at the two secondary objectives, while the last part uses the results from the first two parts to accomplish the main objective.

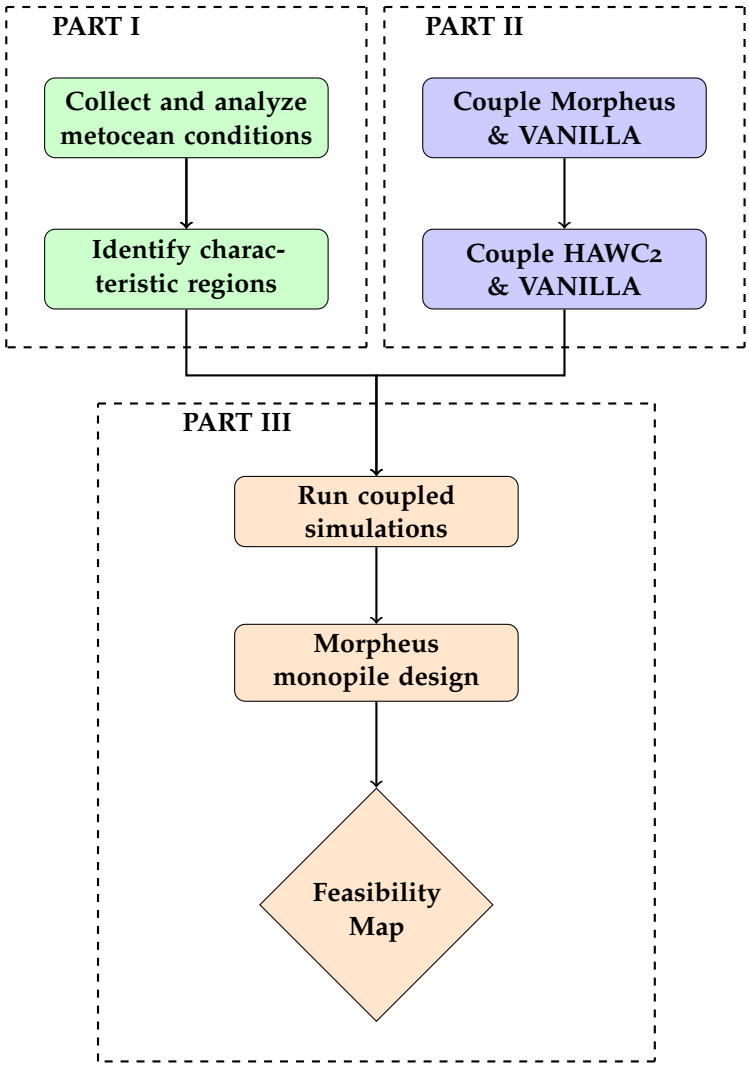

Figure 1.4: Visualization of the applied research framework, including Part I, II and III and the relations between these parts.

1.4.1 Part I

The aim of Part I is to answer the following question:

Which characteristic regions can be identified in the Baltic Sea based on metocean conditions and what are the representative metocean conditions in these regions?

To this purpose Chapter 2 discusses the relevant metocean conditions for the modelling of ice-structure interaction in the Baltic Sea as partly described in a separately published liter-

ature study [van der Stap, 2022]. During the identification of the regions, the focus will be on metocean conditions relating to ice, as that is the primary concern of this research. This includes extreme ice thickness, ice strength coefficient C_R, ice ridge parameters and ice state probabilities.

After identifying the characteristic regions, the corresponding metocean conditions for each of these regions are found. These will serve as input for Part III.

1.4.2 Part II

In Part II begins with the necessary theoretical background of ice mechanics and the ice model VANILLA (Variation of contact Area model for Numerical Ice Load Level Analyses) for assessment of ice crushing loads. Both are presented in Chapter 3. As this research is concerned with monopiles, the focus will be on ice failure modes against vertically-sided structures. This means bending, the governing failure mode on sloping structures, will be excluded from the discussion.

Subsequently, in Chapter 4 the thesis will focus on the coupling of VANILLA into both the WT in-house software MORPHEUS, and the aero-elastic tool HAWC2 (Horizontal Axis Wind turbine simulation Code 2^{nd} generation) with the aim of efficiently simulating coupled aero-elastic and ice-structure interaction simulations. For the coupling, understanding of the time integration methods used in MORPHEUS and HAWC2 is required. To this purpose the necessary background is presented, which aids in presenting the coupled systems. A verification based on statistical measures is proposed and applied to the coupled MORPHEUS/VANILLA model.

1.4.3 Part III

The third and final part of this thesis answers the main question of this research using the metocean input collected in Part I and the model developed in Part II:

Where in the Baltic Sea is it feasible to install monopiles without ice-mitigating measures?

In order to answer this, Chapter 5 outlines the methodology of the design & research procedure. This requires the selection of wind, wave and ice design load cases to be included. This is followed by a presentation of the design methodology of the MORPHEUS optimization algorithm. Based on the proposed research methodology a feasibility map is generated and presented in Chapter 6. This is followed by a thorough discussion of the generated map. Finally, Chapter 7 concludes the research, answers the posed questions, and summarises the limitations of the current research and suggestions for future research.

2 BALTIC SEA - CHARACTERISTIC REGIONS

The first step towards defining a feasibility map for the Baltic Sea, is the identification of characteristic regions and determining the representative metocean data for each region. This is the objective of Part I. This chapter discusses the relevant parameters, methods for the derivation of the parameters and the results. Since the main focus of the research is ice loading, priority was given to parameters that heavily influence ice loading, such as level ice, ridged ice and the C_R coefficient. For the remaining parameters, literature or data provided by the FWT metocean was used. Finally, the characteristic regions are identified based on the derived parameters, and representative parameters for each region are listed. The following parameters will be discussed:

- Ice thickness
  - Level ice
  - Ridged ice
- Ice strength coefficient C_R
- Bathymetry
- Ice drift speed
- Ice state probability
  - Ice thickness distribution
  - Ice days
- Wind & Waves

Section 2.1.1, Section 2.2 and Section 2.3 are succinct summaries of work presented in a separately published literature study [van der Stap, 2022]. However, additional information — specifically with regards to ice ridges, wind & waves, ice drift speed and ice state probabilities — is presented and discussed in this research.

2.1 ICE THICKNESS

For the assessment of ice-structure interaction, an accurate estimate of ice thickness is essential. This section briefly discusses how the level ice as well as the ridge parameters were determined. For the level ice thickness a modified version of Stefan's law was applied with two additional scaling factors, ω and l_{ice}. For the ridge parameters both design standards, and relevant literature are used.

2.1.1 Level ice

For the assessment of the level ice thickness in the Baltic Sea few direct measurements are available. Air temperature data sets, to the contrary, are easily accessible for locations around the entire region. Due to this accessibility and given that air temperature has been shown to provide a decent estimate of ice thickness in the past [Stefan, 1891; Leppäranta, 1993], ice thickness was assessed using air temperature data sets from various weather stations around

the Baltic Sea. After this, the results could be validated and scaled — if necessary — based on both ice thickness measurements and ice charts.

The most common relation between air temperature and ice thickness is referred to as Stefan's law and was originally derived in Stefan [1891]. The key concepts of this derivation are briefly discussed here, but for a full derivation reference is made to van der Stap [2022]. To find the ice thickness Stefan assumed that the air, ice and water are a closed or isolated thermal system and that the air temperature, T_{air}, was constant, and below the freezing temperature T_{fr}. Such a system is shown in Figure 2.1.

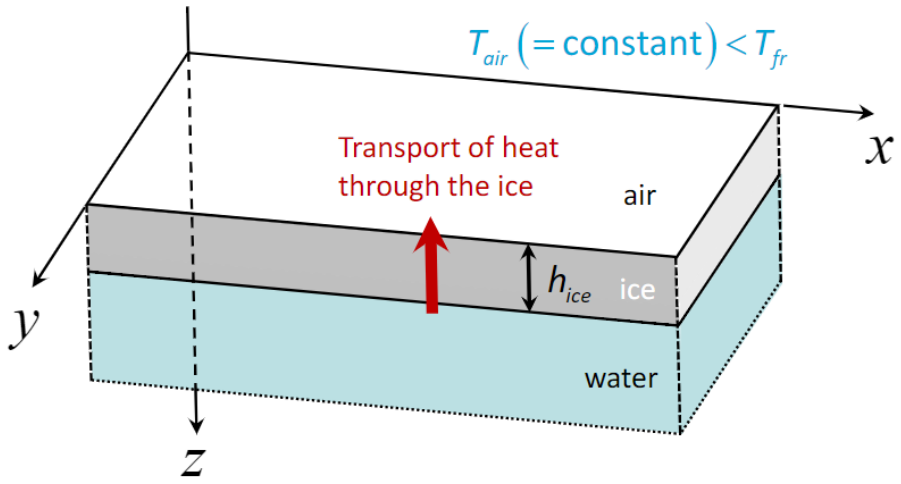

Figure 2.1: Schematic of Stefan's problem for simplified ice growth.

By assuming that 1) the temperature over the ice layer, h_{ice}, is linear, 2) the temperature at the bottom of the layer is equal to T_{fr}, 3) the surface temperature is equal to T_{air} and 4) assuming $h_{\text{ice}}(t = 0) = h_0$, a relation is found for the ice thickness:

$$h = \sqrt{\frac{2k_{\text{ice}}}{\rho_{\text{ice}}\ell} C_{\text{FDD}}} \tag{2.1}$$

where k_{ice} is the thermal conductivity of ice, ρ_{ice} is the density of ice, ℓ is the latent heat of fusion of water and C_{FDD} is number of cumulative freezing degree days. This last parameter is the sum over all days of the difference between the freezing temperature and the average daily air temperature. Note, this is *only* on days with an air temperature below freezing temperature.

For offshore design the ISO19906 [2018] uses a similar method for the calculation of ice thickness as Equation 2.1, however they include a snow cover as well as an empirically derived coefficient, ω, specific to the design location. There is little data available on snow cover extent around the Baltic Sea and including this in the derivation of ice thickness is beyond the scope of this research. When no snow cover data is present the empirical coefficient ω can also be used to scale the thickness to include the insulating effect of a snow cover. It is then typically set to a value in the range of 0.3–0.7. This is also the applied method for the current research, where the thickness can be calculated using:

$$h_{\text{ice}} = \sqrt{\omega \frac{2k_{\text{ice}}}{\rho_{\text{ice}}\ell} C_{\text{FDD}}} \tag{2.2}$$

Once an appropriate value for ω is found, the ice thickness corresponding to once in 50 year ice event can be found by applying a Generalized Extreme Value fit through the data as shown in Figure 2.2.

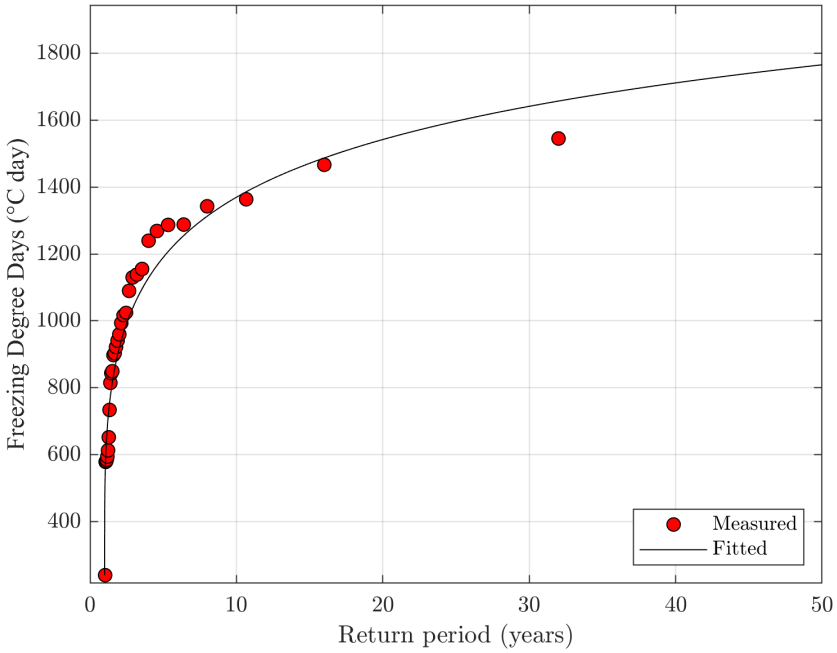

Figure 2.2: Fitted Generalized Extreme Values for C_{FDD} at weather station Ajos in the Bay of Bothnia.

2.1.2 Scaling factors

Besides ω, the factor l_{ice} needs to be determined for the accurate scaling of ice thicknesses. This factor is introduced to scale between the landfast ice region — in which (almost) all the data sets are located — and the drift ice. When ice formation is not landfast, the growth is known to be more limited due to lower temperatures offshore and cooling of a larger water column is required. Different sources were used to estimate the factors and define benchmark ice thicknesses around the Baltic Sea.

The Sveriges Meteorologiska och Hydrologiska Institut (SMHI) and the Finnish Institute of Marine Research (FIMR) provide charts with the maximum ice extent coverage for each year since 1980. For this research it is assumed that at the time of maximum ice extent, the maximum ice thickness is reached. Additionally, some direct ice measurements are available along the Finnish coast from 1981 until 2005, with the exception of the period 1986–1990. The ice charts give good ranges for entire areas, whereas the direct measurements give good estimates for potential local maxima. The ice charts also aid in assessing the difference in drift and landfast ice thickness. The most severe ice conditions in (relatively) recent years were in the winter seasons of 1984/1985 and 1986/1987, which can be seen on the ice charts as provided in Figure A.1 and Figure A.2. These ice charts, the ice measurements and the temperature data sets are in good agreement on the severity of these years.

By using the available data the optimal values for for ω and l_{ice} were found to be 0.55 and 0.8, respectively. For an in-depth discussion and derivation of these values reference is made to van der Stap [2022]. For the locations of all observations stations, reference is made to Figure A.3. Figure 2.3 gives the resulting ice thickness map for a 1/50 year ice event in the Baltic Sea, i.e. h_{50}.

On the whole, the generated map is in good agreement with extreme winters and the most extreme ice measurements. For most given locations, the predicted ice thickness is usually on the side of caution, with the exception of the Gulf of Riga, which may be slightly underestimated. Note, this map is generated for research purposes and should not be used for detailed design, but should only serve as an indication of ice thickness in the Baltic Sea region. For detailed designs, a full in-depth metocean analysis is essential.

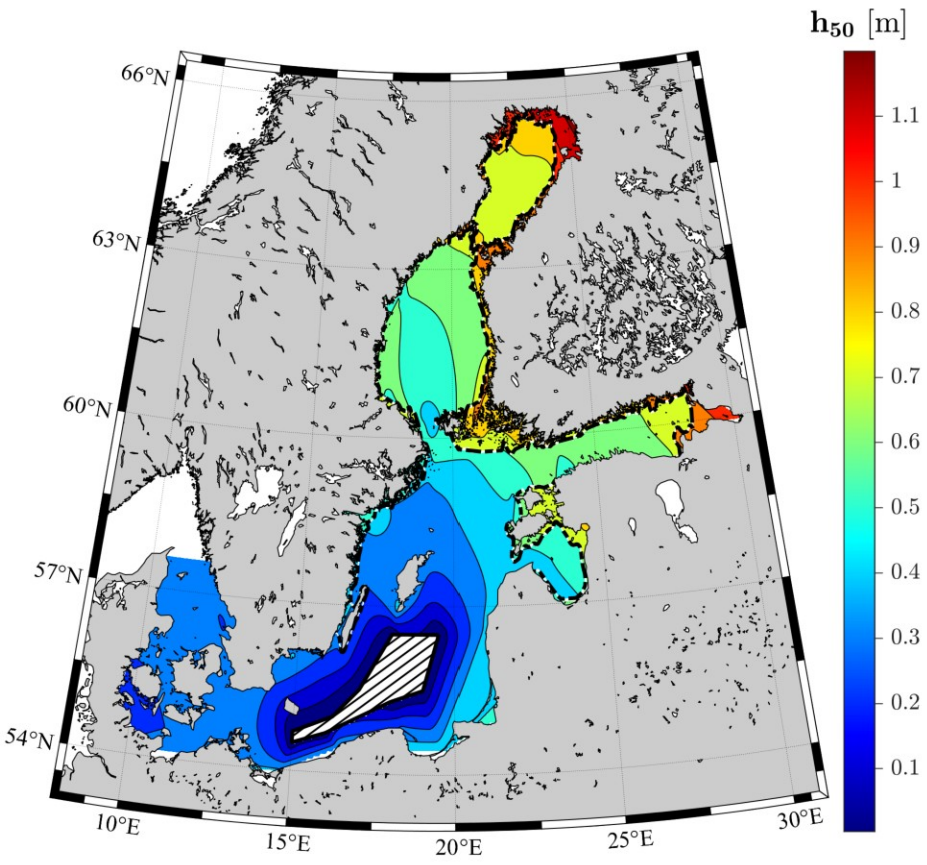

Figure 2.3: Design ice thickness, h_{50}, for a 1/50 year ice event in the Baltic Sea. The hatched area defines the area where no ice is found (< 5 cm), even in extreme winters. The dash-dotted line is denotes the boundary between landfast and drift ice.

2.1.3 Ridged ice

As a result of wind and weather, sheets of level ice are often pressed into one another resulting in the formation of ice ridges. This especially occurs at the boundary between landfast and drift ice, where the dynamic drift ice is being pushed into the rigid landfast ice. A similar situation could present itself in the presence of a wind farm, when drift ice collides with ice stationary against monopiles. This emphasizes the necessity for accurate ridge properties assessment.

The contribution of ice ridges to the total ice mass over large areas can vary drastically depending on the location, with estimates ranging from 10 to 30% for the Baltic Sea [Leppäranta and Hakala, 1992]. Because of this potentially large presence, the effect of ice ridges cannot be neglected. A typical ice ridge consists of a sail, a consolidated layer, and a keel. The sail is neglected during the calculation of the ice action, thus only the contribution to the load of the consolidated layer, F_c, and the keel, F_k, need to be considered [ISO19906, 2018]. The final ridge action is found as the sum of these two actions,

$$F_r = F_c + F_k \tag{2.3}$$

This section will derive all the relevant parameters necessary for calculating this action.

Consolidated layer

The ice action resulting from the consolidated layer crushing against the structure can be calculated with Equation 2.5, which will be discussed thoroughly in Section 2.2. The only unknown in this equation is the thickness, h_c, of the consolidated layer. Both the designs standards and relevant literature suggest a relation between the layer thickness and surrounding ice or the 'parent' ice, i.e. the ice that originally deformed into the ridge.

In absence of location specific data the ISO19906 [2018] suggests a consolidated layer thickness of $2h$, where h is the ice thickness of the parent ice. Accurately determining the thickness of the parent ice sheet is very difficult, and using the extreme 50-year ice thickness would be a significant overestimation. As this thickness occurs briefly at the most severe time during a very severe season. It is therefore highly improbable that two sheets of this extreme thickness were to collide, then impact such that the new layer is twice the original thickness and allowed sufficient time to refreeze. Hence Det Norske Veritas AS [2013] suggest an alternative to relate the extreme ice thickness to the consolidated layer, namely $h_c = 1.5h_{50}$, which is adopted in this research.

Keel

Besides crushing of consolidated layer, the action from the keel of a hummocked ice ridge needs to be considered. This action is given in ISO19906 [2018] by,

$$\begin{aligned} F_K &= \mu_\phi h_k w \left(\frac{h_k \mu_\phi \gamma_e}{2} + 2c \right) \left(1 + \frac{h_k}{6w} \right) \\ \mu_\phi &= \tan\left(45° + \frac{\phi}{2} \right) \\ \gamma_e &= (1 - e)\,(\rho_w - \rho_{ice})\,g; \end{aligned} \tag{2.4}$$

where μ_ϕ is the passive pressure coefficient, which depends on the internal friction angle effect ϕ, h_k is the height of the keel, w is the width of the structure, γ_e is the effective buoyancy and c is the apparent keel cohesion. The effective buoyancy depends on the density of the water, ice and the porosity, which varies between 0.1 and 0.4 according to ISO19906 [2018]. For preliminary designs a value of 0.3 can be applied for the porosity and a value of 35° is advised for the internal friction angle of the ridge.

For the assessment of the keel height, h_k, Det Norske Veritas AS [2013] provides a derivation based on the extreme ice thickness, $12.5\sqrt{h_{50}}$, which is in good agreement with field research on ridge properties Tin and Jeffries [2003].

The advised value for the keel cohesion, c, leads to very high values of the ice ridge, hence this research deviates from the standards with respect to this parameter. The effect of this difference will be investigated in Part III by including ridge action from both methods. The keel cohesion of the ridges is 10 kPa according to ISO19906 [2018] and Det Norske Veritas AS [2013]. The suggested alternative is based on field experiments with first-year ice ridges by Heinonen [2004]. The field experiments determined a relation between the internal friction angle and the maximum keel cohesion as given by Figure 2.4.

For an internal friction angle of 35° the minimum measured keel cohesion was around 6 kPa, and the maximum was 13 kPa, which corresponds to average keel cohesions of 3 and 6.5 kPa. It is assumed that the weakest measured ridge in the severe conditions in the Bay of Bothnia is similar to the strongest ridge in the least severe region in the Southern Baltic Sea. Hence the range of 3–6.5 kPa is assumed and values in between are interpolated based on the length of ice season in the region. With all the aforementioned parameters the ridge action can be determined with Equation 3.1, Equation 2.5 and Equation 2.3, as will be done in Part III of this research. An overview of the applied ridge parameters is given in Table 2.1.

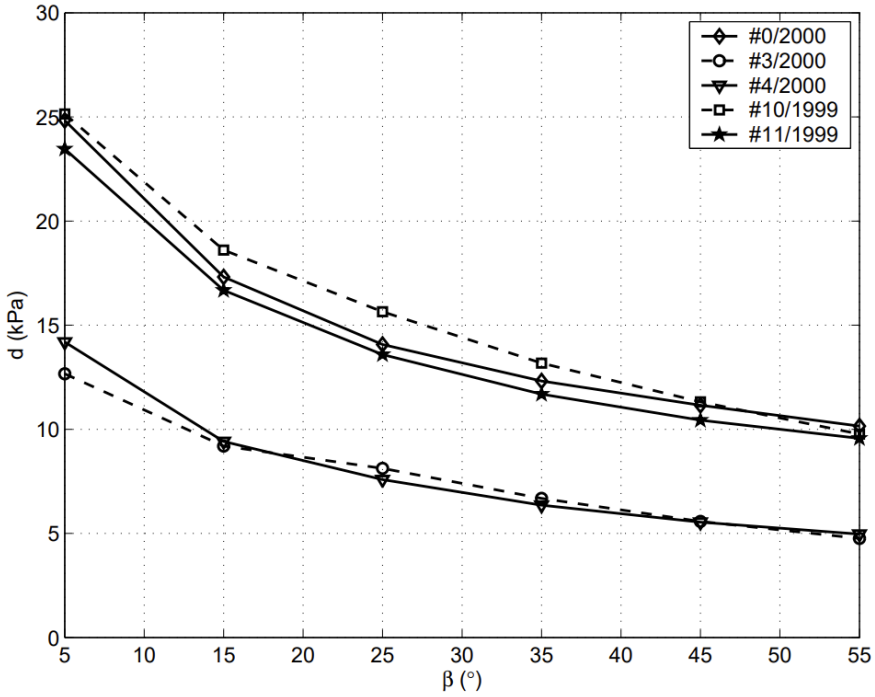

Figure 2.4: Relations between keel cohesion and internal friction angle for various tested ridges in the Bay of Bothnia [Heinonen, 2004].

Table 2.1: Ice ridge parameters according to design standards and field research.

Ridge parameter	Design standards	Alternative
h_c	$1.5h_{50}$	$1.5h_{50}$
h_k	$12.5\sqrt{h}$	$12.5\sqrt{h}$
e	0.3	0.3
ϕ	35°	35°
c	10 kPa	3–6.5 kPa

2.2 ICE STRENGTH COEFFICIENT C_R

The ice strength coefficient C_R is introduced in the ISO19906 [2018] to determine the upper boundary of continuous brittle crushing of ice against a vertical structure. The global average ice pressure and the global ice action can be calculated with the following equations:

$$\begin{aligned} F_G &= p_G h w \\ p_G &= C_R \left[\left(\frac{h}{h_1} \right)^n \left(\frac{w}{h} \right)^m + f_{AR} \right] \end{aligned} \tag{2.5}$$

where F_G is the global ice action, h is the level ice thickness, w is the projected structure width, p_G is the global average ice pressure, C_R is the ice strength coefficient, h_1 is a 1 m reference thickness, both n and m are empirical coefficients, and f_{AR} is an empirical term which should only be included for structures with an aspect ratio < 5.

ISO19906 [2018] gives characteristic values of C_R for arctic, sub-arctic and temperate ice regions, which corresponds to regions with approximately 4000, 2000 and 1000 C_{FDD}, respectively. The Baltic Sea is specifically listed as a temperate ice region. However, there is little literature on inter-region variability of the crushing coefficient, when the C_{FDD} diverges from the default values. The standard does mention three methods to adjust the crushing value if the the region of interest is not clearly categorized by the these values. However, none of these are

satisfactory in the context of this research. Therefore this section suggests a new method, first applied in an informal paper by Hendrikse [2020]. This method will be explained and applied to scale the 1-year and 50-year ice strength coefficients, $C_{R;1}$ and $C_{R;50}$, as measured in full-scale measurements on the Norströmsgrund Lighthouse in the Bay of Bothnia. Reference is made to van der Stap [2022] for an in-depth analysis of the Hendrikse method and the (herein rejected) methods as proposed by the standards.

2.2.1 The Hendrikse method

The original C_R value for the Baltic Sea was determined at the Norströmsgrund Lighthouse (65°6′6″, 22°19′12″) in the Bay of Bothnia, which will serve as reference location. When the rest of the Baltic Sea is compared to this region there are three major differences that may influence the peak ice crushing pressure:

- The length of the winter season is shorter in almost all other regions of the Baltic Sea. This results in less interaction events per winter, which likely results in a lower annual maximum peak pressure.
- The average temperature of the ice is lower in other regions. Warmer ice gives a lower strength and in turn a lower annual maximum peak pressure.
- The salinity in the Bay of Bothnia is lower than in most other regions. Saline ice is known to have less crushing strength compared to freshwater ice.

Data on the length of ice seasons is readily available, whereas data on salinity and temperature of the ice would require plenty of assumptions. Thus the crushing value will only be scaled based on the change in exposure between regions. It should be noted that the coldest, freshest ice will yield the highest crushing coefficient. Since the reference value is based on the Bay of Bothnia, where temperature and salinity is lowest, neglecting the aforementioned effects will give conservative estimates for the rest of the Baltic Sea. For this research the length of the ice season is assumed to be a decent indicator of exposure time. The length of ice season — from ice formation to break-up — was measured in a large scale statistical analysis of ice season in the twentieth century for all observation stations around the Baltic Sea. By assuming similar drift conditions throughout the Baltic Sea, the annual maximum value of the reference locations were correlated to the x-year maximum at a different location in the Baltic based on the length of ice season. With this adjusted return period the reduction factor can be determined using Figure 2.5, which shows the extreme global pressure at the Norströmsgrund Lighthouse as a function of the return period. Note, that the assumption of similar drift conditions throughout the Baltic, means that the C_R value in landfast regions is heavily overestimated. Structures in the landfast zone are exposed to events much less frequently, hence this is very conservative.

The final reduction factor can be found as the ratio between the values found in Figure 2.5. After the reduction factor is obtained for all observation stations, the results were extrapolated across the entire Baltic Sea. The result for 1-year extreme ice strength coefficient, $C_{R;1}$, is given by Figure 2.6. A similar plot for the 50-year maximum coefficient, $C_{R;50}$, can be found in Appendix A.

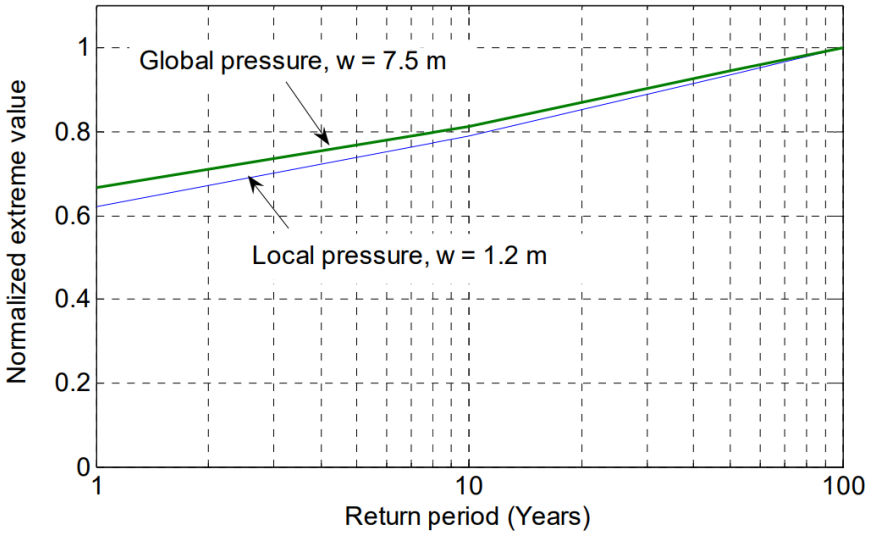

Figure 2.5: Extreme global pressure at the Norströmsgrund lighthouse as a function of the return period. The values were normalized for a penetration distance of 300 m, ice thickness of 0.4 m and for 100-year values for both global and local pressures. For global pressures the width, w, of 7.5 m was taken and for local pressures it was 1.2 m [Gravesen and Kärnä, 2009].

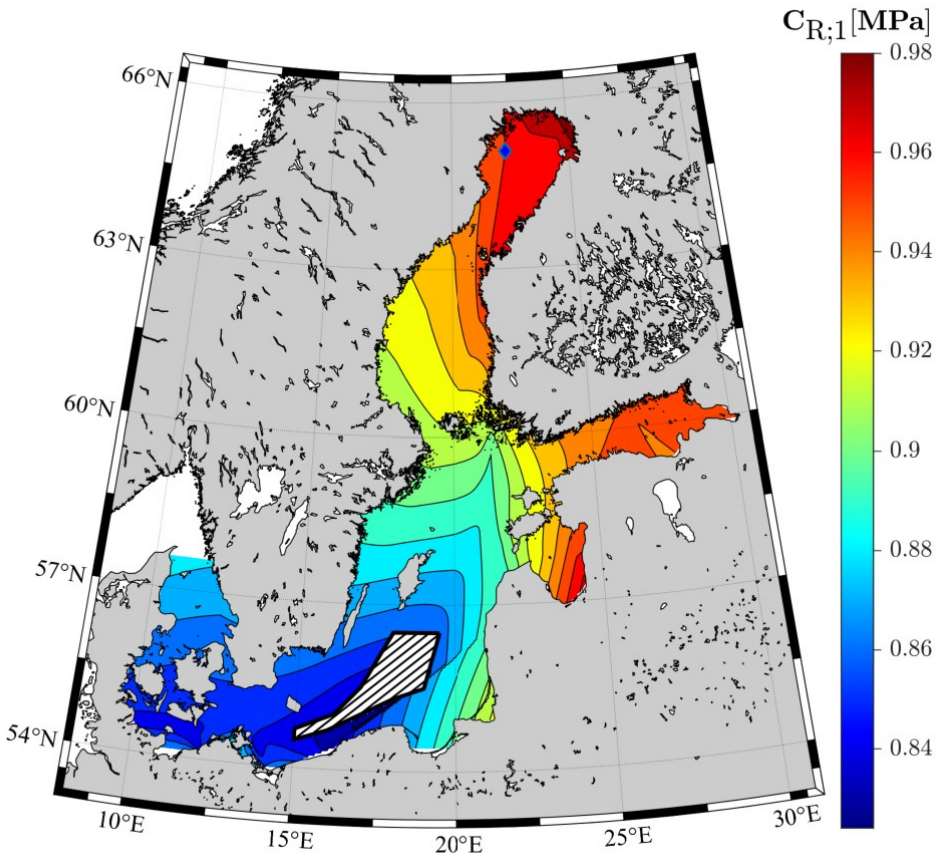

Figure 2.6: Inter-regional variability of the annual maximum crushing coefficient, $C_{R;1}$, in the Baltic Sea. The diamond marker depicts the reference location.

2.3 BATHYMETRY

The bathymetry of the Baltic Sea has a significant impact on the design of fixed wind turbines. Monopiles feasibility water depths depends on turbine size, but for the current generation of 12–15 MW turbines 60-65 m is considered the limit for design. Besides this issue, the bathymetry influences designs in arctic conditions in a different way. The formation of landfast ice depends strongly on the water depth. According to most literature the landfast ice region is defined in the range of the 5 to 15 m isobath [Granskog et al., 2006]. The difference in thickness of landfast ice and drift ice can be substantial as discussed in Section 2.1. This section will provide a map of the bathymetry of the Baltic Sea based on the available data. Additionally, the isobath of 15 m is provided as input for the definition of the landfast region.

Figure 2.7 shows the bathymetry of the Baltic Sea based on the Baltic Sea Bathymetry Database (BSBD), which is developed by Baltic Sea Hydrographic Commission using data sets provided by each national hydrographic authority. Additionally, a map showing all locations where monopiles could be considered as foundations for wind turbines(< 65 m) can be found in Figure A.6.

From the bathymetry defined in Figure 2.7 the isobath at 15 m was also found, which shows close resemblance to the boundary for landfast ice regions on ice charts, especially in the North and East. However, based on these ice charts some adjustments have been made for a more probable result. Notably, in the Southern Baltic Sea the isobath does not necessarily define the landfast region as often no landfast ice is spotted. Furthermore, due to the Finnish archipelago a large landfast zone is observed of the South West coast of Finland. Additionally, the Bay of Bothnia and the Gulf of Finland see large landfast regions. The final boundary for the landfast ice as well as the contour plot up to isobath 15 m is given in Figure A.5.

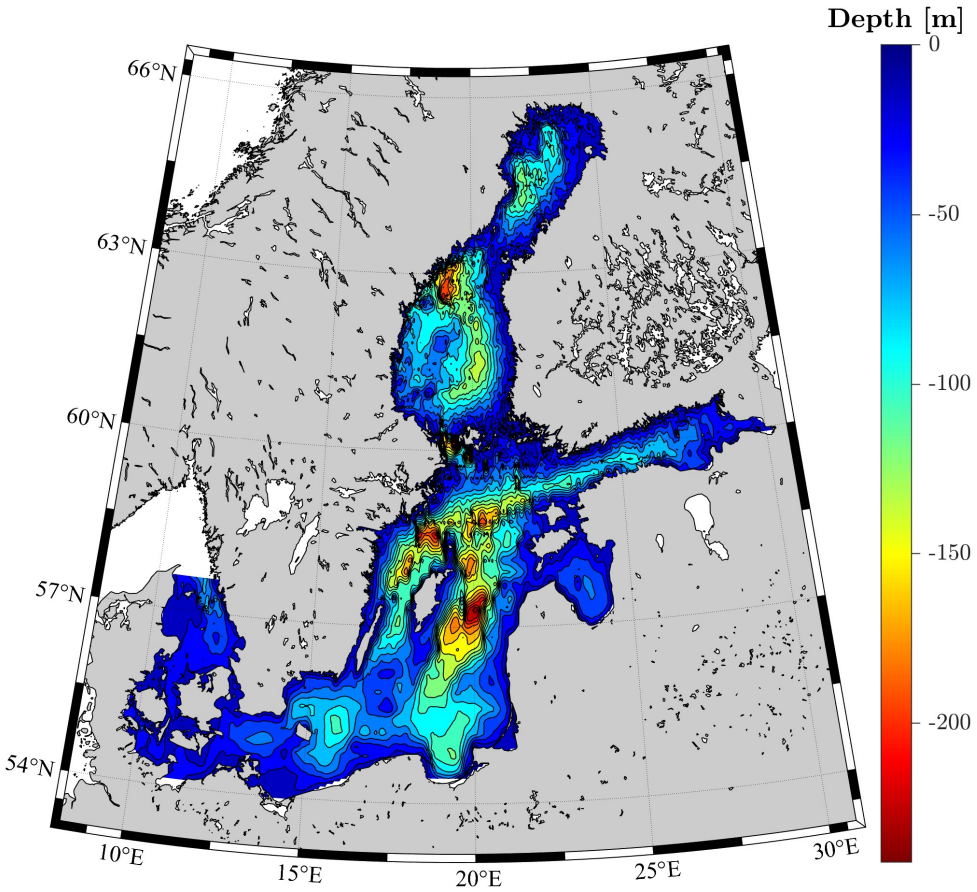

Figure 2.7: Baltic Sea bathymetry generated with the BSBD.

2.4 WIND & WAVES

For the purpose of monopile design, parameters representing wind and wave conditions should be accurately estimated. This has to be done for the 50-year Extreme Sea State (ESS50) as well as for the Normal Sea States (NSS). Since the research is mostly concerned with the ice loading, the data on wind and waves was provided directly by the metocean team of WT. For each region a wind-wave table was generated with probabilities for each sea state. Additionally, the 50-year extreme values were provided by DTU's global wind atlas [Badger et al., 2015]. As the focus was mostly on the effect of ice, the wind and wave conditions were considered to a lesser extent for the identification of the characteristic regions. Rather, the corresponding values were found after the regions were identified. These values are presented in Table 2.2.

2.5 ICE DRIFT SPEED

In this section the ice drift speed is discussed. In the context of monopile design there are two cases which should be considered, the Ultimate Limit State (ULS) and the Fatigue Limit State (FLS). For the former it is critical that the ice drift velocities with the most severe load impact are included in the analysis. While for the latter, an estimate of the likelihood of each individual ice drift speed is required. This section aims to provide reasonable values for both cases.

A multitude of models has been developed with the aim to accurately determine the ice drift speed depending on a range of variables. However, derivation of the exact ice drift using one of these models is unnecessary for the ULS analysis of the monopile. Rather a range of velocities should be considered which 1) are expected to occur and 2) capture the dynamic effects of ice-structure interaction. This approach is in agreement with the design standards such as DNV GL [2016], which states that: *"it shall be analyzed that the dynamic interaction between the structure and the moving sea ice cover leads to a lock-in situation."*

The relevant dynamic regimes are ICR, FLI and CBR, which are defined in Section 3.2. Since the first two occur at relatively low velocities and are known to be governing in terms of the design loads, it suffices to consider a range of speeds from low speeds up until CBR occurs. For all regions ice velocities in the range of 0.01–0.2 $\mathrm{m\,s^{-1}}$ are selected, since these speeds are known to occur in all regions, but also include effects from all regimes, thus ensuring that the peak of the global ice load is captured.

For the FLS cases the likelihood of all potential ice drift velocities and directions need to be determined. Additionally, the likelihood of a specific wind velocity in combination with a ice drift velocity and their relative misalignment should be assessed. Unfortunately, acquiring such a thorough data set is rather strenuous and unrealistic for the scope of this research. Instead, a different approach can be applied. Ice drift is forced by wind and currents, however, research has shown that in the Baltic Sea the contribution of the wind forcing is dominant over the current [Leppäranta, 1981]. This is in line with other research suggesting that a simple wind factor model for the ice drift works equally well as a coupled ice-ocean model [Leppäranta and Omstedt, 1990].

Therefore, the same model is applied in this research with a wind factor of 2% as suggested by Leppäranta and Omstedt [1990]. This assumption implies no misalignment between wind and ice direction, which might be nonconservative. The design standards, however, do not require the assessment of misalignment [DNV GL, 2016].

Since the wind and ice speeds are assumed to be directly related, the probability of each ice velocity is similar to that of its corresponding wind velocity. It is important that this factor is applied to the wind experienced by the ice sheet at sea level, rather than the wind speed at hub

height. The wind speeds at a reference height can be calculated from the wind speeds at hub height using,

$$\frac{U(z)}{U(z_r)} = \left(\frac{z}{z_r}\right)^{\alpha} \tag{2.6}$$

where $U(z)$ and $U(z_r)$ are the wind speeds at height z and at reference height z_r, and α is the power law exponent. For an offshore location at open sea an α of 0.14 can be applied for a reference height of 10 m in accordance with IEC [2019]. The difference in wind speed at the reference height of 10 m and at sea level is considered negligible.

The resulting wind speeds are in the range of 0–0.5 m s^{-1} for each region, which is in correspondence with literature on ice drift speed in the Baltic Sea. Average ice drift speeds were reported in the range of 0.09–0.27 m s^{-1}, while maximum drift speeds were around 0.5–1.0 m s^{-1} depending on the regions [Lilover et al., 2018]. The wind factor model underestimates the maximum occurring ice drift velocities, however, global ice loads decrease during brittle crushing, thus the applied model is conservative. Though, it should be noted that the wind factor model can yield inaccuracies for low wind velocities, as the contribution of currents — now neglected — is more dominant in these cases Leppäranta [1981].

2.6 ICE STATE PROBABILITY

For a proper FLS analysis of the OWT the probability of each ice state needs to be determined, such that during post-processing of the loads the correct probabilities of occurrence are assigned to each simulation. In the previous section it was observed that if wind-ice misalignment is neglected and a wind factor model is applied for the ice drift speed, the probability distribution for the ice drift velocity follows from the wind distribution as the two are directly related. Besides the ice drift velocity distribution, the ice thickness distribution, the number of ice interaction days and the directionality are required for the calculation of the ice state probability, p_{ice}. The derivation of p_{ice} will be the focus of this section.

2.6.1 Ice thickness distribution

In a recent article by Hornnes et al. [2022] drift ice thickness distributions were derived for the design phase of an offshore wind turbine in the Southern Baltic Sea by applying a Copernicus reanalysis product. In this paper the ice occurrence probabilities are provided for a reference case, namely the Danish Kriegers Flak project. Since deriving such a thickness distribution is difficult without a full-scale metocean analysis, similar distributions are assumed for the southern characteristic regions in the Baltic Sea. Note that, similar as with wind & wave data, the assignment of ice thickness distributions and interaction days, was not taken into account during identification of the characteristic regions, but rather performed retro-actively. This is because the scarcity of data of ice thickness distributions and ice interaction days in the Baltic Sea.

For the Northern most region, the Bay of Bothnia, two papers describing ice thickness distribution over one or multiple ice seasons by Hornnes et al. [2020] and Ronkainen et al. [2018] were used. The ice thickness distribution of the former is presented in Figure 2.8. However, these distributions cannot be directly used as no distinction is made between deformed and undeformed ice. Deformed ice is formed due to weather, collisions or other environmental impacts. The deformed ice is much weaker than undeformed ice, but can result in thicker measured ice.

This distinction was also not included in the research on Southern ice thickness distribution, but for the Bay of Bothnia this will have a larger impact as the ice concentration is much higher while the ice season is also longer, giving the ice sheets more opportunity to deform. As a result, all ice thicknesses above the derived extreme ice thickness of 1.25 m are neglected. The resulting probability is applied to the Northern most regions of the Baltic Sea. Educated

estimates are made for the thickness distributions in regions that are bounded by the Northern and Southern regions.

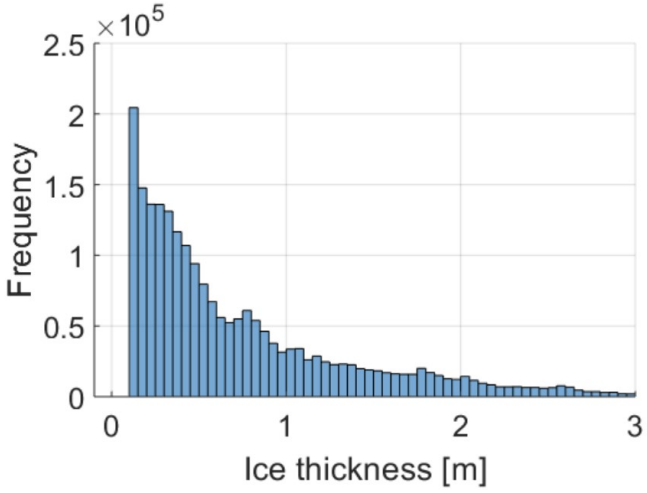

Figure 2.8: Probability of interpolated ice thickness values with a bin width of 0.05 m [Hornnes et al., 2020].

The probability of each ice state, p_{ice}, can then be calculated by multiplying the ice thickness & velocity distributions to generate a combined distribution table, as shown in Table A.1.

2.6.2 Ice days

After the probabilities of specific ice states have been determined, the total number of ice days over the lifetime of a structure has to be assessed. This serves to scale between the wind/wave simulations on one hand and the ice simulations on the other hand. Based on the little data available a method is proposed to determine the total days of ice-interaction based on the length of the ice season and the probability of ice forming in a season, given by,

$$D_{\text{ice}} = \mu_{\text{drift}} \left(L_{\text{s}}\, p_{\text{c}}\, T_{\text{OWT}} - D_{\text{fr}}\, p_{\text{c}}\, T_{\text{OWT}} \right) \tag{2.7}$$

where D_{ice} is the number of interaction days over the lifetime of the structure, L_{s} is the length of the ice season in days (from first ice formation to break up), p_{c} is the probability of ice occurring at the coast, T_{OWT} is the lifetime of the structure in years, D_{fr} is the freeze delay in days and μ_{drift} is the ice drift factor.

In a review of ice seasons in the twentieth century the length of the ice season and the probability of ice occurrence were determined for coastal weather stations all around the Baltic Sea by Jevrejeva et al. [2004]. Since the weather stations are all on the coast a correction is required to account for the slower formation of ice offshore. This is due to lower temperatures and larger water depths, which means a larger water column has to be cooled. To account for this a freeze delay factor, D_{fr}, is included which subtracts a number of days in a season for the formation of ice offshore. This factor also includes the fact that the effect of level ice below 0.15 m is negligible, hence the freeze delay includes days required until the formation of ice above this threshold in open waters. This is approximately 35 days, which is around 5 days for the formation of ice to 0.15 m — calculated with Equation 2.2 — and 30 days for the formation of ice offshore as deduced from ice charts.

Besides the freeze delay, a drift factor, μ_{drift} is included, which accounts for the fact that in most cases the ice is not drifting against the structure. Based on observations at the lighthouse Norströmsgrund, where crushing of drifting ice was only observed 10% of the time, the factor is set to 0.1. With these parameters and an assumed lifetime of 25 years, the total number of

ice interaction days per region were determined and are given in Table 2.2. For the required input data per region, such as the length of ice season and probability of ice formation at the coast, reference is made to Table A.2.

The available data for ice interaction days suggest a total of 8.9 days over the lifetime for an OWT in Kriegers Flak, which lies between the Danish Straits and Baltic Proper South [Hornnes et al., 2022]. The proposed method suggests 9.6 and 11.9 days for these two regions, respectively. Hence, if the data for Kriegers Flak would be accurate, the method is on the conservative side, but within an acceptable range. During full-scale measurements, research found that the total distance travelled of the level ice around the lighthouse in the Bay of Bothnia is around 135 km during one season, when the level ice moves at 0.15 m s^{-1} [Thijssen et al., 2019]. The interaction days from proposed method lead to a total distance travelled of 183 km, which is again an overestimate. However it 1) is within the right order of magnitude and 2) it is conservative assuming that ice damage is larger than wave damage. The latter is very reasonable as wave conditions throughout the Baltic are relatively mild compared to sea states elsewhere.

Finally, the directionality is required to derive p_{ice}. To reduce the number of simulations only one ice direction is included, however it was assumed that ice would be drifting in this direction 35% of the total interaction days. For six total considered directions, this is more than twice the average probability. Without measurements it is hard to determine with certainty, however it is assumed to be on the conservative side.

2.7 CHARACTERISTIC REGIONS

During the review of metocean data, and specifically the data relating to ice, much available data were already grouped into certain known regions in the Baltic Sea. The best example of this is the description of the Baltic Sea in the ISO19906 [2018], which is split over the Gulf of Bothnia (consisting of the Bay of Bothnia & the Bothnian Sea), the Gulf of Finland, the Gulf of Riga, the Baltic Proper and the Danish Straits or Belts.

As a result the identification of the regions is strongly based on these locations, but with slight alterations based on the new analysis of the ice conditions. These changes include the division of the North and South parts of the Bothnian Sea, due to a decrease in ice thickness, ice strength and significant difference in bathymetry. Next, the Archipelago Sea was specifically included, which stands out to adjacent regions due to the very large probability of thick ice as a result of the shallow water. The Gulf of Finland and Riga remain as is. Finally, the Baltic Proper is split in North and South due to difference in ice thickness. The latter of the two is often referred to as the Southern Baltic Sea. However, the Danish Straits are kept separate from this region due to the shallow water in this region, as well as the substantially milder wave conditions. The final identified regions are shown in Figure 2.9 and the corresponding representative conditions are given in Table 2.2. Current velocity, ice drift speed and soil profiles are kept constant for each region. Wind and wave tables are specified for each region specifically, as are extreme wind and wave speeds.

Table 2.2: Identified regions and their characteristic metocean conditions. The * indicates that the average depth exceeds 65, hence 65 m is taken as design limit.

Region	h_{50} [m]	$C_{R;1}$ [MPa]	Depth [m]	$v_{wind;50}$ [m s^{-1}]	$H_{S;50}$ [m]	D_{ice} [days per lifetime]
Danish Straits	0.40	0.88	19	45.06	6.17	9.6
Baltic Proper S.	0.45	0.86	65*	43.44	12.43	11.9
Baltic Proper N.	0.50	0.88	65*	43.88	12.96	73.3
Gulf of Riga	0.55	0.94	26	39.19	9.23	197.6
Gulf of Finland	0.95	0.95	37	35.96	6.44	198.0
Archipelago Sea	0.75	0.92	23	40.28	6.55	96.9
Bothnian Sea S.	0.65	0.92	50	40.72	12.53	228.0
Bothnian Sea N.	1.00	0.94	65*	41.07	11.26	299.8
Bay of Bothnia	1.25	0.98	42	37.70	9.75	352.5

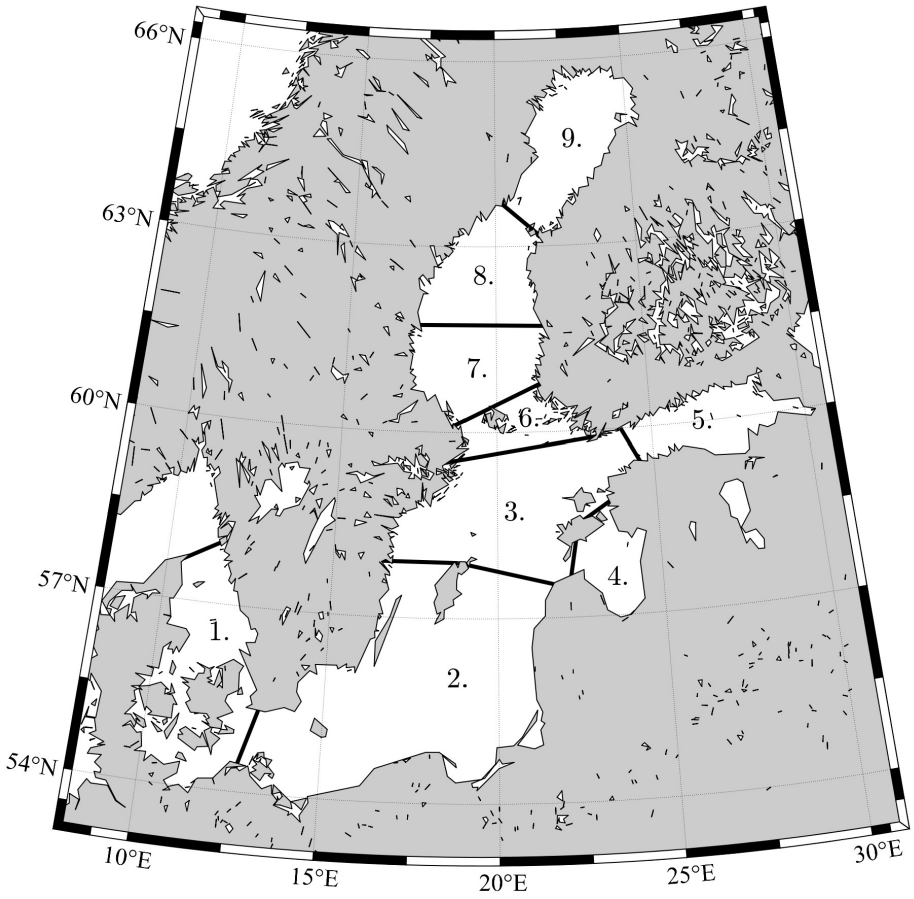

Figure 2.9: The nine identified characteristic regions of the Baltic Sea. The numbers indicate 1 - the Danish Straits, 2 - the Baltic Proper South, 3 - the Baltic Proper North, 4 - the Gulf of Riga, 5 - the Gulf of Finland, 6 - the Archipelago Sea, 7 - the Bothnian Sea South, 8 - the Bothnian Sea North and 9 - the Bay of Bothnia.

3 ICE MECHANICS

To accurately simulate ice-structure interaction of OWT it is necessary to understand ice failure mechanisms against vertical structures. This chapter discusses the relevant ice mechanics, and serves as an introduction to the development of the coupled models, which is the objective of Part II.

Traditionally, most offshore structures concerned foundations for the oil- and gas industry which were very stiff and massive, and could thus (for the most part) be considered as rigid structures. As a result, failure of the ice — and thus the global ice action — was independent of the structural response. As more structures were subject to ice loading, it was observed that the compliance of the structure as well as the ice velocity strongly influenced the ice loading. This chapter provides a short overview of the failure mechanisms typically associated with ice loading as well as the dynamic interactions, known as ice-induces vibrations, for compliant structures. The chapter will conclude with a succinct summary of the theory behind Variation of contact Area model for Numerical Ice Load Level Analyses (VANILLA), which will be used for the modelling of the ice-interaction in the subsequent chapters of the report.

3.1 ICE FAILURE MODES

When level ice interacts with a monopile foundation there are multiple modes of failure, most notably creep, crushing, buckling and splitting. The latter is known to occur in small floes and is believed to be a load-releasing mechanism. This mechanism is the result of a crack through the thickness of the ice propagating towards a free edge of the floe [Lu et al., 2015]. It is assumed that the floes relevant to this research will be of sufficient size that the distance to the nearest free edge is too large for splitting to occur. Hence, splitting is neglected. The occurrence of the other three modes depends on the ice drift velocity, or indentation velocity, and the aspect ratio, which is the diameter of the structure, d, over the thickness of the ice, h. The dependence of the modes on these two parameters is given in Figure 3.1.

3.1.1 Creep, crushing & buckling

At low indentation velocities and low aspect ratios, creep is the dominant failure mechanism. Creep, also known as ductile failure, is a plastic deformation of the ice sheet as it slowly pushes against and around the structure. It is characterized by a very low indentation velocity and, if sustained for longer periods, large deformations due to the uniform pressure along the ice-structure interface. Figure 3.2 depicts, amongst others, the creep failure mode on a vertical structure [Hendrikse, 2017].

For ice-interaction at higher indentation velocities with low aspect ratios, crushing is observed. In this failure mode the higher indentation velocity prevents the development of a full contact area, so only local contact and non-simultaneous failure occurs. The resulting load signal is quasi-random around a mean value [Jordaan, 2001]. In contrast with creep, the high indentation velocities associated with crushing leads to elastic — instead of plastic — deformations before failure [Hendrikse, 2017].

For high aspect ratios buckling is the governing failure mode. Buckling is characterized by out-of-plane deformation, leading to failure once the bending stress exceeds the flexural strength

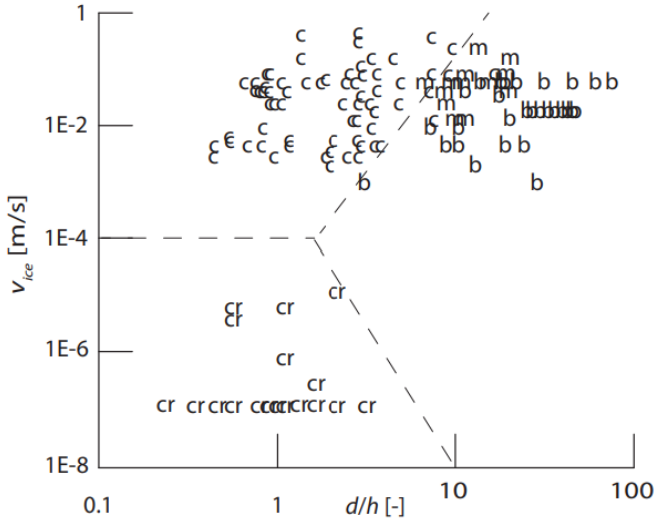

Figure 3.1: Map displaying failure modes of ice depending on the ice indentation velocity and the aspect ratio. Expected transitions between failure modes are given by dashed lines. Letters indicate failure modes: cr – creep, c – crushing failure, b – buckling failure, m – mixed crushing and buckling failure. Note, this map is for model-scale conditions [Hendrikse, 2017].

of the ice sheet [Hendrikse and Metrikine, 2016]. It is often confused with bending failure, also characterized by out-of-plane failure. However, buckling is out-of-plane bending as a result of in-plane forces, while bending is the result of vertical forces on the ice sheet, e.g. being pushed on a sloped structure. At high indentation velocities buckling is sometimes observed to occur after a period of crushing, this is referred to as mixed failure of crushing and buckling [Hendrikse, 2017].

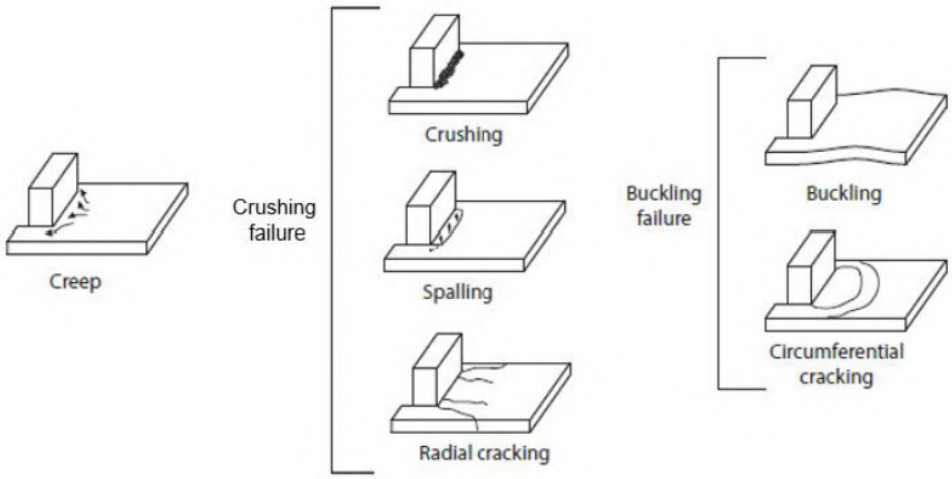

Figure 3.2: Ice failure modes against vertically-sided structures [Hoek, 2021].

3.2 ICE-INDUCED VIBRATIONS

In contrast with rigid structures, dynamic ice-structure interaction needs to be considered when compliant structures are designed. Due to the flexibility in the system the structure and ice interact, which leads to ice-induced vibrations. The load effects of these vibrations are predominantly observed in the transition from creep to crushing, or as it was often referred to:

the ductile to brittle transition [Yue et al., 2002]. This section discusses the three 'traditionally' identified vibrations, or failure regimes given in Figure 3.3. Additionally, recent research has shown that for offshore wind turbines specifically, the traditional terminology does not accurately describe all of the observed regimes. Therefore two additional interaction modes are introduced, namely MMI and MMII as first introduced in Hammer et al. [2022].

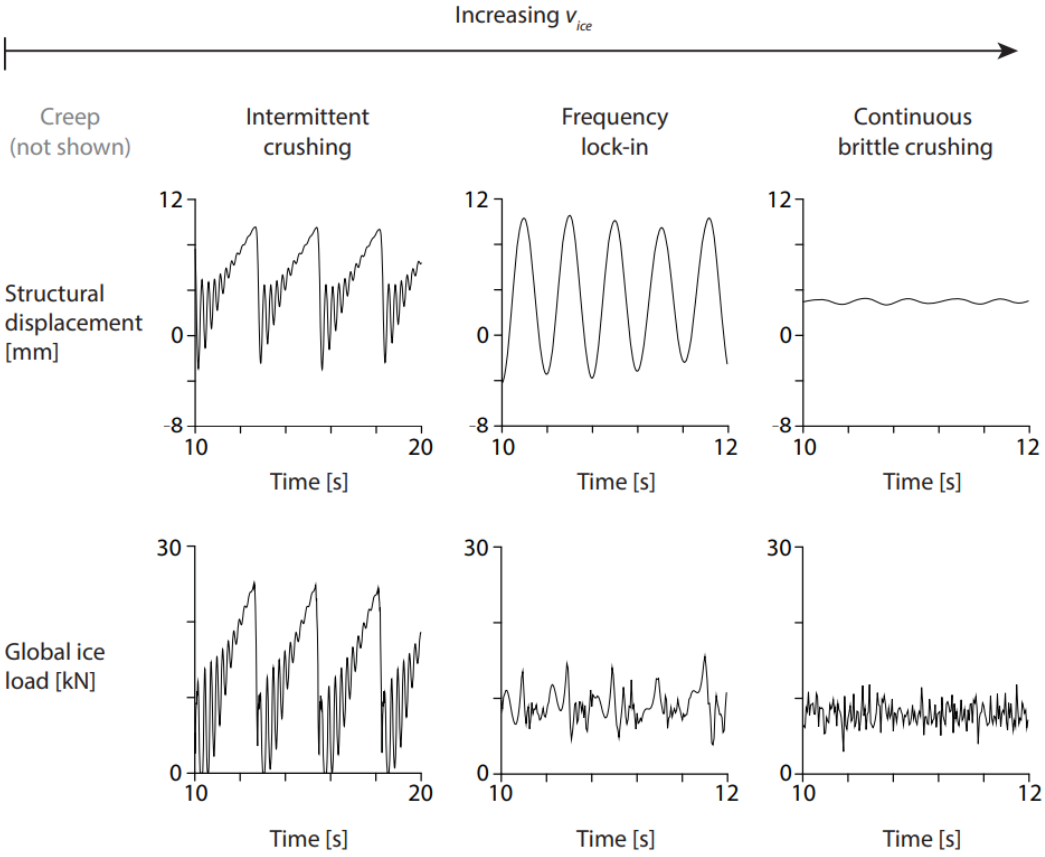

Figure 3.3: Three regimes of ice-induced vibrations as function of ice velocity. Structural displacement is given by the top row, while the bottom row gives the global ice load on the structure [Hendrikse, 2017].

3.2.1 Intermittent crushing

In the transition region from ductile to brittle failure, ICR can develop for the lowest ice velocities. The process starts with the displacement of the structure in direction of the ice motion upon loading. As the the relative velocity of the ice decreases, the ice fails in a ductile manner and the contact area between structure and ice can fully develop. During this phase the load increases as the maximum deflection of the structure is reached, after which the ice starts to fail and the structure begins to move in the opposing direction. Due to the opposing movement of the structure, no full contact area is allowed to develop, so there is brittle failure of the ice and the load drastically decreases [Hoek, 2021]. As the structures continues to move in the opposing ice drift direction its velocity is reduced due to the incoming ice sheet. The process can then repeat itself. As a result the displacement and global load over time are given by the distinctive saw-tooth pattern [Sodhi, 2001]. The peak loads associated with ICR can be up to 4 times higher than peak loads during regular crushing [Singh et al., 1990].

3.2.2 Frequency lock-in

For slightly higher indentation velocities, FLI occurs. During FLI the frequency of ice failure 'locks' in with the one of the natural frequencies of the structure, resulting in periodic oscillations of the structure at a frequency close — usually slightly below — this natural frequency. The reason that this oscillation is not truly, but 'near' harmonic is that as the structure changes its motion in the opposing direction to the ice, the ice does not immediately fail. Rather, some deformation is still imposed on the ice, resulting in a load on the structure, which delays the oscillation. These oscillations may lead to significant damage as a result of structural fatigue [Hendrikse and Koot, 2019]. When the relative velocity of the ice is low, the global load on the structure can rapidly increase. Whereas during periods of high relative velocity the load is similar to that of quasi-random crushing failure. Occasionally the structural velocity exceeds that of the ice sheet, causing a short unloading [Hendrikse, 2017].

3.2.3 Continuous brittle crushing

For high indentation velocities the observed interaction regime is CBR for all structures, independent of the compliance of the structure. Note, the transition region at which this occurs is still dependent on the flexibility. Due to the high speed of the ice sheet, the relative velocity of the ice is constantly high, so the contact area remains small. Hence there is no large periodic transfer of energy, but rather a continuous quasi-random load transfer. The corresponding ice load and displacement are thus quasi-random and oscillate around a mean value [Hendrikse and Nord, 2019]. This mean value is substantially lower than in ICR and FLI, indicating that CBR is less significant for design.

3.2.4 Multi-modal interaction-II

For intermediate ice drift speeds, which are relative to the structure, multi-modal interaction II has been observed. This interaction is characterized by a periodic response of the structure due to loads with higher maxima but similar mean loads as for CBR. The response of the structure is correlated with the second and third mode, with the latter being dominant. The observed load signal is similar in nature to FLI, however FLI is associated with a near-harmonic oscillation, whereas this is highly unlikely to occur for an OWT as higher modes are easily excited. This leads to a response with a steeper slope during the unloading phase compared to the loading phase Hammer et al. [2022], as shown in Figure 3.4b.

3.2.5 Multi-modal interaction-I

For interaction between ice and OWT at low relative ice drift speeds high peaks are observed after a long phase of low relative ice velocity between structure and the incoming ice. Between the peak and the new phase, the load signal resembles that of the the previously introduced MMII. The structural response is characterized by the saw-tooth pattern, similar to ICR. However, in the unloading phase small vibrations associated with the second or third mode can be observed as an additional saw-tooth within the saw-tooth, as indicated by Figure 3.4a. This can be explained due to the low first natural frequency of the structure. This causes a relatively low velocity during the unloading phase, which allows the second and third mode to be excited.

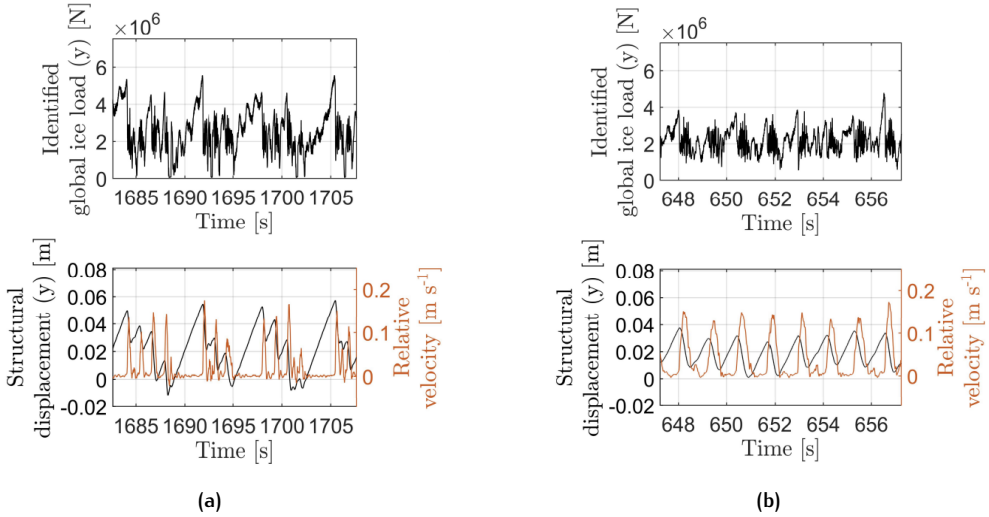

Figure 3.4: (a) Typical load time series (top) and structural response (bottom) of OWT during MMI. (b) Typical load time series (top) and structural response (bottom) of OWT during MMII [Hammer et al., 2022].

3.3 VANILLA

In this research the VANILLA model will be used to simulate ice crushing. This section discusses the latest version of this model. For an overview and comparisons of existing ice models reference is made to van der Stap [2022]. This also contains the reason for selecting VANILLA, which in short is either due to the conservative approaches of other models or non-physical assumptions of the models.

Theoretical background

VANILLA is a phenomenological model developed at the TU Delft which assumes that the development of the contact area between the ice and the structure, as a result of the relative velocity between the two, governs the interaction process. The model has been validated with small- and full-scale measurements on multiple occasions [Hendrikse et al., 2018; Hendrikse and Nord, 2019]. To accurately model the contact area, the model assumes that the ice sheet is partitioned into N independent elements in order to capture the stochastic, non-simultaneous nature of brittle crushing as shown in Figure 3.5a. The elements are each positioned with a uniformly distributed offset to the structure. A combination of (non-)linear springs and dashpots for each individual element is used to model the deformation and failure of the ice once contact is made with the structure as illustrated in Figure 3.5b.

The non-linear dashpot, C_2, at the rear of the ice elements was added to simulate the creep regime, or ductile failure. These creep deformations, occurring at very low velocities, are governed by the 'power law creep', where the deformation is a function of the stress cubed [Hoek, 2021]. The parallel linear spring-dashpot combination, K_1 and C_1, captures the delayed-elastic deformations of the ice in the transition from ductile to brittle failure. The front non-linear springs, K_2 model the local elastic deformations (in compression only) and the failure of the ice when the critical deformation, δ, is reached [Hendrikse et al., 2018]:

$$u_{i,2} - u_{i,1} = \delta \tag{3.1}$$

Once this deformation is exceeded the ice element 'fails', and is removed from its location and replaced. The new ice element position is again drawn from a uniform distribution based on the roughness of the ice edge.

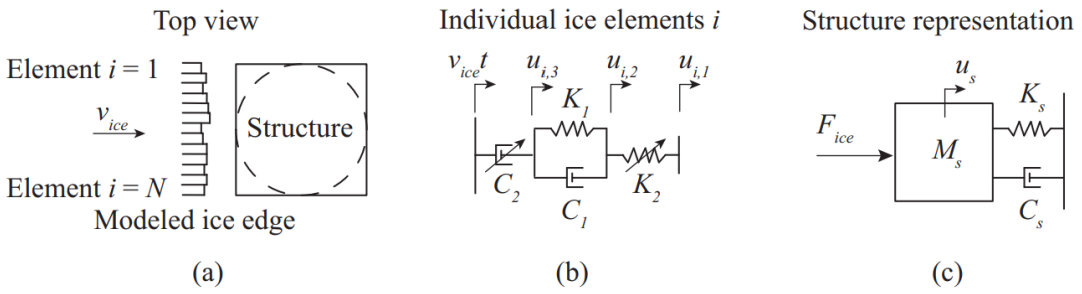

Figure 3.5: VANILLA ice model with (a) ice edge partitioned by N individual elements interacting with a structure which can be of various shapes, (b) combination of (non-)linear springs and dashpots to model each ice element and (c) the structure modelled as simplified SDOF oscillator [Hendrikse et al., 2018].

With the three described components VANILLA is able to simulate ice-structure interaction that has ice velocity dependent deformation and failure of each ice element. This is illustrated in Figure 3.6, where the load resulting from a single ice element is shown as a function of the deformation. Due to the rear dashpot, brittle failure will never occur for low velocities, which is indicated by the line asymptotically approaching the critical load deformation. In contrast, at high ice velocities, the critical load deformation is reached much faster after it develops linearly as a result of the front spring. Finally, at intermediate ice velocities, brittle failure is reached, but much slower than at high velocities. This behaviour corresponds to the linear spring-dashpot combination [Hendrikse and Nord, 2019].

By solving the equations of motions for the ice elements the resulting global ice load can be found as the sum of the contributions of all the elements. When VANILLA is run stand-alone, the response of the system can then be determined by by either assuming that the structure is a simple SDOF oscillator or by solving the system of equations for the structure in the modal domain. The total system is then solved with a 4^{th} order Runge-Kutta solver. Event detection is included in the algorithm to accurately capture the of ice failure. For high velocities a large number of events will occur, thus adaptive time-stepping is included to optimize the time step [Hendrikse et al., 2018; Hendrikse and Nord, 2019].

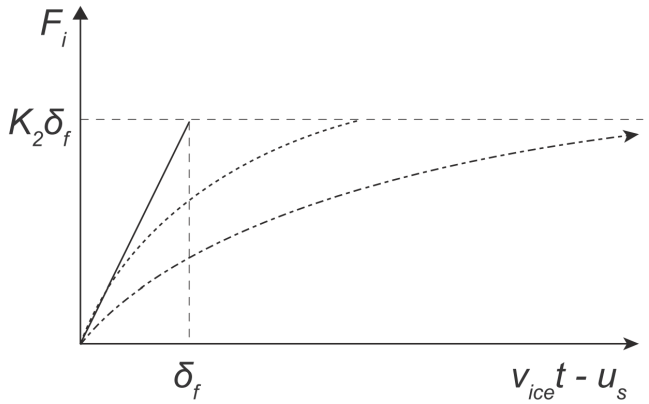

Figure 3.6: Load resulting from a single ice element at different velocities versus the deformation of the element. The solid line corresponds to crushing at high ice speeds, the dashed line to the transition between crushing and creep at intermediate ice speeds and the dash-dotted line to creep at low ice speeds [Hendrikse and Nord, 2019].

As will be discussed in Section 4.2, for the combined MORPHEUS/VANILLA model only the equations of motion for the ice elements are relevant, as the response of the structure is determined by MORPHEUS with a different solver. Hence all relevant equations will be presented in Section 4.2.

Model parameters

Measurements are required to determine the value of the seven input parameters, K_1, K_2, C_1, C_2, N, r_{max} and δ. These measurements should be from the ice action against a rigid structure. This allows for the simulation of flexible structures under similar conditions [Hendrikse and Nord, 2019]. If unavailable these can be scaled using reference measurements [Hendrikse and Metrikine, 2016].

4 ICE-STRUCTURE INTERACTION MODELLING

In this chapter the method for coupling VANILLA with MORPHEUS and the aero-elastic simulation tool HAWC2, is presented. The objective was to create a coupled model which can accurately simulate the response of an OWT subject to ice-, wind- and wave-loading. In order to efficiently combine the models, a thorough understanding of MORPHEUS and HAWC2 is required, specifically with regards to the time integration method applied in the methods, as VANILLA will tie into this. Additionally, the coupling to HAWC2 requires a communication channel between the application and MATLAB, for this purpose the concept of a TCP/IP link will be introduced and applied.

4.1 MORPHEUS

The WT in-house developed software platform MORPHEUS is a framework specifically developed for the holistic design of offshore wind foundations. It includes software for site-conditions assessment, geotechnical assessment, aero-elastic loads generation for integrated load-analysis and software for structural and geotechnical design optimization [Nielsen et al., 2022]. The structure of MORPHEUS is illustrated in Figure 4.1. This research will expand on the load generation module and make use of the design optimization module of MORPHEUS. The MORPHEUS load generation can be performed directly in the software or by using the coupling to the DTU developed code HAWC2. For this research VANILLA will be coupled first to the former, and in the second part to the latter. The core of MORPHEUS is written in MATLAB, which readily facilitates a coupling to VANILLA — also written in MATLAB. This will be the focus of this chapter. In Chapter 6 the optimization module of MORPHEUS is used to assess the effect of the loads by generating optimized foundation designs with and without ice loading. The optimization algorithm for foundation design is presented in Section 5.3.1.

For now, it suffices to state that the OWT is modelled as a finite element model of Timoshenko beam elements and Winkler springs to model the non-linear soil-structure interaction. The Rotor Nacelle Assembly (RNA) is modelled as a lumped mass (or in 3D may also include cou-

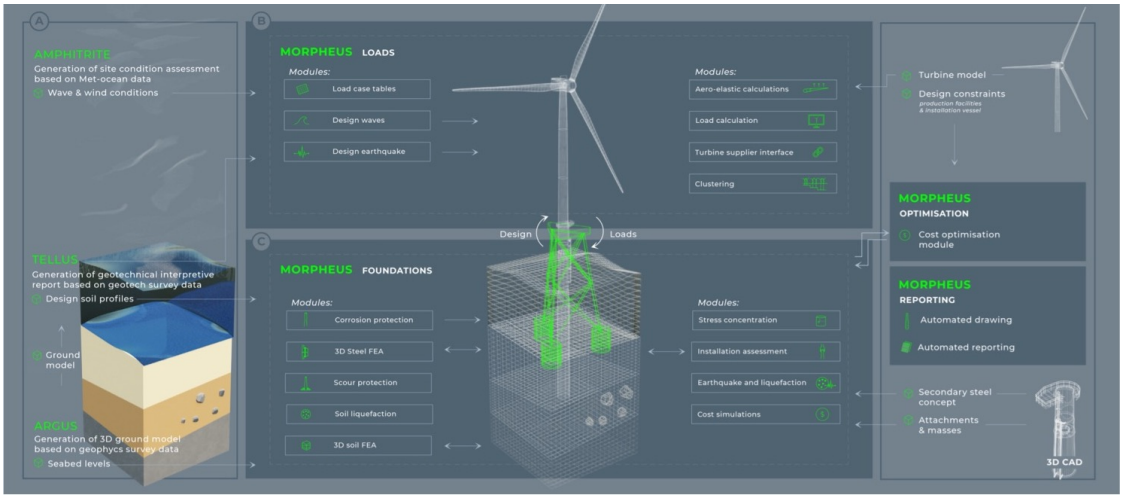

Figure 4.1: Overview of WT's in-house optimization software MORPHEUS [Nielsen et al., 2022].

pling terms, i.e. a fully populated mass matrix) representing the RNA at hub height [Nielsen et al., 2022].

4.2 TIME INTEGRATION ALGORITHM

To accurately simulate the response of an OWT subject to time dependent loads a numerical integration of the equations of motion of the structure is required. For a linear structure the equations of motion can be described with the following system of second order differential equations,

$$\mathbf{M}\ddot{\mathbf{u}} + \mathbf{C}\dot{\mathbf{u}} + \mathbf{K}\mathbf{u} = \mathbf{f}(t) \tag{4.1}$$

where $\mathbf{M}$, $\mathbf{C}$ and $\mathbf{K}$ are the mass, damping and stiffness matrix of the structure, respectively, while $\mathbf{f}(t)$ denotes the (external) load history, in this particular case wind-, wave-, and (soon) ice loading. Solving the equation for the response of the structure, $\mathbf{u}$, further requires $2n$ initial conditions, two for each Degrees of Freedom (DOF), of the form of

$$\mathbf{u}(0) = \mathbf{u}_0 \qquad\qquad \dot{\mathbf{u}}(0) = \dot{\mathbf{u}}_0 \tag{4.2}$$

This section discusses the time integration method applied in MORPHEUS and HAWC2 to determine the response of the OWT, and subsequently discusses the method to include VANILLA generated ice loading into the procedure. An extensive verification is then performed to assess the accuracy of the new methodology.

4.2.1 The generalized α-procedure

The time integration method applied in MORPHEUS is the generalized α-procedure. The procedure is a time integration method based on a discretized structural model. If such a model has n DOF, the displacements are given by $\mathbf{u}(t)^T = [u_1(t), u_2(t), ..., u_n(t)]$, and the time derivatives are indicated by the dot notation such as the velocity, $\dot{\mathbf{u}}$, and the acceleration, $\ddot{\mathbf{u}}$. Linear structures can be fully described at any given time if the load vector, $\mathbf{f}(t)$, and the state vector, $(\mathbf{u}(t), \dot{\mathbf{u}}(t))$, containing the displacements and velocities, at time t, are known [Wood et al., 1980].

The generalized α-procedure computes the state vector $(\mathbf{u}_{n+1}, \dot{\mathbf{u}}_{n+1})$ at time t_{n+1} using the previous state vector, $(\mathbf{u}_n, \dot{\mathbf{u}}_n)$ at time t_n, and the load vectors at time t_n and t_{n+1}, respectively $\mathbf{f}_n$ and $\mathbf{f}_{n+1}$. The procedure consists of two steps. In the first step the increment of the displacement and velocity are expressed as integrals of the acceleration over the time-step interval. In the second step the acceleration is determined with the equations of motion. The generalized α-procedure imposes the equation at motion at both t_{n+1} and t_n by applying weighted mean values as given by [Chung and Hulbert, 1993],

$$\begin{aligned} &\alpha_m \mathbf{M}\,\ddot{\mathbf{u}}_n + (1-\alpha_m)\,\mathbf{M}\,\ddot{\mathbf{u}}_{n+1} + \alpha_f\,(\mathbf{C}\,\dot{\mathbf{u}}_n + \mathbf{K}\,\mathbf{u}_n) \\ &\qquad + (1-\alpha_f)\,(\mathbf{C}\,\dot{\mathbf{u}}_{n+1} + \mathbf{K}\,\mathbf{u}_{n+1}) \qquad\qquad = \alpha_f\,\mathbf{f}_n + (1-\alpha_f)\,\mathbf{f}_{n+1} \end{aligned} \tag{4.3}$$

where the relative weight of the old inertia term and old forcing terms are specified by the parameters α_m and α_f, respectively.

The results of the first step of the algorithm, the integrals of the acceleration over the time step, are,

$$\dot{\mathbf{u}}_{n+1} = \dot{\mathbf{u}}_n + (1-\gamma)\, h\, \ddot{\mathbf{u}}_n + \gamma\, h\, \ddot{\mathbf{u}}_{n+1} \tag{4.4}$$
$$\mathbf{u}_{n+1} = \mathbf{u}_n + h\, \dot{\mathbf{u}}_n + (1-\beta)\, h^2\, \ddot{\mathbf{u}}_n + \beta\, h^2\, \ddot{\mathbf{u}}_{n+1} \tag{4.5}$$

where h is the time step interval $t_{n+1} - t_n$, and $0 < \gamma < 1$ and $0 < \beta < \frac{1}{2}$ are parameters that determine the degree of forward or backward weighting that is applied, e.g. $\gamma = \beta = 0$ corresponds to full backward weighting and $\gamma = 1, \beta = \frac{1}{2}$ is full forward weighting. It can be shown that numerical stability is reached if $\gamma = \frac{1}{2} + \alpha_f - \alpha_m$ and $\beta = \frac{1}{4}(\gamma + \frac{1}{2})^2$ [Krenk, 2009].

Due to the introduced α-weights Equation 4.4 and Equation 4.5 can be simplified by use of,

$$\Delta\ddot{\mathbf{u}} = \ddot{\mathbf{u}}_{n+1} - \ddot{\mathbf{u}}_n \tag{4.6}$$

which allows for the equations to be rewritten into a prediction *without* acceleration increment, and a correction contribution *with* the acceleration increment [Krenk, 2009],

$$\dot{\mathbf{u}}_{n+1} = \dot{\mathbf{u}}_n + \Delta\dot{\mathbf{u}}_* + \gamma\, h\, \Delta\ddot{\mathbf{u}} \tag{4.7}$$
$$\mathbf{u}_{n+1} = \mathbf{u}_n + \Delta\mathbf{u}_* + \beta\, h^2\, \Delta\ddot{\mathbf{u}} \tag{4.8}$$

where the predictors based on accelerations at t_n are given by $\Delta\dot{\mathbf{u}}_* = h\ddot{\mathbf{u}}$ and $\Delta\mathbf{u}_* = h\dot{\mathbf{u}}_n + \frac{1}{2}h^2\, \ddot{\mathbf{u}}_n$. Finally, the weighted equation of motion can be written in the following form:

$$\mathbf{M}_*\, \Delta\ddot{\mathbf{u}} = \mathbf{f}_n - (\mathbf{M}\, \ddot{\mathbf{u}}_n + \mathbf{C}\, \dot{\mathbf{u}}_n + \mathbf{K}\, \mathbf{u}_n) + (1-\alpha_f)\, (\Delta\mathbf{f} - \mathbf{C}\, \Delta\dot{\mathbf{u}}_* - \mathbf{C}\, \Delta\mathbf{u}_*) \tag{4.9}$$

Where $\mathbf{M}_*$ is the modified mass matrix and $\Delta\mathbf{f}$ is the force increment as given by,

$$\mathbf{M}_* = (1-\alpha_m)\, \mathbf{M} + (1-\alpha_f)\, (\gamma\, h\, \mathbf{C} + \beta\, h^2\, \mathbf{K}) \tag{4.10}$$
$$\Delta\mathbf{f} = \Delta\mathbf{f}_{n+1} - \mathbf{f}_n \tag{4.11}$$

Algorithm B.2 provides a numerical implementation of the full procedure.

4.2.2 MORPHEUS/VANILLA coupling

To simplify the integration of VANILLA into the MORPHEUS framework, it can be included in the generalized α-procedure for the evaluation of the structural response. This can be achieved by adding a step after the 'prediction' step, or step 4) in Algorithm B.2, in which the force increment is updated to include the VANILLA generated ice load. This is achieved by including an ice load vector, $\mathbf{f}_{\text{ice}}$, before continuing the algorithm. The ice load vector only contains a non-zero value at ice action point.

The non-zero value is the VANILLA generated ice load at Mean Sea Level (MSL), which can be found by solving the equations of motions for each individual ice elements, i, given by,

$$\begin{aligned} u_{i,1} &= \begin{cases} u_{i,2} & u_{i,1} < u_s \\ u_s & u_{i,1} \geq u_s \end{cases} \\ \dot{u}_{i,2} &= \frac{K_2}{C_1}\,(u_{i,1} - u_{i,2}) + \frac{K_1}{C_1}\,(u_{i,3} - u_{i,2}) + v_{\text{ice}} - \frac{1}{C_2}\,(K_2(u_{i,2} - u_{i,1}))^3 \\ \dot{u}_{i,3} &= v_{\text{ice}} - \frac{1}{C_2}\,(K_2(u_{i,2} - u_{i,1}))^3 \end{aligned} \tag{4.12}$$

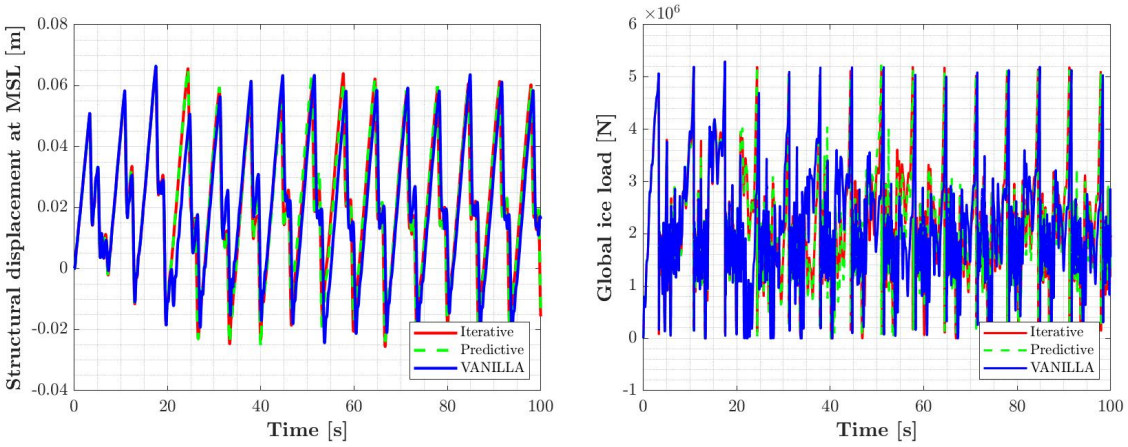

Figure 4.2: Time history of (a) the structural response at MSL and (b) the global ice load based on three methods: stand-alone VANILLA, the MORPHEUS/VANILLA model with iterations (iterative) and without iterations (predictive).

where $u_{i,1}$, $u_{i,2}$ $u_{i,3}$ are the positions of the front, centre and rear of the individual ice element as illustrated in Figure 3.5, K_1, K_2, C_1, K_2 are the model parameters of the (non-) linear springs and dashpots and u_s is the structural displacement at MSL, in this case given by the predictor of the displacement, $u_{n;\text{MSL}} + \Delta u_{*;\text{MSL}}$. The resulting global ice load on the structure is then given by,

$$F_{\text{ice}}(u_s, t) = \sum_{i=1}^{N} F_i = \sum_{i=1}^{N} K_2(u_{i,2} - u_{i,1})H(u_{i,1} - u_s) \tag{4.13}$$

where F_i is the load contribution of a single ice element to the global load, and H is the Heaviside step function which indicates if the ice element and the structure are in contact. The system of equations are solved with a 4^{th} order Runge-Kutta solver as the velocity and acceleration of the structure at MSL are already known, $\dot{u}_s = \dot{u}_{n;\text{MSL}} + \Delta\dot{u}_{*;\text{MSL}}$ and $\ddot{u}_s = \ddot{u}_{n;\text{MSL}}$ respectively. Note, these are the *predicted* values, as they correction is applied after imposing the equation of motion which requires the forcing term (and thus the ice force).

Event detection is included in the algorithm to detect the occurrence of ice failure. For high velocities a large number of events will occur, thus adaptive time-stepping is included to optimize the time step [Hendrikse et al., 2018; Hendrikse and Nord, 2019]. After addition of the ice load vector to $\mathbf{f}_{n+1}$, the generalized α-procedure proceeds as it normally would. The updated procedure is given by Algorithm 4.1.

Step 5-7 of Algorithm 4.1 can be iterated for increased accuracy. Consecutive iterations use the updated state vector from step 7 for the generation of the ice load, which is more accurate as the ice load would otherwise technically 'run behind'. Step 6 and 7 are then executed with the updated VANILLA load. This process is repeated until a predefined tolerance is met.

However, time series such as Figure 4.2 show that although the models accurately predict the vibration regime — MMI in this case — both the iterative and non-iterative model do not fully coincide with VANILLA. The reason for this is twofold. Firstly, VANILLA uses event detection to capture ice failure, in which an element is removed and replaced. The event detection can miss events in the first time step, which is why the time step is split up within VANILLA. However, when the MORPHEUS/VANILLA coupling generates the ice load this can happen more frequently. Secondly, once a single event is missed the entire response is different due to the stochastic nature of the ice crushing, which can clearly be seen in Figure 4.2.

Algorithm 4.1: The generalized α-procedure including VANILLA

1) System matrices:

$$\mathbf{K}, \mathbf{C}, \mathbf{M}$$
$$\mathbf{M}_* = (1-\alpha_m)\,\mathrm{M} + (1-\alpha_f)\,(\gamma\, h\, \mathbf{C} + \beta\, h^2\, \mathbf{K})$$

2) Initial conditions:

$$\mathbf{u}_0, \dot{\mathbf{u}}_0$$
$$\ddot{\mathbf{u}}_0 = \mathbf{M}^{-1}\,(\mathbf{f}_0 - \mathbf{C}\,\dot{\mathbf{u}}_0 - \mathbf{K}\,\mathbf{u}_0)$$

3) Increment time:

$$t_{n+1} = t_{n+1} + h$$

4) Increment predictors:

$$\Delta\dot{\mathbf{u}}_* = h\,\ddot{\mathbf{u}}_n$$
$$\Delta\mathbf{u}_* = h\,\dot{\mathbf{u}}_n + \tfrac{1}{2}h^2\,\ddot{\mathbf{u}}_n$$

5) Generate ice load and update load vector:

$$\Rightarrow \text{VANILLA: } \mathbf{f}_{\text{ice}}(u_{n;\text{MSL}} + \Delta u_{*;\text{MSL}}, \dot{u}_{n;\text{MSL}} + \Delta\dot{u}_{*;\text{MSL}}, \ddot{u}_{n;\text{MSL}})$$
$$\Delta\mathbf{f} = \mathbf{f}_{n+1} + \mathbf{f}_{\text{ice}} - \mathbf{f}_n$$

6) Acceleration increment:

$$\Delta\ddot{\mathbf{u}} = \mathbf{M}_*^{-1}\,(\mathbf{f}_n - (\mathbf{M}\,\ddot{\mathbf{u}}_n + \mathbf{C}\,\dot{\mathbf{u}}_n + \mathbf{K}\,\mathbf{u}_n) + (1-\alpha_f)\,(\Delta\mathbf{f} - \mathbf{C}\,\Delta\dot{\mathbf{u}}_* - \mathbf{C}\,\Delta\mathbf{u}_*))$$

7) State vector update:

$$\ddot{\mathbf{u}}_{n+1} = \ddot{\mathbf{u}}_n + \Delta\ddot{\mathbf{u}}$$
$$\dot{\mathbf{u}}_{n+1} = \dot{\mathbf{u}}_n + \Delta\dot{\mathbf{u}}_* + \gamma\, h\,\Delta\ddot{\mathbf{u}}$$
$$\mathbf{u}_{n+1} = \mathbf{u}_n + \Delta\mathbf{u} + \beta\, h^2\,\Delta\ddot{\mathbf{u}}$$

8) Return to step 3) or stop if $t_{n+1} = t_{\text{end}}$

Thus including the iteration does not lead to increased accuracy, while it does require more computational time. Thus — if verified — the results in both cases are representative and the coupled models would allow for a more detailed structural model — including other load components — to be considered. This would otherwise have been a larger source of discrepancy, i.e. if ice loads were simulated based on a few selected modes only and without simultaneous wind loads and associated aero-elastic damping.

Table 4.1: Ice thickness and ice speed considered in simulations for the different structures. Ice speed provided in MATLAB notation for brevity.

Structure	Ice thickness [m]	Ice drift speed [mm s^{-1}]	Number of seeds [-]
Rigid	0.4, 1.2	[0.1:0.3:0.7][1:3:7] [10:10:190][200:100:500]	6
Compliant	0.4, 1.2	[0.1:0.3:0.7][1:3:7] [10:10:190][200:100:500]	6

Table 4.2: Simulation time per ice drift speed.

Ice drift speed	0.1 mm s^{-1}	0.2–2 mm s^{-1}	3–500 mm s^{-1}
Simulation time	2600 s	1800 s	900 s

4.2.3 Verification

The verification of the MORPHEUS/VANILLA model is performed in two parts. First, the model is verified for a rigid structure. Results for the global ice load are compared between the MORPHEUS/VANILLA model and stand-alone VANILLA. Subsequently, the global ice load and the structural response of a compliant structure is investigated to assess dynamic ice-structure interaction. It should be noted that during all verification simulations no non-linearity is considered in the system, e.g. no wind loads transferred, no soil or fluid coupling. Table 4.1 provides an overview of the simulations used for verification.

For the simulations a range of ice speeds is considered as well as two ice thicknesses. Additionally, six simulations are performed per combination with different 'seeds', which are realizations of the 'same' ice-structure interaction under identical conditions. In total 696 simulations were run: 2 structures x 2 ice thicknesses x 29 ice drift speeds x 6 seeds.

Depending on the drift velocity the simulations ran for different durations as ice failure may take a substantially longer time to occur for low ice velocities in comparison to high velocities. Each simulation runs for at least 600 seconds, but extra time is included to allow for initial conditions and the effect of low ice speeds. For the slowest ice speeds, in which only creep occurs, even more time is simulated to ensure a steady-state has been reached. In these cases, the required simulation time has been determined by trial and error. Table 4.2 shows the duration of the simulations per ice drift speed.

Table 4.3 gives the criteria which were used in the verification process for MORPHEUS/-VANILLA. Due to the stochastic nature of ice failure, the verification is done based on statistical measures such as the mean value, the maximum value and the standard deviation. The statistical measures from Table 4.3 are averaged over the six 'seeds'. The limits for acceptance were determined based on internal discussion on acceptable deviations. Finally, a visual check is performed to determine if the interaction regimes ICR, FLI and CBR occur at similar ice drift velocities. Note, as discussed in section Section 3.2 the traditional interaction regimes do not fully describe the observed interaction for OWTs. Nonetheless, during the verification the terminology is still applied. Thus the vibration regimes MMI and MMII are considered as ICR and FLI, respectively.

Table 4.3: Verification steps and criteria. Note, MV denotes the associated variable according to MORPHEUS/VANILLA and V denotes the associated variable according to stand-alone VANILLA. The limits for acceptance were determined based on internal discussion on acceptable deviations.

Verification step	Type of result		Rejection criteria
Static interaction	1)	Temporal mean global ice load	$\Delta = \frac{\lvert MV-V\rvert}{V} > 2.0\%$
	2)	Temporal root-mean-squared global ice load	$\Delta = \frac{\lvert MV-V\rvert}{V} > 5.0\%$
	3)	Temporal maximum global ice load	$\Delta = \frac{\lvert MV-V\rvert}{V} > 5.0\%$
	4)	Mean-squared spectral density peak location of global ice load	$\Delta = \frac{\lvert MV-V\rvert}{V} > 5.0\%$
Dynamic interaction	Similar to 'Static interaction', but including the following at ice action point:		
	5)	Temporal mean structural displacement	$\Delta = \frac{\lvert MV-V\rvert}{V} > 2.0\%$
	6)	Temporal root-mean-squared structural displacement	$\Delta = \frac{\lvert MV-V\rvert}{V} > 5.0\%$
	7)	Temporal maximum structural displacement	$\Delta = \frac{\lvert MV-V\rvert}{V} > 5.0\%$
	8)	Temporal maximum structural velocity	$\Delta = \frac{\lvert MV-V\rvert}{V} > 5.0\%$
	9)	ICR at **X** ice drift speed	
	10)	FLI at **X** ice drift speed	
	11)	CBR at **X** ice drift speed	

Results: rigid structure

The results of the verification of MORPHEUS/VANILLA for a rigid structure are presented in Table 4.4. The results indicated — based on the criteria from Table 4.3 — stand-alone VANILLA and MORPHEUS/VANILLA are in good agreement. For criteria 4 maxima location of the spectral density peaks are compared, because of this a single seed can heavily influence the results, which occurred during rejection of criteria 4 at ice drift speed of $0.2\,\mathrm{m\,s^{-1}}$.

Results: compliant structure

The results of the verification of the MORPHEUS/VANILLA model for a compliant structure are presented in Table 4.4.

Two key observations from Table 4.5 are 1) errors occur in the transition between interaction regimes and 2) the error in the maximum structural velocity increases with the ice drift velocity.

The first observation is unexpected as it only indicates that the models transition at slightly different regions. Visual inspection of the time series confirms this and also indicates that this discrepancy is well within reason. It should be noted that this effect increased when a thicker ice sheet was considered as can be seen in Table A.3. In this case the transition regions were more widespread over multiple velocities, with some velocities showing different regimes, which lead to larger errors in the verification. This becomes apparent when the range of 0.12–$0.16\,\mathrm{m\,s^{-1}}$ is examined. Both models predicted FLI *and* CBR for each velocity, but depending on the model a different number of seeds predicts one or the other, which leads to exceedance of the criteria.

Table 4.4: Quantitative verification for each ice drift speed in mm s^{-1} against criteria 1–4 from Table 4.3 for a rigid structure with an ice thickness of 0.4 m thickness. Red indicates rejection of the value, given in percent point, and green indicates acceptance.

v_{ice}	1	2	3	4
0.1	0			
0.4	0			
0.7	0			
1	0			
4	0	0	0	0
7	0	0	0	0
10	0	0	1	0
20	0	0	3	0
30	0	0	2	4
40	0	0	2	3
50	0	0	0	2
60	0	0	0	0
70	0	0	0	3
80	0	0	0	0
90	0	0	1	0
100	0	0	0	0
110	0	0	0	0
120	0	0	0	0
130	0	0	0	1
140	0	0	0	0
150	0	0	0	0
160	0	0	0	0
170	0	0	0	1
180	0	0	0	0
190	0	0	0	0
200	0	0	0	10
300	0	0	1	3
400	0	0	0	0
500	0	0	0	1

This is to be expected in the transitions between regimes as they are nonlinear phenomena which are influenced by the stochastic nature of the ice failure and initial conditions or arbitrary conditions. The simulations are sensitive to different initial conditions and perturbations.

The second observation indicates that too much energy is maintained in the system. As this is well within the regime of CBR the force is fortunately not affected, and neither is the mean structural displacement. The most likely reason behind this increased energy is the size of time step. As the velocity of ice increases, more ice failure occurs over each time step. Due to the nature of the interaction between MORPHEUS and VANILLA, it may miss an ice failure since the event detection in VANILLA is less robust when the solver is used over only one time step. If such an event is missed, it is immediately corrected within the same time step, which is why no divergence is observed for the force. This is confirmed by Table 4.6, which shows a drastic decrease in the maximum velocity error when a reduced time step of 0.001 s is used.

A small error still exists, however Figure 4.3 indicate that the model is able to accurately capture the ice-structure interaction. For the ice drift velocities leading to ICR and FLI — where the highest loads are observed — the loads and displacements are accurately predicted. For the highest ice drift velocities leading to CBR the maximum velocity is still exceeded, however 1) this is conservative and 2) for design these velocities will play a marginal role as the velocities and displacements are negligible compared to those due to FLI. Nonetheless, the impact of this overestimation will be investigated during the results.

Table 4.5: Quantitative verification for each ice drift speed in mm s^{-1} against criteria 1-8 from Table 4.3 for a flexible structure with an ice thickness of 0.4 m thickness. Red indicates rejection of the value, given in percent point, and green indicates acceptance. Criteria 9-11 are verified in the second and third column, which present the predicted interaction regime from the stand-alone simulations (V) or from the MORPHEUS/VANILLA simulations (MV). CRP indicates creep, I - intermittent crushing, F - frequency lock-in and C - continuous brittle crushing.

v_{ice}	V	MV	1	2	3	4	5	6	7	8
0.1	CRP	CRP	0				0			
0.4	CRP	CRP	0				0			
0.7	CRP	CRP	0				0			
1	CRP	CRP	0				0			
4	I	I	2	1	0	0	2	1	1	2
7	I	I	1	0	0	0	1	0	0	1
10	I	I	1	1	0	0	2	1	1	2
20	I	I	1	0	0	1	1	0	0	3
30	I/F	I	1	1	1	50	1	0	4	6
40	F	F	2	3	1	0	2	4	5	0
50	F	F	1	1	1	0	1	1	1	2
60	F	F	0	0	2	67	1	1	1	2
70	F	F	0	0	0	22	0	0	1	2
80	F/C	F	2	2	5	44	2	6	12	16
90	C	C	0	0	0	6	0	0	2	12
10	C	C	0	0	1	0	0	0	2	19
110	C	C	0	0	1	2	0	0	1	11
120	C	C	0	0	0	0	0	0	2	19
130	C	C	0	0	0	10	0	0	4	22
140	C	C	0	0	0	7	0	0	4	23
150	C	C	0	0	0	3	0	0	3	22
160	C	C	0	0	0	0	0	0	2	15
170	C	C	0	0	3	0	0	0	5	23
180	C	C	0	0	1	3	0	0	3	26
190	C	C	0	0	1	3	0	0	3	31
200	C	C	0	0	0	4	0	1	4	48
300	C	C	0	0	0	0	0	0	7	85
400	C	C	0	0	1	2	0	0	8	125
500	C	C	0	0	0	6	0	0	14	23

Table 4.6: Quantitative verification for ice drift speed in mm s^{-1} against criteria 1-8 from Table 4.3 for a flexible structure with an ice thickness of 0.4 m thickness and a reduced time step of 0.001 s. Red indicates rejection of the value, given in percent point, and green indicates acceptance. Criteria 9-11 are verified in rows 2 and 3, which present the predicted interaction regime from the stand-alone simulations (V) or from the MORPHEUS/VANILLA simulations (MV). CRP indicates creep, I - intermittent crushing, F - frequency lock-in and C - continuous brittle crushing.

v_{ice}	V	MV	1	2	3	4	5	6	7	8
10	C	C	0	0	2	0	0	0	1	3
120	C	C	0	0	3	0	0	0	3	3
140	C	C	0	0	3	0	0	0	2	7
160	C	C	0	0	4	0	0	0	0	4
180	C	C	0	0	3	0	0	0	28	8
200	C	C	0	0	5	0	0	0	5	6
300	C	C	0	0	4	0	0	0	3	19
400	C	C	0	0	5	0	0	0	12	23
500	C	C	0	0	9	0	0	0	14	15

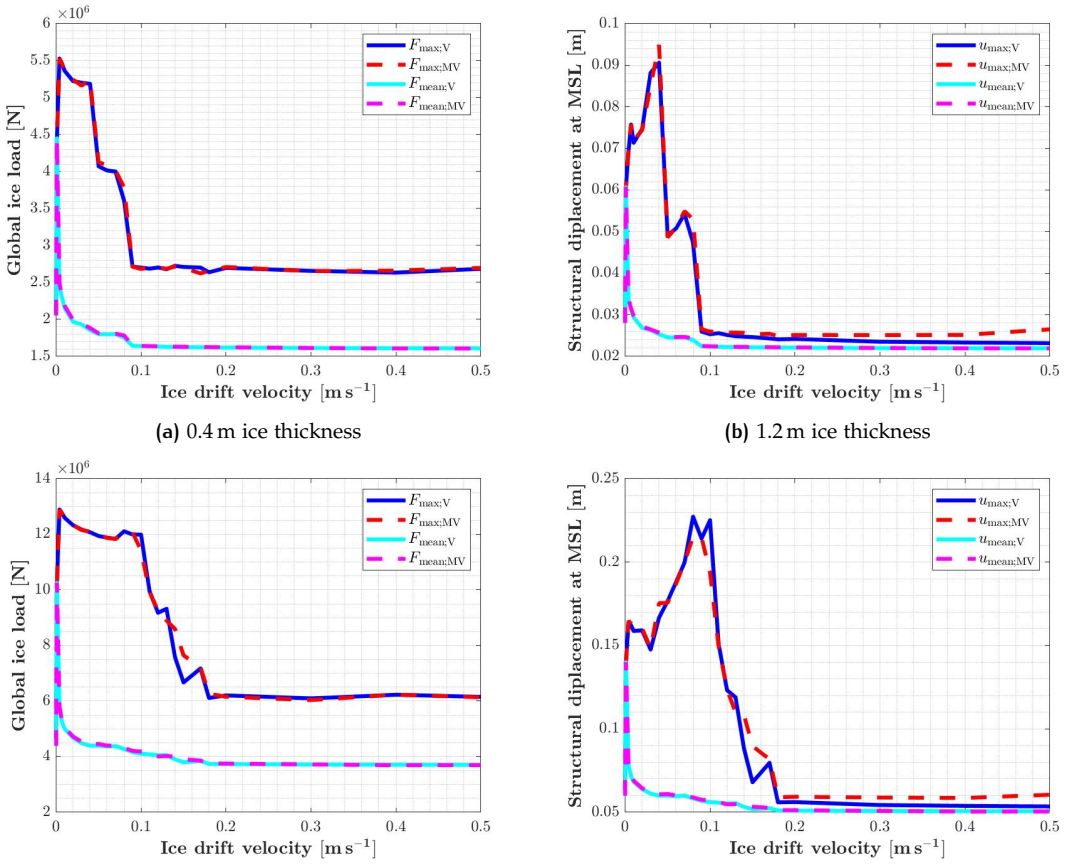

(a) 0.4 m ice thickness

(b) 1.2 m ice thickness

(c) 0.4 m ice thickness

(d) 1.2 m ice thickness

Figure 4.3: Global ice load and structural displacement as a function of the ice drift velocity for 0.4 and 1.2 m ice thickness and time step of 0.01 s.

4.3 HAWC2/VANILLA

After a successful implementation of VANILLA into MORPHEUS, VANILLA is coupled into the aero-elastic tool HAWC2 to simulate both aero-elastic effects and ice loading in a coupled fashion. The proposed coupling method is similar as previously presented, but now a TCP/IP link is required to establish communication between the two applications. This section will first provide a brief introduction to HAWC2, after which the coupling of VANILLA to HAWC2 is discussed by elaborating on the concept of a TCP/IP link.

4.3.1 HAWC2

HAWC2, or Horizontal Axis Wind turbine simulation Code 2^{nd} generation, is an aero-elastic simulation tool developed by the Aero-elastic Design Research Program at DTU Wind Energy. HAWC2 simulates response of the wind turbine in the time domain. It models the structural components based on multi-body dynamics, where the total structure consists of multiple bodies, such as the substructure and tower, which are each connected through a set of constraints. The bodies consist of Timoshenko beam elements with six degrees of freedom for each node. HAWC2 then solves the equations using the the Newmark method, which is a specific form of the generalized-α procedure, when $\alpha_m = \alpha_f = 0$. Typically, the substructure, tower and shaft consist of one body, whereas the blades are made up of several bodies. This allows non-linear effects to be captured. The loading is based on the deformed shape of the structure [Larsen et al., 2005; Larsen and Hansen, 2007].

HAWC2 uses Blade Element Momentum (BEM) theory for the aerodynamic interaction between wind and structure, which requires curves of C_l, C_d, C_m and α as input. Addition-

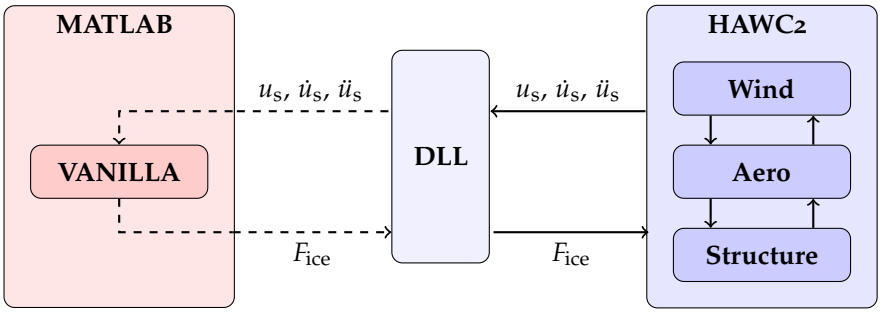

Figure 4.4: Visualization of TCP/IP communication between HAWC2 and VANILLA via a HAWC2 DLL.

ally, a Dynamic Link Library (DLL) can be added to HAWC2 to include other interactions, e.g. controller, soil loads and hydrodynamic loads. The last two are treated as external loads by HAWC2 [Larsen et al., 2005; Larsen and Hansen, 2007].

4.3.2 TCP/IP link

For the coupling of HAWC2 and VANILLA a TCP/IP link was applied. The main benefits of this coupling was that the two applications — written in FORTRAN and MATLAB — could run stand-alone, which prevents having to rewrite the VANILLA or HAWC2 code as much as possible. After setting up communication between the applications via a TCP/IP link, the applications interact similarly as MORPHEUS and VANILLA.

TCP/IP or Transmission Control Protocol/Internet Protocol is a specific mechanism of which the origin outdates the Internet, and was developed for the transfer of data between separate applications and — if required — over multiple networks. The advantage of TCP/IP communication is it's simplicity and ease of configuring. One applications is considered the server, which sets up hosts a server to which the other application, the client, connects. Once the applications are connected both can send and receive information. This means that the two applications can run separately, while exchanging data via the channel. It is non-transactional and non-persistent, i.e. there is no exchange when data is sent/received and the data is not stored anywhere [Barahona et al., 2009].

In previous research HAWC2 was successfully coupled to MATLAB via a TCP/IP link [Garzon et al., 2010], in this case for the integration of the controller. In the particular case of VANILLA the non-transactionality and non-persistence are not an issue, as neither are required for the simulation. The date is only required within the time step (non-persistence) and there is need for proof of transmission (non-transactional), which makes the TCP/IP link a viable mechanism for the coupling of the two applications.

The TCP/IP communication is set-up via a DLL called by HAWC2. This DLL starts the TCP server, to which MATLAB connects. The DLL then exchanges the required data each time step. As a result HAWC2 runs the simulations independently, but continuously sends and receives data via the TCP/IP socket [Garzon et al., 2010].

The coupling is then similar to that as described in Section 4.2. The structural displacement, velocity and acceleration according to HAWC2 are sent — via the TCP/IP link — to MATLAB, which generates a global ice load. This is then imposed as external load on the structure. The coupling is visualized in Figure 4.4.

A downside of the coupled HAWC2/VANILLA model is the long computational time required for simulations. To accurately capture ice-structure interaction small time steps are required, i.e. 0.01 s or smaller, which makes HAWC2 very slow. A potential solution could be the use of a reduced structural model, or superelement, which splits the structure into boundary and interface nodes. The use of a superelement is already possible for the MORPHEUS/VANILLA model, but for a superelement coupling of HAWC2 and VANILLA more development is necessary.

5 BALTIC SEA MONOPILE DESIGN - METHODOLOGY

This chapter outlines the methodology of Part III in which the limit of applicability for monopiles is investigated, by defining a feasibility map in the Baltic Sea. For each region one cycle of the design procedure is performed both for a 'non-ice' — the 'reference' case — and for an 'ice' case. For one such design cycle all necessary steps are described. This includes the identification of the 'usual suspects', the Design Load Case (DLC)s usually governing for design. By cutting down the DLCs to this essential set, the required simulation time of the design cycle is greatly reduced, while confidence in the result is maintained.

For the ice case, the five load cases, as prescribed by DNV GL [2016], are discussed. For both the reference and the ice case the relevant metocean conditions have been provided in Chapter 2. Based on the loads from the metocean conditions and an initial geometry, new design loads can be determined, which in turn can be used in MORPHEUS to generate an optimized monopile design based on design & fabrication criteria. Finally, the designed foundations are compared to define a feasibility map.

The methodology of the research — and more specifically Part III of the research — as presented in this section is visualized in Figure 5.1.

5.1 SIMULATION SET-UP

Before any simulations can be performed initial loads are required in order to determine an initial monopile geometry. For this purpose the load-scaling tool of MORPHEUS is used, which determines loads based on the turbine properties, relevant metocean conditions and reference projects. The selected turbine is the IEA 15 MW reference turbine designed by DTU Wind Energy. The corresponding tower provided by DTU, however, is scaled from a diameter of 10 to 8 m, which is the industry standard for turbines of this size. The moment of inertia was kept constant by scaling the thickness. After the scaled loads are found, a full monopile design is generated by MORPHEUS. The method for MORPHEUS monopile design is evaluated in Section 5.3.1. Besides the initial geometry, both the water depth and the ridge action are required for each region.

5.1.1 Water depth

This procedure is performed for three design cases: a shallow, intermediate and deep position, which correspond to respectively 25, 35 and 45 m water depth. Rather than designing for an individual depth for each region, three clusters were chosen, as this is often done in the industry. The nine identified regions are grouped in the three clusters based on the average water depth values found in Chapter 2. The deepest cluster is set at 45 m depth rather than the previously discussed value of 65 m. This choice was made in order for the research to remain realistic, as designing for a monopile under ice loading would be most unlikely in 65 m deep water. Hence the chosen depth for each region is based on what can be reasonably assumed to be the deepest design cluster for an actual project in that region. Only the deepest position per region is considered as the effect of ice loading is assumed to be most detrimental at these positions due to the larger moment-arm of the ice at the seafloor. The division of the regions over the chosen cluster is given in Table 5.1.

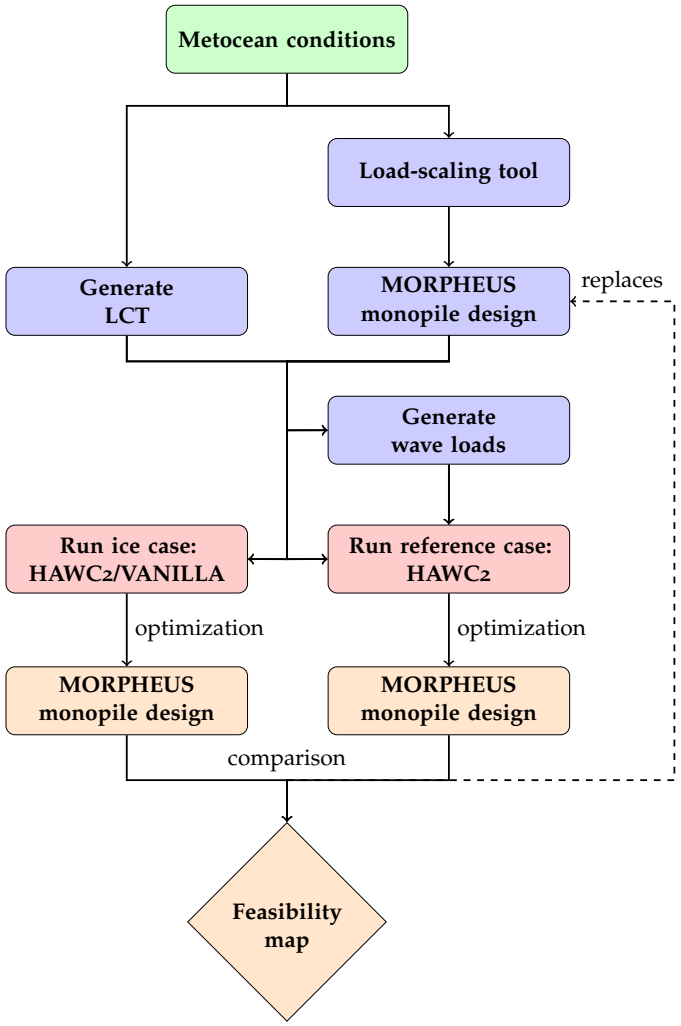

Figure 5.1: Research methodology for the development of a monopile feasibility map in the Baltic Sea. Green indicates data collection as performed in Part I of the project, blue indicates pre-processing of loads, red is generating loads by running simulations, and orange is post-processing of the loads, which involves updating design and generating the feasibility map. Note that the the dashed line depicts the iterative process which is the applied approach during detailed design if the optimized design violates design constraints, e.g. diameter, frequency, stiffness.

Table 5.1: Division of identified Baltic Sea regions over the water depth clusters.

SHALLOW 25 m	INTERMEDIATE 35 m	DEEP 45 m
Danish Straits	Gulf of Finland	Baltic Proper S.
Gulf of Riga	Bothnian Sea S.	Baltic Proper N.
Archipelago Sea	Bay of Bothnia	Bothnian Sea N.

5.1.2 Ridge action

By using the ridge parameters from Table 2.1, Equation 3.1 and Equation 2.3 the ridge actions could be determined. The results are presented in Table 5.2.

Table 5.2: Ice ridge actions according to design standards and field research.

Region	Ridge action [MN]	ISO ridge action [MN]
Danish Straits	5.09	6.95
Baltic Proper South	5.48	7.47
Baltic Proper North	6.30	8.16
Gulf of Riga	7.56	9.05
Gulf of Finland	12.09	14.06
Archipelago Sea	9.10	11.42
Bothnian Sea South	9.13	10.81
Bothnian Sea North	11.75	13.38
Bay of Bothnia	16.20	17.90

5.2 SIMULATIONS

After all simulation input is defined, the relevant simulations are then run in the coupled HAWC2/VANILLA model. For this purpose a Load Case Table (LCT) is defined in which all relevant DLCs with corresponding metocean conditions are listed. This section presents the DLCs which were deemed essential for the design procedure.

For the wind and wave simulations, the generation of wave loads is required. The in-house wave-generation module of WT was used for this purpose. Based on wave and current data of each identified region, the relevant wave loads are generated, which are applied as external load at individual nodes at each time step in HAWC2. In accordance with DNV GL [2016] no wave loads are considered for DLCs relating to ice. Once the wave loads are generated, all simulations can be executed. Around 550-600 simulations were performed for each region for the reference case, and around 200-300 simulations were done for the ice case.

5.2.1 Design load cases: "the usual suspects"

This section identifies and discusses the DLCs that commonly govern monopile design, aptly named "the usual suspects". The naming convention of DNV GL [2016] for DLCs is applied. There are three turbine conditions characterizing the DLCs: power production, parked condition and parked plus fault condition. During power production the turbine functions as specified by the manufacturer, but errors to the ideal operating conditions, e.g. control system delays and yaw misalignment, should be included. The relevant DLCs included in the research are DLC1.2, 1.4 and 1.6. When the turbine is in parked conditions the rotor is idling or at standstill. Yaw misalignment is still considered. The relevant DLCs included in the research are DLC6.1 and 6.4. The parked plus fault conditions refers to a situation in which the turbine is idling or at standstill as a result of a fault. Note that this differs from the parked conditions as it can occur both outside and inside the range of operating wind speeds. The relevant DLC included in the research is DLC7.2. Below a brief description per DLC is provided.

- DLC1.2: Fatigue damage of the structure is considered as a result of NSS over its lifetime. Misalignment of wind and waves as well as multi-directionality of metocean conditions is included. Relevant wind-wave tables have been derived in Part I. A wind discretization of $2\,\mathrm{m\,s^{-1}}$ and a direction discretization of 60° is applied.
- DLC1.4: The ULS of the structure is considered when the turbine is subject to sudden change of wind direction during NSS. Three wind speeds are considered: V_{rated}, V_{rated} + and V_{rated} - $2\,\mathrm{m\,s^{-1}}$. Twelve seeds per wind speed are used.
- DLC1.6: The ULS of the structure is considered when turbine is operating in Severe Sea State (SSS). Wind and wave misalignment is not included, nor is multi-directionality. Extreme waves and wind speeds corresponding to this DLC have been derived in Part I. A wind discretization of $2\,\mathrm{m\,s^{-1}}$ and a direction discretization of 60° is applied. Three seeds per wind speed are used.

- DLC6.1: The ULS of the structure is considered when the turbine is idling or at standstill in ESS50. Wind and wave misalignment is not included, nor is multi-directionality. Extreme waves and wind speeds corresponding to this DLC have been derived in Part I. Twelve seeds are used.

- DLC6.4: Fatigue damage of the structure is considered as result of loads during idling or standstill over its lifetime. Misalignment of wind and waves as well as multi-directionality of metocean conditions is included. Relevant wind-wave tables have been derived in Part I of the research. A wind discretization of $2\,\mathrm{m\,s^{-1}}$ and a direction discretization of 60° is applied.

- DLC7.2: Fatigue damage of the structure is considered as result of loads during idling or standstill — occurring due to fault — over its lifetime. Misalignment of wind and waves as well as multi-directionality of metocean conditions is included. Relevant wind-wave tables have been derived in Part I of the research. A wind discretization of $2\,\mathrm{m\,s^{-1}}$ and a direction discretization of 60° is applied. The expected time in non-power production due to faults has been set to 8%.

These six DLCs were selected as the governing DLCs based on WT's project experience.

5.2.2 Design load cases: ice

This section discusses the DLCs that are required in case of ice presence at a design location. Similar to wind and wave DLCs they cover power production, parked condition and parked plus fault condition, albeit the latter does not have an explicit case as before. During the consideration of ice DLCs wave loads, wind-wave misalignment and wind-ice misalignment are excluded. Below a brief description per DLC is provided.

- DLC9.1: The ULS of the structure during power production in extreme 50-year ice conditions is considered. Dynamic effects from ice loading are included. An ice velocity discretization of $0.01\,\mathrm{m\,s^{-1}}$ until $0.06\,\mathrm{m\,s^{-1}}$ is applied. Beyond this a discretization of $0.02\,\mathrm{m\,s^{-1}}$ is applied until $0.2\,\mathrm{m\,s^{-1}}$. This is done as trial and error confirmed that the dynamic effects for the simulated structures occur at the lower velocities leading to increased loads due to ICR and FLI. At higher velocities CBR occurs and the loads decrease. The considered wind speeds are V_{rated} and $V_{\text{cut-out}}$.

- DLC9.2: Fatigue damage of the structure is considered as a result of ice-structure interaction during power production over its lifetime. A wind discretization of $2\,\mathrm{m\,s^{-1}}$ and wind factor of 0.02 for the ice drift is applied.

- DLC9.3: The ULS of the structure as a result of loads from ice ridges during both power production and standstill/idling is considered. DNV GL [2016] only requires the the ridge action to be simulated as a static load on the structure. The considered wind speeds are V_{rated}, $V_{cut-out}$ and $V_{\text{wind;1}}$*. It should be noted that the inclusion of ice ridges during power production is not prescribed by DNV GL [2016].

- DLC9.4: Fatigue damage of the structure is considered as a result of ice-structure interaction during standstill or idling over its lifetime. A wind discretization of $2\,\mathrm{m\,s^{-1}}$ and wind factor of 0.02 for the ice drift is applied.

- DLC9.5: The ULS of the structure during standstill or idling in extreme 50-year ice conditions is considered. Dynamic effects from ice loading are included. An ice velocity discretization of $0.01\,\mathrm{m\,s^{-1}}$ until $0.06\,\mathrm{m\,s^{-1}}$ is applied. Beyond this a discretization of $0.02\,\mathrm{m\,s^{-1}}$ is applied until $0.02\,\mathrm{m\,s^{-1}}$. This is done as trial and error confirmed that for the simulated structures ICR and FLI occurred at these lower velocities leading to increased loads. The fine discretization ensures that the peak load is captured. At higher velocities CBR occurs and the loads decreases. The considered wind speed is the 1-year extreme wind speed $V_{\text{wind;1}}$*.

Table 5.3: Associated IEC DLCs [IEC, 2019].

DNV GL	IEC
DLC9.1	DLC D3
DLC9.2	DLC D4
DLC9.3	DLC D6
DLC9.4	DLC D7
DLC9.5	DLC D8

The * is included since the current report applied $V_{\text{wind;50}}$ instead of the $V_{\text{wind;1}}$ prescribed by the standard. The results remain unaffected as will be discussed in Chapter 6. Reference is made to Figure A.9 for the extended DLC table covering ice conditions as provided by DNV GL [2016]. For clarity the Table 5.3 provides the associated IEC ice DLCs.

5.3 POST-PROCESSING

In the final phase of the design cycle, the loads are post-processed to generate load envelopes for both ULS and FLS of the structure. For the latter it is necessary to accurately assess the probability of occurrence of each simulated sea state. For the wind & wave simulations these were given in the wind-wave tables provided by the WT metocean team. For the ice simulations the probabilities were determined based on ice thickness distribution and ice interaction days as discussed in Section 2.6. For simplicity this research assumed the ice to drift in a single direction. This direction is given a weight of 35%, which for a wind discretization of 60° is considered conservative.

Once the loads are known, a new optimized monopile is designed by MORPHEUS. Section 4.1 discusses the design methodology applied by MORPHEUS. The optimization is based on certain design and fabrication criteria, which also serve to compare the results. Section 5.3.2 presents and discusses these criteria. The monopiles are optimized for both the reference and the ice case. Note, that in the case where ice is considered, all other DLCs are still considered, but the probabilities of the FLS DLCs are altered as ice is present. The final designs of the optimized monopiles are then compared to each other and used as measure for the feasibility of monopiles in the Baltic Sea.

5.3.1 MORPHEUS optimization

During the design procedure of an OWT foundation the main design variables considered are the bottom diameter of the monopile, D, the wall thickness, t, and the embedded pile length, L_{pile}, as shown in Figure 5.2. The diameter at the top of the foundation is constrained by the tower diameter and the bottom diameter is in practice often limited by fabrication and installation constraints, but both the optimization of the wall thickness and the embedded pile length provide a great potential for steel savings [Nielsen et al., 2022]. During traditional pile design, the design variables are selected and manually adjusted until verification ensures a sufficient design. In contrast, in MORPHEUS the design procedure is fully optimized. The design variables are optimized while complying with both the standards and design, installation and fabrication constraints [Nielsen et al., 2022].

MORPHEUS models the structures as a finite element model of 2D Timoshenko beam elements and Winkler springs to model the non-linear soil-structure interaction. The RNA is modelled as a lumped mass at hub height [Nielsen et al., 2022]. The model is then optimized. A simplified version of the optimization loop is presented in Algorithm 5.1.

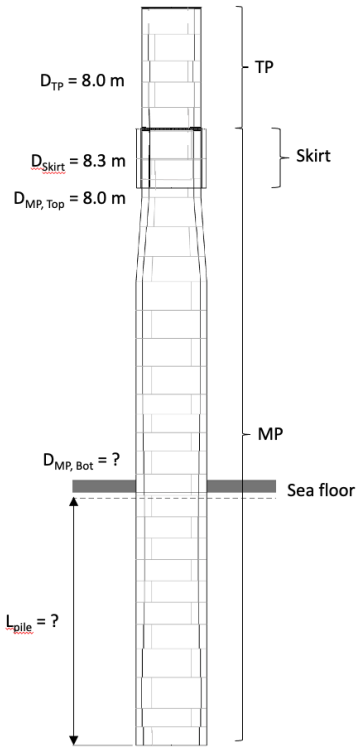

Figure 5.2: Initial monopile geometry consisting of a transition piece (TP), skirt and monopile (MP) [Nielsen et al., 2022].

During the FLS check, MORPHEUS considers Stress Concentration Factor (SCF) for various attachments, holes or other structures. Note, during the optimization in this research, the FLS check is based on a damage equivalent moment ΔM_{eq}. This moment, applied over a chosen number of reference cycles (10^7) causes equivalent damage as if it would be calculated using a moment time history and a SN curve [Nielsen et al., 2022].

For the current research all design checks are performed at intervals of 0.5 m, whereas during detailed design an interval of at least 0.1 m is applied. In step 4, the pile is divided into can sections. Each can section should satisfy the fabrication constraints, e.g. minimum and maximum weight, height and maximum wall thickness t. To ensure the FLS checks of all circumferential welds are still satisfactory, wall thicknesses may be updated [Nielsen et al., 2022].

5.3.2 Design, fabrication & installation criteria

During the optimization of MORPHEUS, the design should satisfy a predefined set of design and fabrication criteria. In terms of design criteria, the required first natural frequency should be met, within the 1P and 3P limits. Furthermore, both the frequency and the stiffness of the foundation have to be comparable to the model used for load generation.

For the stiffness of the structure WT has defined multiple parameters, one of which is a flexibility parameter, α_k. This is the static displacement of the structure at MSL in mm MN^{-1}, when 1 MN is applied at this elevation. If the structure does not meet the minimum required stiffness (or frequency), pile length or wall thickness, at selected cans, is added until the criterion is satisfied. MORPHEUS adds either pile length or wall thickness, depending on the amount of steel required, i.e. the more economic option is selected. For each water depth an initial value is chosen based on reference projects. During optimization α_k is slightly adjusted based on each individual region to reach a more efficient design.

Algorithm 5.1: MORPHEUS-FOUNDATIONS algorithm

1) Find minimum embedded pile length:

   Based on design loads in ULS
   Based on permanent pile rotation in Serviceability Limit State (SLS)

2) Check ULS according to relevant standards:

   Based on combined bending, shear and axial forces
   Based on global column buckling

3) Check FLS according to relevant standards:

   Based on constant amplitude equivalent moment ΔM_{eq}

4) Divide pile into can sections and check:

   Based on fabrication constraints

   $\Rightarrow$ Can wall thickness updated if necessary

5) Dynamic properties of foundation are checked:

   First natural frequency of OWT within 1P and 3P limits
   Frequency and stiffness comparable to model used for load generation

   $\Rightarrow$ Wall thickness and/or embedded pile length increased if necessary

6) Repeat steps 1-5 until:

   Convergence is realized
   Constraints and designs checks are satisfied

For wave-induced fatigue, an increase α_k — which increases the flexibility — the fatigue loads are scaled one-to-one, however, if α_k is decreased the fatigue loads are scaled down with only 50% of the α_k-scaling to remain conservative. A similar relation was assumed in this research for ice-induced fatigue. This relation will be investigated.

If possible, the α_k will be kept constant between the reference and the ice case. However, if necessary due to violations of the fabrication constraints, the stiffness is increased. The fabrication constraints are based on industry practice and are as follows:

- Maximum D/t ratio of 130 for monopile
- Maximum D/t ratio of 180 for for transition piece and skirt
- Maximum wall thickness of 150 mm
- Maximum can weight of 100 t
- Can height range of 2000–4200 mm for cylindrical cans
- Can height range of 2000–3500 mm for conical cans
- Maximum foundation weight of 2000 t

After the optimization the feasibility of the various monopiles is considered. The outlined design, fabrication & installation criteria define technical feasibility of the monopile, i.e. a design is technically feasible if it satisfies the constraints and vice versa.

Besides technical feasibility, economic feasibility is considered, in terms of the weight increase of the foundations under ice loading, i.e. excessive weight increase indicates an infeasible design.

5.3.3 UR plots

After the design optimization MORPHEUS is able to provide a utilization ratio plot for the various design checks, which indicates the governing factor at each elevation. Figure 5.3 provides an example of such a plot. The plots include utilization ratio of ULS buckling & yielding, FLS longitudinal, circular & attachment welds, damage due to transport & installation and maximum allowable D/t ratio [Nielsen et al., 2022].

The investigation of these plots provides insight into the driving factors for the pile design at each elevation, and in the case of this research will be used to assess the specific effect of ice loading compared to the reference case.

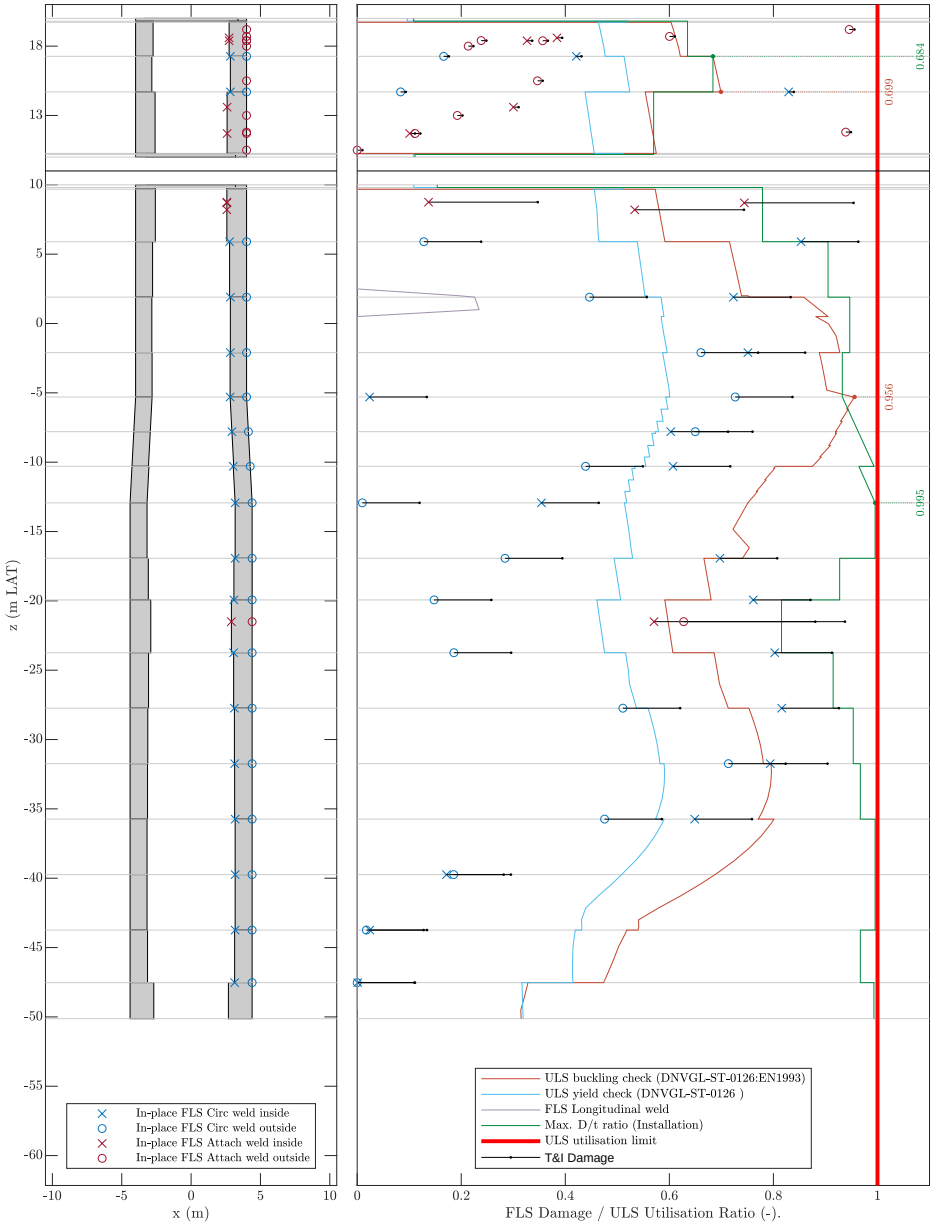

Figure 5.3: Utilization ratios for various limit states

6 BALTIC SEA MONOPILE DESIGN - FEASIBILITY MAP

In the previous chapter the methodology to obtain a feasibility map for monopiles in the Baltic Sea was presented. In this chapter, the results of the research are presented and discussed. The results include load envelopes of the various simulated DLCs, foundation designs for monopiles in all regions and feasibility maps based on weight and fabrication constraints, which is the main objective of Part III.

First, the governing loads are evaluated for the various regions by investigating the load envelopes for each region. By evaluating the load envelopes the impact of ice on the loads can be assessed. However, one or more governing ice DLCs do not directly imply a *load effect* on the design, as it may not be driving for design. To investigate the load effect, the monopile designs generated by MORPHEUS are compared between the reference and the ice case. Based on these monopile designs a feasibility map for monopiles in the Baltic Sea is generated.

This is followed by a discussion on the impact of various input parameters or assumptions on the research, namely the ridge action, the ice interaction days and the water depth. Finally, the effect of ice-mitigating measures on the current research is discussed.

6.1 LOADS

First the ULS load envelopes as well as the damage equivalent moment, ΔM_{eq}, for monopiles in the nine regions are discussed.

6.1.1 Ultimate Limit State

The load envelopes of the overturning moments from all DLCs are provided in Figure 6.1 for two regions, the Danish Straits and the Bay of Bothnia, which are considered as the least and most severe regions in terms of ice conditions, respectively. Reference is made to Figure A.7 for similar plots of all other regions.

For all regions — if calculated according to the design standards — DLC9.3 during power production is shown to be governing. This is extensively discussed in Section 6.3, but in the current section only the ridge action DLC calculated according to literature is considered. The load case due to this alternative ridge action is shown to be governing for at least some section of the foundation in eight out of nine regions.

From Figure 6.1a it can be observed that for the Danish Straits the governing DLC is — for the most part — DLC1.4, which is a sudden gust in another direction. Due to the large RNA mass of the IEA 15 MW, it is unsurprising that this DLC is driving for the design. Especially since wave conditions in this region were relatively mild. The ice DLCs are almost negligible for this region, with only DLC9.1 exceeding the DLC1.4 at the mudline.

For the Bay of Bothnia the ice DLCs were governing over the entire foundation as indicated by Figure 6.1b. Since the largest ice thicknesses and crushing coefficients occur in these regions, it is unsurprising that the foundations were subject to substantial loads and displacements. Similar results were found for the Gulf of Finland, the Bothnian Sea South & the Bothnian Sea North.

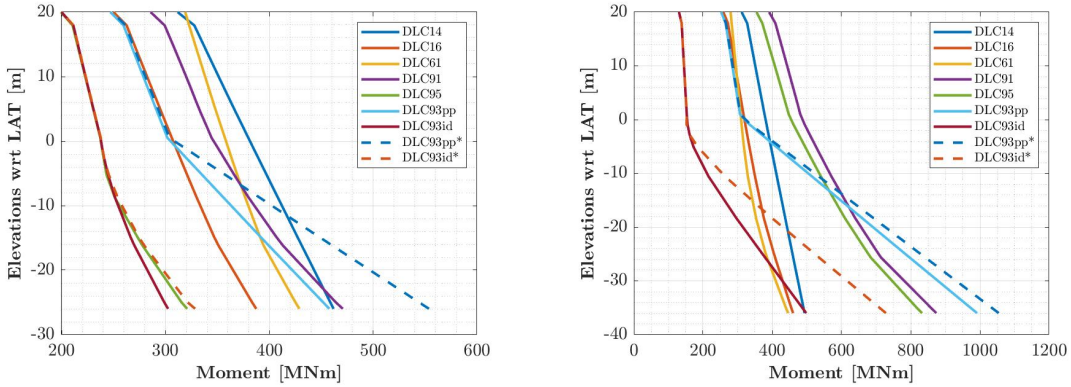

Figure 6.1: Overturning moment load envelopes for a monopile in (a) the Danish Straits and (b) the Bay of Bothnia. For DLC9.3, "id" and "pp" indicate idling and power production, and the dashed line indicates the ridge action according to the design standards.

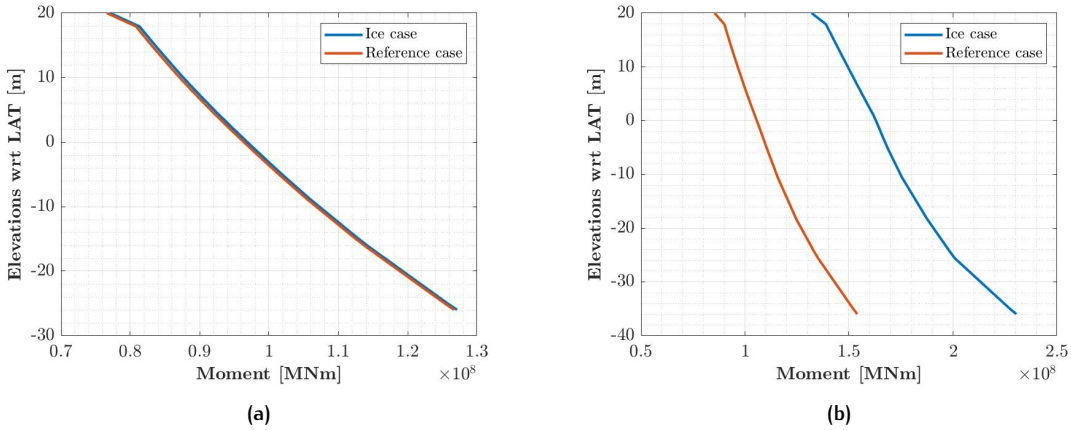

Figure 6.2: Damage equivalent moment in the most unfavourable direction for a monopile in (a) the Danish Straits and (b) the Bay of Bothnia.

The load envelopes for all other regions indicated that as ice conditions worsen, the load envelope is increasingly more governed by the ice DLCs, which is in line with expectations.

Additionally, by comparing the load envelopes of the Archipelago Sea and the Bothnian Sea South the impact of the water depth can be observed. The former has a higher extreme ice thickness, yet DLC9.1 is only governing from MSL onward. While in the Bothnian Sea South — for less extreme ice conditions — the same DLC is governing over the entire length of the foundation.

The load envelopes show that ice loading was the governing DLC for most regions. This suggest that there will be a influence on the design. The exact nature of this influence is discussed in Section 6.2.

6.1.2 Fatigue Limit State

The fatigue loads were represented with the damage equivalent moment ΔM_{eq}, which is given in Figure 6.2 for the Danish Straits and the Bay of Bothnia. The damage equivalent moment for the other regions is given by Figure A.8.

The results confirm that the ice caused significantly more damage — around 50% more in terms of ΔM_{eq} — in the Bay of Bothnia than in the Danish Straits. This was expected, as the OWT interacts with ice for approximately 10 days over its lifetime in the Danish Straits, versus

approximately 350 days in the Bay of Bothnia. In the Danish Straits the increased damage equivalent moment was almost negligible compared to wind & wave contributions. Figure 6.3 shows the correlation between the ice interaction days and the increase in ΔM_{eq}, which is quite strong. The various outliers are likely a result of differences in extreme ice thickness and/or wave conditions.

Examination of the fatigue due to ice showed that more than 90% of the damage as a result of ice is due to simulations at low speeds, specifically those resulting in FLI. However, this research is concerned with the load effect, i.e. what the fatigue damage ΔM_{eq} leads to *and* the required design changes resulting from it. The load effect due to the increased ULS & FLS loads is investigated in the following section.

An important note with regards to the generation of the loads is that only the combination of a 50-year extreme ice thickness and a 1-year extreme C_R were used. For simplicity it was assumed that this was the governing case, but other combinations may be governing. Furthermore, during time domain simulations the research assumed that limit stress is always governing over limit force & energy, i.e. driving forces are always sufficient for ice failure. In reality, this may not be the case as ice sheets — especially ridges — could come to halt against the structures. With increasing size of the foundations this effect may be more prevalent [Croasdale, 1984].

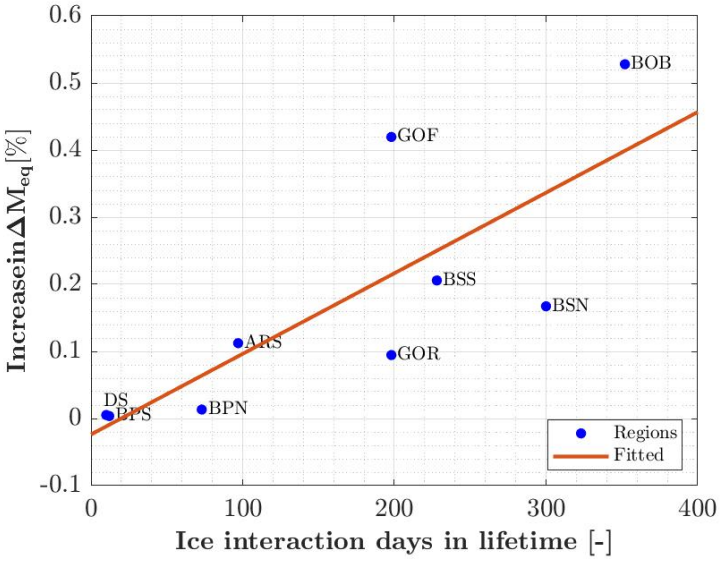

Figure 6.3: Increased damage equivalent moment as a function of ice interaction days.

6.2 LOAD EFFECT

The load effect was investigated by generating optimized monopile designs for all regions based on 1) the reference loads (wind & waves only) and 2) both the reference loads and the ice loads. Figure 6.4 indicates the weight increase per monopile if all the design & fabrication constraints are satisfied.

For the Danish Straits, Baltic Proper South, Baltic Proper North, Gulf of Riga and Archipelago Sea monopile designs could be generated without increasing the stiffness — and decreasing the fatigue loads — of the structure. For the Baltic Proper North, Gulf of Finland and the Southern Bothnian Sea a small increase in stiffness (3–4%) was required to adhere to the fabrication constraints as the maximum can weight of 100 t was slightly exceeded. For the Northern Bothnian Sea and the Bay of Bothnia the stiffness had to be drastically increased, 23 and 43% respectively, with a significant increase in weight as a result. Before the stiffness was increased both the maximum can weight and thickness were exceeded.

The results are summarized in Table 6.1. It should be noted that the frequency constraint was relaxed as the IEA 15 MW tower was scaled based on moment of inertia, not frequency. As a result the frequency constraint was driving for all designs, and no weight increase was observed.

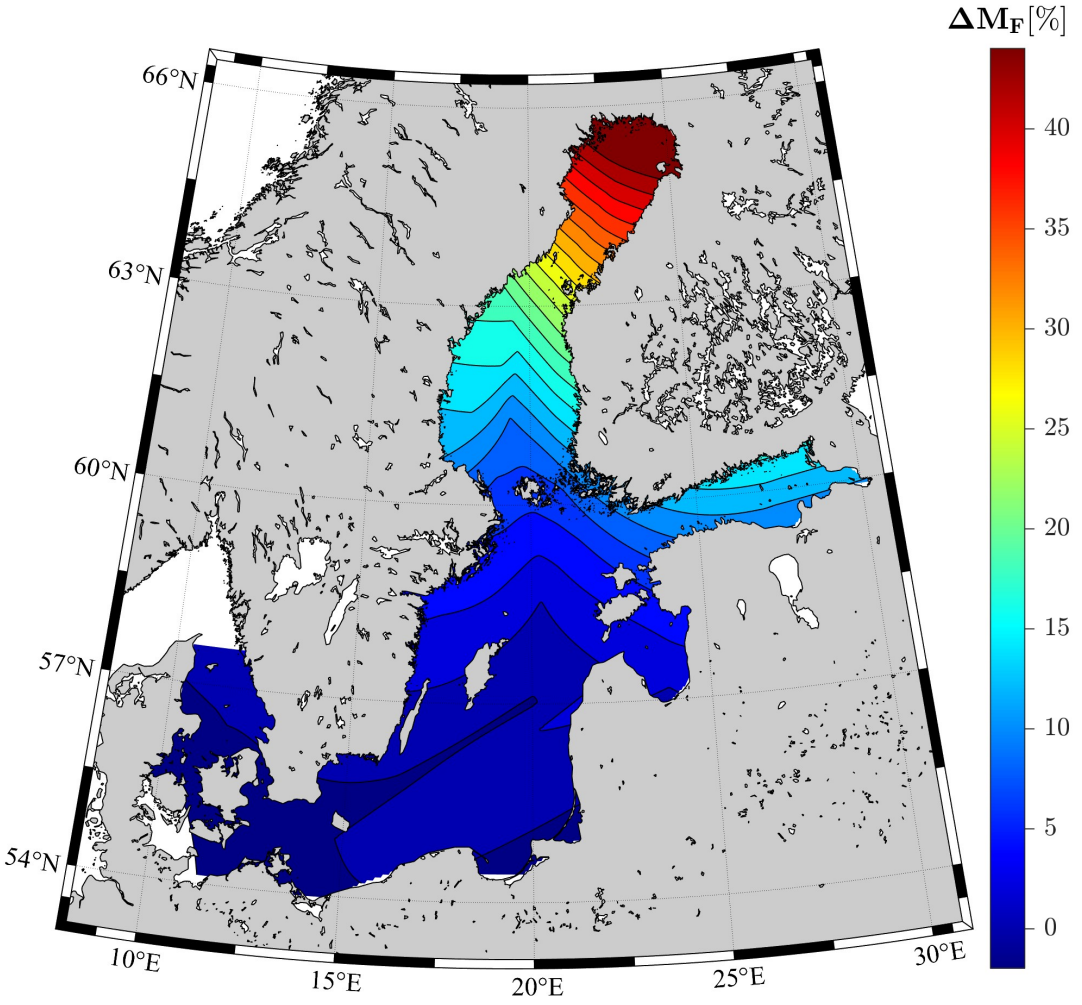

Figure 6.4: The change in foundation mass, ΔM_F for a monopile subject to ice loading in the Baltic Sea for the simulated water depth in each region (25–45 m).

Table 6.1: Summary of results for monopile design optimization for the nine identified regions in the Baltic Sea. The letters indicate DS - Danish Straits, BPS - Baltic Proper South, BPS - Baltic Proper South, GOR - Gulf of Riga, GOF - Gulf of Finland, ARS - Archipelago Sea, BSS - Bothnian Sea South, BSN - Bothnian Sea North, BOB - Bay of Bothnia.

		Reference case			Ice case			Comparison	
Region	**Depth [m]**	M_{MP} [t]	M_{TP} [t]	α_k [mm MN^{-1}]	M_{MP} [t]	M_{TP} [t]	α_k [mm MN^{-1}]	ΔM_F [t]	ΔM_F [%]
DS	25	910	166	9.9	907	166	9.9	-3	0
BPS	45	1911	230	14.8	1907	230	14.9	-4	0
BPN	45	1913	234	14.9	1964	230	14.3	46	2
GOR	25	912	170	9.9	937	181	9.9	36	3
GOF	35	1306	179	12.8	1447	227	12.3	189	13
ARS	25	915	163	9.9	977	181	9.7	81	8
BSS	35	1341	199	12.4	1464	231	11.9	155	10
BSN	45	1821	235	15.9	2178	232	12.9	353	17
BOB	35	1323	194	12.8	1930	230	8.9	643	42

6.2.1 UR plots

The utilization ratio plots generated by MORPHEUS provide the ability to investigate the driving factors of all the designs. The UR plots for the reference case and the ice case of the Gulf of Finland are shown in Figure 6.7 and Figure 6.8. UR plots for the other regions are included in Appendix C.

The UR plots, Figure 6.5 & Figure 6.6 for the Danish Straits was near identical for the reference and the ice case. This corresponds to the observed weight increase of 0%. For this region the ice DLCs was only governing close to sea bed. This does not translate to any load effect on the design. Similarly, the occurrence of ice was too low for the fatigue loads to have a load effect. A similar result is observed for the Baltic Proper South, Baltic Proper North and the Gulf of Riga. However, as the ice conditions become more extreme, more weight increase (up to 2–3%) is observed due to mostly fatigue loading.

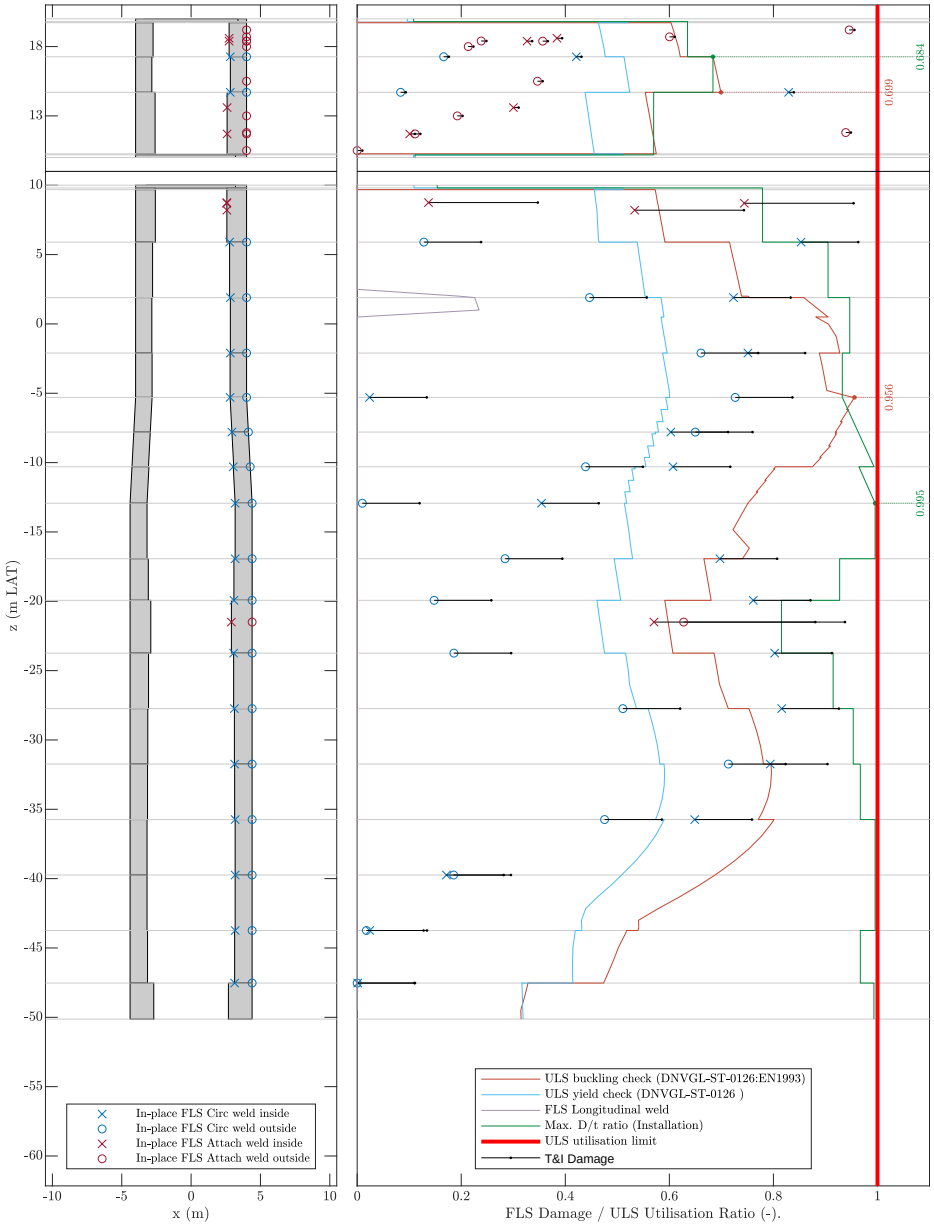

Figure 6.5: UR plot of reference case - Danish Straits

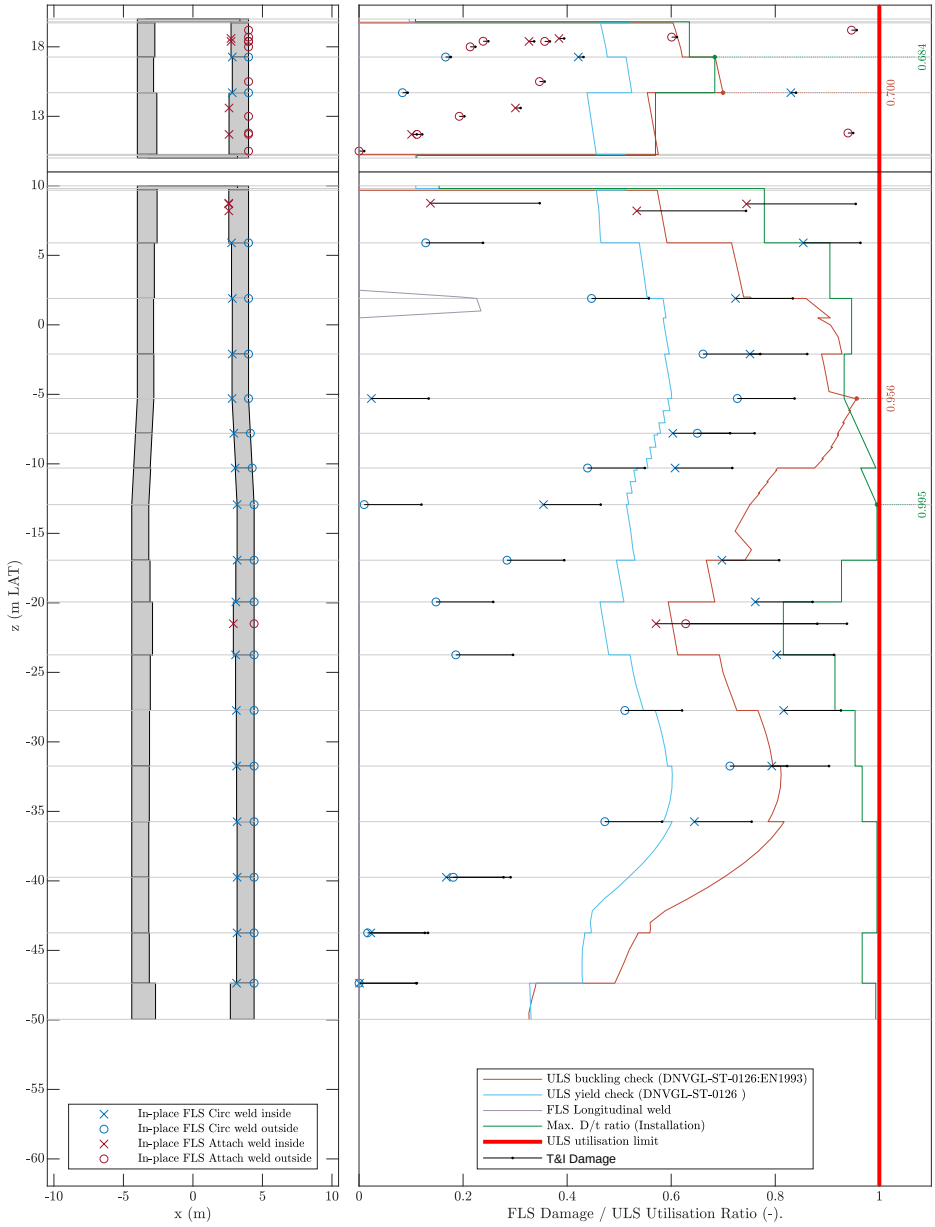

Figure 6.6: UR plot of ice case - Danish Straits

The Gulf of Finland required a small increase in stiffness to satisfy all the design & fabrication constraints. From the UR plot, Figure 6.7 & Figure 6.8, it was observed that this is a result of the fatigue loads, which are governing for most of the foundation. Additionally, the ULS loads were governing near the bottom of the foundation. The design drawings confirmed that increased wall thickness weight was required along the entire length of the foundation. Similar results were found for the Archipelago Sea and the Bothnian Sea South. Fatigue loads were governing over the entire length of the foundation leading to substantial weight increases around the top of the monopile and the transition piece. Either no or small increases in stiffness was required.

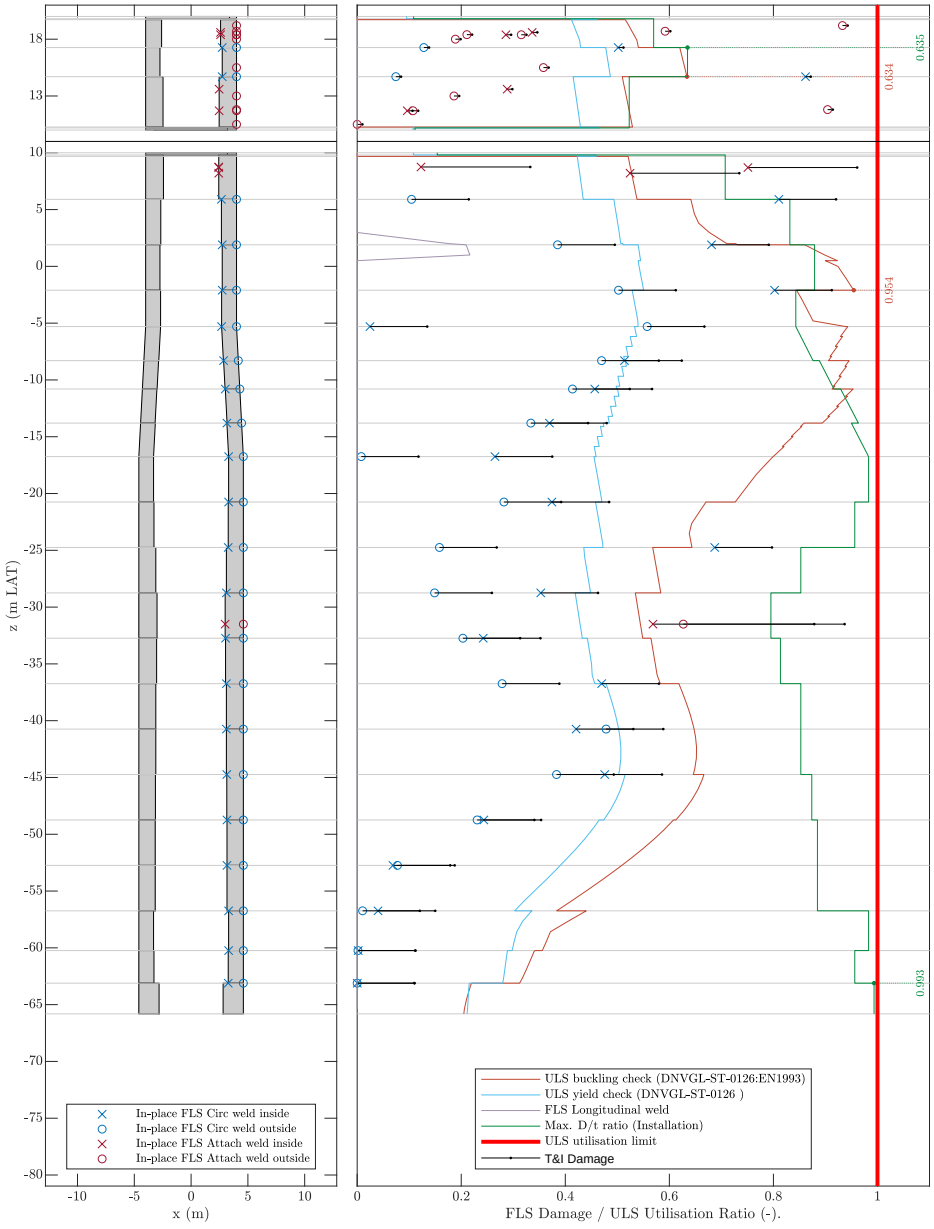

Figure 6.7: UR plot of reference case - Gulf of Finland

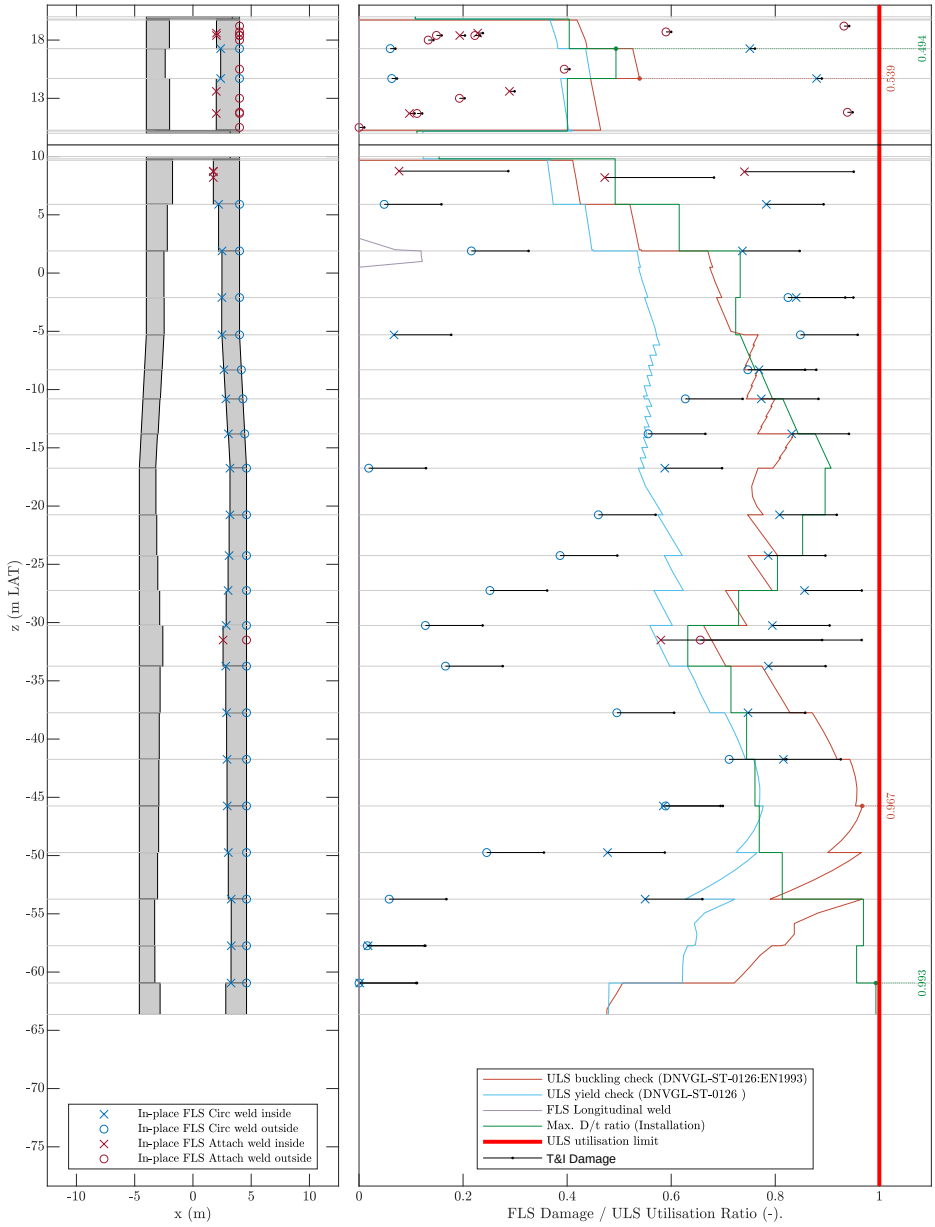

Figure 6.8: UR plot of ice case - Gulf of Finland

The UR plot for the Bay of Bothnia, Figure 6.9 & Figure 6.10, changed drastically between the reference case and the ice case. The stiffness had to be increased substantially, which results in a very inefficient design for the bottom half of the monopile. The UR plots indicate that the increased stiffness is required due to the fatigue loads driving the top half of the monopile design, which punishes the bottom half of the monopile by adding the required steel. The Bothnian Sea South showed similar results.

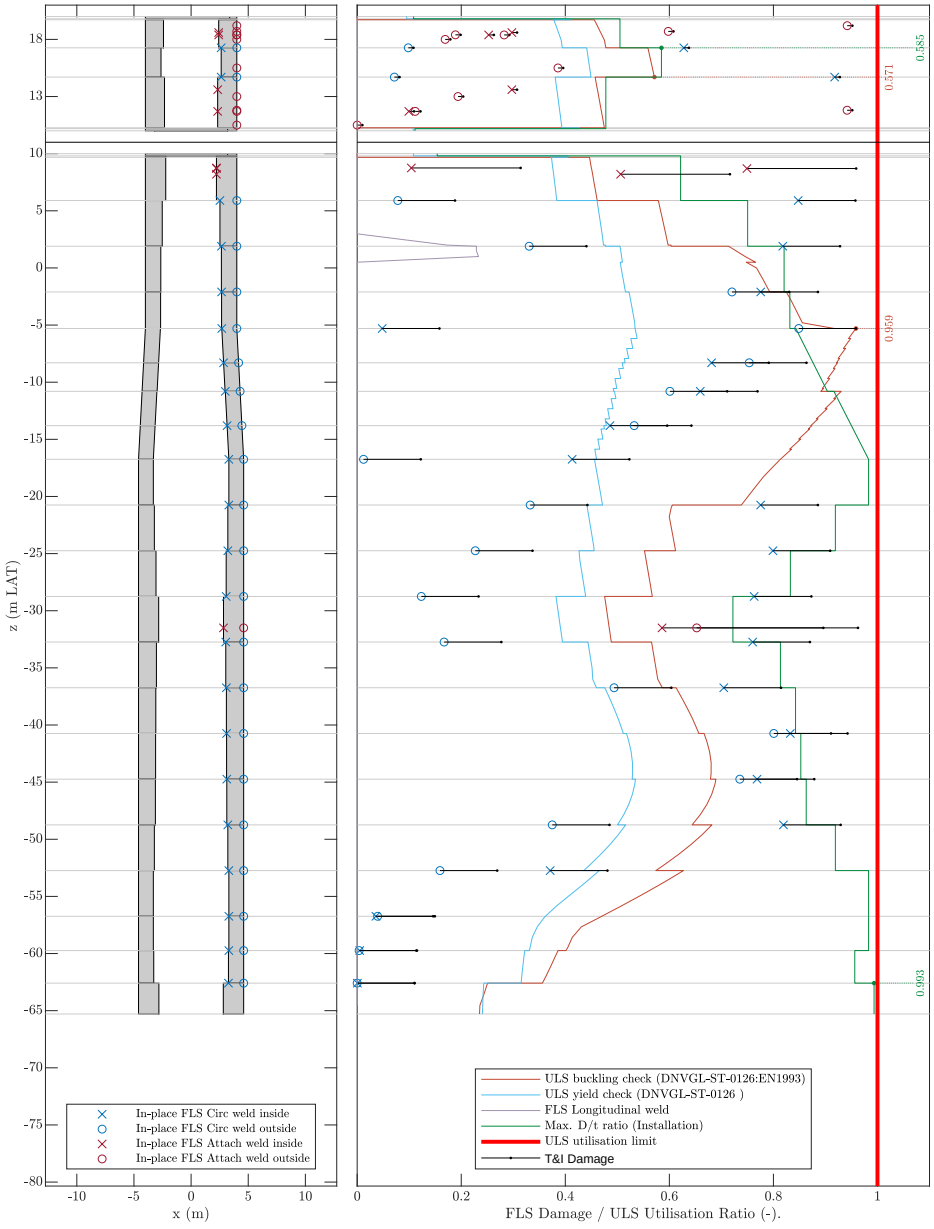

Figure 6.9: UR plot of reference case - Bay of Bothnia

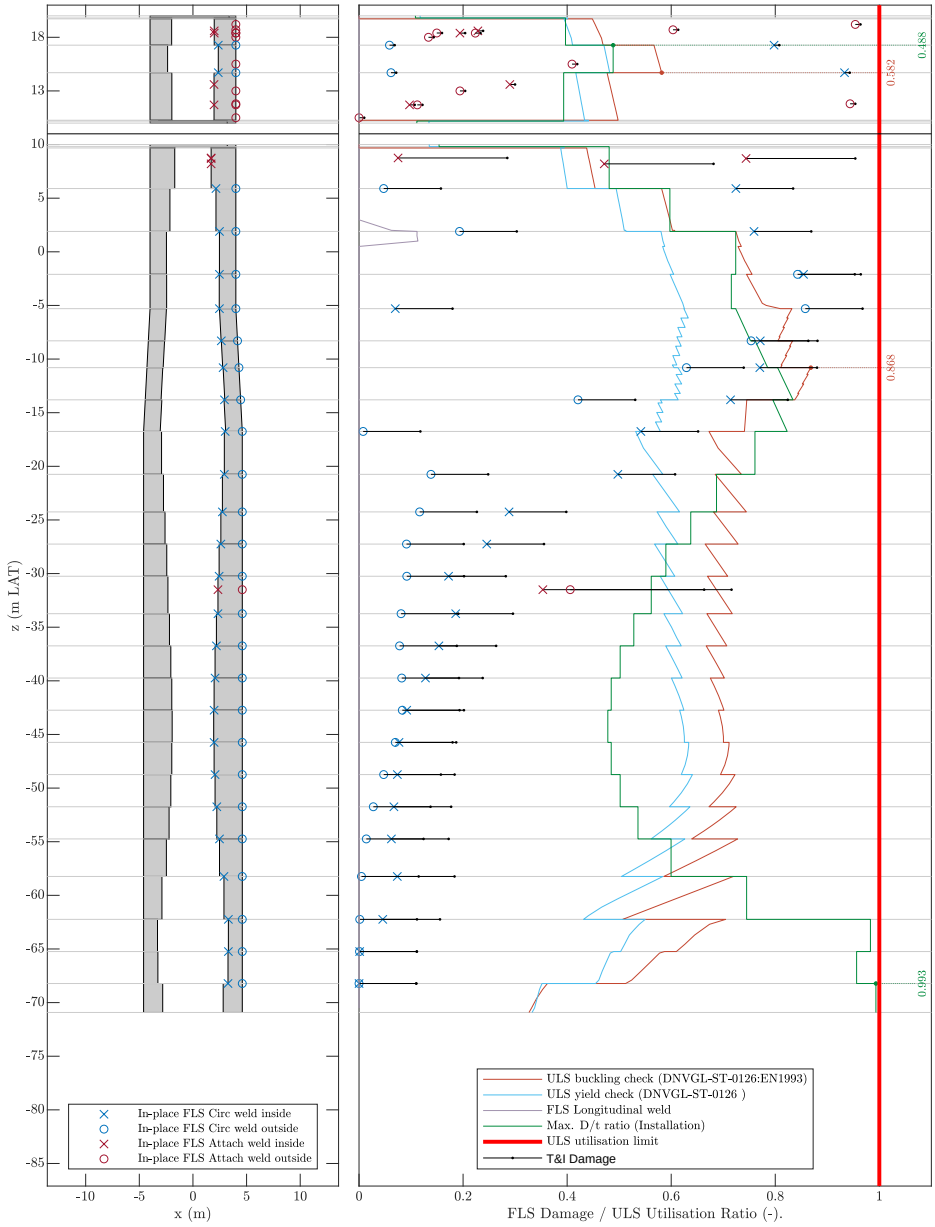

Figure 6.10: UR plot of ice case - Bay of Bothnia

An additional design was generated by MORPHEUS with relaxed fabrication constraints. The resulting UR plots, also provided in Appendix C, and design drawings showed that 1) the fatigue was governing for the design and 2) that specifically the top half of the monopile exceeded the constraints substantially, which is further discussed in the following section.

6.2.2 Fabrication constraints

The design drawings of the monopile and the transition piece are presented for the various cases in Appendix D. With the drawings the impact of the ice loading for specific can sections was investigated. Drawings have also been provided for the ice case with relaxed fabrication constraints to indicate were the designs exactly exceeded the limitations.

For designs that initially exceeded the fabrication constraints for the ice case, the cans causing the problem were the bottom can of the transition piece, the top can of the monopile and the

lowest can above the seabed. The reason for this was the presence of welded attachments and/or holes, which are susceptible to fatigue damage, and include high SCFs.

For the Baltic Proper North, the Gulf of Finland and the Bothnian Sea South the only fabrication constraint that was exceeded was the maximum can weight. The designs could satisfy the constraints and the stiffness requirement if the maximum can weight was increased to from 100 to 110 t. However, slightly increasing the stiffness was more beneficial in terms of total foundation weight.

For the Bothnian Sea North and the Bay of Bothnia the opposite was true, i.e. relaxing the fabrication constraints saved more steel than increasing the stiffness. However, the new required fabrication constraints were less realistic as both the maximum can weight *and* the maximum thickness were exceeded substantially. The maximum can weight was, respectively, 120 and 130 t for the Bothnian Sea North and the Bay of Bothnia, while the maximum wall thickness was 162 and 171 mm.

Besides the fabrication constraints, the installation constraint was exceeded one of the designs. The monopile in the Bothnian Sea North weighs more than 2000 t, which is often considered the maximum allowed weight, as it corresponds to the maximum crane capacity of most commercial lifting vessels for monopile installation. If the monopile requires installation vessels with higher crane capacity the overall cost are expected to increase. Recently installed monopiles that exceeded this weight had to be installed by vessels with capacity of 5000 t. This increased capacity most likely comes at a steep price increase [DEME, 2022].

6.2.3 Feasibility Map

For the simulated water depth in each region, monopile designs were deemed feasible in the following regions: the Danish Straits, the Baltic Proper South, Baltic Proper North, Gulf of Riga, Archipelago Sea.

Based on the observed increased in weight and the inefficient utilization the Bothnian Sea North and the Bay of Bothnia were deemed infeasible for monopile design under ice loading.

For both the Bothnian Sea South and the Gulf of Finland feasibility is difficult to assess. An efficient design that satisfies all criteria is possible. However, a substantial weight increase is observed (10–13%), which despite the technical feasibility, may indicate economic infeasibility. For the Gulf of Finland it should be noted that the mild wave conditions play a role. As a result the wave contribution to the total fatigue damage was low compared to other regions. However, the increased weight was still substantial and should be compared to alternative solutions with ice-mitigating measures. This will be discussed in Section 6.6. The final feasibility map is presented in Figure 6.11. Note, this is for *region specific* water depths.

A recent study by the European Commission indicated that the potential capacity of offshore wind in the Baltic Sea is estimated at 93.5 GW. Since the map is now generated it is possible to investigate if the potential capacity regions and feasibility regions coincide. The study reports that in the Baltic Sea Denmark, Germany, Poland, Lithuania and Latvia combined account for 58.5 GW (63%) of the potential capacity. These countries are all adjacent to feasible regions. Furthermore, Sweden accounts for another 20 GW (21%), which is spread along its coast, in both feasible and infeasible regions. The total capacity within monopile feasible regions is thus likely even higher [European Commission and Directorate-General for Energy, 2019]. Note, this is not entirely accurate as only specific water depths are considered for each region.

6.3 ICE RIDGES

This section discusses the effect of two methods for ice ridge action. Figure 6.12 illustrates the increased weight difference between the two cases, which indicates that diverging from the

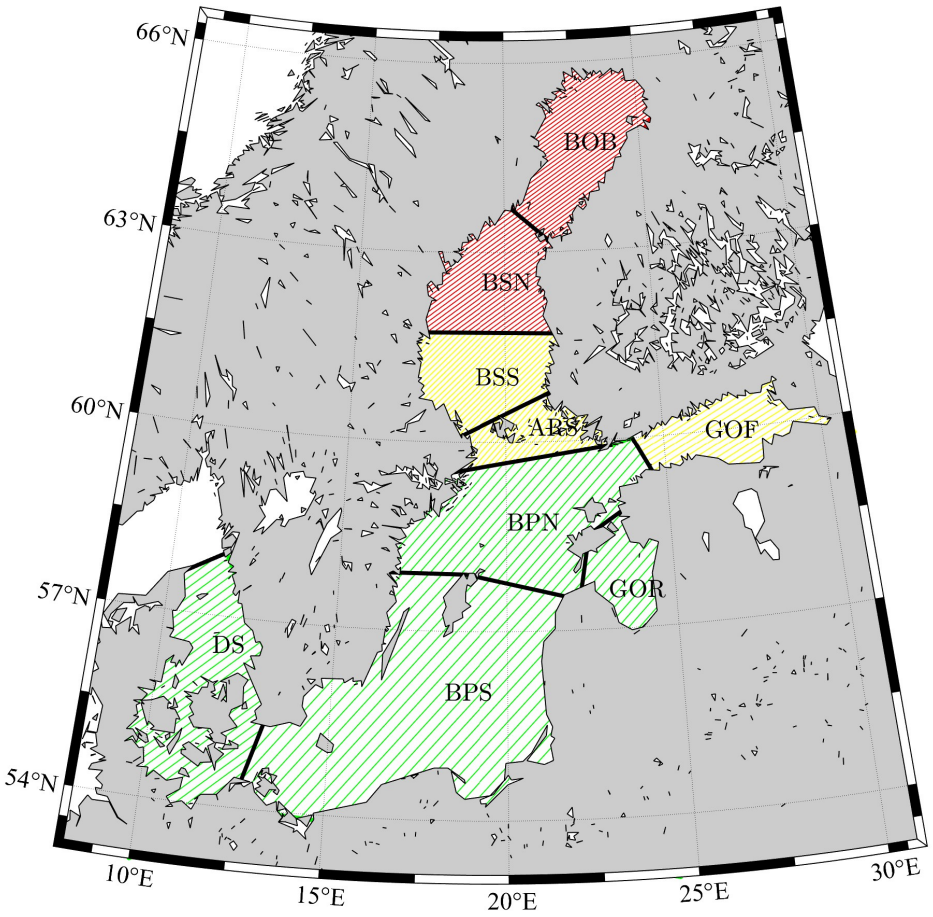

Figure 6.11: Feasibility map for monopiles in the Baltic Sea for region specific water depths. Green indicates a feasible design, yellow indicates that it depends on alternative options, and red indicates infeasible design. The letters indicate DS - Danish Straits, BPS - Baltic Proper South, BPS - Baltic Proper South, GOR - Gulf of Riga, GOF - Gulf of Finland, ARS - Archipelago Sea, BSS - Bothnian Sea South, BSN - Bothnian Sea North, BOB - Bay of Bothnia.

standard saves 1–2% in steel for three of the nine regions, namely the Gulf or Riga, Gulf of Finland & the Archipelago Sea.

This is unsurprising as these were the only regions for which the UR plots indicated that the ULS loads were governing for a (small) section of the design. Overall, the result indicated that ULS does not greatly influence the design and thus the increase in ridge action does not have a significant load effect for most regions.

However, further research into the ridge properties is required as it was the governing ULS load case for many regions and there was a — albeit small — load effect, which seemed to affect the non-deep positions mostly. Due to the infrequency of ice seasons, especially in the Southern regions, assessing the governing ridge geometry required assumptions. Three key factors which strongly influenced the ridge action were 1) the consolidated layer, 2) the keel depth and the 3) keel cohesion.

The current research assumed a factor of 1.5 between the extreme level ice thickness and the consolidated layer. The keel depth and keel cohesion were determined based on experimental data and measurements. The experiments, however, were all conducted on ridges in the Bay of Bothnia. Properly scaling this to the Southern regions is difficult, but might reduce the ridge actions further.

Moreover, the ice ridge action in this research was applied during power production, which is not necessary according to the standards. However, the reason the design standards omit

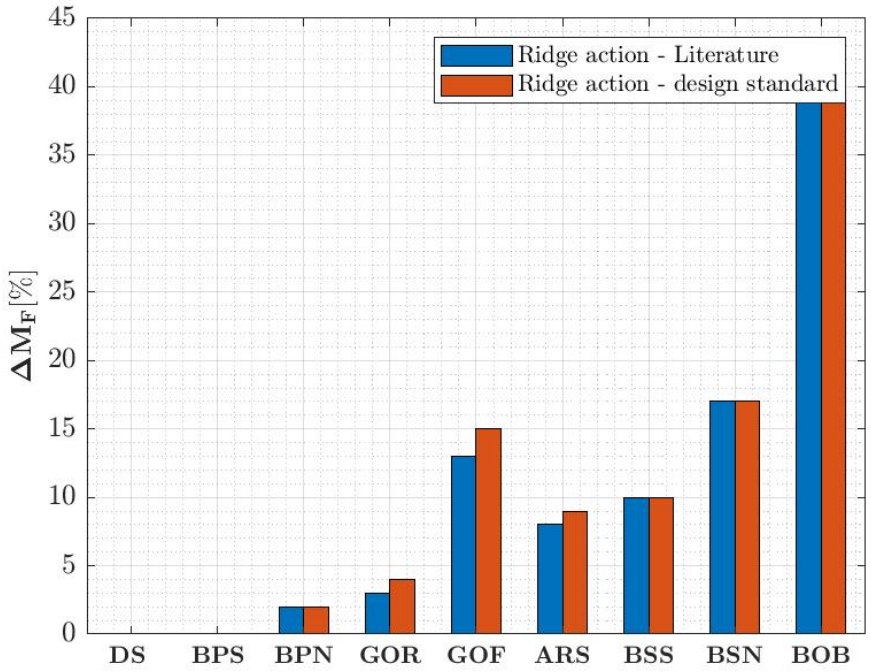

Figure 6.12: Weight increase of the foundation design due to ice loading for a ridge action calculated according to literature and design standards. The letters indicate DS - Danish Straits, BPS - Baltic Proper South, BPS - Baltic Proper South, GOR - Gulf of Riga, GOF - Gulf of Finland, ARS - Archipelago Sea, BSS - Bothnian Sea South, BSN - Bothnian Sea North, BOB - Bay of Bothnia.

this load case is unclear. A potential reason would be that ridge formation occurs only in such extreme winter conditions that the wind farm is pre-emptively shut down. This is deemed rather unlikely as the design standard does consider extreme level ice, which in most regions would also lead to ridges. The presence of a wind farm likely also increases the chances for ridge formation, as drifting ice may interact with ice stationary against the monopiles. However, if there is a valid reason for the exclusion of the ridge DLC during power production, then it can be concluded that ridges do not impact design, since the idling ridge DLC is never governing.

6.4 ICE OCCURRENCE

Recent research has suggested that the applied probability of ice occurrence has a greater impact on design than the applied extreme ice thickness [Hornnes et al., 2022]. Since there is little information on this variable, this research was forced to make assumptions with regards to the ice interaction days as mentioned in Section 2.6.2. The applied interaction days were — compared to the literature — on the conservative side. The effect of this can be observed in Figure 6.13, which provides the weight difference when the ice interaction days were halved.

The results indicate, that the interaction days are of paramount importance on the design. This also follows from the UR plots, which show that for most regions fatigue is driving for design. This further emphasizes the necessity for extensive metocean information with regards to ice occurrence.

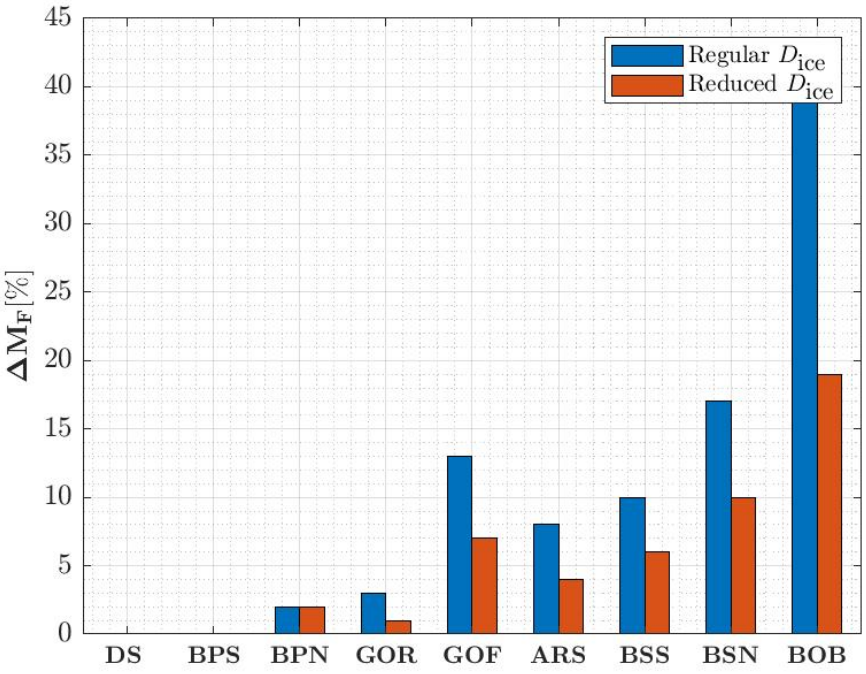

Figure 6.13: Weight increase of the foundation design due to ice loading for regular number of ice interaction days and the 50% reduction of the interaction days. The letters indicate DS - Danish Straits, BPS - Baltic Proper South, BPS - Baltic Proper South, GOR - Gulf of Riga, GOF - Gulf of Finland, ARS - Archipelago Sea, BSS - Bothnian Sea South, BSN - Bothnian Sea North, BOB - Bay of Bothnia.

6.4.1 Ice direction

Additionally, the occurrence of ice in specific directions should be investigated. The current research assumed the ice to be one-directional and weighted this direction with 35%, twice the average probability for a discretization of 60°. Without data it is difficult to determine whether this is conservative or not. However, as discussed in Section 2.5, the ice drift is strongly governed by wind throughout the Baltic Sea. As a result a wind factor model was suggested to be an accurate estimate of the drift speed [Leppäranta, 1981; Leppäranta and Omstedt, 1990]. Since the two are strongly correlated, the directionality can be assumed to strongly correlate as well. By investigating the probabilities of the wind directions for the regions, it can be shown that the applied 35% is very conservative. The occurrence of the governing wind direction varies for all regions, but is at most 23%. Reducing the directionality would have similar effects as reducing the interaction days, as the fatigue load is more evenly distributed over the directions.

It should also be noted that the wind factor model has one — until now — ignored assumption, the current contribution to the ice forcing is neglected. For low wind speeds this might not be accurate, as the relative contribution of the current becomes larger [Leppäranta, 1981; Leppäranta and Omstedt, 1990]. For the FLS simulations this implies that at lower wind speeds the simulated ice drift velocities may have been underestimated, as including the current contribution would have increased it. Since the lower drift velocities contribute significantly to the fatigue damage due to the occurring vibration regimes, including the current contribution might lead to more efficient and less conservative designs.

The current research assumed — in line with requirements from the design standards — no wind-ice misalignment. However, wind-ice misalignment may result in bi-directional vibrations, thus potentially negatively affecting the design of the foundation [Zhu et al., 2021].

Table 6.2: Summary of results for monopile design optimization for the nine identified regions in the Baltic Sea. The letters indicate DS - Danish Straits, BPS - Baltic Proper South, BPS - Baltic Proper South, GOR - Gulf of Riga, GOF - Gulf of Finland, ARS - Archipelago Sea, BSS - Bothnian Sea South, BSN - Bothnian Sea North, BOB - Bay of Bothnia.

		Reference case			Ice case			Comparison	
Region	**Depth [m]**	M_{MP} [t]	M_{TP} [t]	α_k [mm MN^{-1}]	M_{MP} [t]	M_{TP} [t]	α_k [mm MN^{-1}]	ΔM_F [t]	ΔM_F [%]
BSS	35	1341	199	12.4	1464	231	11.9	155	10
BSS	45	1905	235	14.9	2097	234	13.4	190	9

6.5 WATER DEPTH

In the methodology a deeper water depth was assumed to be unfavourable for ice loading. This section investigates and discusses this assumption.

The load envelopes confirm that for the ULS of the foundations the deeper positions were increasingly more governed by the ice DLCs. However, since fatigue was shown to be governing over the ULS loads, this may not directly result in a larger load effect. To investigate this, a second water depth was considered for one of the regions, the Bothnian Sea South.

Besides the original water depth of 35 m a deeper position was considered at 45 m. The results are given in Table 6.2. The increase of foundation mass in percentage is similar between the two regions — even slightly smaller for the deep position — but the increase in absolute weight increases since the foundation is substantially larger for the deep design. As a result, the overall mass exceeds the installation constraint of 2000 t.

The UR plots of the intermediate and deep positions all indicated that fatigue was driving for design. Specifically, the fatigue loads in the top section of the foundation were often governing. The welds around the transition piece and in the top of the monopile were very susceptible to fatigue damage. The results indicated that this fatigue damage is similarly detrimental to the intermediate and deep position, in terms of relative foundation increase.

However, as deeper positions are considered a smaller relative weight increase can lead to large complications. With the current size of foundations for OWT, any increase will push the overall foundation weight beyond the installation requirements. This was shown to be the case for the Bothnian Sea South, Bothnian Sea North, Bay of Bothnia and the Gulf of Finland. No deep and intermediate position were simulated for the Archipelago Sea and the Gulf of Riga.

Hence the original assumption that the ice load effect is worst for deep positions does not seem to be entirely correct. The ULS load envelopes showed that for larger positions the ice DLC govern larger parts of the foundation. However, the ice load effect is similar between intermediate and deep position. Nonetheless, the deeper position will more frequently be infeasible for design as it is closer to the installation constraint. The effect of water depth should be carefully investigated for each region individually.

Table 6.3 provides the feasibility of monopiles in the Baltic Sea for varying water depths, with help of some assumptions. Firstly, the Gulf of Finland is considered infeasible for design, while the Bothnian Sea South is considered feasible for design. This is based on a preliminary assessment of ice-mitigating measures, presented in Section 6.6. Secondly, it is assumed that design is possible for all water depths in the Danish Straits, as ice & wave conditions are worse for the Baltic Proper South, yet this region was shown to be feasible for design. Thirdly, the Gulf of Riga was deemed feasible for intermediate positions as it has similar (mild) wave conditions and interaction days as the Gulf of Finland, but almost half the ice thickness. Finally, it is assumed that the intermediate deep position for the Bothnian Sea North is infeasible for design as ice conditions are significantly worse than in its Southern counter part, where the feasibility of the design is already questionable.

Table 6.3: Increased weight in percent point for a monopile within a specific region as well as feasibility of monopiles in the Baltic Sea for shallow (25 m), intermediate (35 m) and deep water position (45 m). The colors indicate green - feasible, yellow - inconclusive, red - infeasible and gray - unknown. The letters indicate DS - Danish Straits, BPS - Baltic Proper South, BPS - Baltic Proper South, GOR - Gulf of Riga, GOF - Gulf of Finland, ARS - Archipelago Sea, BSS - Bothnian Sea South, BSN - Bothnian Sea North, BOB - Bay of Bothnia.

	DS	BPS	BPN	GOR	GOF	ARS	BSS	BSN	BOB
SHALLOW	0			3		8			
INTERMEDIATE					13		10		42
DEEP		0	2				9	17	

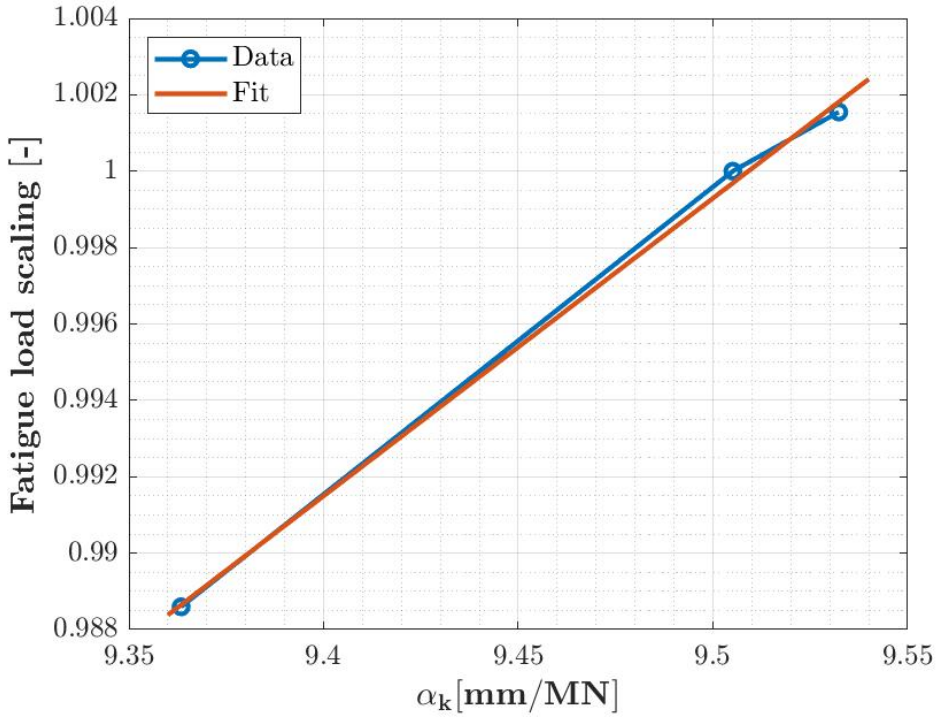

Figure 6.14: Fatigue scaling versus the flexibility parameter α_k.

6.5.1 Flexibility sensitivity

In this research the fatigue loads were assumed to scale linearly with the flexibility parameter α_k. This relation was also investigated by comparing fatigue damage for 3 monopiles with varying stiffness. The results are given in Figure 6.14. This indicates that fatigue loads do indeed scale with the flexibility parameter, however with only 3 data point it is difficult to distinguish if the relation is linear, thus more research is required.

6.6 ICE-MITIGATING MEASURES

In order to fully assess the feasibility of monopiles in the Baltic Sea under ice loading, it is necessary to discuss the mitigating measures or alternative substructures. This section discusses the ice cone as mitigating measures as well as the jacket & the GBS.

6.6.1 Ice cones

Ice cones are the most common ice-mitigating measure. The inclined surface of the cones reduces the peak ice loads by changing the ice failure mode from crushing to bending, which

also reduce the effects of ice-induced vibrations. Note, the effects of ice-induced vibrations cannot be completely ignored as they can still occur if the ice break-up frequency matches the frequency of the structure [Wang et al., 2013]. However, ice cones have shown to significantly reduce the measured ice loads [Brown and Määttänen, 2009].

Steel

It is possible to make a crude estimate around the additional cost required to include an ice cone. By comparing this to the previously designed monopiles this can indicate whether it is economically feasible to design a monopile *with* or *without* ice cone in each region.

To calculate the cost of an ice cone, its geometry has to be determined. Previous literature on cones in the Baltic Sea has considered cone angles in in the range of 50–65°, cone heights of 5–6 m and a wall thickness around 25 mm [Gravesen et al., 2005; Rissanen and Heinonen, 2016]. This corresponds to about 80 to 120 t of steel, assuming a density of 7850 kg/m^3 , and including 25% additional steel, such as internal stiffeners.

However, integrating an ice cone is not as straightforward as simply adding the amount of steel. A multitude of factors need to be considered. Firstly, the fabrication of conical steel section is more tedious than cylindrical sections. This is normally accounted for in the industry by a cost factor of 1.1 for conical steel.

The second factor is the transport & assembly of the ice cones. If the assembly is done prior to installation it might increase cost of transport of monopiles as they can be transported less efficiently. If the assembly is performed after the installation, the cones need to be transported on a separate barge and the assembly is done offshore, which is very labour-intensive and leads to increased costs [Zhu et al., 2021]. Little data is available on the additional cost for transport and assembly of ice cones. However, the additional costs are quantified in terms of steel for the ice cone by another factor of 1.2.

The third, and potentially most vital, factor which has to be considered is the increase in hydrodynamic loads due to an increased diameter at the waterline. The current generation of monopiles has seen a large increase in diameters. Further increasing this will draw very large loads to the monopile as the inertia contribution of the wave-load is related to the diameter squared.

For the ice cones described before, the diameter would be in the range of 12–18 m. To mitigate the hydrodynamic loading, a downward-facing cone could be installed, which ensures the largest diameter is above the waterline, illustrated by Figure 6.15b. An alternative solution is an up-downward cone, shown in Figure 6.15a, which reduces the maximum diameter at the waterline and is shown to have the best performance under wave-loading [Tang et al., 2021]. Additionally, the up-downward cone requires less steel. However, fabrication and installation cost will most likely increase due to the complexity of the cone.

Assuming that the increased weight of the monopile due to the hydrodynamic loads on the cone is around 2% of the foundation weight, the total additional steel required for a monopile design *with* ice cone is in the range of 150–200 t.

Figure 6.16 shows the feasibility map for monopiles *without* ice cones, thus including a maximum weight increase constraint of 175 t. The map shows that the Bay of Bothnia and the Bothnian Sea South are infeasible for monopiles. The Gulf of Finland also exceeds this threshold, however, it is very close and the observed weight increase of approximately 190 t actually falls within the range of additional steel due to the ice cone. Further research into the implications of an ice cone on monopile design is therefore required for conclusive results.

Cost

The extra steel required for designing in (sub-)arctic conditions increases the total cost as well as the CO_2 emissions of the project. The additional financial and environmental cost due to the inclusion of ice loading into the design of a monopile is given by Figure 6.17a. Figure 6.17b is

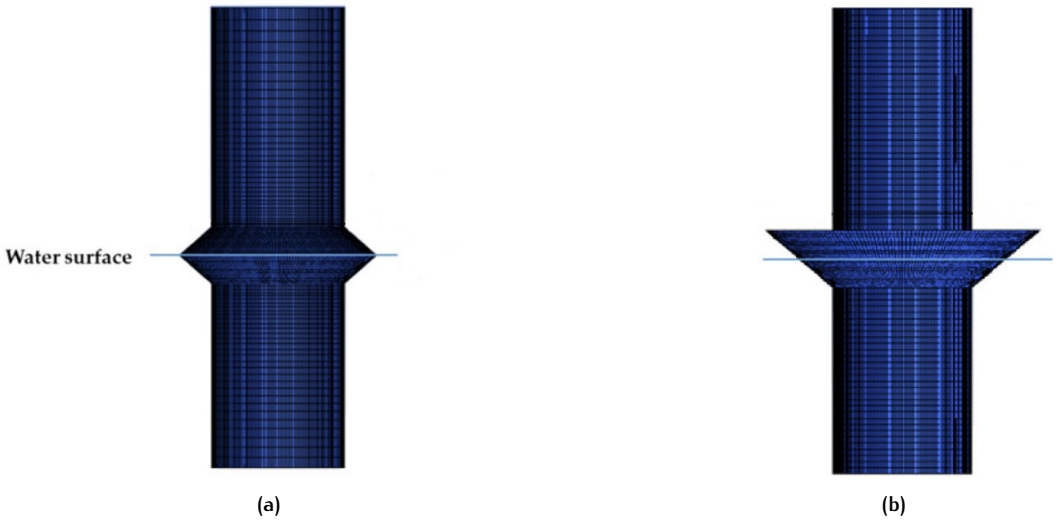

Figure 6.15: Ice breaking cone configurations: (a) up-downward cone; (b) downward cone [Tang et al., 2021].

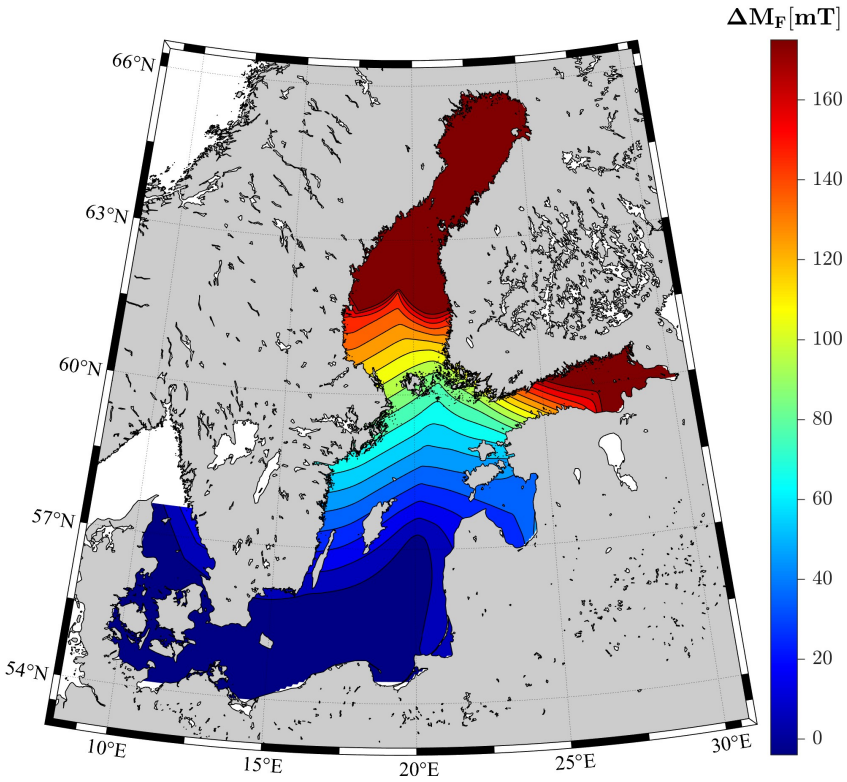

Figure 6.16: Weight increase in t for monopiles design in the Baltic Sea when ice loading is included. The dark red signifies that the threshold of 175 t is exceeded, which indicates that an ice cone design is more efficient.

an indication of the costs gained or lost by implementing an ice cone into the final design. The calculation assumed a cost of steel of €2000/t and an associated emission of 1.97 t CO_2/t steel [Sandberg et al., 2001]. Substantial costs can be saved by including ice-mitigating measures or alternative substructures in the Bay of Bothnia and the Bothnian Sea North. This conclusion is supported by the only existing wind farm in the Bay of Bothnia, Ajos, which made artificial islands for each individual turbine [OX2, 2021].

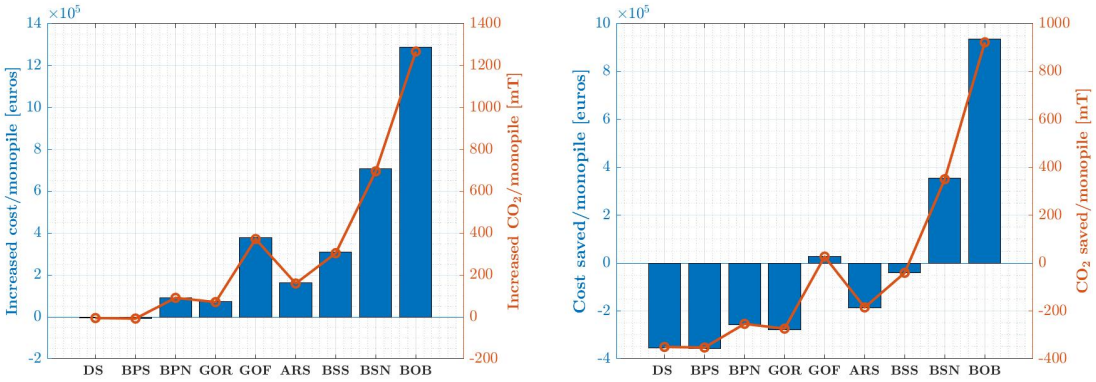

Figure 6.17: Financial and environmental cost of designing monopiles in the Baltic Sea: (a) Increased cost due to ice loading; (b) Cost saved due to ice cone. The letters indicate DS - Danish Straits, BPS - Baltic Proper South, BPS - Baltic Proper South, GOR - Gulf of Riga, GOF - Gulf of Finland, ARS - Archipelago Sea, BSS - Bothnian Sea South, BSN - Bothnian Sea North, BOB - Bay of Bothnia.

Figure 6.17b also shows that the Gulf of Finland and the Bothnian Sea South are close to breaking even. Hence, developers should always consider alternative options during development in these regions.

6.6.2 Alternative substructures

The current research has focused on the monopile as substructure for OWTs due to its simplicity in both design and installation (often) resulting in the lowest LCOE. However, alternative fixed substructures could also be considered for many of the identified regions. Two will be discussed here, namely the jacket and the GBS.

Jacket structure

For inclined structures the threshold angle for ice failing in crushing instead of bending is between 70 and 110°, meaning that the ice will fail in crushing if the angle between the incoming ice sheet and the structure lies within this range [Hoek, 2021]. The legs of a jacket, despite having a slight incline, fall within in this range and the governing failure mode of the ice will still be crushing. This means the structure will still be subject to substantial loads. Regular jackets include bracing in the waterline, which increases the ice loading on the structure. However, the omission of bracing at the waterline is unfavourable due to design and fabrication complexity, less redundancy and thicker jacket legs. Hence recent research has focused on designing jackets in ice conditions, while keeping the braces in the waterline, which was deemed feasible [Hoek, 2021].

It should be noted that this research focused on the ULS of the jackets, rather than the FLS. The current research suggests that as the ice interaction days increase throughout the Baltic regions, the fatigue damage becomes driving for design. The effect of this should be investigated, as the tubular joints of jackets are very susceptible to fatigue damage [Zhang et al., 2018; Li et al., 2008]. On the other hand the global ice load will be reduced due to the shielding effect of the legs, while the negative effects of jamming — accumulation of ice between adjacent members/legs — are less significant due to the size of the next generation OWT substructures Huang et al. [2007]; Hoek [2021].

Further research is required to assess the feasibility of jackets in the Baltic Sea, however, it is expected that the fatigue of the tubular joints will be the main concern.

Gravity Based Structure

The GBS is often suggested as foundation for OWTs in (sub-)arctic conditions, as it is easy to manufacture with an inclined ice-structure interface and is known to resist very high ice-loads [Anku-Vinyoh et al., 2021].

In terms of ice resistance the GBS will be sufficient for all occurring ice loading in the Baltic Sea as it has proven itself in more extreme conditions [Li et al., 2015]. Another advantage of the GBS is its relative ease of fabrication and installation [Esteban et al., 2019]. The crucial aspect for the feasibility of the GBS is the economics of the substructure, especially when deeper waters are concerned. In the offshore wind sector GBS are found up to 20 m of water depth, but usually are only considered for water depths less than 10 m. For deeper locations the increased costs lead to noncompetitive designs compared to the monopile [Esteban et al., 2019]. However, based on the current research this might not be the case under extreme ice conditions, as the monopile design increases drastically in price.

7 CONCLUSION

The aim of the present research was to develop a feasibility map for monopiles in the Baltic Sea. The research was split into three parts, each necessary for producing the feasibility map. This chapter provides the conclusions, limitations & recommendations of each of these parts and answers the research question:

Where in the Baltic Sea is it feasible to install monopiles without ice-mitigating measures?

7.1 PART I

The first step in defining the feasibility map was the analysis of metocean data of the Baltic Sea in order to answer the following question:

Which characteristic regions can be identified in the Baltic Sea based on metocean conditions and what are the representative metocean conditions in these regions?

In Part I the following nine characteristic regions were identified: the Danish Straits, the Baltic Proper South, the Baltic Proper North, the Gulf of Riga, the Gulf of Finland, the Archipelago Sea, the Bothnian Sea South, the Bothnian Sea North and the Bay of Bothnia. The minimum and maximum reported 50-year extreme ice thickness were 0.40 and 1.25 m in the Danish Straits and the Bay of Bothnia, respectively. The corresponding 1-year extreme crushing coefficients for these regions were 0.86 and 0.98 MPa. Two methods to determine the ridge action were presented, one based on the design standards and one based on the literature, as the design standard was assumed to be overly conservative for regions other than the Bay of Bothnia.

A major issue surrounding the ice conditions in the Baltic Sea is the lack of data. In most regions, other than the Bay of Bothnia, the occurrence of ice is not as frequent. Especially in the Southern parts of the Baltic Sea, where ice seasons are so infrequent that little data are available and therefore data from more extreme regions have to be scaled. During the derivation or scaling of such parameters, the research aimed to be conservative. This was the case for the ice thickness calculation (snow cover neglected), the ice thickness scaling (ω & l_{ice}), the C_R (salinity neglected), the ice direction and the ice interaction days.

Despite these efforts, it is difficult to determine whether the chosen values were *actually* conservative without data. Further research is required to accurately determine the ice conditions in the Baltic Sea, outside the extreme regions. Furthermore, the current velocity and soil profiles were kept constant between the regions. The former does not greatly affect the results, but the latter can have tremendous effects on monopile design and should be thoroughly investigated for each region. Finally, the ice drift speed was determined using a wind factor model. More sophisticated models can be applied as the wind factor model most likely underestimates the drift velocity at low wind speeds, since the contribution of the current to the forcing is neglected.

7.2 PART II

In Part II of the research VANILLA was coupled to both MORPHEUS and HAWC2. Due to the stochastic nature of ice failure, a verification based on statistical measures was performed. This

showed that the model was in great agreement, except when higher ice drift velocities were simulated, which resulted in an overestimation of the maximum structural velocity. The reason for this is likely the event detection of the VANILLA which may miss events — ice element failures — in the first time step, thus leaving too much energy in the system. At higher velocities more ice element failures occur and as a result more may be missed. Hence, a smaller time step was shown to reduce this error, substantially.

No increased accuracy was observed when the generalized-α procedure was applied iteratively. Due to the aforementioned event detection flaw and the stochastic nature of the ice failure, the solutions always diverge slightly. This was also the reason for verification based on statistical measures.

For the coupling to HAWC2 a TCP/IP link was used, which allows for MATLAB and HAWC2 to run stand-alone. As a result minimal changes were required to the existing codes, but fully coupled aero-elastic ice-structure interaction simulations could be run. The coupled model is computationally expensive due to the small required time step for ice crushing. Further research into the reduction of computational time could prove very useful. A potential solution could be the use of a reduced structural model, or superelement, which splits the structure into boundary and interface nodes. The use of a superelement is already possible for the MORPHEUS/VANILLA model, but more development is required for the superelement coupling of HAWC2 and VANILLA.

7.3 PART III

In Part III the methodology for the generation of the feasibility map was presented and executed in order to answer the research question:

Where in the Baltic Sea is it feasible to install monopiles without ice-mitigating measures?

The results of this study showed that monopile designs without ice-mitigating measures were feasible both economically and technically in the Danish Straits, the Baltic Proper South, the Baltic Proper North, the Gulf of Riga and the Archipelago Sea. In contrast, designing monopiles in the Bothnian Sea North and the Bay of Bothnia without ice-mitigating measures led to very heavy designs. This was a result of the substantial increase in stiffness required to withstand the fatigue damage. Hence these regions were deemed infeasible for monopile design. Finally, monopile design in the Bothnian Sea South and Gulf of Finland is technically feasible without mitigating measures, yet the alternatives should be thoroughly investigated as the economic feasibility is questioned due to large weight increases. This was largely a result of the increase in fatigue damage from the ice loading.

The applied method in this research was to categorize the regions into three water depths — shallow (25 m), intermediate (35 m) & deep (45 m) — based on their bathymetry. Wind, wave and ice loads were generated for initial geometries in all regions. The load envelopes showed that in most regions ice loading was governing for the ULS of the foundations. The damage equivalent moment — used for FLS analysis — was also shown to be strongly correlated to the number of ice interaction days.

The load effect was subsequently investigated by generating monopile designs for both the reference case consisting of only the wind & wave loads, and the ice case consisting of wind, wave & ice loads. The results showed little to no weight increase for the Danish Straits (0%), the Baltic Proper South (0%), the Baltic Proper North (2%) and the Gulf of Riga (3%).

In the Bothnian Sea North and the Bay of Bothnia, the fatigue loads in the top of the foundation were so large that a significant increase in stiffness was required to satisfy the design & fabrication constraints. The resulting UR plots showed that the stiffness constraint governed the bottom half, effectively punishing this section of the foundation in order to resist the fatigue damage in the top half. As a result the weight of the designs increased by 17 and 42% for the Bothnian Sea North and the Bay of Bothnia, respectively.

Monopiles in the Archipelago Sea, the Bothnian Sea South and the Gulf of Finland showed a larger increase in weight, around 8%, 10% and 17%, respectively. All three designs satisfied all fabrication constraints and are technically feasible. However, the economic feasibility is questionable. The former of the three is considered feasible as the weight increase is below 10% and due to the shallow position relatively small in absolute weight increase. Further analysis is required to assess the feasibility of monopiles in the other two regions, as it strongly depends on the cost of the ice-mitigating measures.

One such a measure is the installation of an ice cone, as it reduces the ice loading by changing the ice failure mode from crushing to bending. A preliminary estimate of the additional cost for an ice cone, in terms of steel, ranges between 150–200 t. Though, care should be taken with an ice cone design as the additional diameter in the waterline may have very detrimental effects on the overall design. Hence a more thorough research in the behaviour — and specifically the hydrodynamic performance — of monopiles fitted with ice cones is required.

Other ice-mitigating measures include considering an alternative substructure such as a jacket substructure or a GBS. Since the current research shows that fatigue is the limiting factor for design, the jacket structure is suspected to be too vulnerable due to its tubular joints. A GBS can most certainly be designed to withstand ice loading, however, existing GBSs for OWT are in the range of 5–20 m water depth. Due to the size of these foundations, economic feasibility of this substructure needs to be investigated as the costs drastically increase with water depth.

Two different methods to assess the ridge action were applied, one based on ridge literature and one based on the design standards, which was larger in each region. The larger ridge actions were shown only to impact the design slightly (< 2% weight increase). The affected regions were the Gulf of Riga, the Gulf of Finland and the Archipelago Sea. The regions were either shallow or intermediate and also showed relatively mild wave conditions. As a result the ULS ridge DLC had more impact on design in these regions, but not significantly.

Overall the increase in fatigue damage due to ice loading was the governing factor for design in most regions. For all regions, investigation of the individual simulations showed that the fatigue damage due to ice was largely a result of the simulations involving FLI, which led to the large structural vibrations, which was especially detrimental to the design of the transition piece and the top of the monopile.

For the Bothnian Sea South another water depth was simulated. This showed that the deeper positions, showed a similar relative weight increase. However, since the foundations are closer to the installation constraint this will likely limit the design of monopiles for deeper water in these region. However, further research should investigate this relation for each specific region.

In addition, recommendations for further research include a diameter sensitivity analysis for the design positions. This study did not change the diameter between the reference case and the ice case, but doing so might provide the necessary stiffness more efficiently, i.e. use less steel. Other limitations include — amongst others — the soil conditions, which were kept constant for each region, the selection of a subset of wind & wave DLCs and the assumed one-directionality of the ice. Further research could build on the current work by investigating the effect of each listed limitation. The large scope of the thesis forced the research to limit these parameters, but inclusion will improve the quality of the findings.

BIBLIOGRAPHY

Anku-Vinyoh, J., Oja, S., Ajosmäki, A., Sjölund, J., Hübler, M., Ferrer Mur, S., Kaschube, D., Erdem, C., and Knüppel, P. (2021). Gravity base foundation concept for a platform in icy shallow waters. In *A Holistic Approach to Ship Design*, pages 285–326. Springer.

Badger, J., Hahmann, A., Larsén, X. G., Badger, M., Kelly, M., Olsen, B. T., and Mortensen, N. G. (2015). The global wind atlas: An eudp project carried out by dtu wind energy.

Barahona, B., Adersen, P., Hansen, A. D., Cutululis, N. A., and Sørensen, P. (2009). Integrated design of wind power systems: Matlabhawc2 interface. In *50th International Conference of Scandinavian Simulation Society (SIMS 50)*, pages 107–113.

Bosch, J., Staffell, I., and Hawkes, A. D. (2019). Global levelised cost of electricity from offshore wind. *Energy*, 189:116357.

Brown, T. G. and Määttänen, M. (2009). Comparison of kemi-i and confederation bridge cone ice load measurement results. *Cold Regions Science and Technology*, 55(1):3–13.

Chung, J. and Hulbert, G. (1993). A time integration algorithm for structural dynamics with improved numerical dissipation: the generalized-α method.

Croasdale, K. (1984). The limiting driving force approach to ice loads. In *Offshore Technology Conference*. OnePetro.

DEME (2022). Monopile installation completed at arcadis ost 1 offshore wind farm. URL: https://www.deme-group.com/news/monopile-installation-completed-arcadis-ost-1-offshore-wind-farm.

Det Norske Veritas AS (2013). Icestruct jip guideline: Ice actions and actions effects on offshore structures. *Geneva: ISO*.

DNV GL (2016). Loads and site conditions for wind turbines. *DNVGL-ST-0437*.

Esteban, M. D., Diez, J. J., López, J. S., and Negro, V. (2011). Why offshore wind energy? *Renewable energy*, 36(2):444–450.

Esteban, M. D., López-Gutiérrez, J.-S., and Negro, V. (2019). Gravity-based foundations in the offshore wind sector. *Journal of Marine Science and Engineering*, 7(3):64.

European Commission and Directorate-General for Energy (2019). *Study on Baltic offshore wind energy cooperation under BEMIP : final report*. Publications Office.

Finance, B. N. E. (2017). 1h 2017 offshore wind energy market outlook.

Garzon, B. B., Henriksen, L. C., Hansen, A. D., Cutululis, N. A., and Sørensen, P. E. (2010). Coupling of hawc2 and matlab: Towards an integrated simulation platform. In *2010 European Wind Energy Conference and Exhibition*. European Wind Energy Association (EWEA).

Granskog, M., Kaartokallio, H., Kuosa, H., Thomas, D. N., and Vainio, J. (2006). Sea ice in the baltic sea–a review. *Estuarine, Coastal and Shelf Science*, 70(1-2):145–160.

Gravesen, H. and Kärnä, T. (2009). Ice loads for offshore wind turbines in southern baltic sea. In *Proceedings of the International Conference on Port and Ocean Engineering Under Arctic Conditions*, number POAC9-3.

Gravesen, H., Sørensen, S. L., Vølund, P., Barker, A., and Timco, G. (2005). Ice loading on danish wind turbines: Part 2. analyses of dynamic model test results. *Cold regions science and technology*, 41(1):25–47.

Hammer, T., Owen, C., van den Berg, M., and Hendrikse, H. (2022). Classification of ice-induced vibration regimes of offshore wind turbines. In *Proceedings of the ASME 2022 41st International Conference on Ocean, Offshore and Arctic Engineering*.

Heinonen, J. (2004). Constitutive modelling of ice rubble in first-year ridge keel. Master's thesis, Helsinki University of Technology.

Hendrikse, H. (2017). *Ice-induced vibrations of vertically sided offshore structures*. PhD thesis, Delft University of Technology.

Hendrikse, H. (2020). Ice strength coefficient c_R. *Informal paper*.

Hendrikse, H. and Koot, J. (2019). Consideration of ice drift in determining the contribution of ice-induced vibrations to structural fatigue. In *Proc. 25th International Conference on Port and Ocean engineering under Arctic Conditions, Delft, The Netherlands*.

Hendrikse, H. and Metrikine, A. (2016). Ice-induced vibrations and ice buckling. *Cold Regions Science and Technology*, 131:129–141.

Hendrikse, H. and Nord, T. S. (2019). Dynamic response of an offshore structure interacting with an ice floe failing in crushing. *Marine Structures*, 65:271–290.

Hendrikse, H., Ziemer, G., and Owen, C. (2018). Experimental validation of a model for prediction of dynamic ice-structure interaction. *Cold Regions Science and Technology*, 151:345–358.

Hoek, J. (2021). Dynamic ice-structure interaction for jacket substructures. Master's thesis, Delft University of Technology.

Hornnes, V., Hammer, T., Høyland, K. V., Hendrikse, H., and Turner, J. (2022). On the use of drift ice thickness statistics from a copernicus reanalysis product for fatigue damage calculation. In *Proceedings of the 26th IAHR International Symposium on Ice*.

Hornnes, V., Høyland, K. V., Turner, J. D., Gedikli, E. D., and Bjerkås, M. (2020). Combined distribution of ice thickness and speed based on local measurements at the norströmsgrund lighthouse 2000-2003. In *PROCEEDINGS OF THE 25th INTERNATIONAL SYMPOSIUM ON ICE Trondheim, Norway, 23rd–25th November 2020*. The International Association for Hydro-Environment Engineering and Research ....

Huang, Y., Shi, Q., and Song, A. (2007). Model test study of the shielding effect of multi-pile structures on ice force. In *Proceedings of the International Conference on Port and Ocean Engineering Under Arctic Conditions*.

IEC (2019). Wind energy generation systems – part 3-1: Design requirements for fixed offshore wind turbines. *IEC 61400-3-1*.

ISO19906, I. (2018). Petroleum and natural gas industries–arctic offshore structures. *Geneva: ISO*.

Jevrejeva, S., Drabkin, V., Kostjukov, J., Lebedev, A., Leppäranta, M., Mironov, Y. U., Schmelzer, N., and Sztobryn, M. (2004). Baltic sea ice seasons in the twentieth century. *Climate research*, 25(3):217–227.

Jordaan, I. J. (2001). Mechanics of ice–structure interaction. *Engineering Fracture Mechanics*, 68(17-18):1923–1960.

Kalliosaari, S. and Seinä, A. (1987). Jäätalvet 1981–1985 suomen merialueilla. ice winters 1981–1985 along the finnish coast.

Krenk, S. (2009). *Non-linear modeling and analysis of solids and structures*. Cambridge University Press.

Larsen, T. J. and Hansen, A. M. (2007). *How 2 HAWC2, the user's manual*. Risø National Laboratory.

Larsen, T. J., Madsen, H. A., Hansen, A. M., and Thomsen, K. (2005). Investigations of stability effects of an offshore wind turbine using the new aeroelastic code hawc2. *Proceedings of Copenhagen Offshore Wind 2005, Copenhagen, Denmark*, pages 25–28.

Leppäranta, M. (1981). An ice drift model for the baltic sea. *Tellus*, 33(6):583–593.

Leppäranta, M. (1993). A review of analytical models of sea-ice growth. *Atmosphere-Ocean*, 31(1):123–138.

Leppäranta, M. and Hakala, R. (1992). The structure and strength of first-year ice ridges in the baltic sea. *Cold Regions Science and Technology*, 20(3):295–311.

Leppäranta, M. and Omstedt, A. (1990). Dynamic coupling of sea ice and water for an ice field with free boundaries. *Tellus A: Dynamic Meteorology and Oceanography*, 42(4):482–495.

Li, G., Liu, X., Liu, Y., and Yue, Q. (2008). Optimum design of ice-resistant offshore jacket platforms in the bohai gulf in consideration of fatigue life of tubular joints. *Ocean engineering*, 35(5-6):484–493.

Li, H., Dang, X., Zhu, K., and Ni, Y. (2015). Review and outlook on arctic offshore facilities & technologies. In *OTC Arctic Technology Conference 2015*, pages 777–800.

Lilover, M.-J., Pavelson, J., Kõuts, T., Lepparanta, M., et al. (2018). Characteristics of high-resolution sea ice dynamics in the gulf of finland, baltic sea. *Boreal Environment Research*.

Lu, W., Lubbad, R., and Løset, S. (2015). In-plane fracture of an ice floe: A theoretical study on the splitting failure mode. *Cold Regions Science and Technology*, 110:77–101.

Nielsen, M. B., Hindhede, D., Palmer, M., and Thilsted, C. L. (2022). A highly efficient and rapid cost-optimization framework for offshore wind turbine foundations for an entire windfarm site (submitted). In *Proceedings of ASME 2022 International Offshore Wind Technical Conference (IOWTC2022)*, Boston, Massachusetts.

OX2 (2021). Ajos.

Rissanen, S. and Heinonen, J. (2016). Simulations of drifting sea ice loads on offshore wind turbine. *Winterwind 2016*, 1(1):p1–19.

Ronkainen, I., Lehtiranta, J., Lensu, M., Rinne, E., Haapala, J., and Haas, C. (2018). Interannual sea ice thickness variability in the bay of bothnia. *The Cryosphere*, 12(11):3459–3476.

Sandberg, H., Lagneborg, R., Lindblad, B., Axelsson, H., and Bentell, L. (2001). Co2 emissions of the swedish steel industry. *Scandinavian journal of metallurgy*, 30(6):420–425.

Singh, S., Timco, G., Frederking, R., and Jordaan, I. (1990). Tests of ice crushing on a flexible structure. In *Proc. 9th OMAE Conf. Houston*, volume 4, pages 89–94.

Sodhi, D. S. (2001). Crushing failure during ice–structure interaction. *Engineering Fracture Mechanics*, 68(17-18):1889–1921.

Stefan, J. (1891). Über die theorie der eisbildung, insbesondere über die eisbildung im polarmeere. *Annalen der Physik*, 278(2):269–286.

Tang, Y., Shi, W., You, J., and Michailides, C. (2021). Effects of nonlinear wave loads on large monopile offshore wind turbines with and without ice-breaking cone configuration. *Journal of Marine Science and Technology*, 26(1):37–53.

The Crown Estate (2017). Offshore wind operational report. URL: https://www.thecrownestate.co.uk/media/2400/offshore-wind-operational-report_digital.pdf.

Thijssen, J., Fuglem, M., and Ralph, F. (2019). Level ice crushing pressures for estimating mooring loads. In *Proceedings of the 25th International Conference on Port and Ocean Engineering under Arctic Conditions (POAC)*, pages 9–13.

Tin, T. and Jeffries, M. O. (2003). Morphology of deformed first-year sea ice features in the southern ocean. *Cold regions science and technology*, 36(1-3):141–163.

van der Stap, F. (2022). Ice-structure interaction in the baltic sea: Identifying characteristic regions based on metocean conditions. Literature review, Delft University of Technology.

Voigt, T., Füssel, H.-M., Gärtner-Roer, I., Huggel, C., Marty, C., and Zemp, M. (2010). Impacts of climate change on snow, ice, and permafrost in europe: Observed trends, future projections, and socio-economic relevance. *ETC/ACC Technical Paper*, 13:1–117.

Wang, S., Yue, Q., and Zhang, D. (2013). Ice-induced non-structure vibration reduction of jacket platforms with isolation cone system. *Ocean engineering*, 70:118–123.

WindEurope (2020). *Offshore Wind in Europe Key trends and statistics 2020*.

Wood, W., Bossak, M., and Zienkiewicz, O. (1980). An alpha modification of newmark's method. *International journal for numerical methods in engineering*, 15(10):1562–1566.

Wu, X., Hu, Y., Li, Y., Yang, J., Duan, L., Wang, T., Adcock, T., Jiang, Z., Gao, Z., Lin, Z., et al. (2019). Foundations of offshore wind turbines: A review. *Renewable and Sustainable Energy Reviews*, 104:379–393.

Yue, Q., Bi, X., Zhang, X., and Karna, T. (2002). Dynamic ice forces caused by crushing failure. In *Proc. 16 IAHR Int. Symp. on Ice. Dunedin, New Zealand*, pages 134–141.

Zhang, D., Wang, G., and Yue, Q. (2018). Evaluation of ice-induced fatigue life for a vertical offshore structure in the bohai sea. *Cold Regions Science and Technology*, 154:103–110.

Zhu, B., Sun, C., and Jahangiri, V. (2021). Characterizing and mitigating ice-induced vibration of monopile offshore wind turbines. *Ocean Engineering*, 219:108406.

A ADDITIONAL FIGURES AND TABLES

This appendix consists of Figures to further clarify specific topics, but were excluded from the main text for brevity.

A.1 METOCEAN CONDITIONS

For the ice thickness scaling additional figures were used to find the correct scale factors. Figure A.1 and Figure A.2 were used as they provide ice charts at maximum ice extent in the severe ice winters of 1984–1985 and 1986–1987, respectively. The final empirical values were then found and presented in Section 2.1.1.

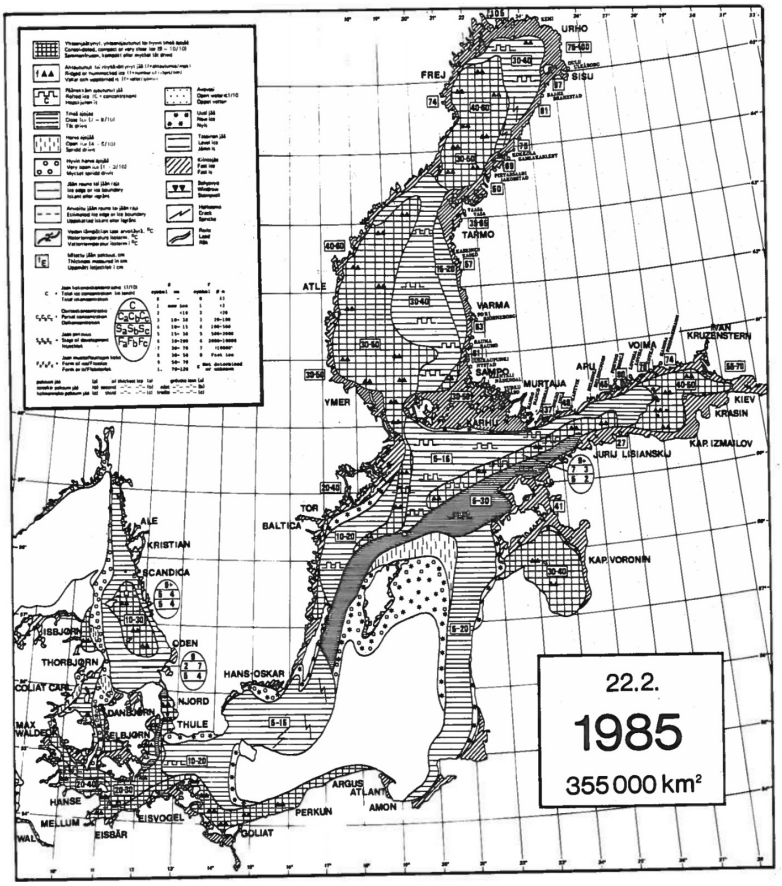

Figure A.1: Maximum ice extent of the Baltic Sea in the extremely severe ice winter 1984–1985 [Kalliosaari and Seinä, 1987].

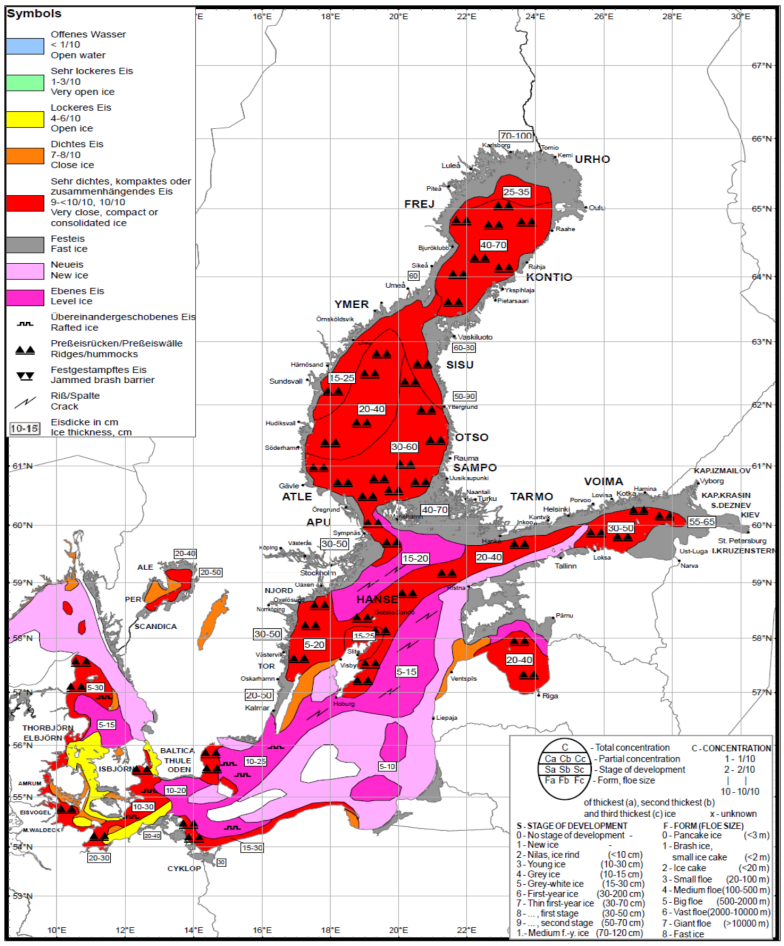

Figure A.2: Maximum ice extent of the Baltic Sea in the extremely severe ice winter 1986–1987 [Voigt et al., 2010].

Besides the ice charts, actual air temperature data were used for the ice thickness determination. Figure A.3 provides the location of all the weather stations around the Baltic Sea which were used for determining the ice thickness based on air temperature data sets.

In Section 2.2 a method was proposed for finding the correct ice crushing coefficient. For design the worst possible combination of ice thickness and ice crushing coefficient for once in 50 years should be considered. This could be the 1-year maximum thickness with the 50 year ice strength coefficient or vice versa. But other options, e.g. the 2- or 5-year ice maximum with the 25- or 10-year crushing coefficient, should also be considered. For clarity Figure A.4 shows the crushing coefficient corresponding to a 50 year ice event.

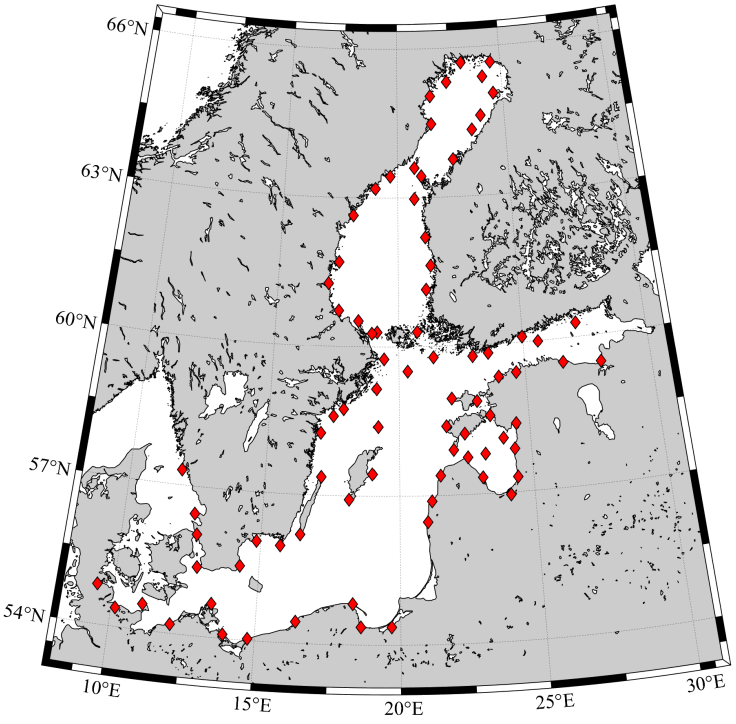

Figure A.3: Location of weather stations around the Baltic Sea with available air temperature data sets.

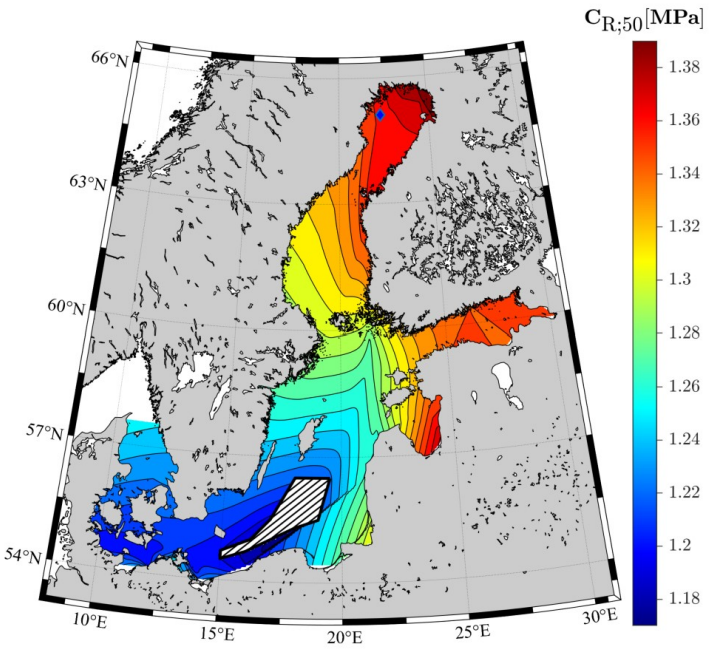

Figure A.4: Inter-regional variability of the annual maximum crushing coefficient, $C_{R;50}$, in the Baltic Sea. The diamond marker depicts the reference location.

Section 2.3 discussed the impact of bathymetry for design both for the landfast ice formation and for overall monopile design. Figure A.5 and Figure A.6 give the bathymetry plots for the Baltic Sea with a limit at either 15 or 65 m. The first serves as indication for the landfast ice region, the second as indication for possible monopile locations.

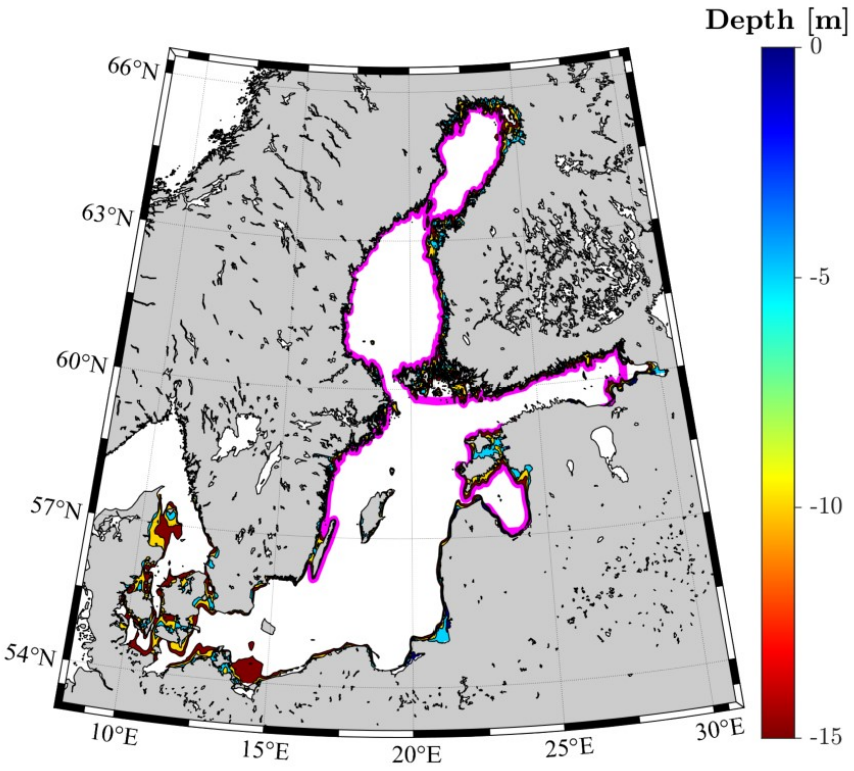

Figure A.5: Baltic Sea bathymetry up to depth of 15 m. The boundary for the landfast ice zone, in magenta, is largely defined by the 15 m isobath with adjustments based on observations from ice charts.

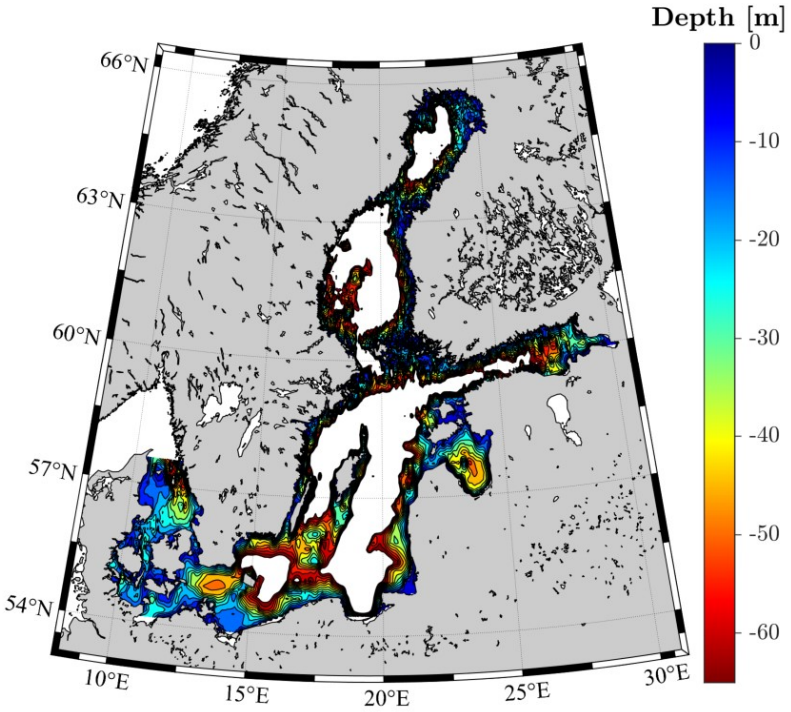

Figure A.6: Baltic Sea bathymetry up to depth of 65 m. Current industry standard for monopiles is up to 65 m, thus the map provides locations which can be considered for monopile design.

For each region an ice thickness-velocity distribution table was generated as discussed in Section 2.5. Table A.1 provides an example of such an ice thickness-velocity distribution table, which is used to find the the probability of each ice state, p_{ice}.

Table A.1: Ice thickness and velocity distribution for probability of individual ice states for Danish Straits. The probability of each ice state, p_{ice}, is determined as the product of the probability of the specific wind/ice speed and the probability of occurrence of the specific ice thickness, 35, 50 and 15% in this case.

v_{wind} [m s^{-1}] at hub height	v_{wind} [m s^{-1}] at 10 m	v_{ice} [m s^{-1}]	p_{wind} [%]	Ice thickness	0.2 m p_{ice} [%]	0.3 m p_{ice} [%]	0.4 m p_{ice} [%]
1	0.68	0.01	1.45%		0.51%	0.73%	0.22%
2	1.37	0.03	2.95%		1.03%	1.48%	0.44%
3	2.05	0.04	3.80%		1.33%	1.90%	0.57%
4	2.74	0.05	4.43%		1.55%	2.21%	0.66%
5	3.42	0.07	4.96%		1.74%	2.48%	0.74%
6	4.11	0.08	5.38%		1.88%	2.69%	0.81%
8	5.48	0.11	11.58%		4.05%	5.79%	1.74%
10	6.84	0.14	12.43%		4.35%	6.22%	1.87%
12	8.21	0.16	13.13%		4.59%	6.56%	1.97%
14	9.58	0.19	12.68%		4.44%	6.34%	1.90%
16	10.95	0.22	10.56%		3.70%	5.28%	1.58%
18	12.32	0.25	7.50%		2.63%	3.75%	1.13%
20	13.69	0.27	4.40%		1.54%	2.20%	0.66%
22	15.06	0.30	2.52%		0.88%	1.26%	0.38%
24	16.43	0.33	1.30%		0.46%	0.65%	0.20%
26	17.80	0.36	0.63%		0.22%	0.31%	0.09%
28	19.16	0.38	0.17%		0.06%	0.08%	0.03%
30	20.53	0.41	0.07%		0.03%	0.04%	0.01%
32	21.90	0.44	0.03%		0.01%	0.01%	0.00%
34	23.27	0.47	0.01%		0.00%	0.00%	0.00%
36	24.64	0.49	0.00%		0.00%	0.00%	0.00%
38	26.01	0.52	0.00%		0.00%	0.00%	0.00%
		Sum	100.00%	**Sum**	35.00%	50.00%	15.00%

In Section 2.6.2 a method was proposed to calculate the number of ice interaction days. Table A.2 gives the required input for the calculation of the number of ice interaction days in each region as well as the actual number of interaction days.

Table A.2: Ice season, probability of ice occurrence and ice interaction days for each characteristic region in the Baltic Sea. Note, the probability of ice occurrence listed here is the probability of ice forming at the coast, which should not be confused with the probability of ice forming in open waters.

Region	Ice season [days]	Ice occurrence [%]	Ice interaction [days/lifetime]
Danish Straits	44	43	9.6
Baltic Proper South	44	53	11.9
Baltic Proper North	75	73	73.3
Gulf of Riga	128	85	197.6
Gulf of Finland	134	80	198.0
Archipelago Sea	77	92	96.9
Bothnian Sea South	131	95	228.0
Bothnian Sea North	159	97	299.8
Bay of Bothnia	176	100	352.5

A.2 VERIFICATION

Table A.3 presents the verification of the MORPHEUS/VANILLA model for a flexible structure interacting with an ice thickness of 1.2 m.

Table A.3: Quantitative verification for each ice drift speed in mm s^{-1} against criteria 1-8 from Table 4.3 for a flexible structure with an ice thickness of 1.2 m thickness. Red indicates rejection of the value, given in percent point, and green indicates acceptance. Criteria 9-11 are verified in the second and third column, which present the predicted interaction regime from the stand-alone simulations (V) or from the MORPHEUS/VANILLA simulations (MV). CRP indicates creep, I - intermittent crushing, F - frequency lock-in and C - continuous brittle crushing.

v_{ice}	V	MV	1	2	3	4	5	6	7	8
0.1	CRP	CRP	0				0			
0.4	CRP	CRP	0				0			
0.7	CRP	CRP	0				0			
1	CRP	CRP	0				0			
4	I	I	1	1	0	0	1	2	1	1
7	I	I	1	0	0	1	1	1	1	0
10	I	I	1	1	0	1	1	1	1	2
20	I	I	1	0	0	0	1	1	1	1
30	I/F	I/F	1	0	0	50	1	1	0	0
40	I/F	F	1	1	0	17	1	1	5	6
50	F	F	1	1	1	0	1	1	1	2
60	F	F	1	0	0	0	1	0	1	6
70	F	F	0	0	0	0	0	2	0	4
80	F/C	F	1	1	1	21	1	3	5	6
90	C	C	1	1	1	10	1	1	0	5
100	C	C	2	1	5	56	2	4	14	8
110	C	C	1	0	0	0	1	2	1	2
120	C	C	1	1	1	4	1	0	0	9
130	C	C	1	1	5	427	1	3	8	14
140	C	C	3	3	13	60	3	9	23	43
150	C	C	3	4	15	37	3	11	32	89
160	C	C	3	4	15	40	3	11	34	97
170	C	C	0	0	1	3	0	1	3	8
180	C	C	1	1	2	0	1	1	5	40
190	C	C	0	0	1	0	1	1	6	46
200	C	C	0	0	1	3	1	1	6	54
300	C	C	0	0	1	2	0	0	8	111
400	C	C	1	1	0	1	0	0	9	124
500	C	C	0	0	0	26	0	0	13	206

A.3 LOADS

In Section 6.1 loads for the Danish Straits and the Bay of Bothnia are presented. For brevity the loads of the other regions were not included in the main text, but for clarity they are included here.

Figure A.7 shows the ULS load envelopes for monopiles in the various regions, while Figure A.8 shows the damage equivalent moment in the most unfavourable direction.

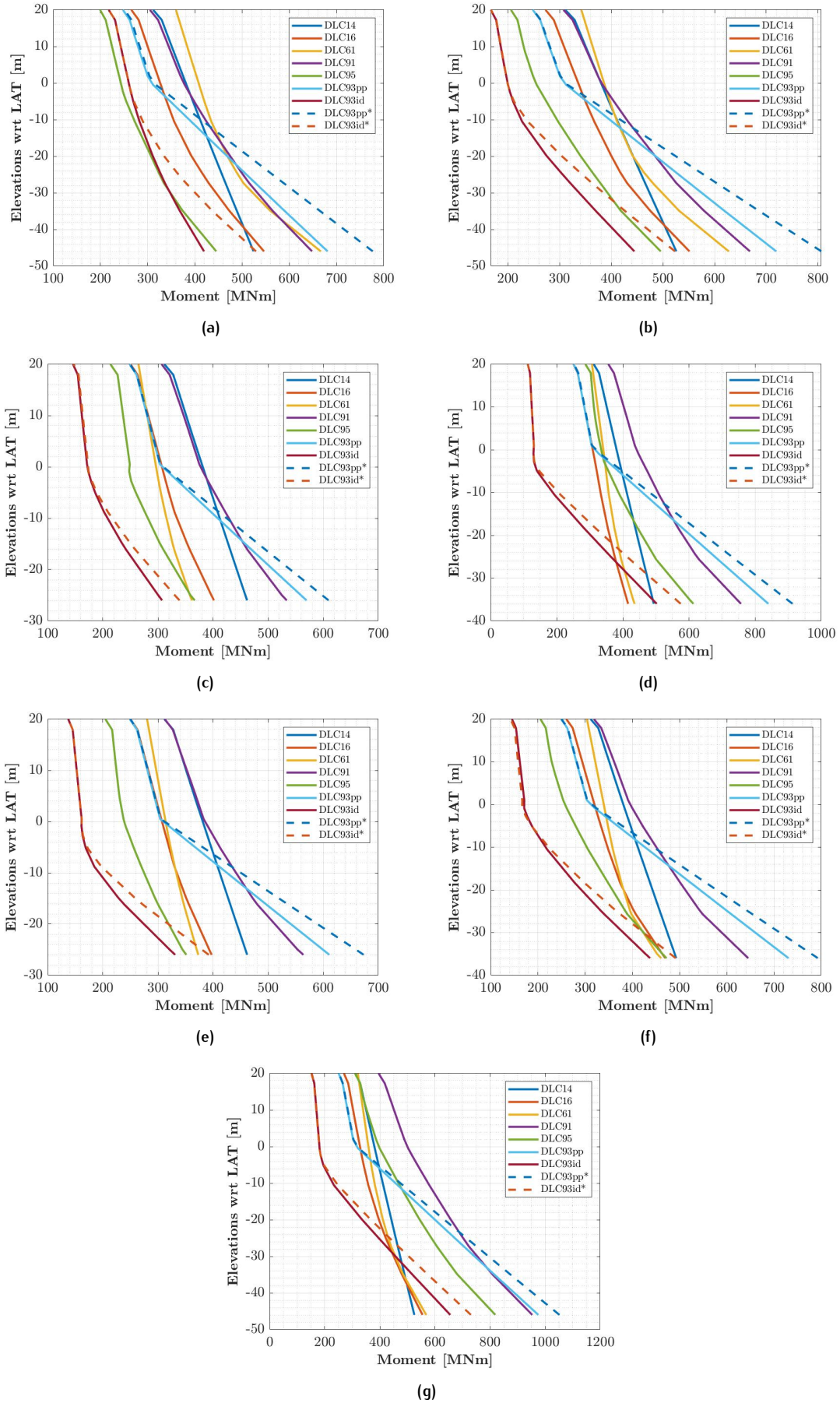

Figure A.7: Overturning moment load envelopes for (a) Baltic Proper South, (b) Baltic Proper North, (c) Gulf of Riga, (d) Gulf of Finland, (e) Archipelago Sea, (f) Bothnian Sea South and (g) Bothnian Sea North. For DLC9.3, “id" and “pp" indicate idling and power production, and the dashed line indicates the ridge action according to the design standards.

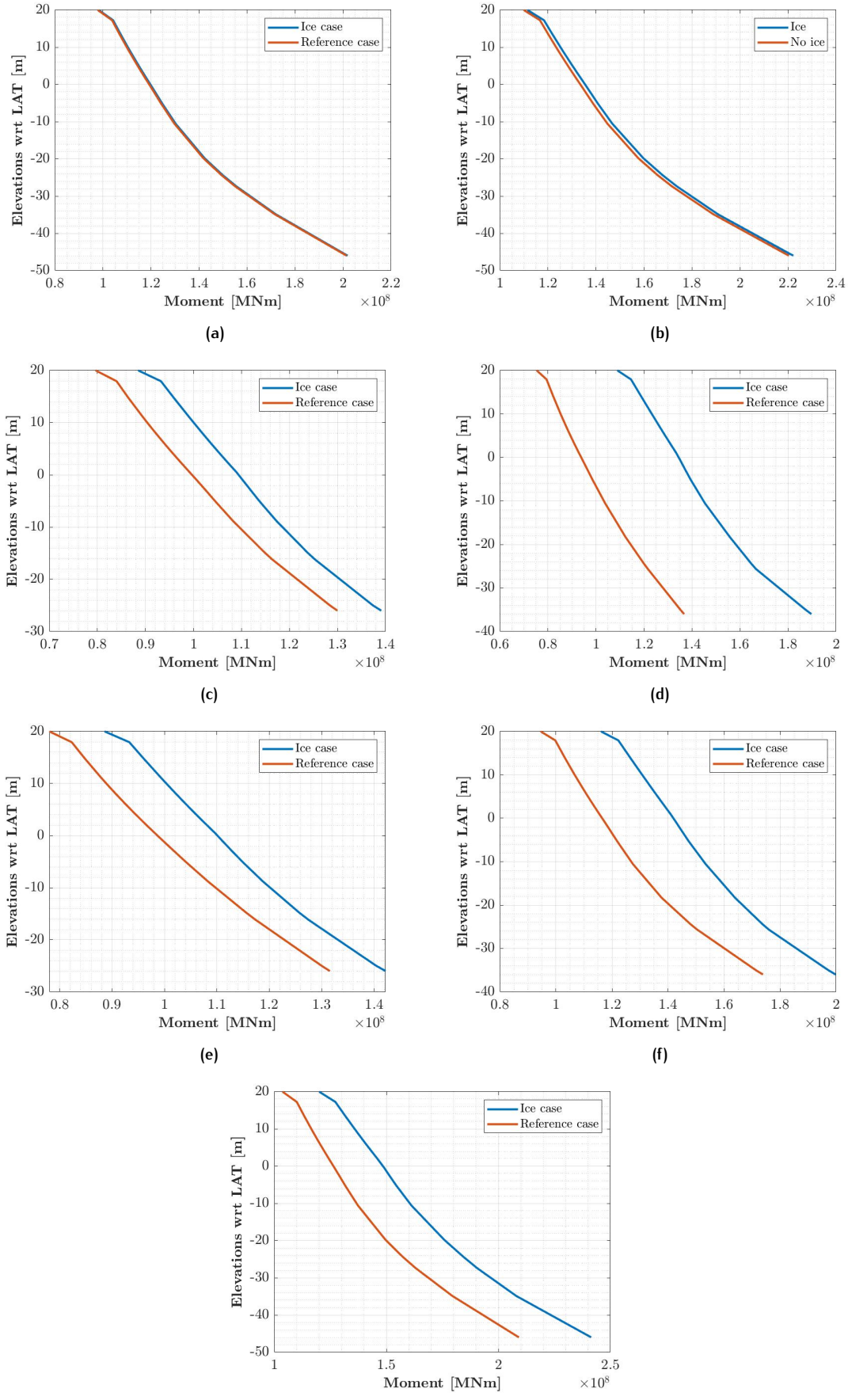

Figure A.8: Damage equivalent moment in the most unfavourable direction in (a) Baltic Proper South, (b) Baltic Proper North, (c) Gulf of Riga, (d) Gulf of Finland, (e) Archipelago Sea, (f) Bothnian Sea South and (g) Bothnian Sea North.

Figure A.9 is the extended design load case table of DNV GL [2016], which covers all DLCs relating to ice.

Design Situation	DLC	Wind Condition	Marine Condition				Other Conditions:	Type of Analysis		Partial safety factor
			Waves	Wind and wave directionality	Sea Currents	Water Level		Onshore	Offshore	
Drifting sea ice (power production)	9.1	NTM $V_{in} < V_{hub} < V_{out}$	No waves	n/a	NCM	NWLR	Ice load in horizontal direction from moving ice at relevant velocities. $h = h_{50}$ or largest value of moving ice Dynamic effects from ice loading – frequency lock-in effects	-	U	N
	9.2	NTM $V_{in} < V_{hub} < V_{out}$	No waves	n/a	NCM	NWLR	Ice load in horizontal direction from moving ice at relevant velocities *Use values of h corresponding to expected history of moving ice occurring* Dynamic effects from ice loading – frequency lock-in effects	-	F/U	F/N
Drifting sea ice (parked, standing still or idling)	9.3	Turbulent - EWM $V_{hub} = V_1$	No waves	n/a	NCM	NWLR	Pressure from hummocked ice and ice ridges	-	U	N
	9.4	NTM $V_{hub} < 0.7\ V_{50}$	No waves	n/a	NCM	NWLR	Horizontal load from moving ice at relevant velocities *Use values of h corresponding to expected history of moving ice occurring*) Dynamic effects from ice loading – frequency lock-in effects	-	F/U	F/N
	9.5	Turbulent - EWM $V_{hub} = V_1$	No waves	n/a	NCM	NWLR	Horizontal load from moving ice at relevant velocities. $h = h_{50}$ or largest value of moving ice Dynamic effects from ice loading – frequency lock-in effects	-	U	N
Temperature effects (power production)	10.1	NWP $V_{in} \leq V_{hub} \leq V_{out}$	$H=H_s(V)$	COD, UNI	NCM	MSL	Temperature effects	F/U	F/U	F/N

Figure A.9: Extended design load cases covering ice conditions as listed in DNV GL [2016].

B ALGORITHMS

This appendix presents two algorithms, the full Newmark numerical algorithm (which is a specific case of the generalized-*alpha* procedure) and the generalized-*alpha* procedure.

Algorithm B.1 provides the full Newmark numerical algorithm, which is found when the weighted

---

Algorithm B.1: The Newmark algorithm

---

1) System matrices:

$$\mathbf{K}, \mathbf{C}, \mathbf{M}$$
$$\mathbf{M}_* = \mathrm{M} + \gamma\, h\, \mathbf{C} + \beta\, h^2\, \mathbf{K}$$

2) Initial conditions:

$$\mathbf{u}_0,\ \dot{\mathbf{u}}_0$$
$$\ddot{\mathbf{u}}_0 = \mathbf{M}^{-1}(\mathbf{f}_0 - \mathbf{C}\,\dot{\mathbf{u}}_0 - \mathbf{K}\,\mathbf{u}_0)$$

3) Increment time:

$$t_{n+1} = t_{n+1} + h$$

4) Increment predictors:

$$\dot{\mathbf{u}}^*_{n+1} = \dot{\mathbf{u}}_n + (1-\gamma)\, h\, \ddot{\mathbf{u}}_n$$
$$\mathbf{u}^*_{n+1} = \mathbf{u}_n + h\,\dot{\mathbf{u}}_n + (1-\beta)\, h^2\, \ddot{\mathbf{u}}_n$$

5) Corrections:

$$\ddot{\mathbf{u}}_{n+1} = \mathbf{M}_*^{-1}(\mathbf{f}_{n+1} - \mathbf{C}\,\dot{\mathbf{u}}^*_{n+1} - \mathbf{K}\,\mathbf{u}^*_{n+1})$$
$$\dot{\mathbf{u}}_{n+1} = \dot{\mathbf{u}}^*_{n+1} + \Delta\dot{\mathbf{u}}_* + \gamma\, h\, \Delta\ddot{\mathbf{u}}$$
$$\mathbf{u}_{n+1} = \mathbf{u}^*_{n+1} + \beta\, h^2\, \ddot{\mathbf{u}}_{n+1}$$

6) Return to step 3) or stop if $t_{n+1} = t_{end}$

B.1 THE GENERALIZED α–PROCEDURE

Algorithm B.2 shows the numerical implementation of the generalized α-procedure.

Algorithm B.2: The generalized α-procedure

1) System matrices:

$$\mathbf{K}, \mathbf{C}, \mathbf{M}$$
$$\mathbf{M}_* = (1-\alpha_m)\mathrm{M} + (1-\alpha_f)(\gamma h\mathbf{C} + \beta h^2\mathbf{K})$$

2) Initial conditions:

$$\mathbf{u}_0, \dot{\mathbf{u}}_0$$
$$\ddot{\mathbf{u}}_0 = \mathbf{M}^{-1}(\mathbf{f}_0 - \mathbf{C}\dot{\mathbf{u}}_0 - \mathbf{K}\mathbf{u}_0)$$

3) Increment time:

$$t_{n+1} = t_{n+1} + h$$

4) Increment predictors:

$$\Delta\dot{\mathbf{u}}_* = h\ddot{\mathbf{u}}_n$$
$$\Delta\mathbf{u}_* = h\dot{\mathbf{u}}_n + \tfrac{1}{2}h^2\ddot{\mathbf{u}}_n$$
$$\Delta\mathbf{f} = \mathbf{f}_{n+1} - \mathbf{f}_n$$

5) Acceleration increment:

$$\Delta\ddot{\mathbf{u}} = \mathbf{M}_*^{-1}(\mathbf{f}_n - (\mathbf{M}\ddot{\mathbf{u}}_n + \mathbf{C}\dot{\mathbf{u}}_n + \mathbf{K}\mathbf{u}_n) + (1-\alpha_f)(\Delta\mathbf{f} - \mathbf{C}\Delta\dot{\mathbf{u}}_* - \mathbf{C}\Delta\mathbf{u}_*))$$

6) State vector update:

$$\ddot{\mathbf{u}}_{n+1} = \ddot{\mathbf{u}}_n + \Delta\ddot{\mathbf{u}}$$
$$\dot{\mathbf{u}}_{n+1} = \dot{\mathbf{u}}_n + \Delta\dot{\mathbf{u}}_* + \gamma h\Delta\ddot{\mathbf{u}}$$
$$\mathbf{u}_{n+1} = \mathbf{u}_n + \Delta\mathbf{u} + \beta h^2\Delta\ddot{\mathbf{u}}$$

7) Return to step 3) or stop if $t_{n+1} = t_{end}$

C | UR PLOTS

All the relevant UR plots of the research are presented in this appendix. For each region first the UR plot of the reference case is presented, followed by the ice case. For the Bothnian Sea North and the Bay of Bothnia the plots for relaxed fabrication constraints are also included.

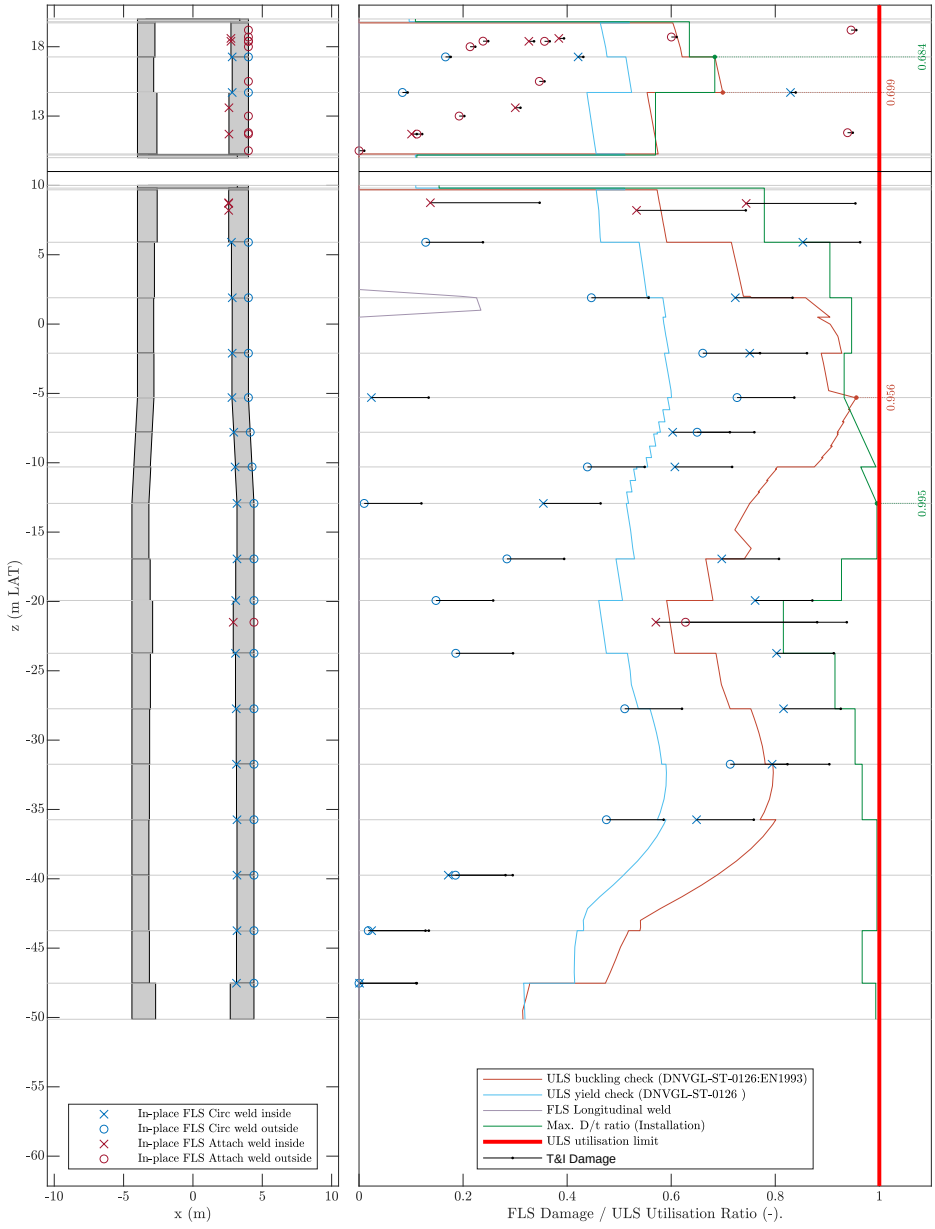

Figure C.1: UR plot of reference case - Danish Straits

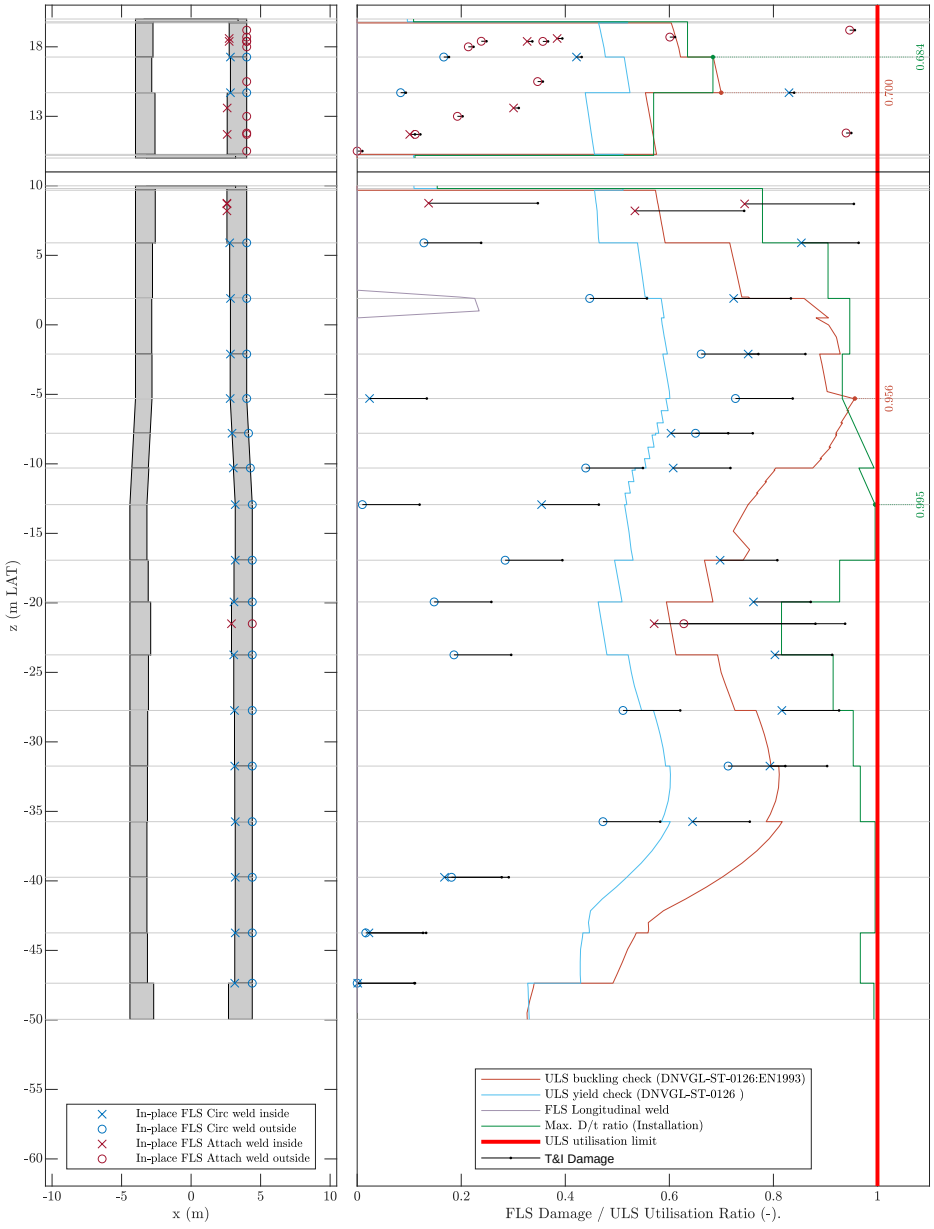

Figure C.2: UR plot of ice case - Danish Straits

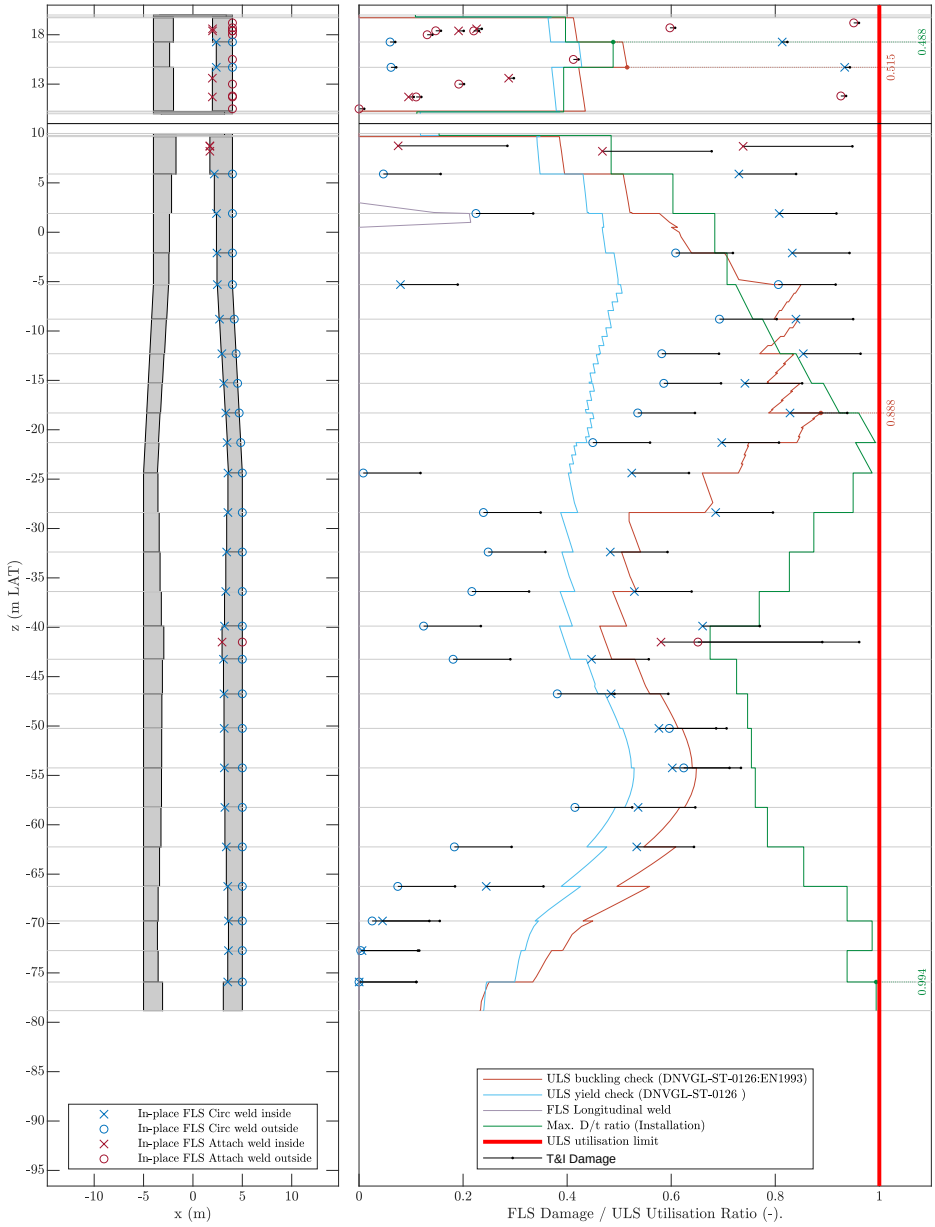

Figure C.3: UR plot of reference case - Baltic Proper South

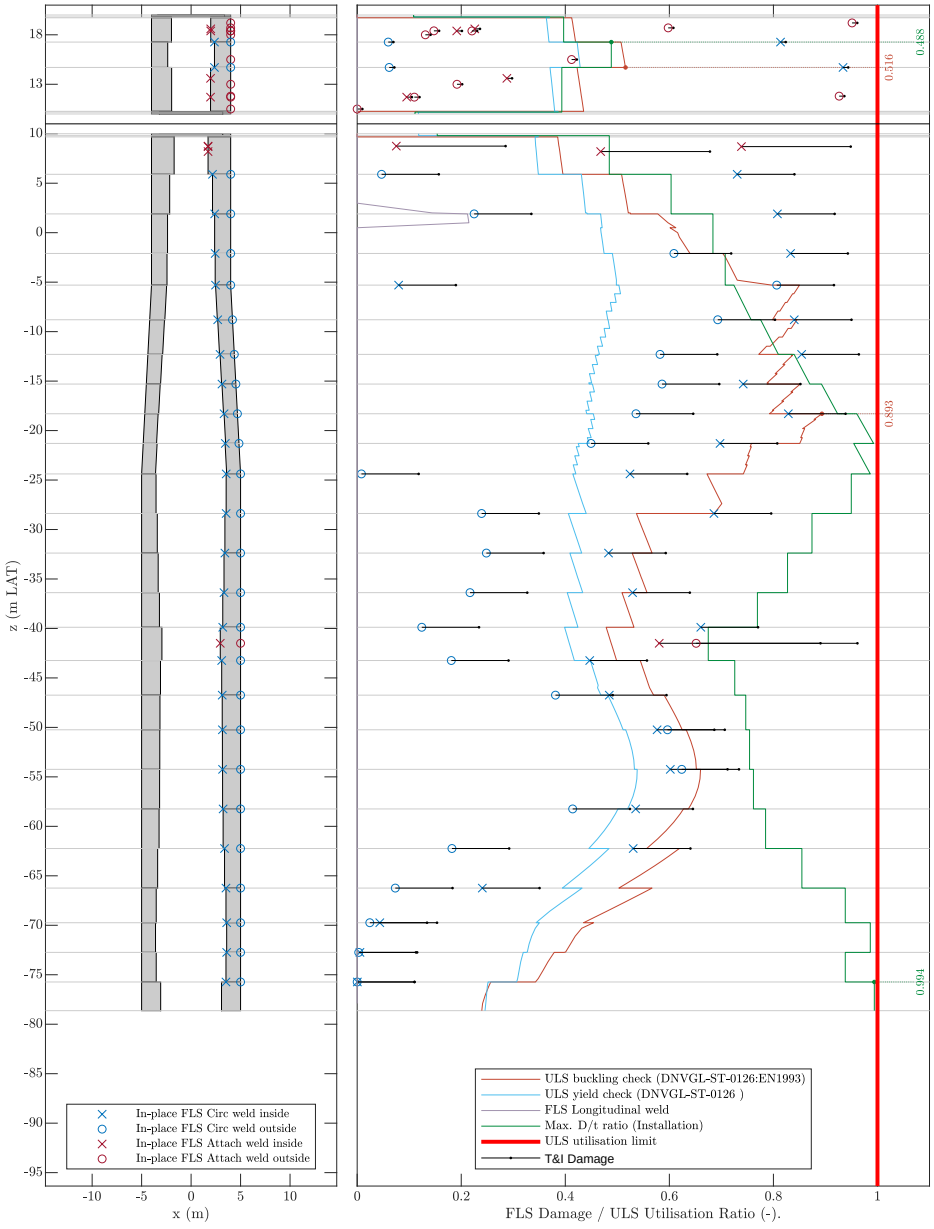

Figure C.4: UR plot of ice case - Baltic Proper South

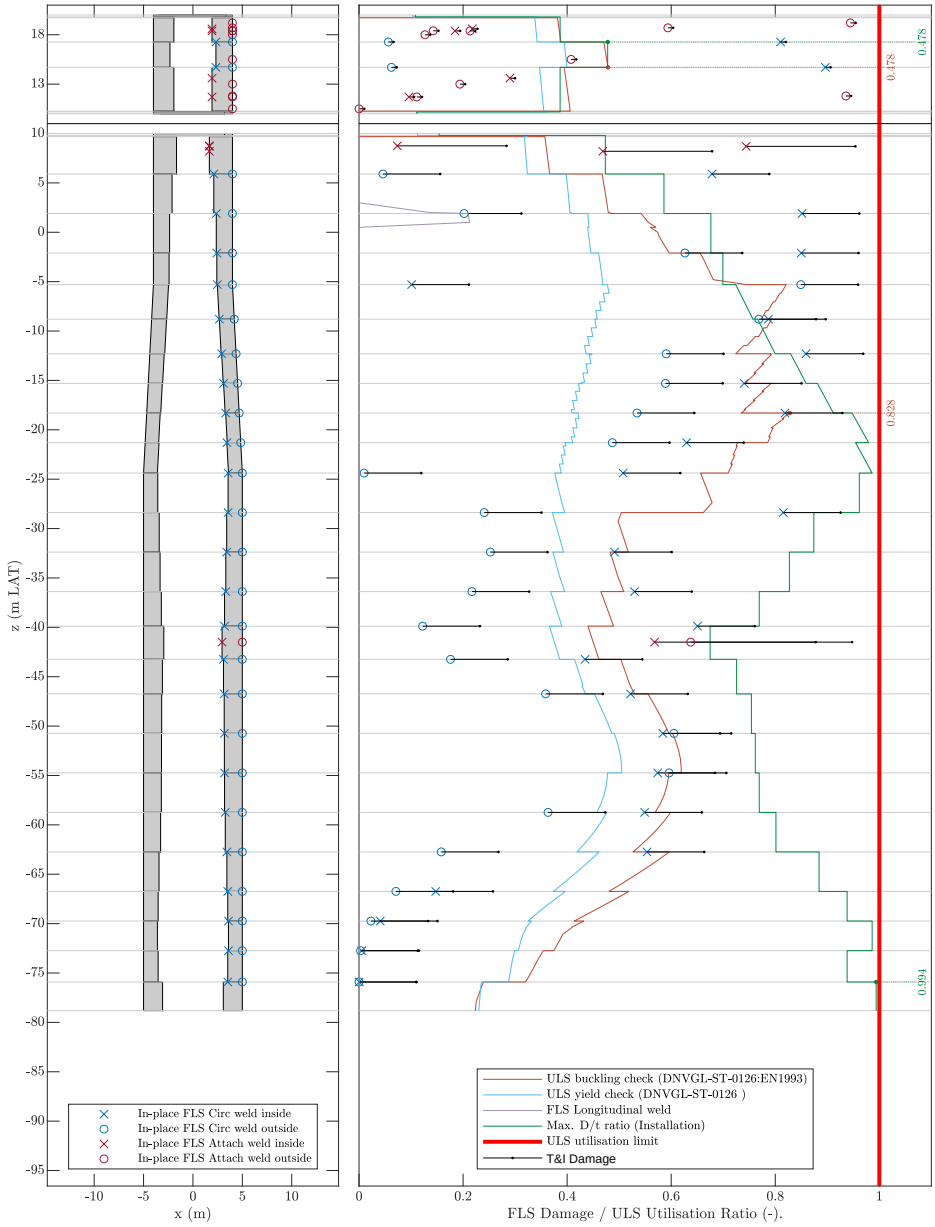

Figure C.5: UR plot of reference case - Baltic Proper North

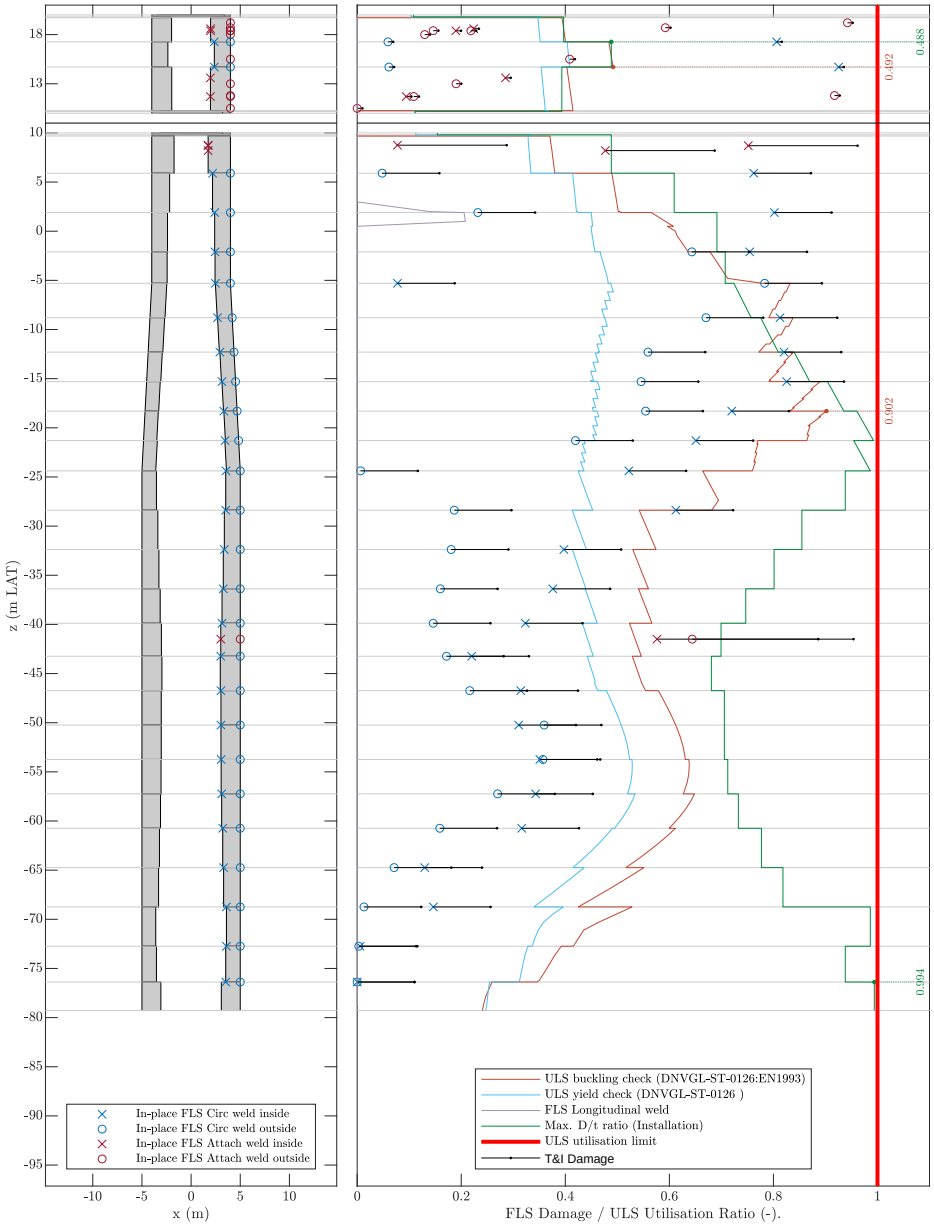

Figure C.6: UR plot of ice - Baltic Proper North

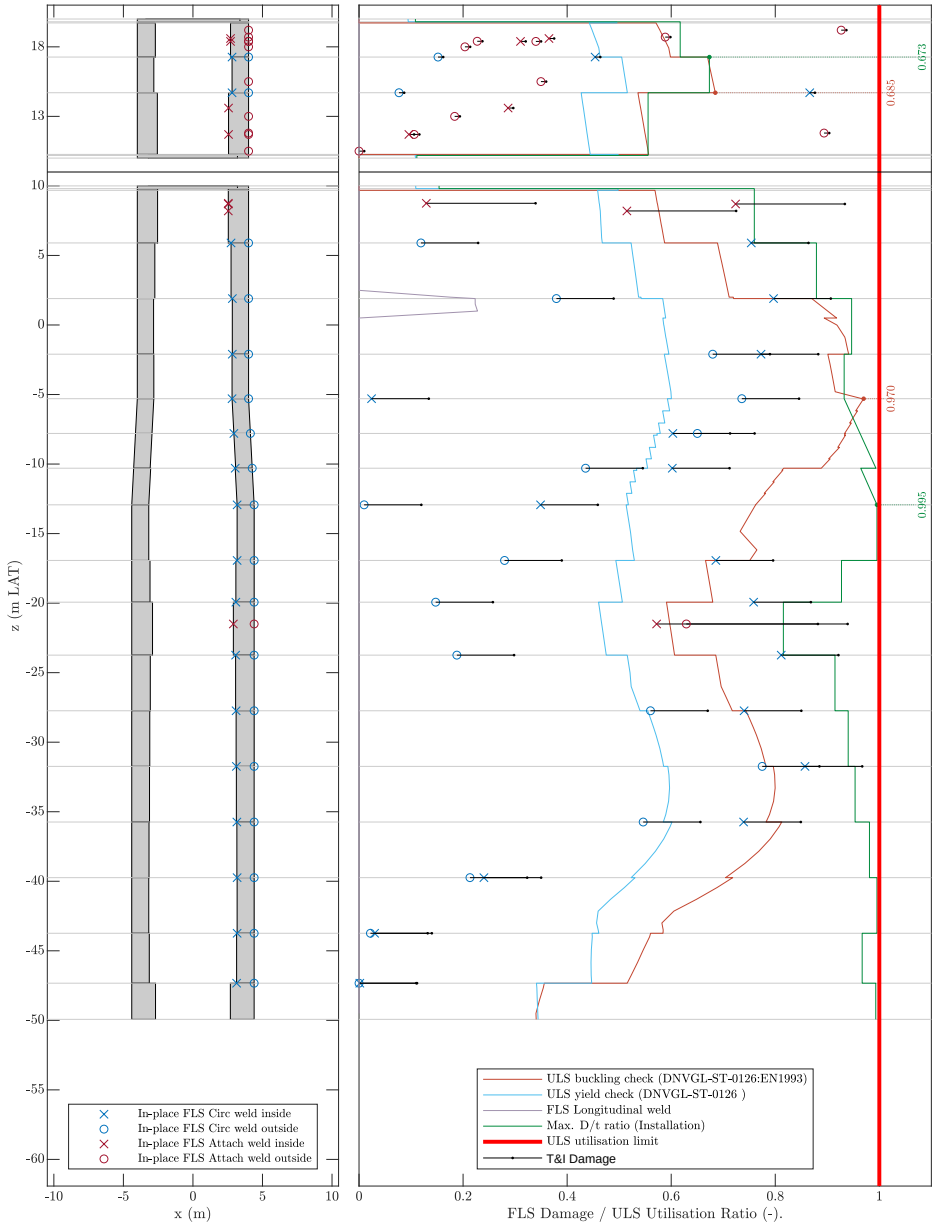

Figure C.7: UR plot of reference case - Gulf of Riga

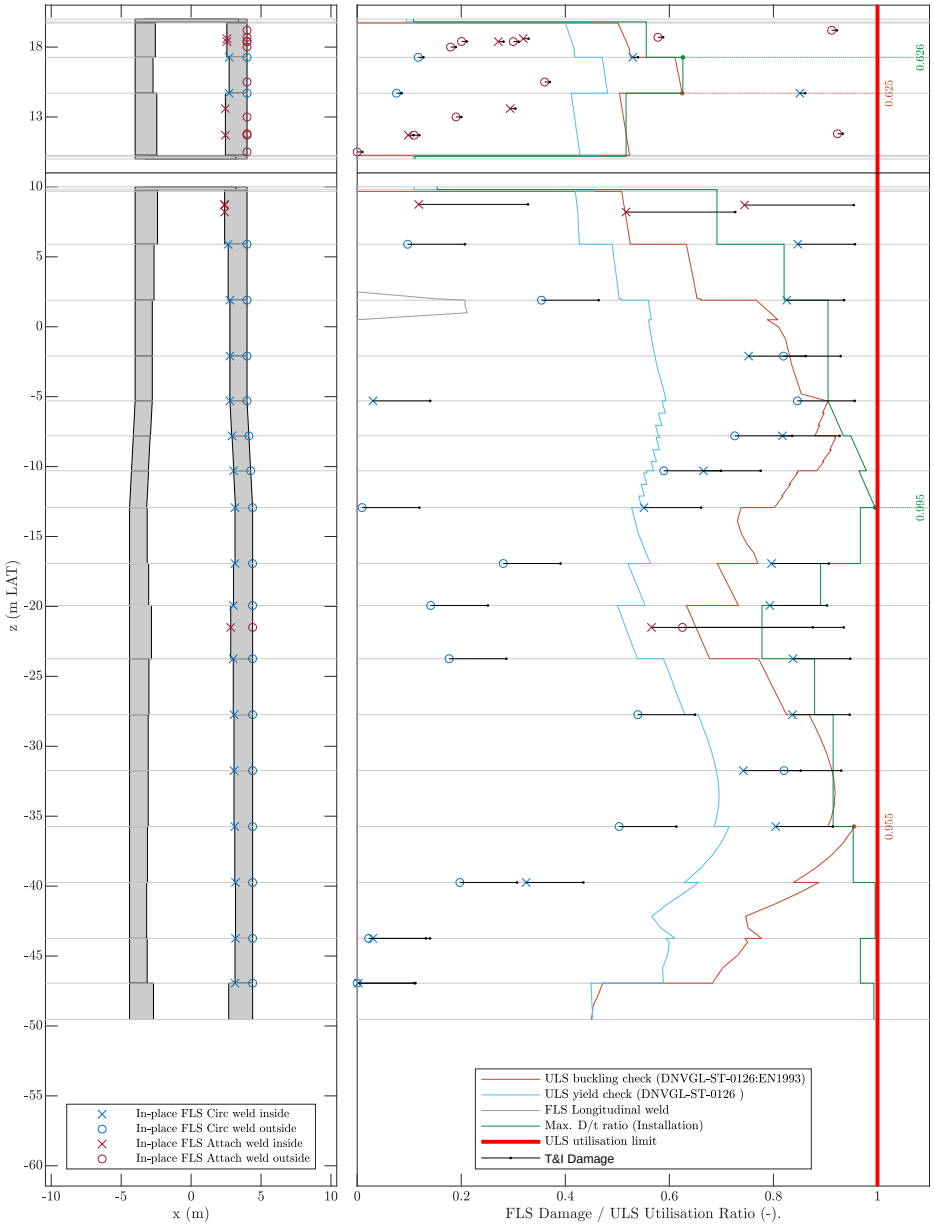

Figure C.8: UR plot of ice case - Gulf of Riga

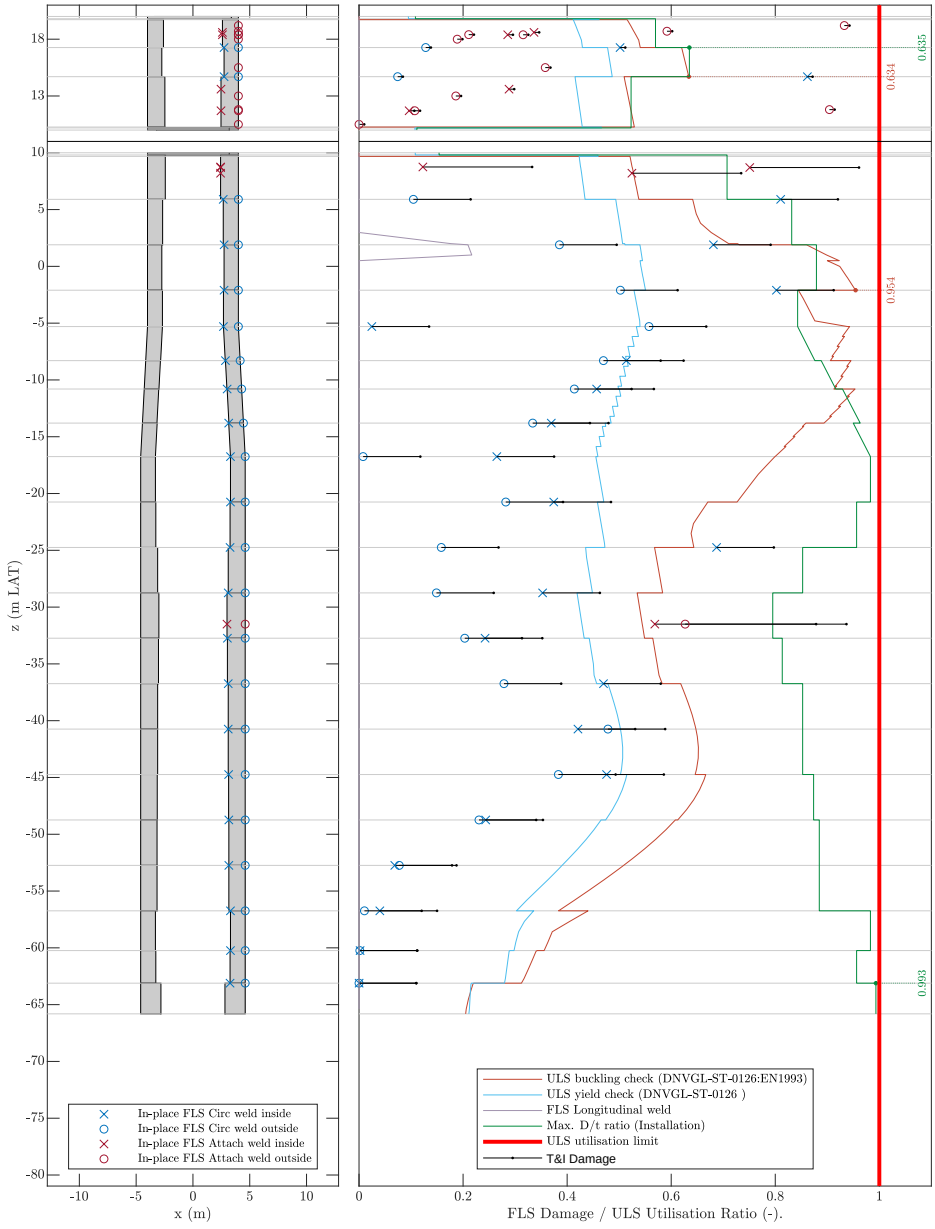

Figure C.9: UR plot of reference case - Gulf of Finland

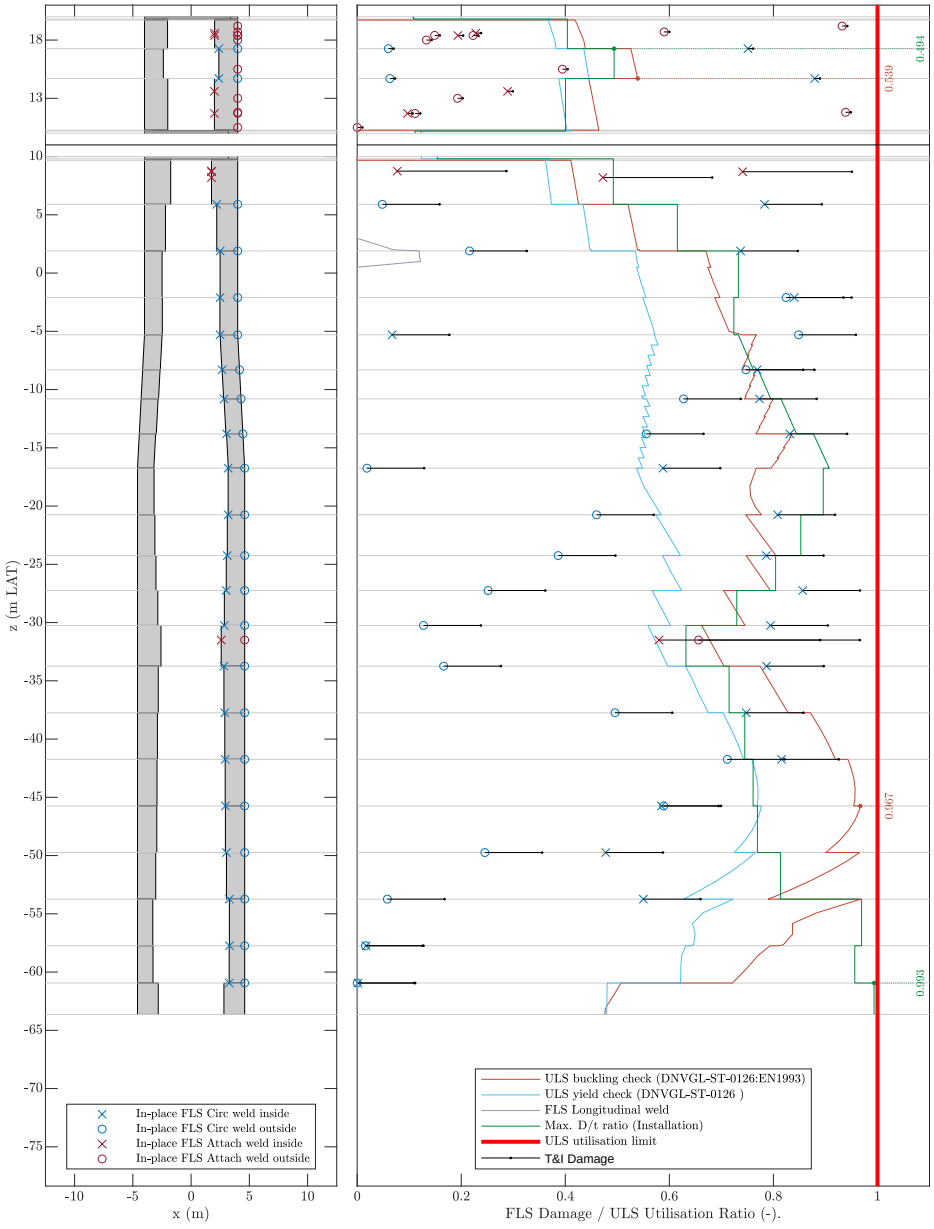

Figure C.10: UR plot of ice case - Gulf of Finland

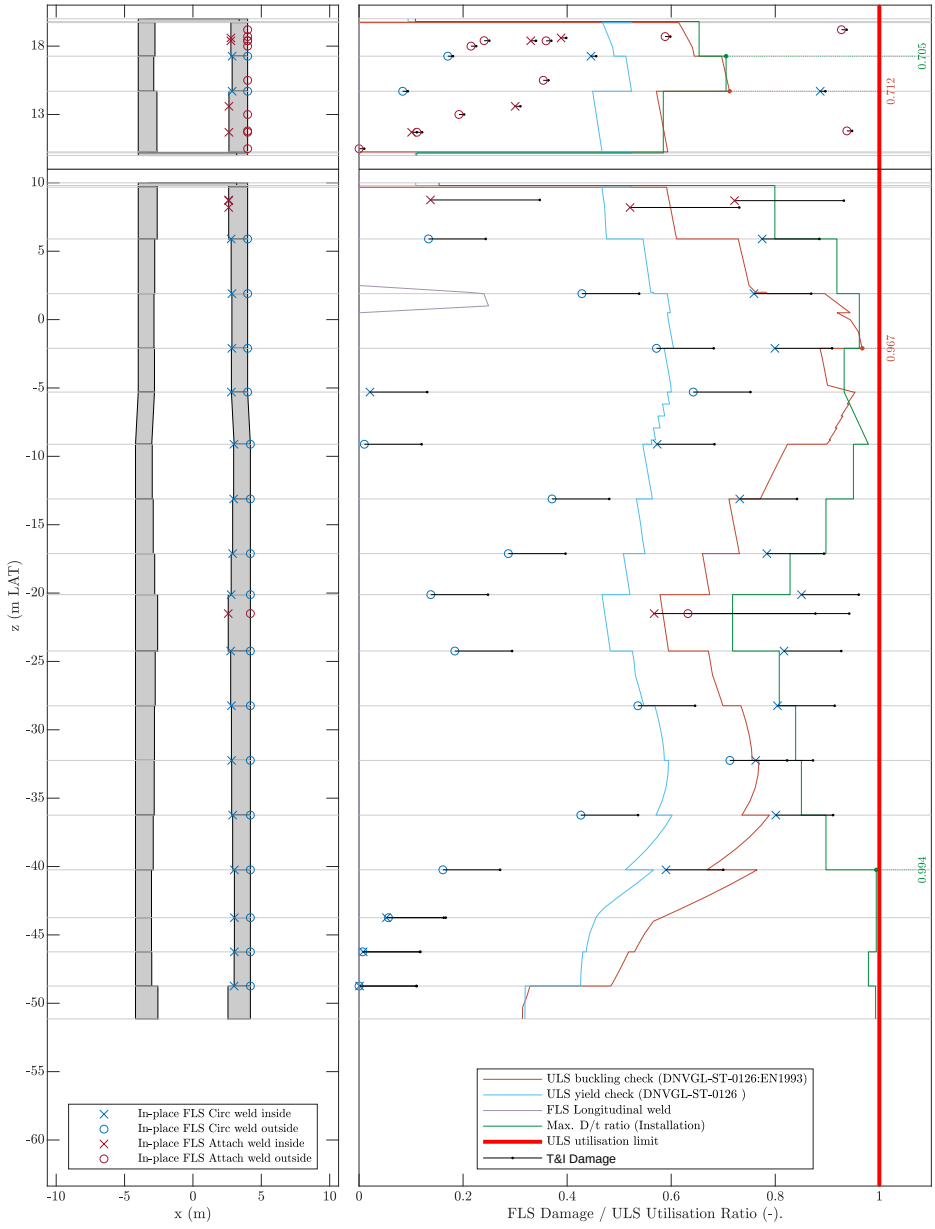

Figure C.11: UR plot of reference case -Archipelago Sea

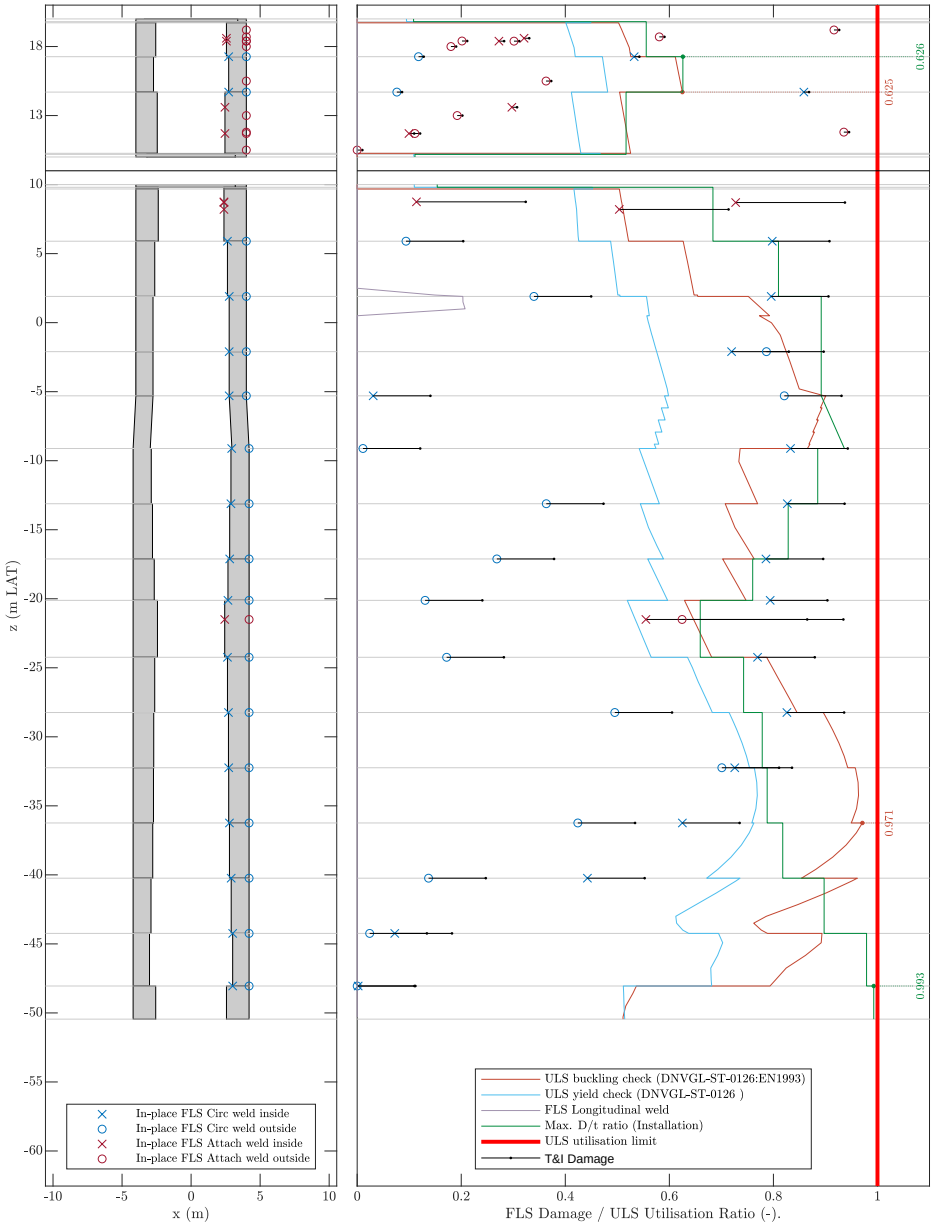

Figure C.12: UR plot of ice case -Archipelago Sea

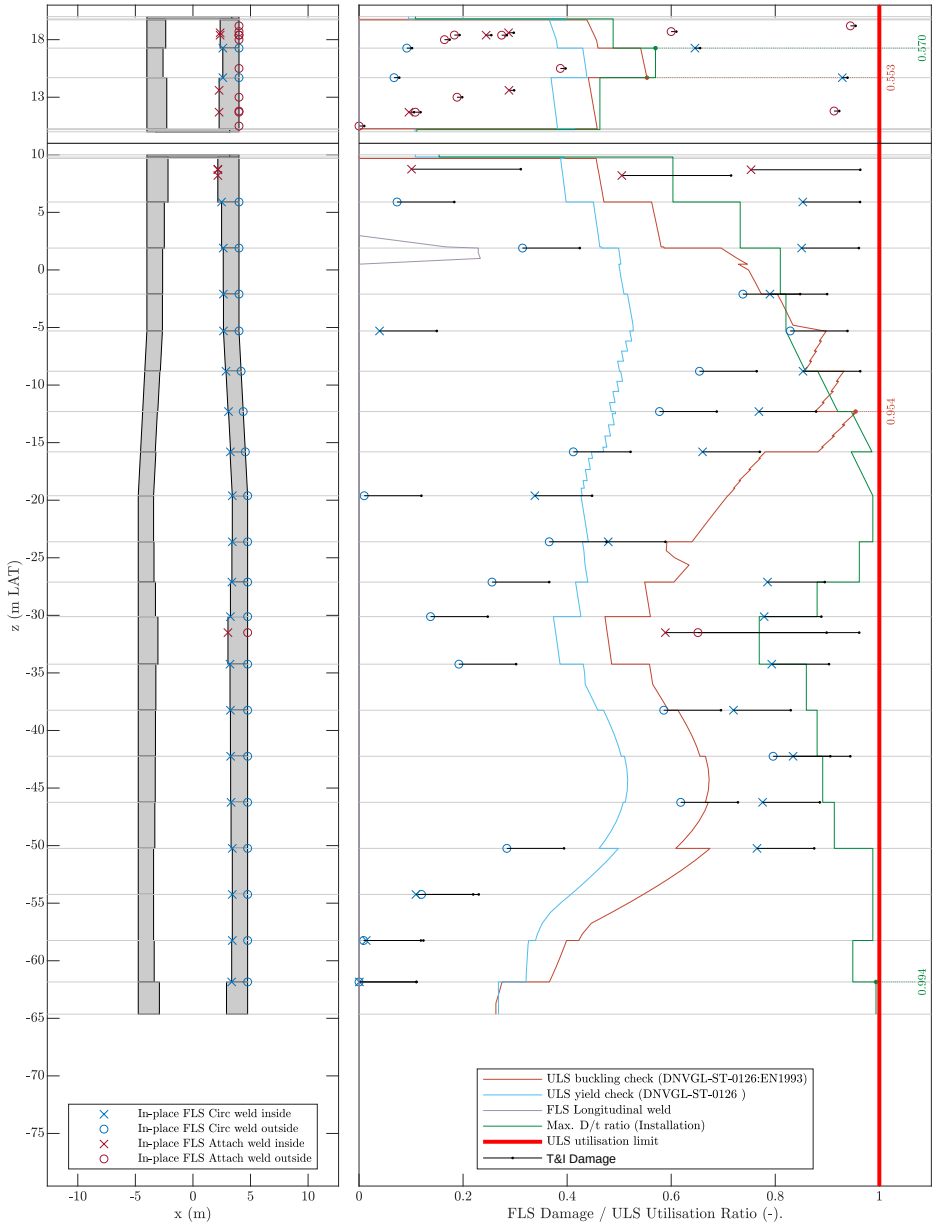

Figure C.13: UR plot of reference case - Bothnian Sea South

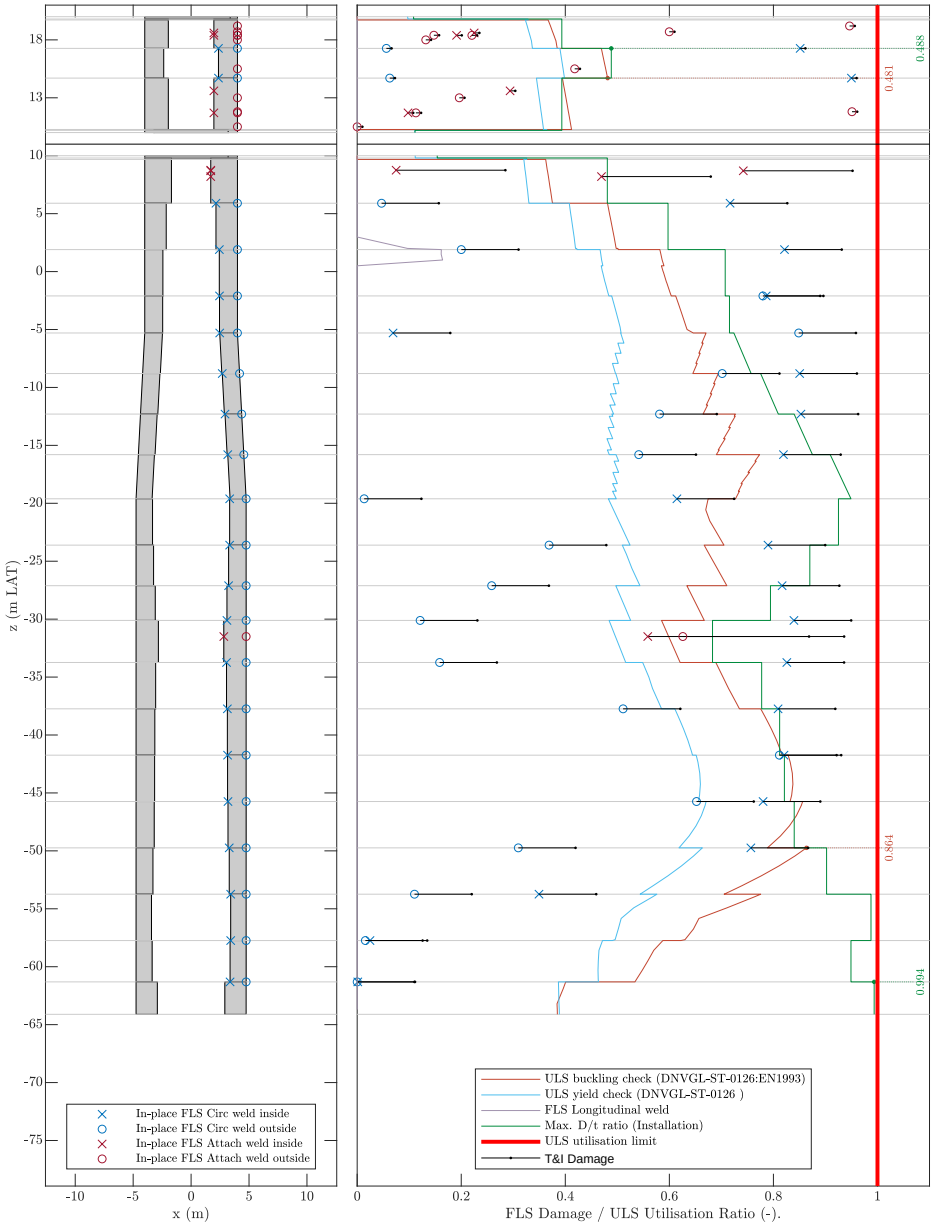

Figure C.14: UR plot of ice case - Bothnian Sea South

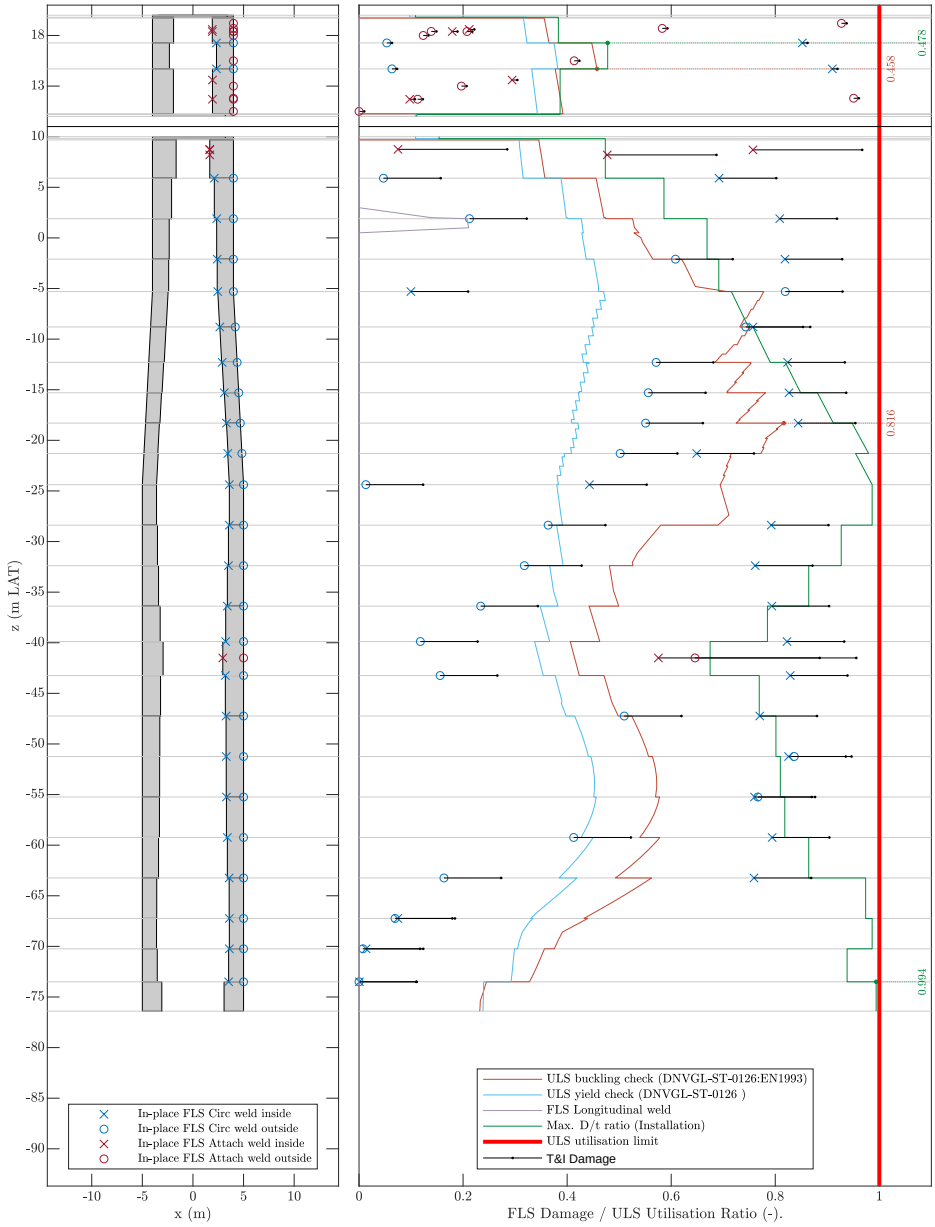

Figure C.15: UR plot of reference case - Bothnian Sea North

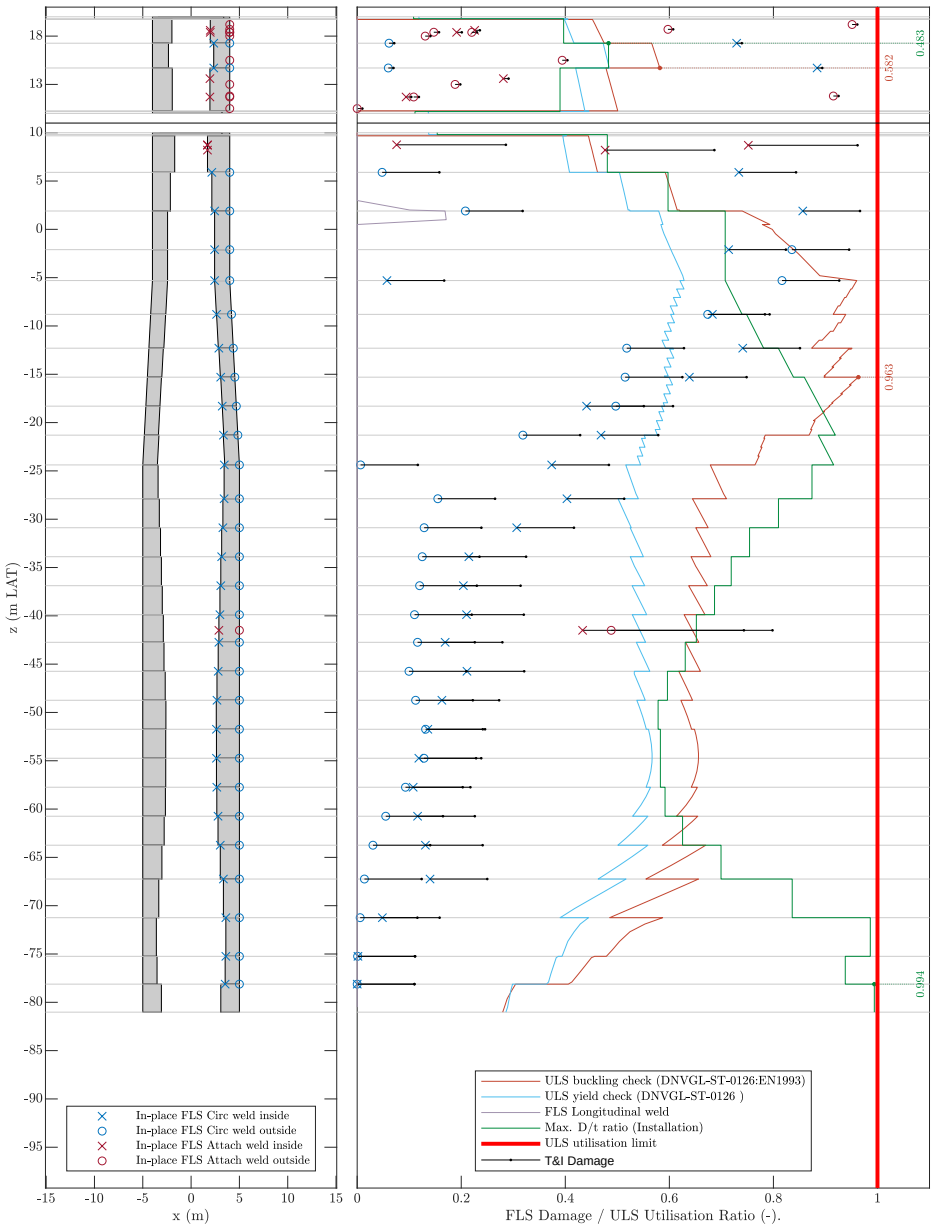

Figure C.16: UR plot of ice case - Bothnian Sea North

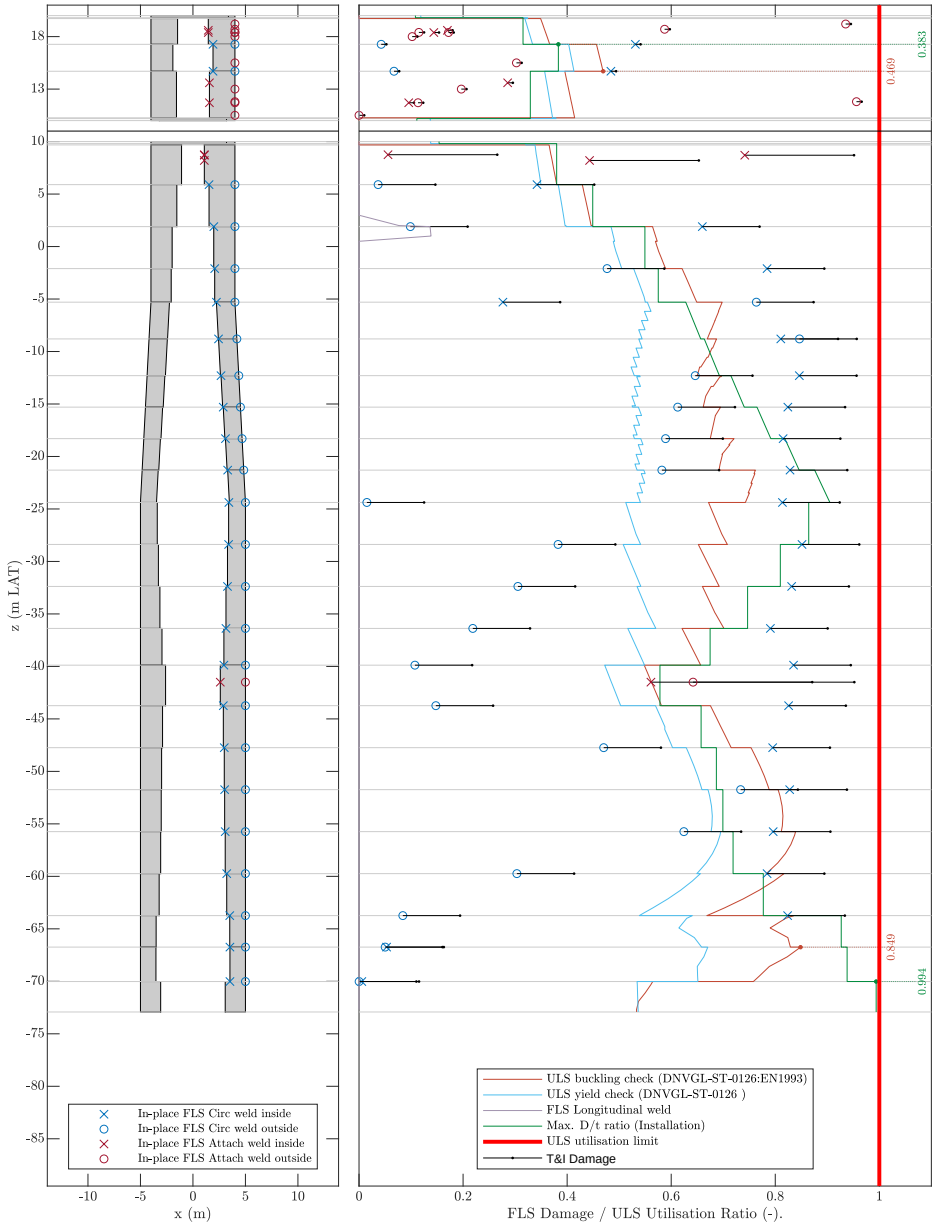

Figure C.17: UR plot of ice case for relaxed fabrication constraints - Bothnian Sea North

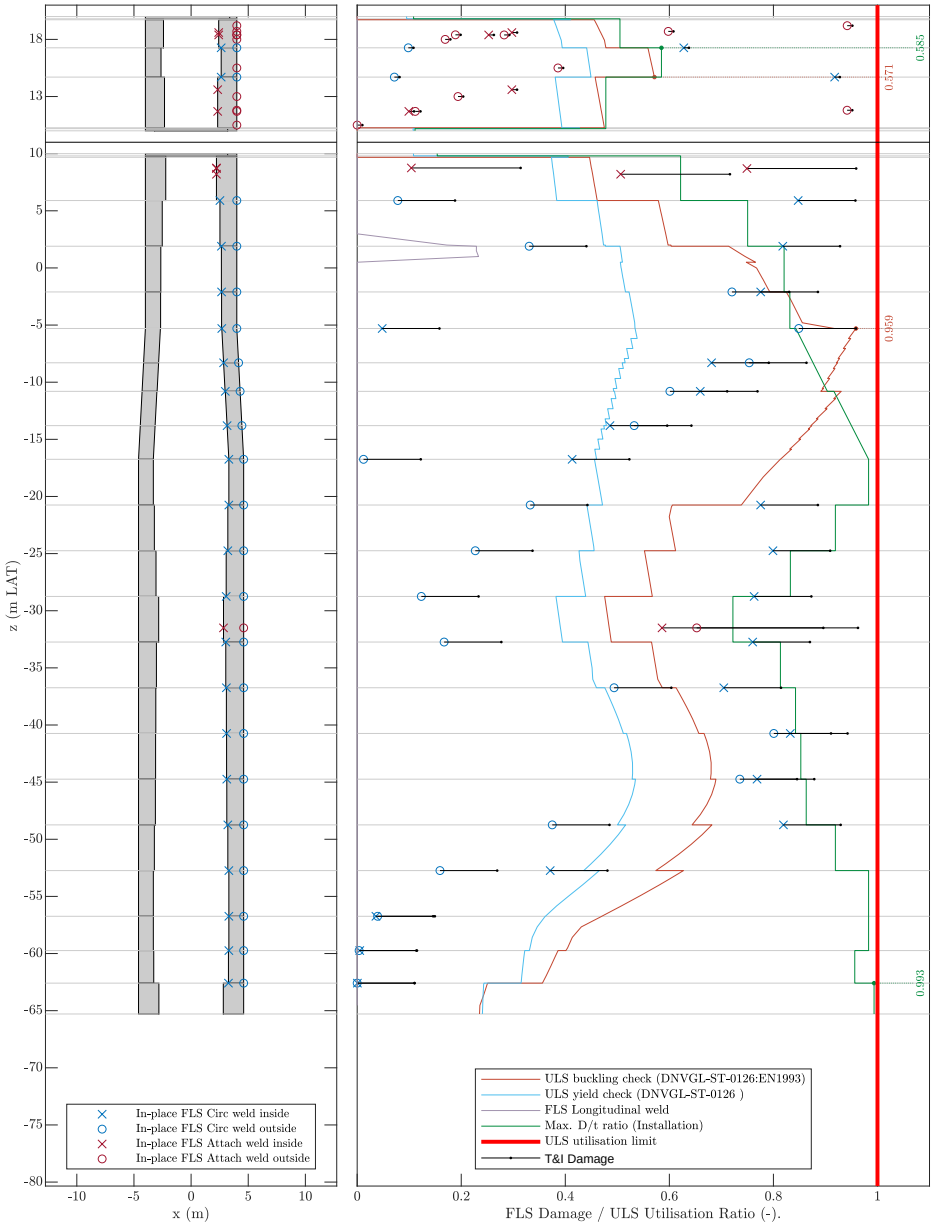

Figure C.18: UR plot of reference case - Bay of Bothnia

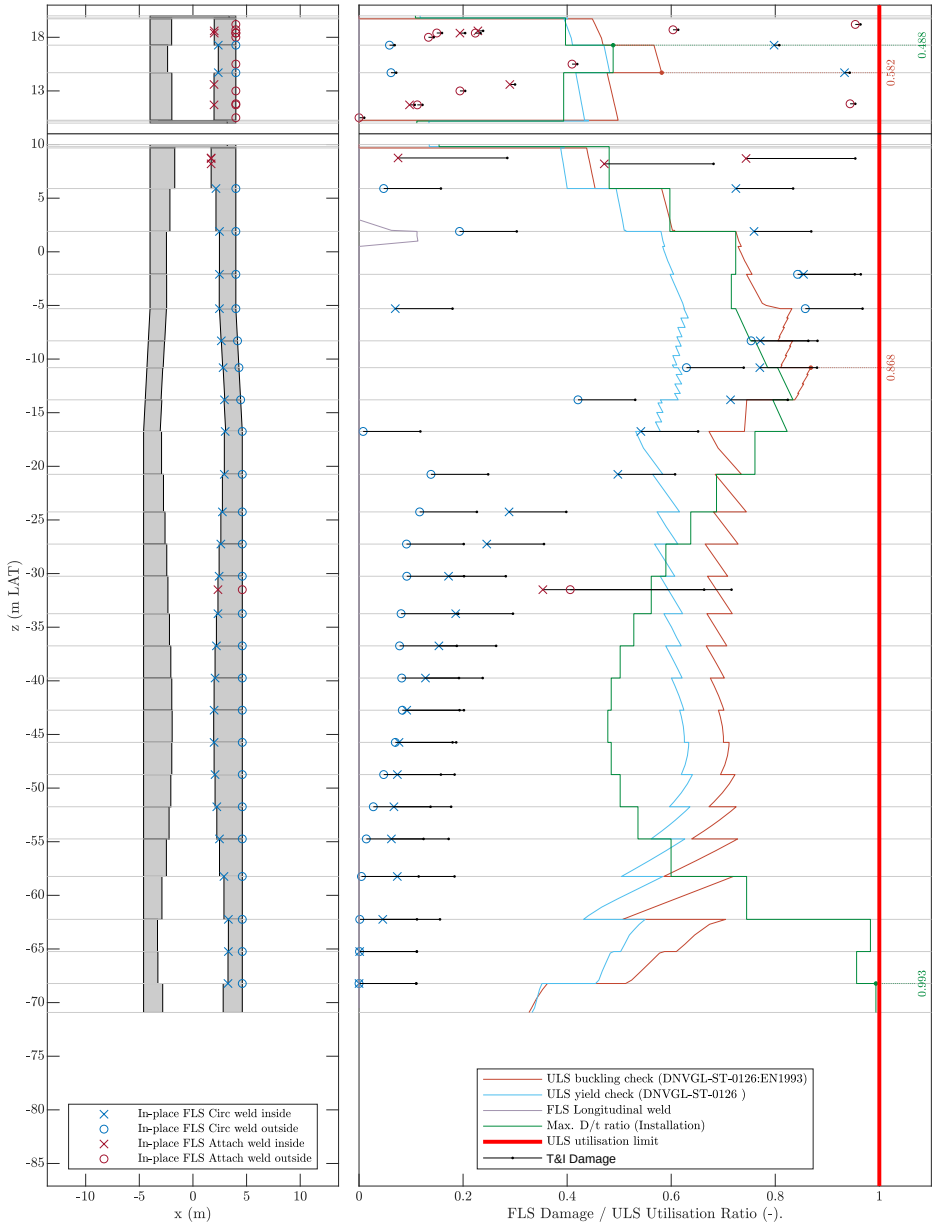

Figure C.19: UR plot of ice case - Bay of Bothnia

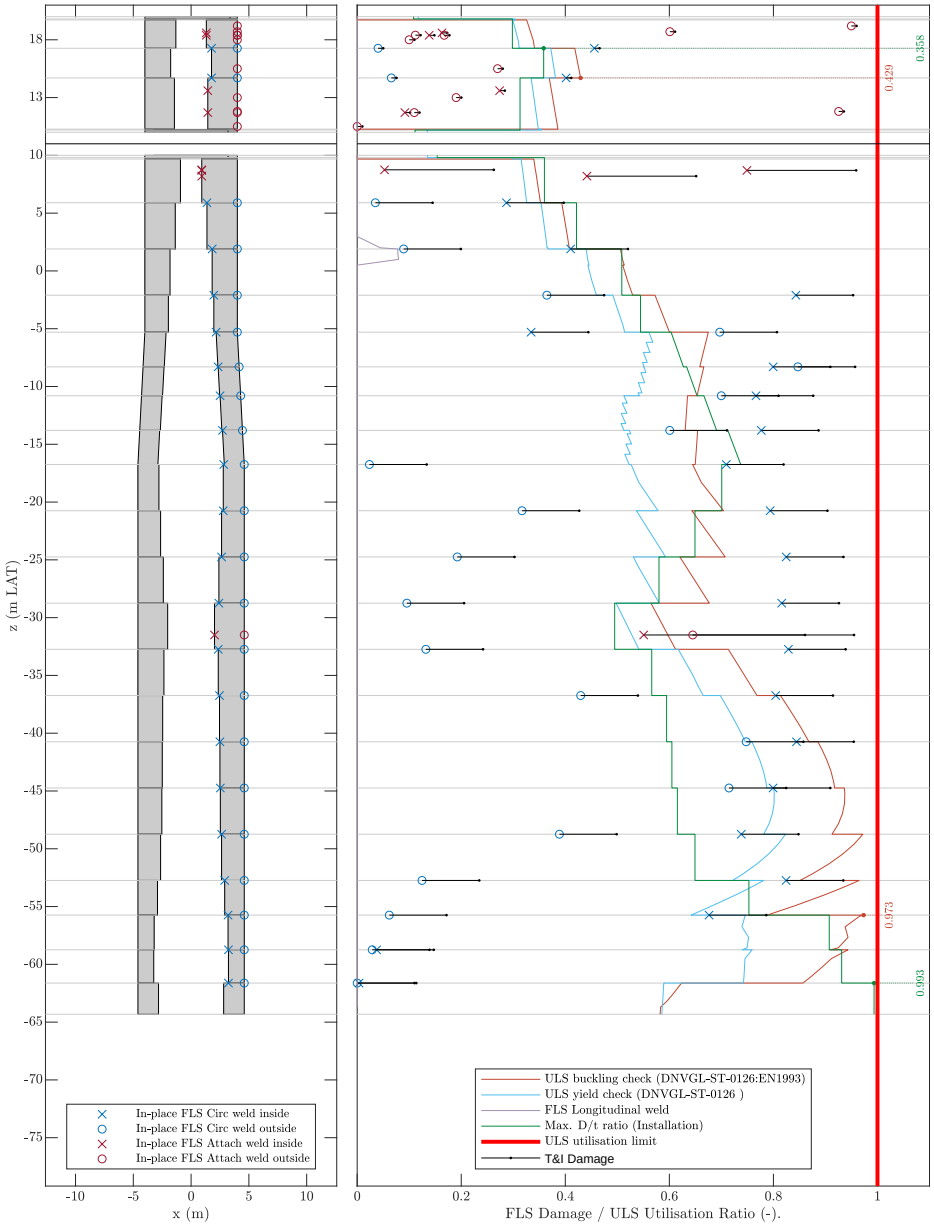

Figure C.20: UR plot of ice case for relaxed fabrication constraints - Bay of Bothnia

D TECHNICAL DESIGN DRAWINGS

All the generated Technical design drawings for the research are presented in this appendix. For each region the monopile and transition piece drawing are included for both the reference and ice case.

If during initial generation of the monopile under ice loading, the fabrication constraints were exceeded, two monopiles were generated. For one design the stiffness was increased (and fabrication constraints kept constant), which is referred to as the ice case. For the second design the fabrication constraints were relaxed, which is referred to as the relaxed case. Drawings for both cases are included.

TP (incl. flanges)

M: 166.5 t

L: 10.0 m

V: 21.1 m^3

D: 8.00 m

A_{ext}: 251.3 m^2

A_{int}: 246.0 m^2

Legend:

Grind: Grind weld flush

Plate tapering (angle 1:4)

Center of gravity

Hole

Longitudinal welds (LW):

Weld ID	No	length	thi	Grinding		IC*	
-	-	mm	mm	in	out	in	out
LW-1	1	2455	70	-	-	II	II
LW-2	1	2565	65	-	-	II	II
LW-3	2	4435	78	-	-	II	II

LW total length: 13.9 m
LW average thickness: 74.2 mm

Circumferential welds (CW):

Weld ID	length	thi	Grinding		IC*	
-	mm	mm	in	out	in	out
CW-1	25133	70-70	-	-	I	I
CW-2	25133	70-65	-	-	II	II
CW-3	25133	65-78	-	-	I	II
CW-4	25133	78-78	-	-	I	I

CW total length: 100.5 m
CW average thickness: 69.5 mm

Steel (TP total excl. flanges)

S355NL/ML:	32.6 t
S355NL/ML+Z35:	101.2 t

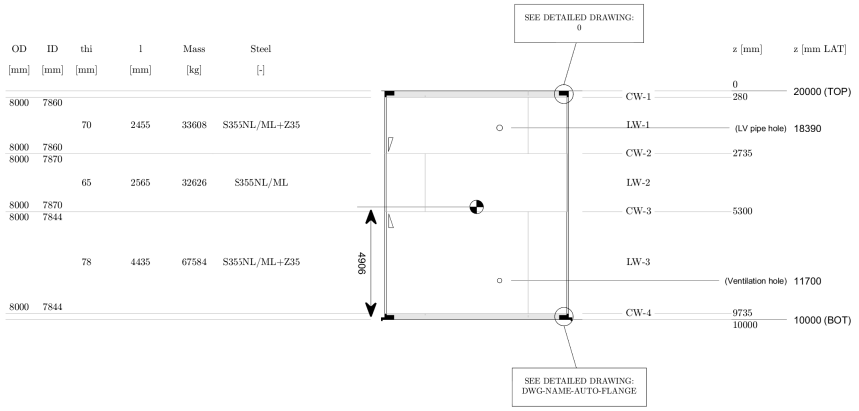

10 m 5 m 1 m 0 m

NOTES:

Drawings are for scheme design and show design intent only. Full detailed design analysis is required prior to fabrication. Secondary steel concept is not shown.

REV	DATE	REVISION DESCRIPTION	PREP.	QA	APPR
A	XXXX.XX.XXX	Issued for Client Review	EMS	XX	XX

DESIGN BY: WOOD THILSTED PARTNERS
APPROVED BY: XX — DATE: 12 Aug 2022
CHECKED BY: XX — DATE: 12 Aug 2022
PREPARED BY: EMS — DATE: 12 Aug 2022
SCALE: NOTED
WT PROJECT NO. 9993

NAN

WOOD THILSTED

GENERIC MORPHEUS MODEL
IEA15MW
TRANSITION PIECE: WTG_01

DRAWING NO. WT-9993-nan-DWG-WTG_01-TP — REV. A

DRAWING NO. WT-9993-nan-DWG-WTG_01-TP
REV. A

Figure D.1: Transition piece design drawing of reference case - Danish Straits

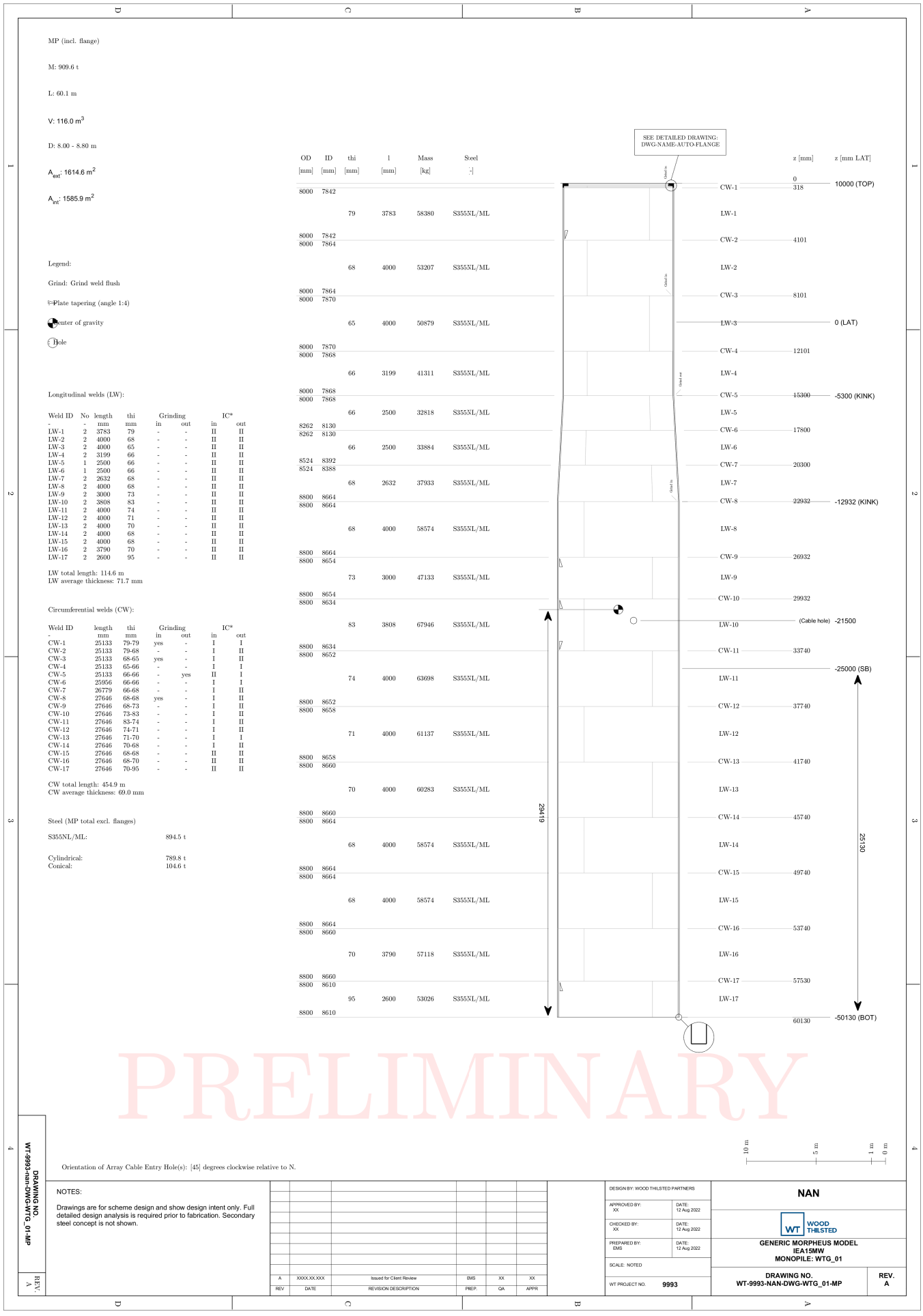

Figure D.2: Monopile design drawing of reference case - Danish Straits

TP (incl. flanges)

M: 166.5 t

L: 10.0 m

V: 21.1 m^3

D: 8.00 m

A_{ext}: 251.3 m^2

A_{int}: 246.0 m^2

Legend:

Grind: Grind weld flush

Plate tapering (angle 1:4)

Center of gravity

Hole

Longitudinal welds (LW):

Weld ID	No	length	thi	Grinding		IC*	
-	-	mm	mm	in	out	in	out
LW-1	1	2455	70	-	-	II	II
LW-2	1	2565	65	-	-	II	II
LW-3	2	4435	78	-	-	II	II

LW total length: 13.9 m
LW average thickness: 74.2 mm

Circumferential welds (CW):

Weld ID	length	thi	Grinding		IC*	
-	mm	mm	in	out	in	out
CW-1	25133	70-70	-	-	I	I
CW-2	25133	70-65	-	-	II	II
CW-3	25133	65-78	-	-	I	II
CW-4	25133	78-78	-	-	I	I

CW total length: 100.5 m
CW average thickness: 69.5 mm

Steel (TP total excl. flanges)

S355NL/ML:	32.6 t
S355NL/ML+Z35:	101.2 t

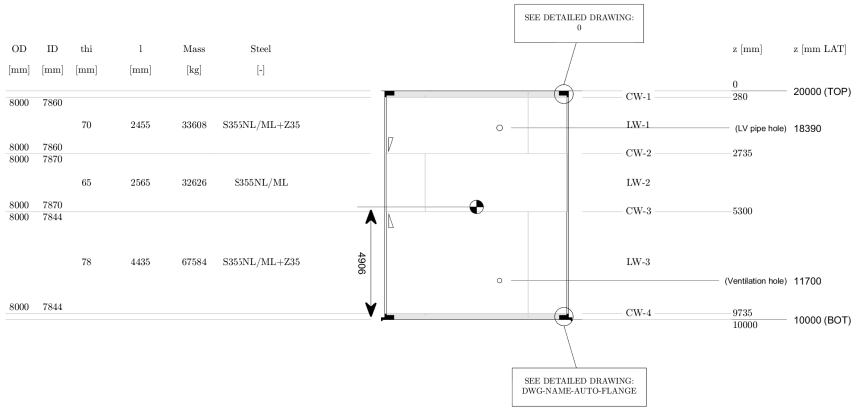

10 m 5 m 1 m 0 m

NOTES:

Drawings are for scheme design and show design intent only. Full detailed design analysis is required prior to fabrication. Secondary steel concept is not shown.

REV	DATE	REVISION DESCRIPTION	PREP.	QA	APPR
A	XXXX.XX.XXX	Issued for Client Review	EMS	XX	XX

DESIGN BY: WOOD THILSTED PARTNERS
APPROVED BY: XX — DATE: 15 Aug 2022
CHECKED BY: XX — DATE: 15 Aug 2022
PREPARED BY: EMS — DATE: 15 Aug 2022
SCALE: NOTED
WT PROJECT NO. 9993

NAN

WOOD THILSTED

GENERIC MORPHEUS MODEL
IEA15MW
TRANSITION PIECE: WTG_01

DRAWING NO. WT-9993-NAN-DWG-WTG_01-TP — REV. A

DRAWING NO. WT-9993-nan-DWG-WTG_01-TP
REV. A

Figure D.3: Transition piece design drawing of ice case - Danish Straits

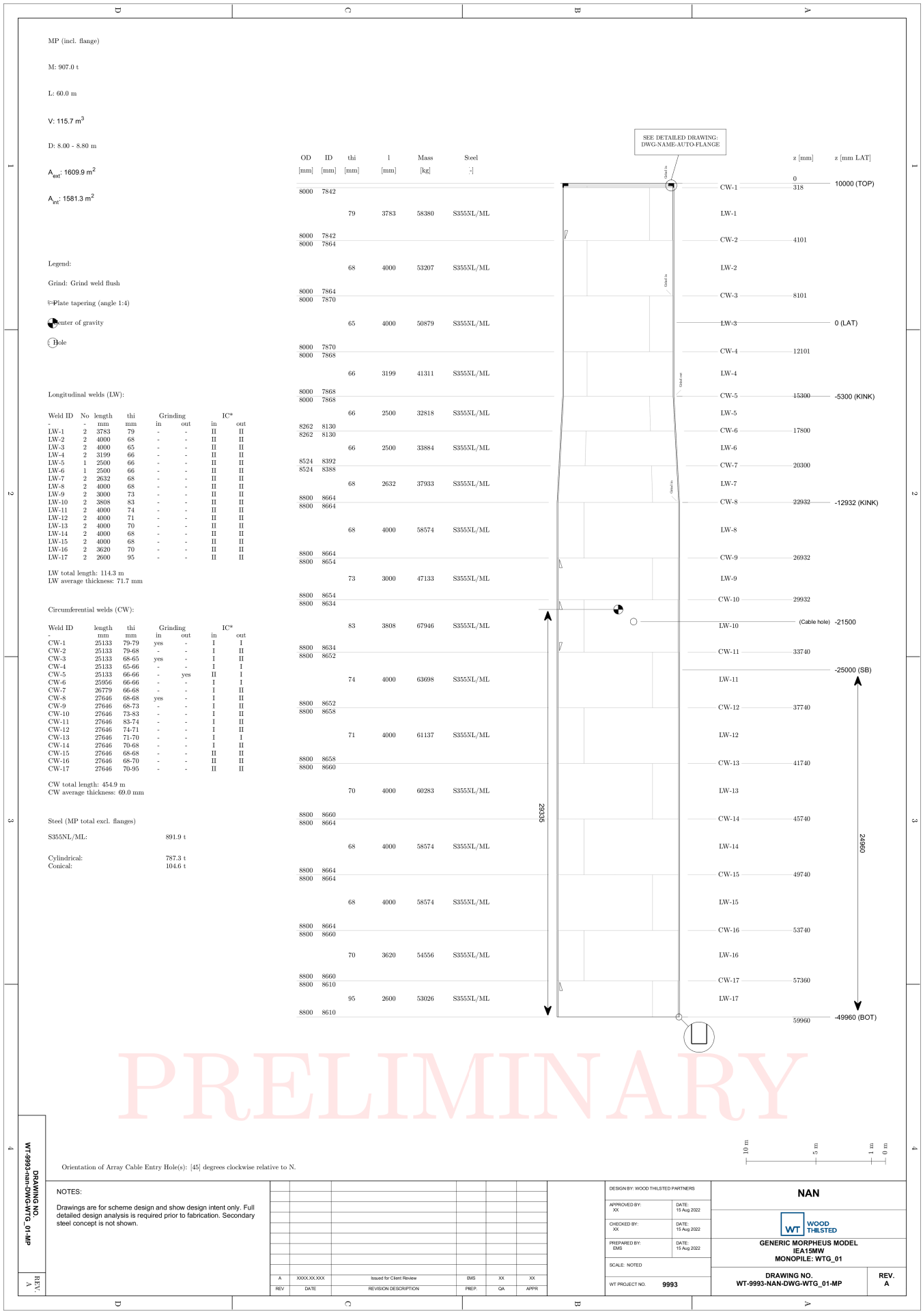

Figure D.4: Monopile design drawing of ice case - Danish Straits

TP (incl. flanges)

M: 230.3 t

L: 10.0 m

V: 29.2 m^3

D: 8.00 m

A_{ext}: 251.3 m^2

A_{int}: 243.9 m^2

Legend:

Grind: Grind weld flush

Plate tapering (angle 1:4)

Center of gravity

Hole

Longitudinal welds (LW):

Weld ID	No	length	thi	Grinding		IC*	
-	-	mm	mm	in	out	in	out
LW-1	2	2455	112	-	-	II	II
LW-2	2	2565	91	-	-	II	II
LW-3	3	4435	113	-	-	II	II

LW total length: 23.3 m
LW average thickness: 108.0 mm

Circumferential welds (CW):

Weld ID	length	thi	Grinding		IC*	
-	mm	mm	in	out	in	out
CW-1	25133	112-112	-	-	I	I
CW-2	25133	112-91	-	-	I	II
CW-3	25133	91-113	-	-	I	II
CW-4	25133	113-113	-	-	I	I

CW total length: 100.5 m
CW average thickness: 101.8 mm

Steel (TP total excl. flanges)

S355NL/ML:	45.5 t
S355NL/ML+Z35:	151.0 t

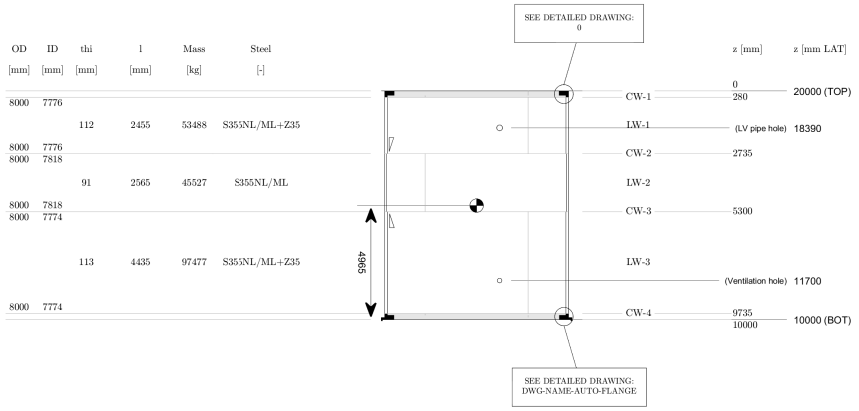

10 m 5 m 1 m 0 m

NOTES:

Drawings are for scheme design and show design intent only. Full detailed design analysis is required prior to fabrication. Secondary steel concept is not shown.

REV	DATE	REVISION DESCRIPTION	PREP.	QA	APPR
A	XXXX.XX.XXX	Issued for Client Review	EMS	XX	XX

DESIGN BY: WOOD THILSTED PARTNERS
APPROVED BY: XX — DATE: 12 Aug 2022
CHECKED BY: XX — DATE: 12 Aug 2022
PREPARED BY: EMS — DATE: 12 Aug 2022
SCALE: NOTED
WT PROJECT NO. 9993

NAN
WOOD THILSTED
GENERIC MORPHEUS MODEL
IEA15MW
TRANSITION PIECE: WTG_01
DRAWING NO. WT-9993-NAN-DWG-WTG_01-TP
REV. A

DRAWING NO. WT-9993-nan-DWG-WTG_01-TP
REV. A

Figure D.5: Transition piece design drawing of reference case - Baltic Proper South

MP (incl. flange)

M: 1911.1 t

L: 88.8 m

V: 243.6 m^3

D: 8.00 - 10.00 m

A_{ext}: 2635.0 m^2

A_{int}: 2579.4 m^2

Legend:

Grind: Grind weld flush

Plate tapering (angle 1:4)

Center of gravity

Hole

Longitudinal welds (LW):

Weld ID	No	length	thi	Grinding		IC*	
-	-	mm	mm	in	out	in	out
LW-1	3	3783	127	-	-	II	II
LW-2	3	4000	102	-	-	II	II
LW-3	3	4000	90	-	-	II	II
LW-4	2	3199	87	-	-	II	II
LW-5	2	3500	85	-	-	II	II
LW-6	2	3500	83	-	-	II	II
LW-7	2	3000	80	-	-	II	II
LW-8	2	3000	78	-	-	II	II
LW-9	2	3000	75	-	-	II	II
LW-10	2	3081	78	-	-	II	II
LW-11	3	4000	81	-	-	II	II
LW-12	3	4000	88	-	-	II	II
LW-13	3	4000	93	-	-	II	II
LW-14	3	3500	100	-	-	II	II
LW-15	3	3360	114	-	-	II	II
LW-16	3	3500	106	-	-	II	II
LW-17	3	3500	103	-	-	II	II
LW-18	3	4000	102	-	-	II	II
LW-19	3	4000	101	-	-	II	II
LW-20	3	4000	98	-	-	II	II
LW-21	3	4000	90	-	-	II	II
LW-22	3	3500	82	-	-	II	II
LW-23	2	3000	78	-	-	II	II
LW-24	2	3179	82	-	-	II	II
LW-25	3	2900	107	-	-	II	II

LW total length: 237.0 m
LW average thickness: 94.4 mm

Circumferential welds (CW):

Weld ID	length	thi	Grinding		IC*	
-	mm	mm	in	out	in	out
CW-1	25133	127-127	yes	-	I	I
CW-2	25133	127-102	-	-	I	II
CW-3	25133	102-90	yes	-	I	II
CW-4	25133	90-87	-	-	I	I
CW-5	25133	87-85	-	yes	II	I
CW-6	26285	85-83	-	-	I	I
CW-7	27438	83-80	-	-	I	II
CW-8	28426	80-78	-	-	I	II
CW-9	29414	78-75	-	-	I	II
CW-10	30401	75-78	-	-	I	II
CW-11	31416	78-81	yes	-	I	II
CW-12	31416	81-88	-	-	I	II
CW-13	31416	88-93	-	-	II	II
CW-14	31416	93-100	-	-	II	II
CW-15	31416	100-114	-	-	I	II
CW-16	31416	114-106	-	-	II	II
CW-17	31416	106-103	-	-	II	II
CW-18	31416	103-102	-	-	II	I
CW-19	31416	102-101	-	-	I	I
CW-20	31416	101-98	-	-	II	II
CW-21	31416	98-90	-	-	II	II
CW-22	31416	90-82	-	-	II	II
CW-23	31416	82-78	-	-	II	II
CW-24	31416	78-82	-	-	II	II
CW-25	31416	82-107	-	-	II	II

CW total length: 738.9 m
CW average thickness: 89.5 mm

Steel (MP total excl. flanges)

S355NL/ML: 1894.8 t

Cylindrical: 1559.7 t
Conical: 335.2 t

OD [mm]	ID [mm]	thi [mm]	l [mm]	Mass [kg]	Steel -]
8000	7746				
		127	3783	93282	S355NL/ML
8000	7746				
8000	7796				
		102	4000	79469	S355NL/ML
8000	7796				
8000	7820				
		90	4000	70226	S355NL/ML
8000	7820				
8000	7826				
		87	3199	54312	S355NL/ML
8000	7826				
8000	7830				
		85	3500	59417	S355NL/ML
8367	8197				
8367	8201				
		83	3500	60661	S355NL/ML
8734	8568				
8734	8574				
		80	3000	52150	S355NL/ML
9048	8888				
9048	8892				
		78	3000	52672	S355NL/ML
9363	9207				
9363	9213				
		75	3000	52408	S355NL/ML
9677	9527				
9677	9521				
		78	3081	57847	S355NL/ML
10000	9844				
10000	9838				
		81	4000	79256	S355NL/ML
10000	9838				
10000	9824				
		88	4000	86045	S355NL/ML
10000	9824				
10000	9814				
		93	4000	90888	S355NL/ML
10000	9814				
10000	9800				
		100	3500	85452	S355NL/ML
10000	9800				
10000	9772				
		114	3360	93387	S355NL/ML
10000	9772				
10000	9788				
		106	3500	90524	S355NL/ML
10000	9788				
10000	9794				
		103	3500	87989	S355NL/ML
10000	9794				
10000	9796				
		102	4000	99593	S355NL/ML
10000	9796				
10000	9798				
		101	4000	98626	S355NL/ML
10000	9798				
10000	9804				
		98	4000	95726	S355NL/ML
10000	9804				
10000	9820				
		90	4000	87982	S355NL/ML
10000	9820				
10000	9836				
		82	3500	70198	S355NL/ML
10000	9836				
10000	9844				
		78	3000	57258	S355NL/ML
10000	9844				
10000	9836				
		82	3179	63760	S355NL/ML
10000	9836				
10000	9786				
		107	2900	75706	S355NL/ML
10000	9786				

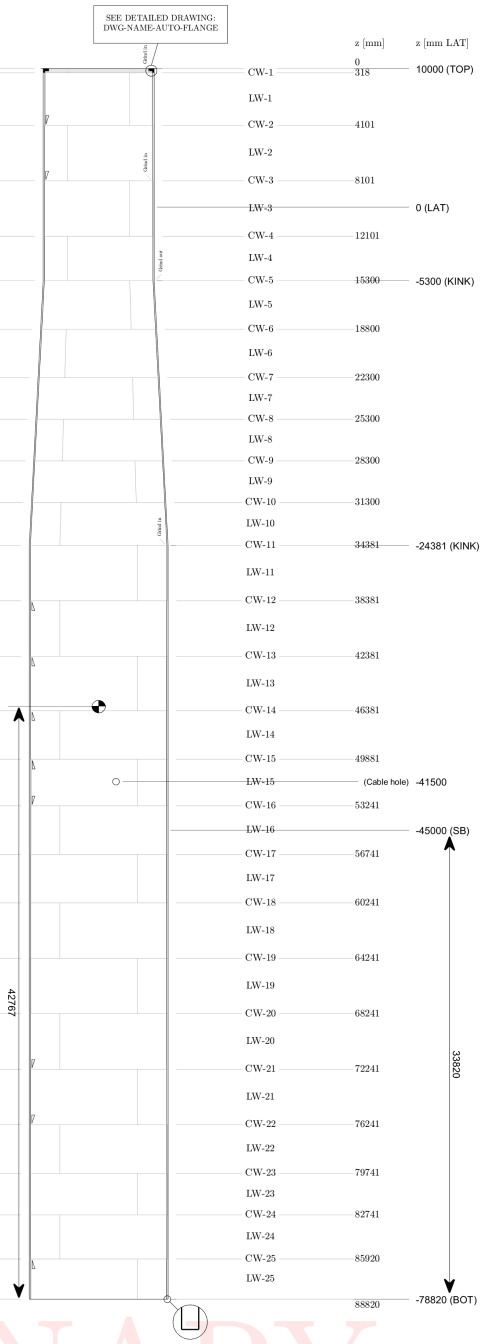

Orientation of Array Cable Entry Hole(s): [45] degrees clockwise relative to N.

10 m 5 m 1 m 0 m

NOTES:

Drawings are for scheme design and show design intent only. Full detailed design analysis is required prior to fabrication. Secondary steel concept is not shown.

REV	DATE	REVISION DESCRIPTION	PREP.	QA	APPR
A	XXXX.XX.XXX	Issued for Client Review	BMS	XX	XX

DESIGN BY: WOOD THILSTED PARTNERS
APPROVED BY: XX — DATE: 12 Aug 2022
CHECKED BY: XX — DATE: 12 Aug 2022
PREPARED BY: EMB — DATE: 12 Aug 2022
SCALE: NOTED
WT PROJECT NO. 9993

NAN

WOOD THILSTED

GENERIC MORPHEUS MODEL
IEA15MW
MONOPILE: WTG_01

DRAWING NO. WT-9993-NAN-DWG-WTG_01-MP
REV. A

DRAWING NO. WT-9993-nan-DWG-WTG_01-MP
REV. A

Figure D.6: Monopile design drawing of reference case - Baltic Proper South

TP (incl. flanges)

M: 230.3 t

L: 10.0 m

V: 29.2 m^3

D: 8.00 m

A_{ext}: 251.3 m^2

A_{int}: 243.9 m^2

Legend:

Grind: Grind weld flush

Plate tapering (angle 1:4)

Center of gravity

Hole

Longitudinal welds (LW):

Weld ID	No	length	thi	Grinding		IC*	
-	-	mm	mm	in	out	in	out
LW-1	2	2455	112	-	-	II	II
LW-2	2	2565	91	-	-	II	II
LW-3	3	4435	113	-	-	II	II

LW total length: 23.3 m
LW average thickness: 108.0 mm

Circumferential welds (CW):

Weld ID	length	thi	Grinding		IC*	
-	mm	mm	in	out	in	out
CW-1	25133	112-112	-	-	I	I
CW-2	25133	112-91	-	-	I	II
CW-3	25133	91-113	-	-	I	II
CW-4	25133	113-113	-	-	I	I

CW total length: 100.5 m
CW average thickness: 101.8 mm

Steel (TP total excl. flanges)

S355NL/ML:	45.5 t
S355NL/ML+Z35:	151.0 t

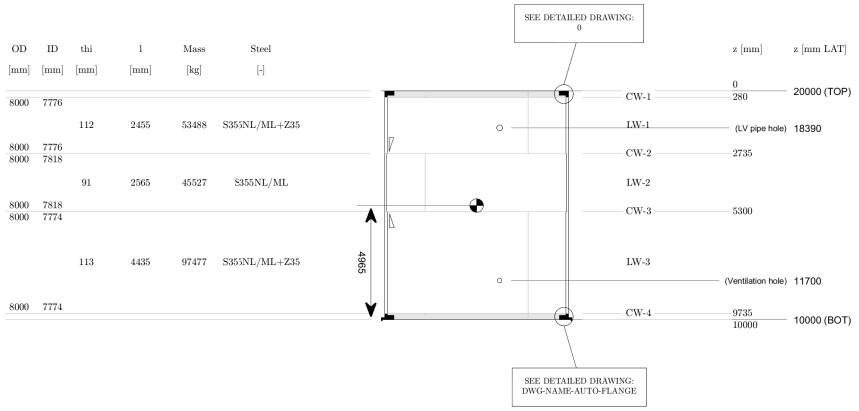

10 m 5 m 1 m 0 m

NOTES:

Drawings are for scheme design and show design intent only. Full detailed design analysis is required prior to fabrication. Secondary steel concept is not shown.

REV	DATE	REVISION DESCRIPTION	PREP.	QA	APPR
A	XXXX.XX.XXX	Issued for Client Review	EMS	XX	XX

DESIGN BY: WOOD THILSTED PARTNERS
APPROVED BY: XX — DATE: 15 Aug 2022
CHECKED BY: XX — DATE: 15 Aug 2022
PREPARED BY: EMS — DATE: 15 Aug 2022
SCALE: NOTED
WT PROJECT NO. 9993

NAN
WOOD THILSTED
GENERIC MORPHEUS MODEL
IEA15MW
TRANSITION PIECE: WTG_01
DRAWING NO. WT-9993-NAN-DWG-WTG_01-TP
REV. A

DRAWING NO. WT-9993-nan-DWG-WTG_01-TP
REV. A

Figure D.7: Transition piece design drawing of ice case - Baltic Proper South

MP (incl. flange)

M: 1907.3 t

L: 88.6 m

V: 243.1 m^3

D: 8.00 - 10.00 m

A_{ext}: 2629.1 m^2

A_{int}: 2573.5 m^2

Legend:

Grind: Grind weld flush

Plate tapering (angle 1:4)

Center of gravity

Hole

Longitudinal welds (LW):

Weld ID	No	length	thi	Grinding		IC*	
-	-	mm	mm	in	out	in	out
LW-1	3	3783	127	-	-	II	II
LW-2	3	4000	102	-	-	II	II
LW-3	3	4000	90	-	-	II	II
LW-4	2	3199	87	-	-	II	II
LW-5	2	3500	85	-	-	II	II
LW-6	2	3500	83	-	-	II	II
LW-7	2	3000	80	-	-	II	II
LW-8	2	3000	78	-	-	II	II
LW-9	2	3000	75	-	-	II	II
LW-10	2	3081	78	-	-	II	II
LW-11	3	4000	81	-	-	II	II
LW-12	3	4000	88	-	-	II	II
LW-13	3	4000	93	-	-	II	II
LW-14	3	3500	100	-	-	II	II
LW-15	3	3360	114	-	-	II	II
LW-16	3	3500	106	-	-	II	II
LW-17	3	3500	103	-	-	II	II
LW-18	3	4000	102	-	-	II	II
LW-19	3	4000	101	-	-	II	II
LW-20	3	4000	98	-	-	II	II
LW-21	3	4000	90	-	-	II	II
LW-22	3	3500	82	-	-	II	II
LW-23	2	3000	78	-	-	II	II
LW-24	2	2989	82	-	-	II	II
LW-25	3	2900	107	-	-	II	II

LW total length: 236.7 m
LW average thickness: 94.4 mm

Circumferential welds (CW):

Weld ID	length	thi	Grinding		IC*	
-	mm	mm	in	out	in	out
CW-1	25133	127-127	yes	-	I	I
CW-2	25133	127-102	-	-	I	II
CW-3	25133	102-90	yes	-	I	II
CW-4	25133	90-87	-	-	I	I
CW-5	25133	87-85	-	yes	II	I
CW-6	26285	85-83	-	-	I	I
CW-7	27438	83-80	-	-	I	II
CW-8	28426	80-78	-	-	I	II
CW-9	29414	78-75	-	-	I	II
CW-10	30401	75-78	-	-	I	II
CW-11	31416	78-81	yes	-	I	II
CW-12	31416	81-88	-	-	I	II
CW-13	31416	88-93	-	-	II	II
CW-14	31416	93-100	-	-	II	II
CW-15	31416	100-114	-	-	I	II
CW-16	31416	114-106	-	-	II	II
CW-17	31416	106-103	-	-	II	II
CW-18	31416	103-102	-	-	II	I
CW-19	31416	102-101	-	-	I	I
CW-20	31416	101-98	-	-	II	II
CW-21	31416	98-90	-	-	II	II
CW-22	31416	90-82	-	-	II	II
CW-23	31416	82-78	-	-	II	II
CW-24	31416	78-82	-	-	II	II
CW-25	31416	82-107	-	-	II	II

CW total length: 738.9 m
CW average thickness: 89.5 mm

Steel (MP total excl. flanges)

S355NL/ML:	1891.0 t
Cylindrical:	1555.9 t
Conical:	335.2 t

OD [mm]	ID [mm]	thi [mm]	l [mm]	Mass [kg]	Steel -]
8000	7746				
		127	3783	93282	S355NL/ML
8000	7746				
8000	7796				
		102	4000	79469	S355NL/ML
8000	7796				
8000	7820				
		90	4000	70226	S355NL/ML
8000	7820				
8000	7826				
		87	3199	54312	S355NL/ML
8000	7826				
8000	7830				
		85	3500	59417	S355NL/ML
8367	8197				
8367	8201				
		83	3500	60661	S355NL/ML
8734	8568				
8734	8574				
		80	3000	52150	S355NL/ML
9048	8888				
9048	8892				
		78	3000	52672	S355NL/ML
9363	9207				
9363	9213				
		75	3000	52408	S355NL/ML
9677	9527				
9677	9521				
		78	3081	57847	S355NL/ML
10000	9844				
10000	9838				
		81	4000	79256	S355NL/ML
10000	9838				
10000	9824				
		88	4000	86045	S355NL/ML
10000	9824				
10000	9814				
		93	4000	90888	S355NL/ML
10000	9814				
10000	9800				
		100	3500	85452	S355NL/ML
10000	9800				
10000	9772				
		114	3360	93387	S355NL/ML
10000	9772				
10000	9788				
		106	3500	90524	S355NL/ML
10000	9788				
10000	9794				
		103	3500	87989	S355NL/ML
10000	9794				
10000	9796				
		102	4000	99593	S355NL/ML
10000	9796				
10000	9798				
		101	4000	98626	S355NL/ML
10000	9798				
10000	9804				
		98	4000	95726	S355NL/ML
10000	9804				
10000	9820				
		90	4000	87982	S355NL/ML
10000	9820				
10000	9836				
		82	3500	70198	S355NL/ML
10000	9836				
10000	9844				
		78	3000	57258	S355NL/ML
10000	9844				
10000	9836				
		82	2989	59949	S355NL/ML
10000	9836				
10000	9786				
		107	2900	75706	S355NL/ML
10000	9786				

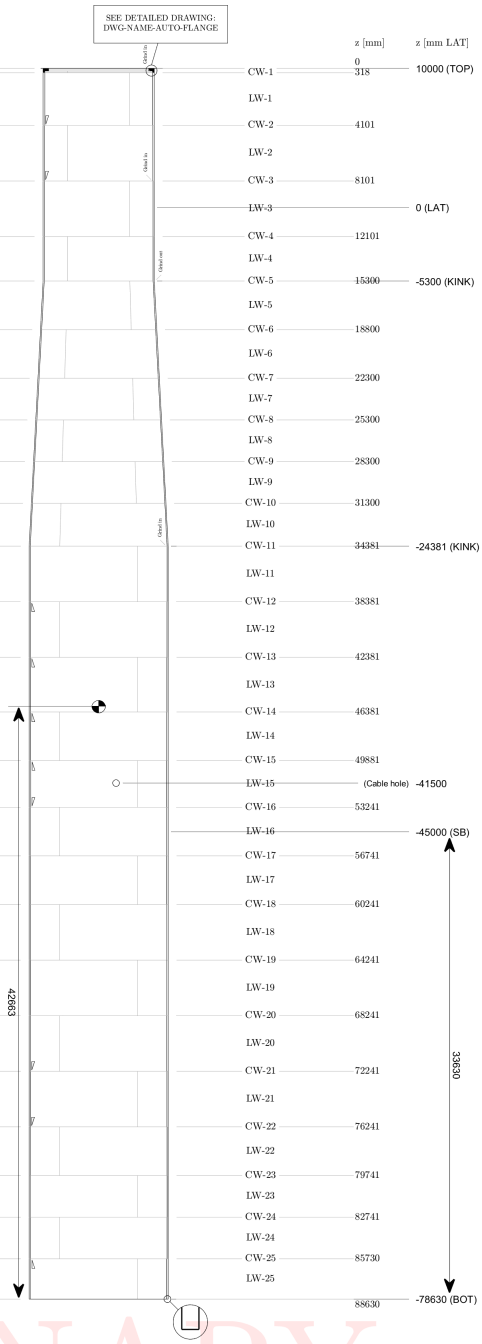

z [mm]	z [mm LAT]
0	
CW-1 318	10000 (TOP)
LW-1	
CW-2 4101	
LW-2	
CW-3 8101	
LW-3	0 (LAT)
CW-4 12101	
LW-4	
CW-5 15300	-5300 (KINK)
LW-5	
CW-6 18800	
LW-6	
CW-7 22300	
LW-7	
CW-8 25300	
LW-8	
CW-9 28300	
LW-9	
CW-10 31300	
LW-10	
CW-11 34381	-24381 (KINK)
LW-11	
CW-12 38381	
LW-12	
CW-13 42381	
LW-13	
CW-14 46381	
LW-14	
CW-15 49881	
LW-15	(Cable hole) -41500
CW-16 53241	
LW-16	-45000 (SB)
CW-17 56741	
LW-17	
CW-18 60241	
LW-18	
CW-19 64241	
LW-19	
CW-20 68241	
LW-20	
CW-21 72241	
LW-21	
CW-22 76241	
LW-22	
CW-23 79741	
LW-23	
CW-24 82741	
LW-24	
CW-25 85730	
LW-25	
88630	-78630 (BOT)

Orientation of Array Cable Entry Hole(s): [45] degrees clockwise relative to N.

10 m 5 m 1 m 0 m

NOTES:

Drawings are for scheme design and show design intent only. Full detailed design analysis is required prior to fabrication. Secondary steel concept is not shown.

REV	DATE	REVISION DESCRIPTION	PREP.	QA	APPR
A	XXXX.XX.XXX	Issued for Client Review	BMS	XX	XX

DESIGN BY: WOOD THILSTED PARTNERS
APPROVED BY: XX — DATE: 15 Aug 2022
CHECKED BY: XX — DATE: 15 Aug 2022
PREPARED BY: EMB — DATE: 15 Aug 2022
SCALE: NOTED
WT PROJECT NO. 9993

NAN

WOOD THILSTED

GENERIC MORPHEUS MODEL
IEA15MW
MONOPILE: WTG_01

DRAWING NO. WT-9993-NAN-DWG-WTG_01-MP — REV. A

DRAWING NO. WT-9993-nan-DWG-WTG_01-MP
REV. A

Figure D.8: Monopile design drawing of ice case - Baltic Proper South

TP (incl. flanges)

M: 234.5 t

L: 10.0 m

V: 29.8 m^3

D: 8.00 m

A_{ext}: 251.3 m^2

A_{int}: 243.7 m^2

Legend:

Grind: Grind weld flush

Plate tapering (angle 1:4)

Center of gravity

Hole

Longitudinal welds (LW):

Weld ID	No	length	thi	Grinding		IC*	
-	-	mm	mm	in	out	in	out
LW-1	2	2455	115	-	-	II	II
LW-2	2	2565	93	-	-	II	II
LW-3	3	4435	115	-	-	II	II

LW total length: 23.3 m
LW average thickness: 110.2 mm

Circumferential welds (CW):

Weld ID	length	thi	Grinding		IC*	
-	mm	mm	in	out	in	out
CW-1	25133	115-115	-	-	I	I
CW-2	25133	115-93	-	-	I	II
CW-3	25133	93-115	-	-	I	II
CW-4	25133	115-115	-	-	I	I

CW total length: 100.5 m
CW average thickness: 104.0 mm

Steel (TP total excl. flanges)

S355NL/ML:	46.5 t
S355NL/ML+Z35:	154.1 t

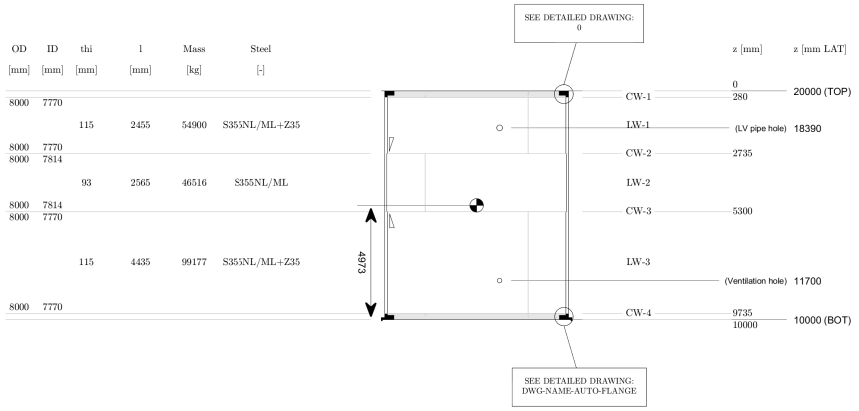

10 m 5 m 1 m 0 m

NOTES:

Drawings are for scheme design and show design intent only. Full detailed design analysis is required prior to fabrication. Secondary steel concept is not shown.

REV	DATE	REVISION DESCRIPTION	PREP.	QA	APPR
A	XXXX.XX.XXX	Issued for Client Review	EMS	XX	XX

DESIGN BY: WOOD THILSTED PARTNERS
APPROVED BY: XX — DATE: 12 Aug 2022
CHECKED BY: XX — DATE: 12 Aug 2022
PREPARED BY: EMS — DATE: 12 Aug 2022
SCALE: NOTED
WT PROJECT NO. 9993

NAN

WOOD THILSTED

GENERIC MORPHEUS MODEL
IEA15MW
TRANSITION PIECE: WTG_01

DRAWING NO. WT-9993-NAN-DWG-WTG_01-TP — REV. A

DRAWING NO. WT-9993-nan-DWG-WTG_01-TP
REV. A

Figure D.9: Transition piece design drawing of reference case - Baltic Proper North

MP (incl. flange)

M: 1913.4 t

L: 88.8 m

V: 243.9 m^3

D: 8.00 - 10.00 m

A_{ext}: 2634.7 m^2

A_{int}: 2578.9 m^2

Legend:

Grind: Grind weld flush

Plate tapering (angle 1:4)

Center of gravity

Hole

Longitudinal welds (LW):

Weld ID	No	length	thi	Grinding		IC*	
-	-	mm	mm	in	out	in	out
LW-1	3	3783	130	-	-	II	II
LW-2	3	4000	105	-	-	II	II
LW-3	3	4000	91	-	-	II	II
LW-4	2	3199	88	-	-	II	II
LW-5	2	3500	85	-	-	II	II
LW-6	2	3500	84	-	-	II	II
LW-7	2	3000	81	-	-	II	II
LW-8	2	3000	79	-	-	II	II
LW-9	2	3000	76	-	-	II	II
LW-10	2	3081	78	-	-	II	II
LW-11	3	4000	80	-	-	II	II
LW-12	3	4000	88	-	-	II	II
LW-13	3	4000	93	-	-	II	II
LW-14	3	3500	100	-	-	II	II
LW-15	3	3359	114	-	-	II	II
LW-16	3	3500	106	-	-	II	II
LW-17	3	4000	102	-	-	II	II
LW-18	3	4000	101	-	-	II	II
LW-19	3	4000	100	-	-	II	II
LW-20	3	4000	96	-	-	II	II
LW-21	3	4000	87	-	-	II	II
LW-22	2	3000	82	-	-	II	II
LW-23	2	3000	78	-	-	II	II
LW-24	2	3170	82	-	-	II	II
LW-25	3	2900	107	-	-	II	II

LW total length: 234.0 m
LW average thickness: 94.7 mm

Circumferential welds (CW):

Weld ID	length	thi	Grinding		IC*	
-	mm	mm	in	out	in	out
CW-1	25133	130-130	yes	-	I	I
CW-2	25133	130-105	-	-	I	II
CW-3	25133	105-91	yes	-	I	II
CW-4	25133	91-88	-	-	I	I
CW-5	25133	88-85	-	yes	II	I
CW-6	26285	85-84	-	-	I	I
CW-7	27438	84-81	-	-	I	I
CW-8	28426	81-79	-	-	I	II
CW-9	29414	79-76	-	-	I	II
CW-10	30401	76-78	-	-	I	II
CW-11	31416	78-80	yes	-	I	II
CW-12	31416	80-88	-	-	I	II
CW-13	31416	88-93	-	-	II	II
CW-14	31416	93-100	-	-	II	II
CW-15	31416	100-114	-	-	I	II
CW-16	31416	114-106	-	-	II	II
CW-17	31416	106-102	-	-	II	II
CW-18	31416	102-101	-	-	II	I
CW-19	31416	101-100	-	-	II	I
CW-20	31416	100-96	-	-	II	II
CW-21	31416	96-87	-	-	II	II
CW-22	31416	87-82	-	-	II	II
CW-23	31416	82-78	-	-	II	II
CW-24	31416	78-82	-	-	II	II
CW-25	31416	82-107	-	-	II	II

CW total length: 738.9 m
CW average thickness: 89.6 mm

Steel (MP total excl. flanges)

S355NL/ML:	1897.0 t
Cylindrical:	1559.2 t
Conical:	337.9 t

SEE DETAILED DRAWING: DWG-NAME-AUTO-FLANGE

OD [mm]	ID [mm]	thi [mm]	l [mm]	Mass [kg]	Steel -]
8000	7740				
		130	3783	95450	S355NL/ML
8000	7740				
8000	7790				
		105	4000	81775	S355NL/ML
8000	7790				
8000	7818				
		91	4000	70997	S355NL/ML
8000	7818				
8000	7824				
		88	3199	54929	S355NL/ML
8000	7824				
8000	7830				
		85	3500	59417	S355NL/ML
8367	8197				
8367	8199				
		84	3500	61385	S355NL/ML
8734	8566				
8734	8572				
		81	3000	52796	S355NL/ML
9048	8886				
9048	8890				
		79	3000	53342	S355NL/ML
9363	9205				
9363	9211				
		76	3000	53101	S355NL/ML
9677	9525				
9677	9521				
		78	3081	57847	S355NL/ML
10000	9844				
10000	9840				
		80	4000	78285	S355NL/ML
10000	9840				
10000	9824				
		88	4000	86045	S355NL/ML
10000	9824				
10000	9814				
		93	4000	90888	S355NL/ML
10000	9814				
10000	9800				
		100	3500	85452	S355NL/ML
10000	9800				
10000	9772				
		114	3359	93359	S355NL/ML
10000	9772				
10000	9788				
		106	3500	90524	S355NL/ML
10000	9788				
10000	9796				
		102	4000	99593	S355NL/ML
10000	9796				
10000	9798				
		101	4000	98626	S355NL/ML
10000	9798				
10000	9800				
		100	4000	97660	S355NL/ML
10000	9800				
10000	9808				
		96	4000	93791	S355NL/ML
10000	9808				
10000	9826				
		87	4000	85075	S355NL/ML
10000	9826				
10000	9836				
		82	3000	60170	S355NL/ML
10000	9836				
10000	9844				
		78	3000	57258	S355NL/ML
10000	9844				
10000	9836				
		82	3170	63579	S355NL/ML
10000	9836				
10000	9786				
		107	2900	75706	S355NL/ML
10000	9786				

z [mm]	z [mm LAT]	
0		
318	10000	(TOP)
4101		
8101		
0	(LAT)	
12101		
15300	-5300	(KINK)
18800		
22300		
25300		
28300		
31300		
34381	-24381	(KINK)
38381		
42381		
46381		
49881		
-41500	(Cable hole)	
53240		
-45000	(SB)	
56740		
60740		
64740		
68740		
72740		
76740		
79740		
82740		
85910		
88810	-78810	(BOT)

42969

33810

Orientation of Array Cable Entry Hole(s): [45] degrees clockwise relative to N.

10 m 5 m 1 m 0 m

NOTES:

Drawings are for scheme design and show design intent only. Full detailed design analysis is required prior to fabrication. Secondary steel concept is not shown.

REV	DATE	REVISION DESCRIPTION	PREP.	QA	APPR
A	XXXX.XX.XXX	Issued for Client Review	EMS	XX	XX

DESIGN BY: WOOD THILSTED PARTNERS

APPROVED BY: XX	DATE: 12 Aug 2022
CHECKED BY: XX	DATE: 12 Aug 2022
PREPARED BY: EMS	DATE: 12 Aug 2022

SCALE: NOTED

WT PROJECT NO. 9993

NAN

WOOD THILSTED

GENERIC MORPHEUS MODEL
IEA15MW
MONOPILE: WTG_01

DRAWING NO. WT-9993-NAN-DWG-WTG_01-MP

REV. A

DRAWING NO. WT-9993-nan-DWG-WTG_01-MP

REV. A

Figure D.10: Monopile design drawing of reference case - Baltic Proper North

TP (incl. flanges)

M: 230.3 t

L: 10.0 m

V: 29.2 m^3

D: 8.00 m

A_{ext}: 251.3 m^2

A_{int}: 243.9 m^2

Legend:

Grind: Grind weld flush

Plate tapering (angle 1:4)

Center of gravity

Hole

Longitudinal welds (LW):

Weld ID	No	length	thi	Grinding		IC*	
-	-	mm	mm	in	out	in	out
LW-1	2	2455	112	-	-	II	II
LW-2	2	2565	91	-	-	II	II
LW-3	3	4435	113	-	-	II	II

LW total length: 23.3 m
LW average thickness: 108.0 mm

Circumferential welds (CW):

Weld ID	length	thi	Grinding		IC*	
-	mm	mm	in	out	in	out
CW-1	25133	112-112	-	-	I	I
CW-2	25133	112-91	-	-	I	II
CW-3	25133	91-113	-	-	I	II
CW-4	25133	113-113	-	-	I	I

CW total length: 100.5 m
CW average thickness: 101.8 mm

Steel (TP total excl. flanges)

S355NL/ML:	45.5 t
S355NL/ML+Z35:	151.0 t

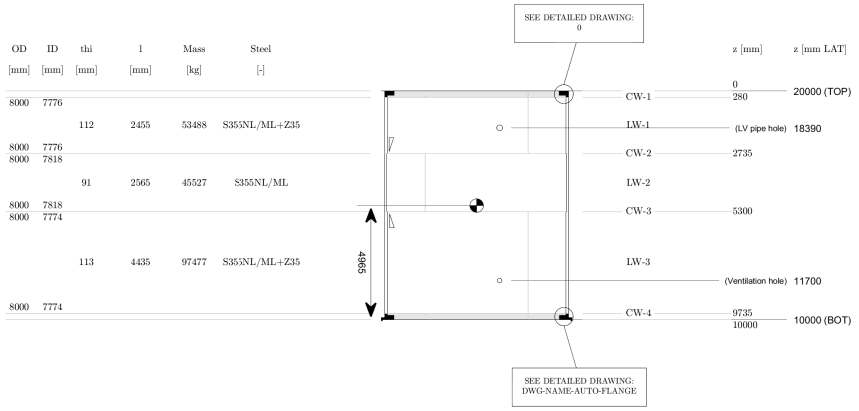

10 m 5 m 1 m 0 m

NOTES:

Drawings are for scheme design and show design intent only. Full detailed design analysis is required prior to fabrication. Secondary steel concept is not shown.

REV	DATE	REVISION DESCRIPTION	PREP.	QA	APPR
A	XXXX.XX.XXX	Issued for Client Review	EMS	XX	XX

DESIGN BY: WOOD THILSTED PARTNERS
APPROVED BY: XX — DATE: 15 Aug 2022
CHECKED BY: XX — DATE: 15 Aug 2022
PREPARED BY: EMS — DATE: 15 Aug 2022
SCALE: NOTED
WT PROJECT NO. 9993

NAN

WOOD THILSTED

GENERIC MORPHEUS MODEL
IEA15MW
TRANSITION PIECE: WTG_01

DRAWING NO. WT-9993-NAN-DWG-WTG_01-TP — REV. A

DRAWING NO. WT-9993-nan-DWG-WTG_01-TP
REV. A

Figure D.11: Transition piece design drawing of ice case - Baltic Proper North

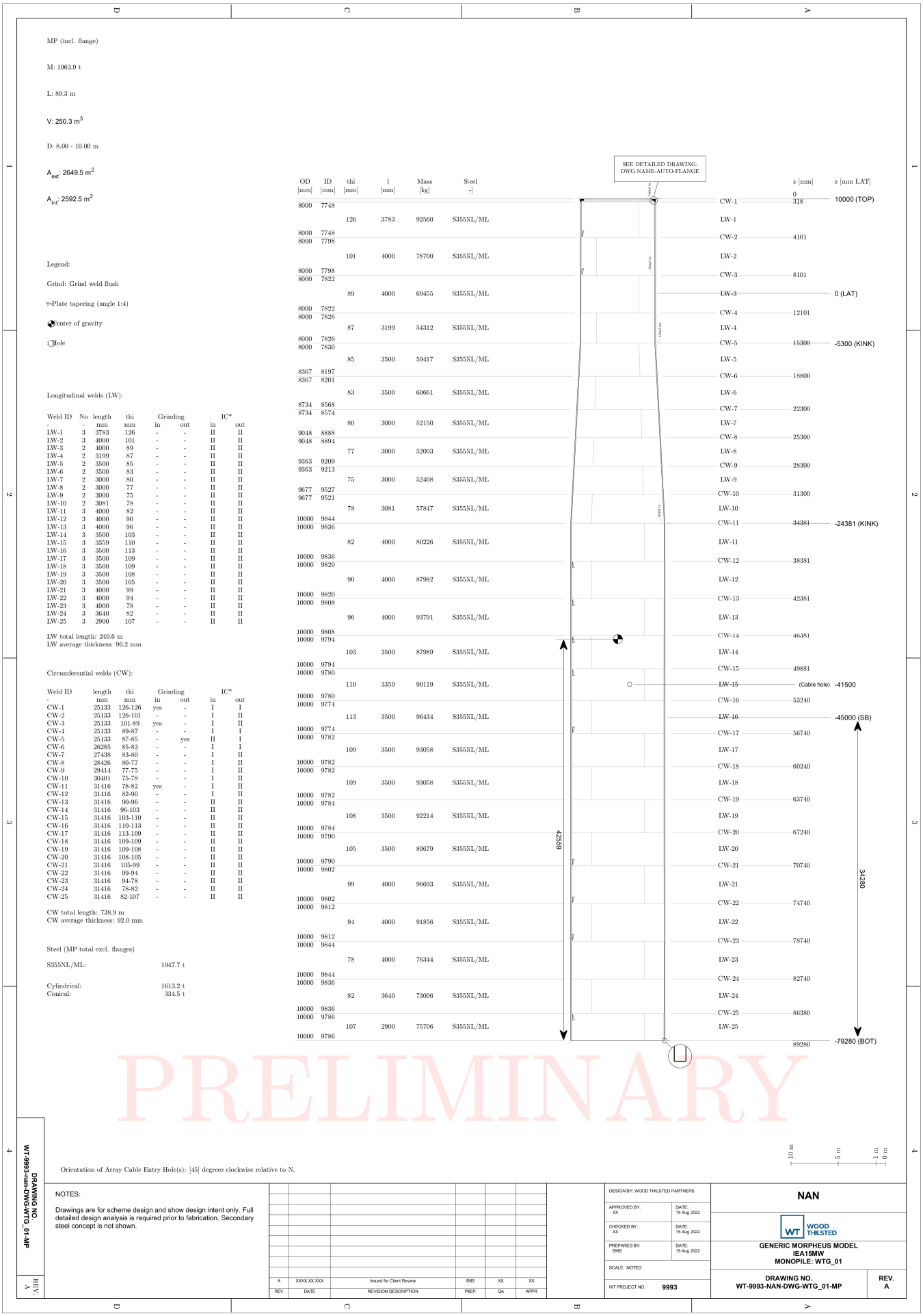

Figure D.12: Monopile design drawing of ice case - Baltic Proper North

TP (incl. flanges)

M: 237.7 t

L: 10.0 m

V: 30.2 m^3

D: 8.00 m

A_{ext}: 251.3 m^2

A_{int}: 243.6 m^2

Legend:

Grind: Grind weld flush

Plate tapering (angle 1:4)

Center of gravity

Hole

Longitudinal welds (LW):

Weld ID	No	length	thi	Grinding		IC*	
-	-	mm	mm	in	out	in	out
LW-1	2	2455	117	-	-	II	II
LW-2	2	2565	94	-	-	II	II
LW-3	3	4435	117	-	-	II	II

LW total length: 23.3 m
LW average thickness: 111.9 mm

Circumferential welds (CW):

Weld ID	length	thi	Grinding		IC*	
-	mm	mm	in	out	in	out
CW-1	25133	117-117	-	-	I	I
CW-2	25133	117-94	-	-	I	II
CW-3	25133	94-117	-	-	I	II
CW-4	25133	117-117	-	-	I	I

CW total length: 100.5 m
CW average thickness: 105.5 mm

Steel (TP total excl. flanges)

S355NL/ML:	47.0 t
S355NL/ML+Z35:	156.7 t

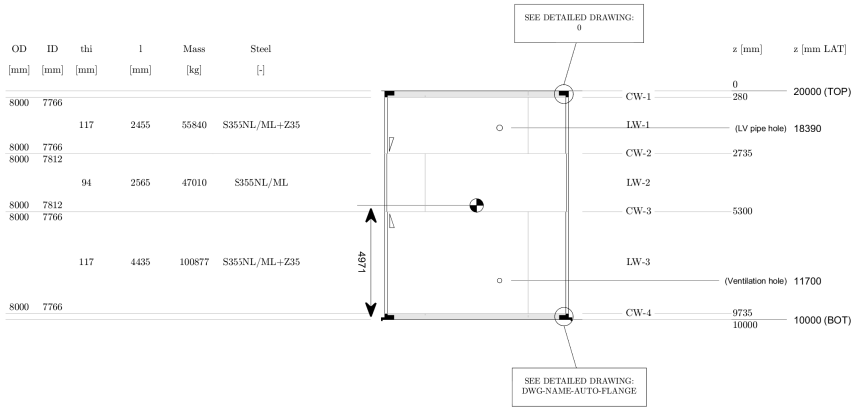

10 m 5 m 1 m 0 m

NOTES:

Drawings are for scheme design and show design intent only. Full detailed design analysis is required prior to fabrication. Secondary steel concept is not shown.

REV	DATE	REVISION DESCRIPTION	PREP.	QA	APPR
A	XXXX.XX.XXX	Issued for Client Review	EMS	XX	XX

DESIGN BY: WOOD THILSTED PARTNERS
APPROVED BY: XX — DATE: 15 Aug 2022
CHECKED BY: XX — DATE: 15 Aug 2022
PREPARED BY: EMS — DATE: 15 Aug 2022
SCALE: NOTED
WT PROJECT NO. 9993

NAN

WOOD THILSTED

GENERIC MORPHEUS MODEL
IEA15MW
TRANSITION PIECE: WTG_01

DRAWING NO. WT-9993-NAN-DWG-WTG_01-TP
REV. A

DRAWING NO. WT-9993-nan-DWG-WTG_01-TP
REV. A

Figure D.13: Transition piece design drawing of relaxed case - Baltic Proper North

MP (incl. flange)

M: 1919.6 t

L: 88.7 m

V: 244.7 m^3

D: 8.00 - 10.00 m

A_{ext}: 2630.6 m^2

A_{int}: 2574.7 m^2

Legend:

Grind: Grind weld flush

t–t Plate tapering (angle 1:4)

Center of gravity

Hole

Longitudinal welds (LW):

Weld ID	No	length	thi	Grinding		IC*	
-	-	mm	mm	in	out	in	out
LW-1	3	3783	132	-	-	II	II
LW-2	3	4000	107	-	-	II	II
LW-3	3	4000	93	-	-	II	II
LW-4	2	3199	90	-	-	II	II
LW-5	2	3500	86	-	-	II	II
LW-6	2	3500	85	-	-	II	II
LW-7	2	3000	82	-	-	II	II
LW-8	2	3000	79	-	-	II	II
LW-9	2	3000	76	-	-	II	II
LW-10	2	3081	78	-	-	II	II
LW-11	3	4000	80	-	-	II	II
LW-12	3	4000	87	-	-	II	II
LW-13	3	4000	95	-	-	II	II
LW-14	3	3500	100	-	-	II	II
LW-15	4	3859	114	-	-	II	II
LW-16	3	4000	106	-	-	II	II
LW-17	3	4000	102	-	-	II	II
LW-18	3	4000	101	-	-	II	II
LW-19	3	4000	99	-	-	II	II
LW-20	3	4000	94	-	-	II	II
LW-21	3	4000	84	-	-	II	II
LW-22	3	4000	78	-	-	II	II
LW-23	3	4040	82	-	-	II	II
LW-24	3	2900	107	-	-	II	II

LW total length: 246.7 m
LW average thickness: 94.9 mm

Circumferential welds (CW):

Weld ID	length	thi	Grinding		IC*	
-	mm	mm	in	out	in	out
CW-1	25133	132-132	yes	-	I	I
CW-2	25133	132-107	-	-	I	II
CW-3	25133	107-93	yes	-	I	II
CW-4	25133	93-90	-	-	I	I
CW-5	25133	90-86	-	yes	II	I
CW-6	26285	86-85	-	-	I	I
CW-7	27438	85-82	-	-	I	II
CW-8	28426	82-79	-	-	I	II
CW-9	29414	79-76	-	-	I	II
CW-10	30401	76-78	-	-	I	II
CW-11	31416	78-80	yes	-	I	II
CW-12	31416	80-87	-	-	I	II
CW-13	31416	87-95	-	-	I	II
CW-14	31416	95-100	-	-	II	II
CW-15	31416	100-114	-	-	I	II
CW-16	31416	114-106	-	-	II	II
CW-17	31416	106-102	-	-	II	II
CW-18	31416	102-101	-	-	I	I
CW-19	31416	101-99	-	-	I	II
CW-20	31416	99-94	-	-	II	II
CW-21	31416	94-84	-	-	II	II
CW-22	31416	84-78	-	-	II	II
CW-23	31416	78-82	-	-	II	II
CW-24	31416	82-107	-	-	II	II

CW total length: 707.5 m
CW average thickness: 90.1 mm

Steel (MP total excl. flanges)

S355NL/ML:	1903.2 t
Cylindrical:	1563.3 t
Conical:	339.9 t

OD [mm]	ID [mm]	thi [mm]	l [mm]	Mass [kg]	Steel -]
8000	7736				
		132	3783	96893	S355NL/ML
8000	7736				
8000	7786				
		107	4000	83312	S355NL/ML
8000	7786				
8000	7814				
		93	4000	72539	S355NL/ML
8000	7814				
8000	7820				
		90	3199	56163	S355NL/ML
8000	7820				
8000	7828				
		86	3500	60108	S355NL/ML
8367	8195				
8367	8197				
		85	3500	62108	S355NL/ML
8734	8564				
8734	8570				
		82	3000	53441	S355NL/ML
9048	8884				
9048	8890				
		79	3000	53342	S355NL/ML
9363	9205				
9363	9211				
		76	3000	53101	S355NL/ML
9677	9525				
9677	9521				
		78	3081	57847	S355NL/ML
10000	9844				
10000	9840				
		80	4000	78285	S355NL/ML
10000	9840				
10000	9826				
		87	4000	85075	S355NL/ML
10000	9826				
10000	9810				
		95	4000	92823	S355NL/ML
10000	9810				
10000	9800				
		100	3500	85452	S355NL/ML
10000	9800				
10000	9772				
		114	3859	107256	S355NL/ML
10000	9772				
10000	9788				
		106	4000	103456	S355NL/ML
10000	9788				
10000	9796				
		102	4000	99593	S355NL/ML
10000	9796				
10000	9798				
		101	4000	98626	S355NL/ML
10000	9798				
10000	9802				
		99	4000	96693	S355NL/ML
10000	9802				
10000	9812				
		94	4000	91856	S355NL/ML
10000	9812				
10000	9832				
		84	4000	82167	S355NL/ML
10000	9832				
10000	9844				
		78	4000	76344	S355NL/ML
10000	9844				
10000	9836				
		82	4040	81029	S355NL/ML
10000	9836				
10000	9786				
		107	2900	75706	S355NL/ML
10000	9786				

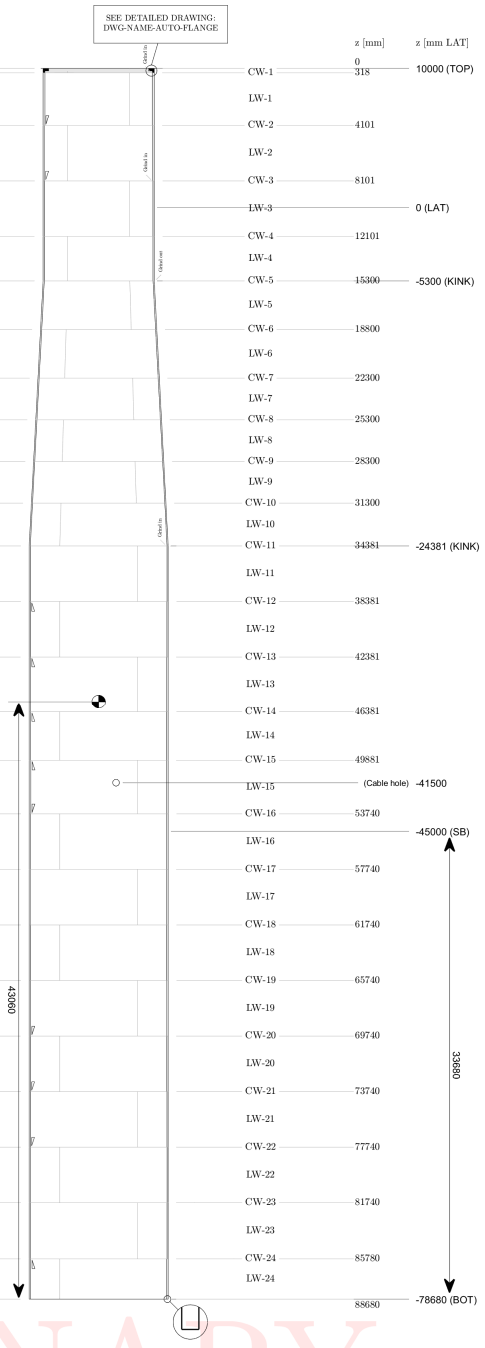

Orientation of Array Cable Entry Hole(s): [45] degrees clockwise relative to N.

10 m 5 m 1 m 0 m

NOTES:

Drawings are for scheme design and show design intent only. Full detailed design analysis is required prior to fabrication. Secondary steel concept is not shown.

REV	DATE	REVISION DESCRIPTION	PREP.	QA	APPR
A	XXXX.XX.XXX	Issued for Client Review	BMS	XX	XX

DESIGN BY: WOOD THILSTED PARTNERS
APPROVED BY: XX — DATE: 15 Aug 2022
CHECKED BY: XX — DATE: 15 Aug 2022
PREPARED BY: EMB — DATE: 15 Aug 2022
SCALE: NOTED
WT PROJECT NO. 9993

NAN

WOOD THILSTED

GENERIC MORPHEUS MODEL
1EA15MW
MONOPILE: WTG_01

DRAWING NO. WT-9993-NAN-DWG-WTG_01-MP
REV. A

DRAWING NO. WT-9993-nan-DWG-WTG_01-MP
REV. A

Figure D.14: Monopile design drawing of relaxed case - Baltic Proper North

TP (incl. flanges)

M: 169.7 t

L: 10.0 m

V: 21.5 m^3

D: 8.00 m

A_{ext}: 251.3 m^2

A_{int}: 245.9 m^2

Legend:

Grind: Grind weld flush

Plate tapering (angle 1:4)

Center of gravity

Hole

Longitudinal welds (LW):

Weld ID	No	length	thi	Grinding		IC*	
-	-	mm	mm	in	out	in	out
LW-1	1	2455	72	-	-	II	II
LW-2	1	2565	66	-	-	II	II
LW-3	2	4435	80	-	-	II	II

LW total length: 13.9 m
LW average thickness: 76.0 mm

Circumferential welds (CW):

Weld ID	length	thi	Grinding		IC*	
-	mm	mm	in	out	in	out
CW-1	25133	72-72	-	-	I	I
CW-2	25133	72-66	-	-	II	II
CW-3	25133	66-80	-	-	I	II
CW-4	25133	80-80	-	-	I	I

CW total length: 100.5 m
CW average thickness: 71.0 mm

Steel (TP total excl. flanges)

S355NL/ML:	33.1 t
S355NL/ML+Z35:	103.9 t

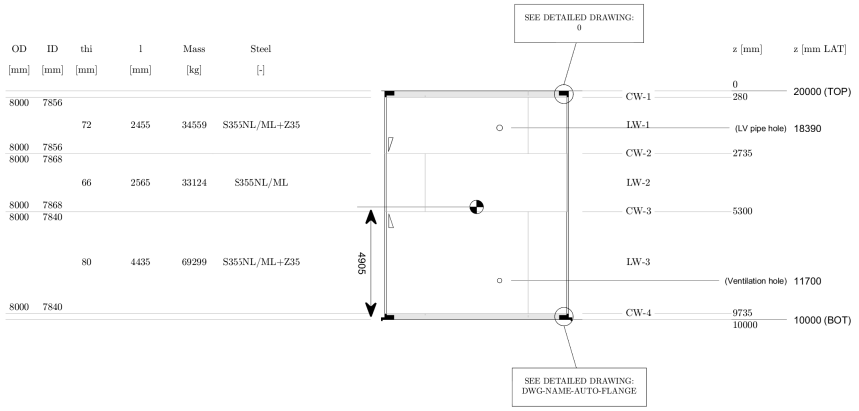

10 m 5 m 1 m 0 m

NOTES:

Drawings are for scheme design and show design intent only. Full detailed design analysis is required prior to fabrication. Secondary steel concept is not shown.

REV	DATE	REVISION DESCRIPTION	PREP.	QA	APPR
A	XXXX.XX.XXX	Issued for Client Review	EMS	XX	XX

DESIGN BY: WOOD THILSTED PARTNERS
APPROVED BY: XX — DATE: 12 Aug 2022
CHECKED BY: XX — DATE: 12 Aug 2022
PREPARED BY: EMS — DATE: 12 Aug 2022
SCALE: NOTED
WT PROJECT NO. 9993

NAN

WOOD THILSTED

GENERIC MORPHEUS MODEL
IEA15MW
TRANSITION PIECE: WTG_01

DRAWING NO. WT-9993-nan-DWG-WTG_01-TP — REV. A

Figure D.15: Transition piece design drawing of reference case - Gulf of Riga

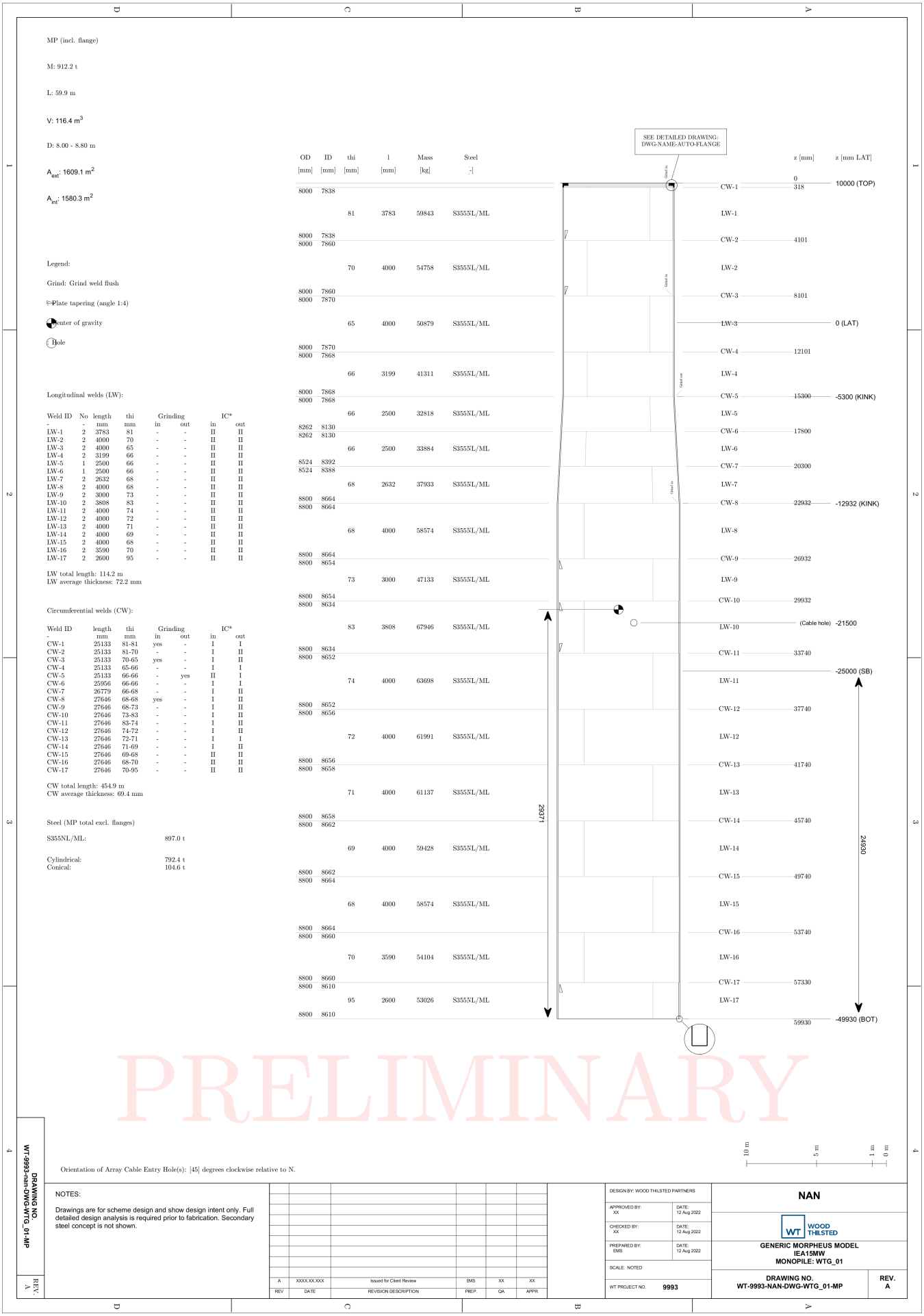

Figure D.16: Monopile design drawing of reference case - Gulf of Riga

TP (incl. flanges)

M: 181.3 t

L: 10.0 m

V: 23.0 m^3

D: 8.00 m

A_{ext}: 251.3 m^2

A_{int}: 245.5 m^2

Legend:

Grind: Grind weld flush

Plate tapering (angle 1:4)

Center of gravity

Hole

Longitudinal welds (LW):

Weld ID	No	length	thi	Grinding		IC*	
-	-	mm	mm	in	out	in	out
LW-1	2	2455	80	-	-	II	II
LW-2	2	2565	71	-	-	II	II
LW-3	3	4435	86	-	-	II	II

LW total length: 23.3 m
LW average thickness: 81.4 mm

Circumferential welds (CW):

Weld ID	length	thi	Grinding		IC*	
-	mm	mm	in	out	in	out
CW-1	25133	80-80	-	-	I	I
CW-2	25133	80-71	-	-	II	II
CW-3	25133	71-86	-	-	I	II
CW-4	25133	86-86	-	-	I	I

CW total length: 100.5 m
CW average thickness: 77.0 mm

Steel (TP total excl. flanges)

S355NL/ML:	35.6 t
S355NL/ML+Z35:	112.8 t

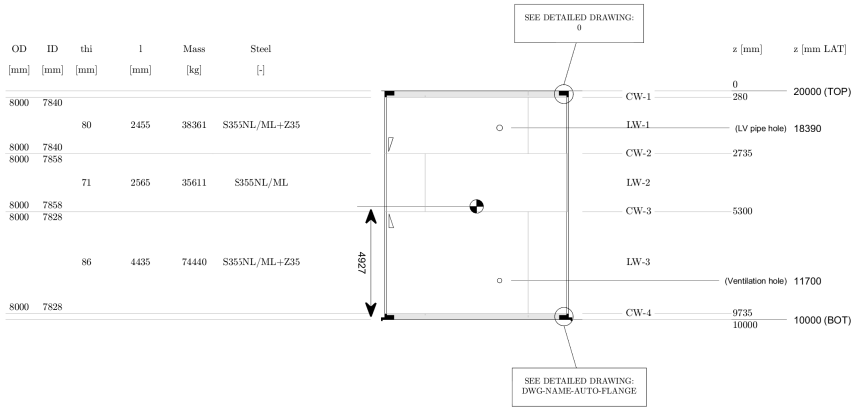

10 m 5 m 1 m 0 m

DRAWING NO. WT-9993-nan-DWG-WTG_01-TP
REV. A

NOTES:

Drawings are for scheme design and show design intent only. Full detailed design analysis is required prior to fabrication. Secondary steel concept is not shown.

REV	DATE	REVISION DESCRIPTION	PREP.	QA	APPR
A	XXXX.XX.XXX	Issued for Client Review	EMS	XX	XX

DESIGN BY: WOOD THILSTED PARTNERS
APPROVED BY: XX — DATE: 15 Aug 2022
CHECKED BY: XX — DATE: 15 Aug 2022
PREPARED BY: EMS — DATE: 15 Aug 2022
SCALE: NOTED
WT PROJECT NO. 9993

NAN
WOOD THILSTED
GENERIC MORPHEUS MODEL
IEA15MW
TRANSITION PIECE: WTG_01
DRAWING NO. WT-9993-NAN-DWG-WTG_01-TP
REV. A

Figure D.17: Transition piece design drawing of ice case - Gulf of Riga

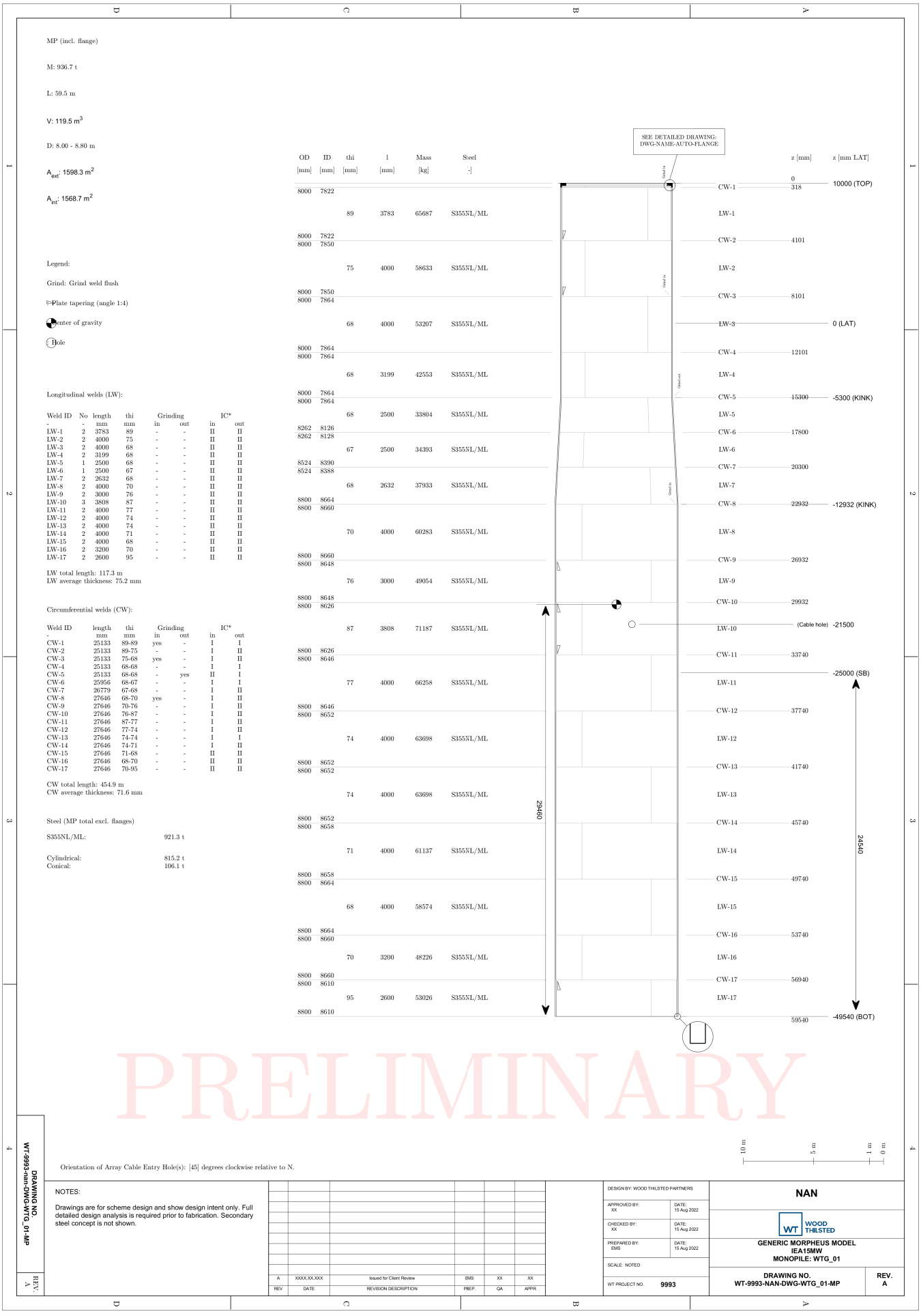

Figure D.18: Monopile design drawing of ice case - Gulf of Riga

TP (incl. flanges)

M: 179.0 t

L: 10.0 m

V: 22.7 m^3

D: 8.00 m

A_{ext}: 251.3 m^2

A_{int}: 245.6 m^2

Legend:

Grind: Grind weld flush

Plate tapering (angle 1:4)

Center of gravity

Hole

Longitudinal welds (LW):

Weld ID	No	length	thi	Grinding		IC*	
-	-	mm	mm	in	out	in	out
LW-1	2	2455	78	-	-	II	II
LW-2	2	2565	70	-	-	II	II
LW-3	3	4435	85	-	-	II	II

LW total length: 23.3 m
LW average thickness: 80.2 mm

Circumferential welds (CW):

Weld ID	length	thi	Grinding		IC*	
-	mm	mm	in	out	in	out
CW-1	25133	78-78	-	-	I	I
CW-2	25133	78-70	-	-	II	II
CW-3	25133	70-85	-	-	I	II
CW-4	25133	85-85	-	-	I	I

CW total length: 100.5 m
CW average thickness: 75.7 m

Steel (TP total excl. flanges)

S355NL/ML:	35.1 t
S355NL/ML+Z35:	111.0 t

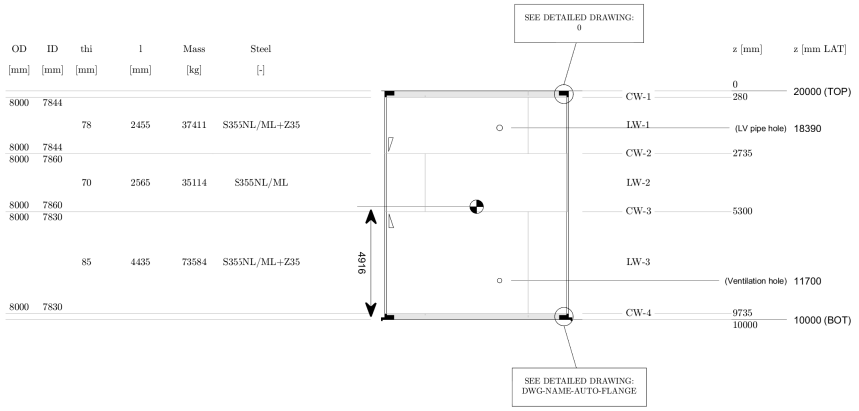

10 m 5 m 1 m 0 m

NOTES:

Drawings are for scheme design and show design intent only. Full detailed design analysis is required prior to fabrication. Secondary steel concept is not shown.

REV	DATE	REVISION DESCRIPTION	PREP.	QA	APPR
A	XXXX.XX.XXX	Issued for Client Review	EMS	XX	XX

DESIGN BY: WOOD THILSTED PARTNERS
APPROVED BY: XX — DATE: 12 Aug 2022
CHECKED BY: XX — DATE: 12 Aug 2022
PREPARED BY: EMS — DATE: 12 Aug 2022
SCALE: NOTED
WT PROJECT NO. 9993

NAN

WOOD THILSTED

GENERIC MORPHEUS MODEL
IEA15MW
TRANSITION PIECE: WTG_01

DRAWING NO. WT-9993-NAN-DWG-WTG_01-TP — REV. A

DRAWING NO. WT-9993-nan-DWG-WTG_01-TP
REV. A

Figure D.19: Transition piece design drawing of reference case - Gulf of Finland

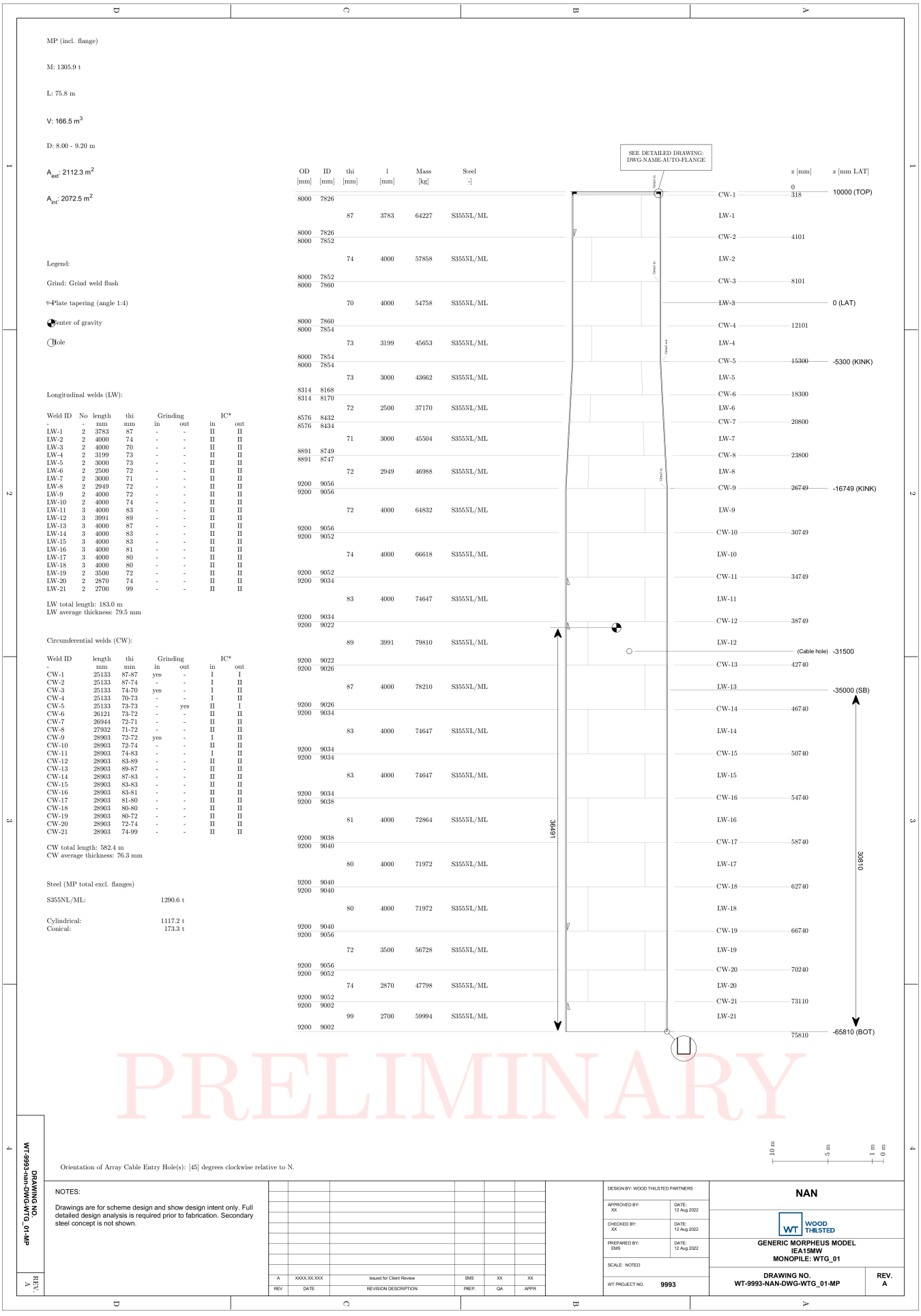

Figure D.20: Monopile design drawing of reference case - Gulf of Finland

TP (incl. flanges)

M: 227.1 t

L: 10.0 m

V: 28.8 m^3

D: 8.00 m

A_{ext}: 251.3 m^2

A_{int}: 244.0 m^2

Legend:

Grind: Grind weld flush

Plate tapering (angle 1:4)

Center of gravity

Hole

Longitudinal welds (LW):

Weld ID	No	length	thi	Grinding		IC*	
-	-	mm	mm	in	out	in	out
LW-1	2	2455	110	-	-	II	II
LW-2	2	2565	90	-	-	II	II
LW-3	3	4435	111	-	-	II	II

LW total length: 23.3 m
LW average thickness: 106.2 mm

Circumferential welds (CW):

Weld ID	length	thi	Grinding		IC*	
-	mm	mm	in	out	in	out
CW-1	25133	110-110	-	-	I	I
CW-2	25133	110-90	-	-	I	II
CW-3	25133	90-111	-	-	I	II
CW-4	25133	111-111	-	-	I	I

CW total length: 100.5 m
CW average thickness: 100.2 mm

Steel (TP total excl. flanges)

S355NL/ML:	45.0 t
S355NL/ML+Z35:	148.3 t

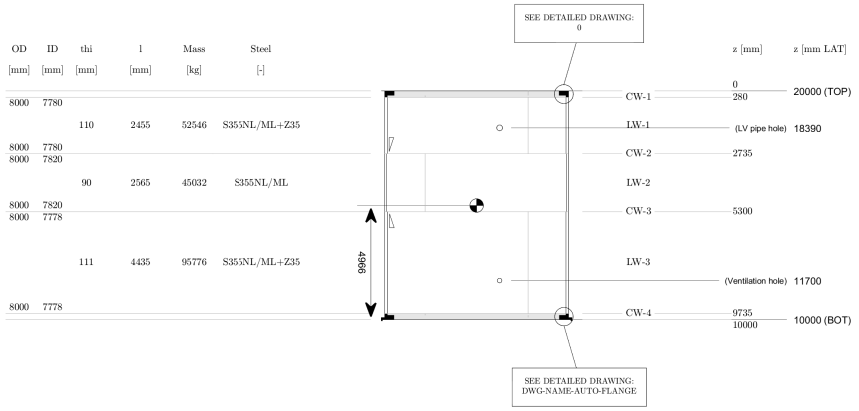

10 m 5 m 1 m 0 m

NOTES:

Drawings are for scheme design and show design intent only. Full detailed design analysis is required prior to fabrication. Secondary steel concept is not shown.

REV	DATE	REVISION DESCRIPTION	PREP.	QA	APPR
A	XXXX.XX.XXX	Issued for Client Review	EMS	XX	XX

DESIGN BY: WOOD THILSTED PARTNERS
APPROVED BY: XX — DATE: 15 Aug 2022
CHECKED BY: XX — DATE: 15 Aug 2022
PREPARED BY: EMS — DATE: 15 Aug 2022
SCALE: NOTED
WT PROJECT NO. 9993

NAN

WOOD THILSTED

GENERIC MORPHEUS MODEL
IEA15MW
TRANSITION PIECE: WTG_01

DRAWING NO. WT-9993-NAN-DWG-WTG_01-TP — REV. A

DRAWING NO. WT-9993-nan-DWG-WTG_01-TP
REV. A

Figure D.21: Transition piece design drawing of ice case - Gulf of Finland

MP (incl. flange)

M: 1446.7 t

L: 73.6 m

V: 184.5 m^3

D: 8.00 - 9.20 m

A_{ext}: 2049.6 m^2

A_{int}: 2005.4 m^2

Legend:

Grind: Grind weld flush

Plate tapering (angle 1:4)

Center of gravity

Hole

Longitudinal welds (LW):

Weld ID	No	length	thi	Grinding in	Grinding out	IC* in	IC* out
-	-	mm	mm	in	out	in	out
LW-1	3	3783	125	-	-	II	II
LW-2	3	4000	100	-	-	II	II
LW-3	2	4000	84	-	-	II	II
LW-4	2	3199	85	-	-	II	II
LW-5	2	3000	84	-	-	II	II
LW-6	2	2500	83	-	-	II	II
LW-7	2	3000	81	-	-	II	II
LW-8	2	2949	78	-	-	II	II
LW-9	3	4000	79	-	-	II	II
LW-10	2	3500	83	-	-	II	II
LW-11	2	3000	88	-	-	II	II
LW-12	2	3000	97	-	-	II	II
LW-13	3	3492	112	-	-	II	II
LW-14	3	4000	99	-	-	II	II
LW-15	3	4000	95	-	-	II	II
LW-16	3	4000	93	-	-	II	II
LW-17	3	4000	92	-	-	II	II
LW-18	3	4000	87	-	-	II	II
LW-19	2	4000	73	-	-	II	II
LW-20	2	3199	74	-	-	II	II
LW-21	2	2700	99	-	-	II	II

LW total length: 181.9 m
LW average thickness: 91.8 mm

Circumferential welds (CW):

Weld ID	length	thi	Grinding in	Grinding out	IC* in	IC* out
-	mm	mm	in	out	in	out
CW-1	25133	125-125	yes	-	I	I
CW-2	25133	125-100	-	-	I	II
CW-3	25133	100-84	yes	-	I	II
CW-4	25133	84-85	-	-	I	I
CW-5	25133	85-84	-	yes	II	I
CW-6	26121	84-83	-	-	I	I
CW-7	26944	83-81	-	-	I	I
CW-8	27932	81-78	-	-	I	II
CW-9	28903	78-79	yes	-	I	II
CW-10	28903	79-83	-	-	I	II
CW-11	28903	83-88	-	-	I	II
CW-12	28903	88-97	-	-	I	II
CW-13	28903	97-112	-	-	I	II
CW-14	28903	112-99	-	-	I	II
CW-15	28903	99-95	-	-	I	II
CW-16	28903	95-93	-	-	I	I
CW-17	28903	93-92	-	-	II	II
CW-18	28903	92-87	-	-	II	II
CW-19	28903	87-73	-	-	II	II
CW-20	28903	73-74	-	-	II	II
CW-21	28903	74-99	-	-	II	II

CW total length: 582.4 m
CW average thickness: 86.9 mm

Steel (MP total excl. flanges)

S355NL/ML:	1430.5 t
Cylindrical:	1234.8 t
Conical:	195.7 t

OD [mm]	ID [mm]	thi [mm]	l [mm]	Mass [kg]	Steel -]
8000	7750				
		125	3783	91837	S355NL/ML
8000	7750				
8000	7800				
		100	4000	77930	S355NL/ML
8000	7800				
8000	7832				
		84	4000	65594	S355NL/ML
8000	7832				
8000	7830				
		85	3199	53077	S355NL/ML
8000	7830				
8000	7832				
		84	3000	50173	S355NL/ML
8314	8146				
8314	8148				
		83	2500	42793	S355NL/ML
8576	8410				
8576	8414				
		81	3000	51853	S355NL/ML
8891	8729				
8891	8735				
		78	2949	50870	S355NL/ML
9200	9044				
9200	9042				
		79	4000	71080	S355NL/ML
9200	9042				
9200	9034				
		83	3500	65316	S355NL/ML
9200	9034				
9200	9024				
		88	3000	59325	S355NL/ML
9200	9024				
9200	9006				
		97	3000	65328	S355NL/ML
9200	9006				
9200	8976				
		112	3492	87656	S355NL/ML
9200	8976				
9200	9002				
		99	4000	88880	S355NL/ML
9200	9002				
9200	9010				
		95	4000	85326	S355NL/ML
9200	9010				
9200	9014				
		93	4000	83548	S355NL/ML
9200	9014				
9200	9016				
		92	4000	82659	S355NL/ML
9200	9016				
9200	9026				
		87	4000	78210	S355NL/ML
9200	9026				
9200	9054				
		73	4000	65725	S355NL/ML
9200	9054				
9200	9052				
		74	3199	53278	S355NL/ML
9200	9052				
9200	9002				
		99	2700	59994	S355NL/ML
9200	9002				

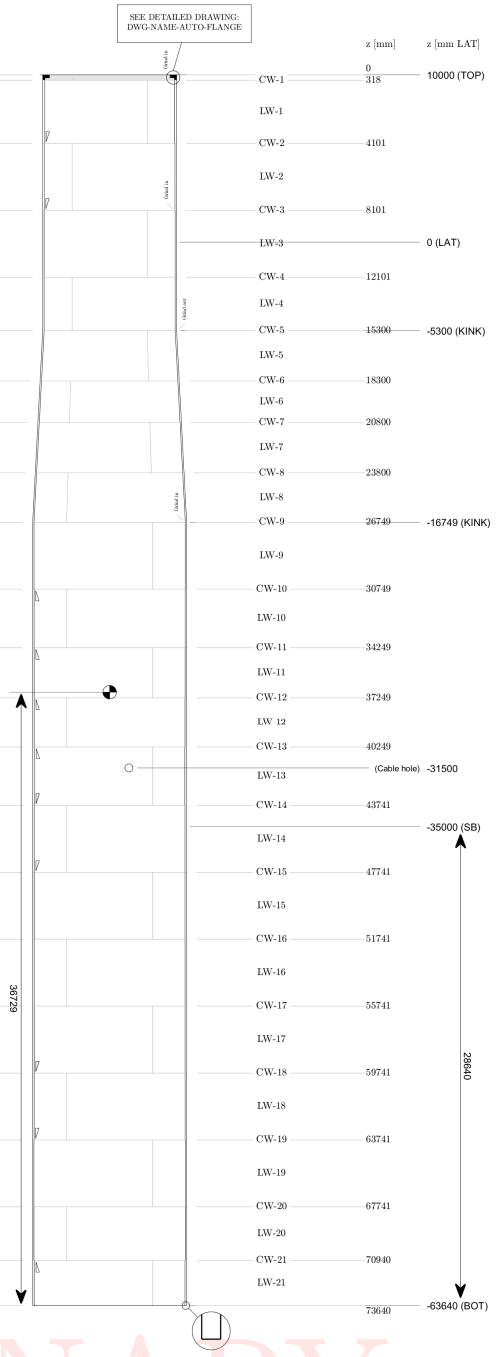

Orientation of Array Cable Entry Hole(s): [45] degrees clockwise relative to N.

10 m 5 m 1 m 0 m

NOTES:

Drawings are for scheme design and show design intent only. Full detailed design analysis is required prior to fabrication. Secondary steel concept is not shown.

REV	DATE	REVISION DESCRIPTION	PREP.	QA	APPR
A	XXXX.XX.XXX	Issued for Client Review	EMS	XX	XX

DESIGN BY: WOOD THILSTED PARTNERS
APPROVED BY: XX — DATE: 15 Aug 2022
CHECKED BY: XX — DATE: 15 Aug 2022
PREPARED BY: EMS — DATE: 15 Aug 2022
SCALE: NOTED
WT PROJECT NO. 9993

NAN

WOOD THILSTED

GENERIC MORPHEUS MODEL
IEA15MW
MONOPILE: WTG_01

DRAWING NO. WT-9993-NAN-DWG-WTG_01-MP — REV. A

DRAWING NO. WT-9993-nan-DWG-WTG_01-MP
REV. A

Figure D.22: Monopile design drawing of ice case - Gulf of Finland

TP (incl. flanges)

M: 235.8 t

L: 10.0 m

V: 29.9 m^3

D: 8.00 m

A_{ext}: 251.3 m^2

A_{int}: 243.7 m^2

Legend:

Grind: Grind weld flush

Plate tapering (angle 1:4)

Center of gravity

Hole

Longitudinal welds (LW):

Weld ID	No	length	thi	Grinding		IC*	
-	-	mm	mm	in	out	in	out
LW-1	2	2455	116	-	-	II	II
LW-2	2	2565	93	-	-	II	II
LW-3	3	4435	116	-	-	II	II

LW total length: 23.3 m
LW average thickness: 110.9 mm

Circumferential welds (CW):

Weld ID	length	thi	Grinding		IC*	
-	mm	mm	in	out	in	out
CW-1	25133	116-116	-	-	I	I
CW-2	25133	116-93	-	-	I	II
CW-3	25133	93-116	-	-	I	II
CW-4	25133	116-116	-	-	I	I

CW total length: 100.5 m
CW average thickness: 104.5 mm

Steel (TP total excl. flanges)

S355NL/ML:	46.5 t
S355NL/ML+Z35:	155.4 t

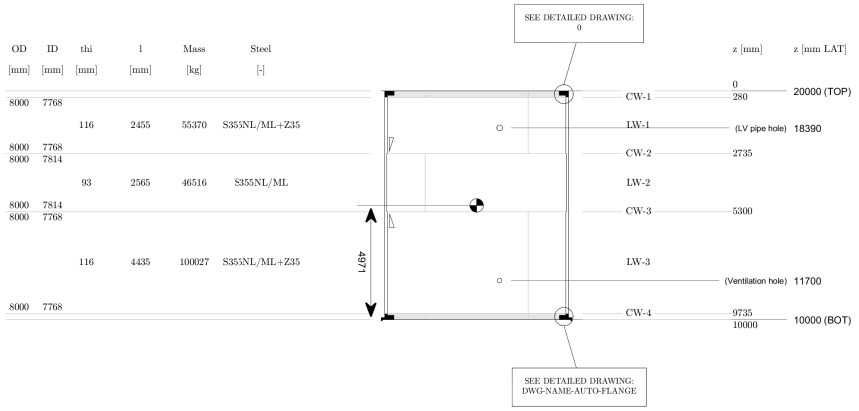

10 m 5 m 1 m 0 m

NOTES:

Drawings are for scheme design and show design intent only. Full detailed design analysis is required prior to fabrication. Secondary steel concept is not shown.

REV	DATE	REVISION DESCRIPTION	PREP.	QA	APPR
A	XXXX.XX.XXX	Issued for Client Review	EMS	XX	XX

DESIGN BY: WOOD THILSTED PARTNERS
APPROVED BY: XX — DATE: 15 Aug 2022
CHECKED BY: XX — DATE: 15 Aug 2022
PREPARED BY: EMS — DATE: 15 Aug 2022
SCALE: NOTED
WT PROJECT NO. 9993

NAN

WOOD THILSTED

GENERIC MORPHEUS MODEL
IEA15MW
TRANSITION PIECE: WTG_01

DRAWING NO. WT-9993-NAN-DWG-WTG_01-TP — REV. A

DRAWING NO. WT-9993-nan-DWG-WTG_01-TP
REV. A

Figure D.23: Transition piece design drawing of relaxed case - Gulf of Finland

MP (incl. flange)

M: 1480.7 t

L: 72.4 m

V: 188.8 m^3

D: 8.00 - 9.20 m

A_{ext}: 2014.9 m^2

A_{int}: 1969.7 m^2

Legend:

Grind: Grind weld flush

Plate tapering (angle 1:4)

Center of gravity

Hole

Longitudinal welds (LW):

Weld ID	No	length	thi	Grinding		IC*	
-	-	mm	mm	in	out	in	out
LW-1	3	3783	132	-	-	II	II
LW-2	3	4000	107	-	-	II	II
LW-3	2	4000	87	-	-	II	II
LW-4	2	3199	88	-	-	II	II
LW-5	2	3000	87	-	-	II	II
LW-6	2	2500	86	-	-	II	II
LW-7	2	3000	84	-	-	II	II
LW-8	2	2949	81	-	-	II	II
LW-9	3	4000	84	-	-	II	II
LW-10	3	4000	90	-	-	II	II
LW-11	3	4000	100	-	-	II	II
LW-12	3	3992	117	-	-	II	II
LW-13	3	4000	102	-	-	II	II
LW-14	3	4000	97	-	-	II	II
LW-15	3	4000	96	-	-	II	II
LW-16	3	4000	94	-	-	II	II
LW-17	3	4000	89	-	-	II	II
LW-18	2	4000	76	-	-	II	II
LW-19	2	2999	74	-	-	II	II
LW-20	2	2700	99	-	-	II	II

LW total length: 188.0 m
LW average thickness: 95.7 mm

Circumferential welds (CW):

Weld ID	length	thi	Grinding		IC*	
-	mm	mm	in	out	in	out
CW-1	25133	132-132	yes	-	I	I
CW-2	25133	132-107	-	-	I	II
CW-3	25133	107-87	yes	-	I	II
CW-4	25133	87-88	-	-	I	I
CW-5	25133	88-87	-	yes	II	I
CW-6	26121	87-86	-	-	I	I
CW-7	26944	86-84	-	-	I	I
CW-8	27932	84-81	-	-	I	II
CW-9	28903	81-84	yes	-	I	II
CW-10	28903	84-90	-	-	I	II
CW-11	28903	90-100	-	-	I	II
CW-12	28903	100-117	-	-	I	II
CW-13	28903	117-102	-	-	I	II
CW-14	28903	102-97	-	-	I	II
CW-15	28903	97-96	-	-	I	I
CW-16	28903	96-94	-	-	I	I
CW-17	28903	94-89	-	-	I	II
CW-18	28903	89-76	-	-	I	II
CW-19	28903	76-74	-	-	II	II
CW-20	28903	74-99	-	-	II	II

CW total length: 553.5 m
CW average thickness: 90.1 mm

Steel (MP total excl. flanges)

S355NL/ML:	1464.3 t
Cylindrical:	1261.5 t
Conical:	202.8 t

OD [mm]	ID [mm]	thi [mm]	l [mm]	Mass [kg]	Steel -]
8000	7736				
		132	3783	96893	S355NL/ML
8000	7736				
8000	7786				
		107	4000	83312	S355NL/ML
8000	7786				
8000	7826				
		87	4000	67911	S355NL/ML
8000	7826				
8000	7824				
		88	3199	54929	S355NL/ML
8000	7824				
8000	7826				
		87	3000	51945	S355NL/ML
8314	8140				
8314	8142				
		86	2500	44324	S355NL/ML
8576	8404				
8576	8408				
		84	3000	53755	S355NL/ML
8891	8723				
8891	8729				
		81	2949	52808	S355NL/ML
9200	9038				
9200	9032				
		84	4000	75538	S355NL/ML
9200	9032				
9200	9020				
		90	4000	80880	S355NL/ML
9200	9020				
9200	9000				
		100	4000	89768	S355NL/ML
9200	9000				
9200	8966				
		117	3992	104623	S355NL/ML
9200	8966				
9200	8996				
		102	4000	91543	S355NL/ML
9200	8996				
9200	9006				
		97	4000	87104	S355NL/ML
9200	9006				
9200	9008				
		96	4000	86215	S355NL/ML
9200	9008				
9200	9012				
		94	4000	84437	S355NL/ML
9200	9012				
9200	9022				
		89	4000	79990	S355NL/ML
9200	9022				
9200	9048				
		76	4000	68404	S355NL/ML
9200	9048				
9200	9052				
		74	2999	49947	S355NL/ML
9200	9052				
9200	9002				
		99	2700	59994	S355NL/ML
9200	9002				

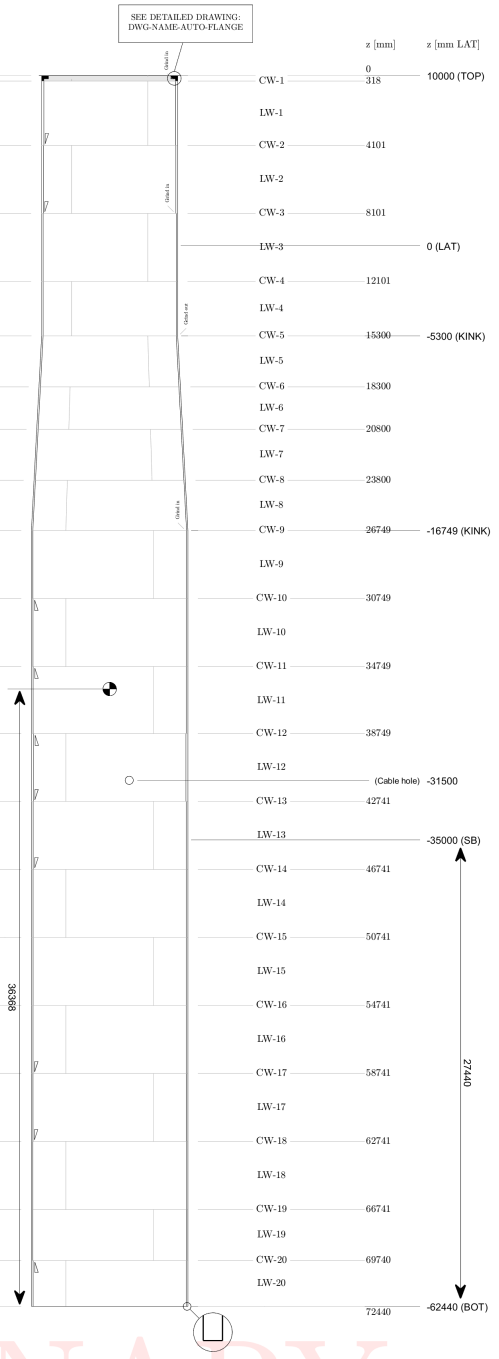

Orientation of Array Cable Entry Hole(s): [45] degrees clockwise relative to N.

10 m 5 m 1 m 0 m

NOTES:

Drawings are for scheme design and show design intent only. Full detailed design analysis is required prior to fabrication. Secondary steel concept is not shown.

REV	DATE	REVISION DESCRIPTION	PREP.	QA	APPR
A	XXXX.XX.XXX	Issued for Client Review	EMS	XX	XX

DESIGN BY: WOOD THILSTED PARTNERS
APPROVED BY: XX — DATE: 15 Aug 2022
CHECKED BY: XX — DATE: 15 Aug 2022
PREPARED BY: EMS — DATE: 15 Aug 2022
SCALE: NOTED
WT PROJECT NO. 9993

NAN

WOOD THILSTED

GENERIC MORPHEUS MODEL
IEA15MW
MONOPILE: WTG_01

DRAWING NO. WT-9993-NAN-DWG-WTG_01-MP
REV. A

Figure D.24: Monopile design drawing of relaxed case - Gulf of Finland

TP (incl. flanges)

M: 162.7 t

L: 10.0 m

V: 20.6 m^3

D: 8.00 m

A_{ext}: 251.3 m^2

A_{int}: 246.1 m^2

Legend:

Grind: Grind weld flush

Plate tapering (angle 1:4)

Center of gravity

Hole

Longitudinal welds (LW):

Weld ID	No	length	thi	Grinding		IC*	
-	-	mm	mm	in	out	in	out
LW-1	1	2455	68	-	-	II	II
LW-2	1	2565	63	-	-	II	II
LW-3	2	4435	76	-	-	II	II

LW total length: 13.9 m
LW average thickness: 72.2 mm

Circumferential welds (CW):

Weld ID	length	thi	Grinding		IC*	
-	mm	mm	in	out	in	out
CW-1	25133	68-68	-	-	I	I
CW-2	25133	68-63	-	-	II	II
CW-3	25133	63-76	-	-	I	II
CW-4	25133	76-76	-	-	I	I

CW total length: 100.5 m
CW average thickness: 67.5 mm

Steel (TP total excl. flanges)

S355NL/ML:	31.6 t
S355NL/ML+Z35:	98.5 t

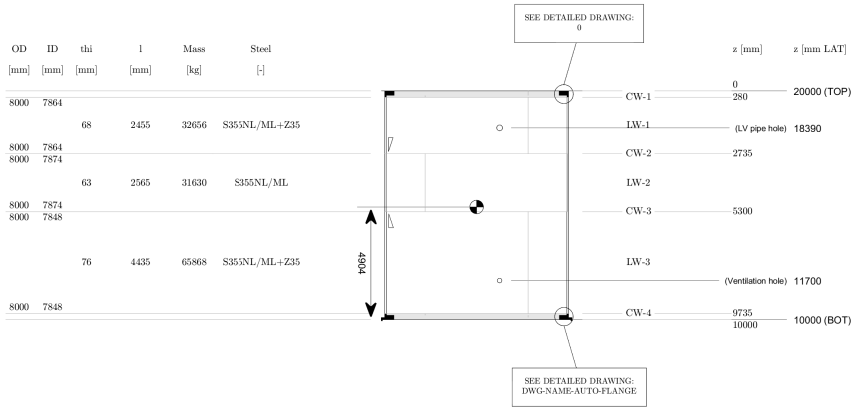

10 m 5 m 1 m 0 m

NOTES:

Drawings are for scheme design and show design intent only. Full detailed design analysis is required prior to fabrication. Secondary steel concept is not shown.

REV	DATE	REVISION DESCRIPTION	PREP.	QA	APPR
A	XXXX.XX.XXX	Issued for Client Review	EMS	XX	XX

DESIGN BY: WOOD THILSTED PARTNERS
APPROVED BY: XX — DATE: 12 Aug 2022
CHECKED BY: XX — DATE: 12 Aug 2022
PREPARED BY: EMS — DATE: 12 Aug 2022
SCALE: NOTED
WT PROJECT NO. 9993

NAN

WOOD THILSTED

GENERIC MORPHEUS MODEL
IEA15MW
TRANSITION PIECE: WTG_01

DRAWING NO. WT-9993-NAN-DWG-WTG_01-TP — REV. A

DRAWING NO. WT-9993-nan-DWG-WTG_01-TP
REV. A

Figure D.25: Transition piece design drawing of reference case - Archipelago Sea

MP (incl. flange)

M: 914.8 t

L: 61.1 m

V: 116.7 m^3

D: 8.00 - 8.40 m

A_{ext}: 1592.0 m^2

A_{int}: 1562.9 m^2

Legend:

Grind: Grind weld flush

Plate tapering (angle 1:4)

Center of gravity

Hole

Longitudinal welds (LW):

Weld ID	No	length	thi	Grinding		IC*	
-	-	mm	mm	in	out	in	out
LW-1	2	3783	77	-	-	II	II
LW-2	2	4000	67	-	-	II	II
LW-3	2	4000	64	-	-	II	II
LW-4	2	3199	66	-	-	II	II
LW-5	2	3816	66	-	-	II	II
LW-6	2	4000	68	-	-	II	II
LW-7	2	4000	72	-	-	II	II
LW-8	2	3000	78	-	-	II	II
LW-9	3	4124	90	-	-	II	II
LW-10	2	4000	80	-	-	II	II
LW-11	2	4000	77	-	-	II	II
LW-12	2	4000	76	-	-	II	II
LW-13	2	4000	72	-	-	II	II
LW-14	2	3500	65	-	-	II	II
LW-15	1	2500	65	-	-	II	II
LW-16	1	2500	66	-	-	II	II
LW-17	2	2400	91	-	-	II	II

LW total length: 120.8 m
LW average thickness: 73.8 mm

Circumferential welds (CW):

Weld ID	length	thi	Grinding		IC*	
-	mm	mm	in	out	in	out
CW-1	25133	77-77	yes	-	I	I
CW-2	25133	77-67	-	-	I	II
CW-3	25133	67-64	yes	-	I	II
CW-4	25133	64-66	-	-	I	II
CW-5	25133	66-66	-	yes	II	I
CW-6	26389	66-68	yes	-	I	II
CW-7	26389	68-72	-	-	I	II
CW-8	26389	72-78	-	-	I	II
CW-9	26389	78-90	-	-	I	II
CW-10	26389	90-80	-	-	I	II
CW-11	26389	80-77	-	-	I	II
CW-12	26389	77-76	-	-	I	I
CW-13	26389	76-72	-	-	I	II
CW-14	26389	72-65	-	-	II	II
CW-15	26389	65-65	-	-	II	II
CW-16	26389	65-66	-	-	II	II
CW-17	26389	66-91	-	-	II	II

CW total length: 442.3 m
CW average thickness: 69.9 mm

Steel (MP total excl. flanges)

S355NL/ML:	899.7 t
Cylindrical:	849.2 t
Conical:	50.5 t

OD [mm]	ID [mm]	thi [mm]	l [mm]	Mass [kg]	Steel -]
8000	7846				
		77	3783	56916	S355NL/ML
8000	7846				
8000	7866				
		67	4000	52431	S355NL/ML
8000	7866				
8000	7872				
		64	4000	50103	S355NL/ML
8000	7872				
8000	7868				
		66	3199	41311	S355NL/ML
8000	7868				
8000	7868				
		66	3816	50521	S355NL/ML
8400	8268				
8400	8264				
		68	4000	55890	S355NL/ML
8400	8264				
8400	8256				
		72	4000	59150	S355NL/ML
8400	8256				
8400	8244				
		78	3000	48025	S355NL/ML
8400	8244				
8400	8220				
		90	4124	76064	S355NL/ML
8400	8220				
8400	8240				
		80	4000	65659	S355NL/ML
8400	8240				
8400	8246				
		77	4000	63219	S355NL/ML
8400	8246				
8400	8248				
		76	4000	62406	S355NL/ML
8400	8248				
8400	8256				
		72	4000	59150	S355NL/ML
8400	8256				
8400	8270				
		65	3500	46763	S355NL/ML
8400	8270				
8400	8270				
		65	2500	33402	S355NL/ML
8400	8270				
8400	8268				
		66	2500	33912	S355NL/ML
8400	8268				
8400	8218				
		91	2400	44753	S355NL/ML
8400	8218				

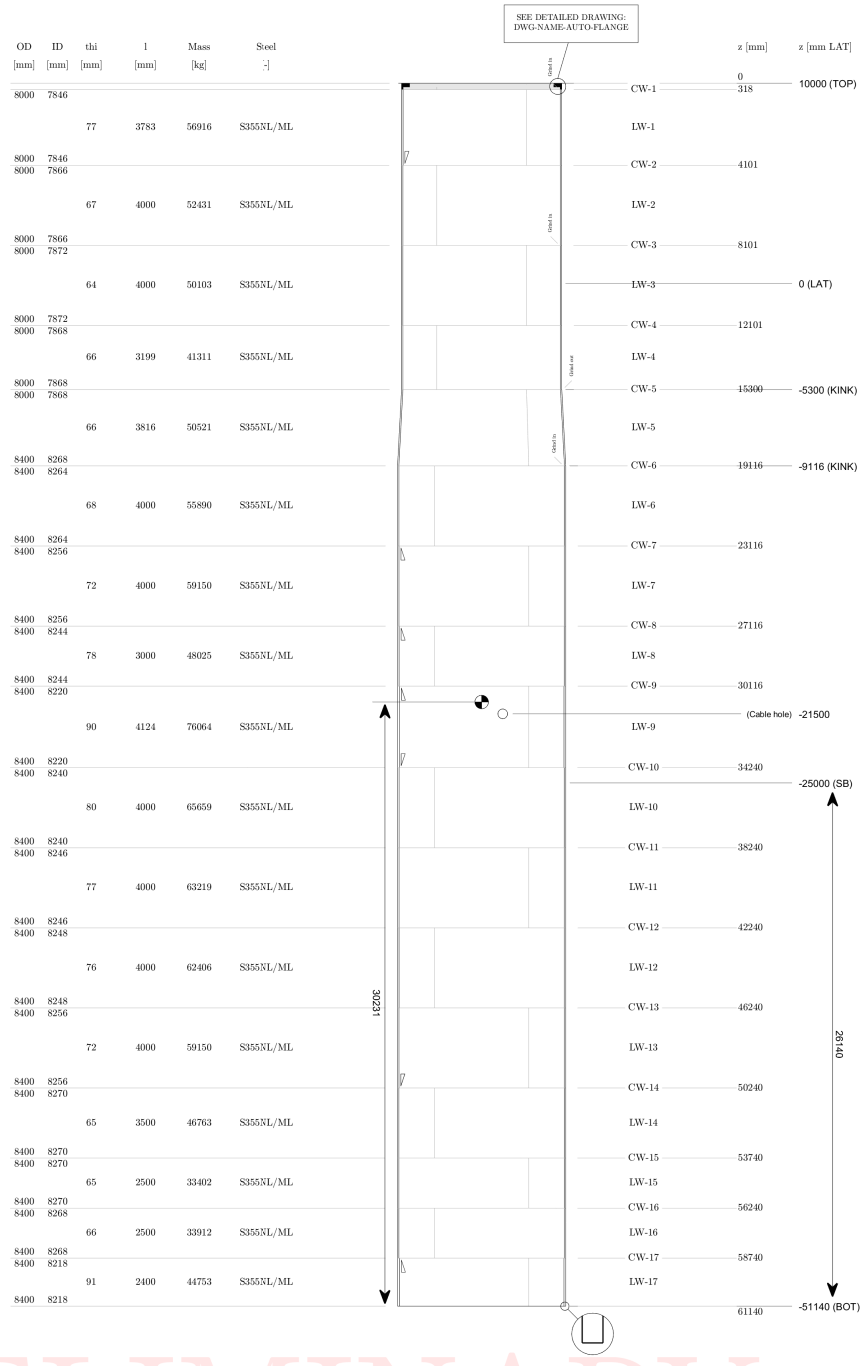

Orientation of Array Cable Entry Hole(s): [45] degrees clockwise relative to N.

10 m 5 m 1 m 0 m

NOTES:

Drawings are for scheme design and show design intent only. Full detailed design analysis is required prior to fabrication. Secondary steel concept is not shown.

REV	DATE	REVISION DESCRIPTION	PREP.	QA	APPR
A	XXXX.XX.XXX	Issued for Client Review	EMS	XX	XX

DESIGN BY: WOOD THILSTED PARTNERS
APPROVED BY: XX DATE: 12 Aug 2022
CHECKED BY: XX DATE: 12 Aug 2022
PREPARED BY: EMS DATE: 12 Aug 2022
SCALE: NOTED
WT PROJECT NO. 9993

NAN

WOOD THILSTED

GENERIC MORPHEUS MODEL
IEA15MW
MONOPILE: WTG_01

DRAWING NO. WT-9993-NAN-DWG-WTG_01-MP
REV. A

DRAWING NO. WT-9993-nan-DWG-WTG_01-MP
REV: A

Figure D.26: Monopile design drawing of reference case - Archipelago Sea

TP (incl. flanges)

M: 181.3 t

L: 10.0 m

V: 23.0 m^3

D: 8.00 m

A_{ext}: 251.3 m^2

A_{int}: 245.5 m^2

Legend:

Grind: Grind weld flush

Plate tapering (angle 1:4)

Center of gravity

Hole

Longitudinal welds (LW):

Weld ID	No	length	thi	Grinding		IC*	
-	-	mm	mm	in	out	in	out
LW-1	2	2455	80	-	-	II	II
LW-2	2	2565	71	-	-	II	II
LW-3	3	4435	86	-	-	II	II

LW total length: 23.3 m
LW average thickness: 81.4 mm

Circumferential welds (CW):

Weld ID	length	thi	Grinding		IC*	
-	mm	mm	in	out	in	out
CW-1	25133	80-80	-	-	I	I
CW-2	25133	80-71	-	-	II	II
CW-3	25133	71-86	-	-	I	II
CW-4	25133	86-86	-	-	I	I

CW total length: 100.5 m
CW average thickness: 77.0 mm

Steel (TP total excl. flanges)

S355NL/ML:	35.6 t
S355NL/ML+Z35:	112.8 t

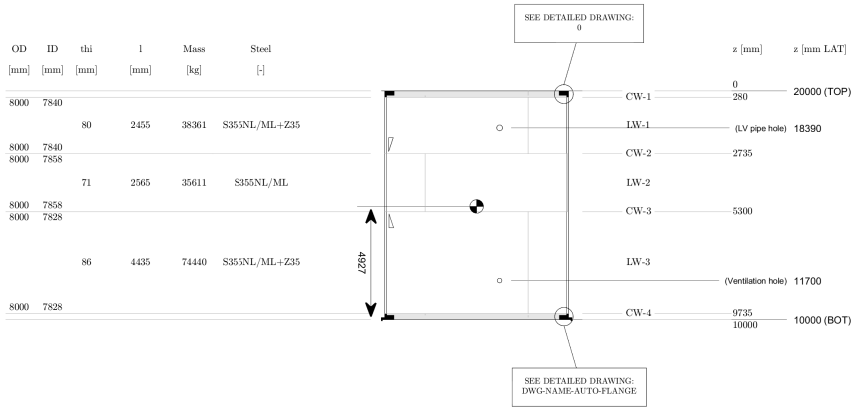

10 m 5 m 1 m 0 m

NOTES:

Drawings are for scheme design and show design intent only. Full detailed design analysis is required prior to fabrication. Secondary steel concept is not shown.

REV	DATE	REVISION DESCRIPTION	PREP.	QA	APPR
A	XXXX.XX.XXX	Issued for Client Review	EMS	XX	XX

DESIGN BY: WOOD THILSTED PARTNERS
APPROVED BY: XX — DATE: 15 Aug 2022
CHECKED BY: XX — DATE: 15 Aug 2022
PREPARED BY: EMS — DATE: 15 Aug 2022
SCALE: NOTED
WT PROJECT NO. 9993

NAN
WOOD THILSTED
GENERIC MORPHEUS MODEL
IEA15MW
TRANSITION PIECE: WTG_01
DRAWING NO. WT-9993-NAN-DWG-WTG_01-TP
REV. A

DRAWING NO. WT-9993-nan-DWG-WTG_01-TP
REV. A

Figure D.27: Transition piece design drawing of ice case - Archipelago Sea

MP (incl. flange)

M: 977.4 t

L: 60.5 m

V: 124.7 m^3

D: 8.00 - 8.40 m

A_{ext}: 1573.7 m^2

A_{int}: 1542.7 m^2

Legend:

Grind: Grind weld flush

Plate tapering (angle 1:4)

Center of gravity

Hole

Longitudinal welds (LW):

Weld ID	No	length	thi	Grinding		IC*	
-	-	mm	mm	in	out	in	out
LW-1	2	3783	90	-	-	II	II
LW-2	2	4000	76	-	-	II	II
LW-3	2	4000	69	-	-	II	II
LW-4	2	3199	69	-	-	II	II
LW-5	2	3816	69	-	-	II	II
LW-6	2	4000	73	-	-	II	II
LW-7	2	4000	78	-	-	II	II
LW-8	2	3000	85	-	-	II	II
LW-9	3	4124	98	-	-	II	II
LW-10	3	4000	87	-	-	II	II
LW-11	2	4000	83	-	-	II	II
LW-12	2	4000	82	-	-	II	II
LW-13	2	4000	79	-	-	II	II
LW-14	2	4000	72	-	-	II	II
LW-15	2	3810	66	-	-	II	II
LW-16	2	2400	91	-	-	II	II

LW total length: 128.4 m
LW average thickness: 79.8 mm

Circumferential welds (CW):

Weld ID	length	thi	Grinding		IC*	
-	mm	mm	in	out	in	out
CW-1	25133	90-90	yes	-	I	I
CW-2	25133	90-76	-	-	I	II
CW-3	25133	76-69	yes	-	I	II
CW-4	25133	69-69	-	-	I	I
CW-5	25133	69-69	-	yes	II	I
CW-6	26389	69-73	yes	-	I	II
CW-7	26389	73-78	-	-	I	II
CW-8	26389	78-85	-	-	I	II
CW-9	26389	85-98	-	-	I	II
CW-10	26389	98-87	-	-	I	II
CW-11	26389	87-83	-	-	I	II
CW-12	26389	83-82	-	-	I	I
CW-13	26389	82-79	-	-	I	II
CW-14	26389	79-72	-	-	II	II
CW-15	26389	72-66	-	-	II	II
CW-16	26389	66-91	-	-	II	II

CW total length: 415.9 m
CW average thickness: 75.8 mm

Steel (MP total excl. flanges)

S355NL/ML:	962.0 t
Cylindrical:	909.2 t
Conical:	52.8 t

OD [mm]	ID [mm]	thi [mm]	l [mm]	Mass [kg]	Steel -]		z [mm]	z [mm LAT]
						CW-1	0 / 318	10000 (TOP)
8000	7820	90	3783	66416	S355NL/ML	LW-1		
8000	7820					CW-2	4101	
8000	7848	76	4000	59407	S355NL/ML	LW-2		
8000	7848					CW-3	8101	
8000	7862	69	4000	53983	S355NL/ML	LW-3		0 (LAT)
8000	7862					CW-4	12101	
8000	7862	69	3199	43173	S355NL/ML	LW-4		
8000	7862					CW-5	15300	-5300 (KINK)
8000	7862	69	3816	52798	S355NL/ML	LW-5		
8400	8262					CW-6	19116	-9116 (KINK)
8400	8254	73	4000	59964	S355NL/ML	LW-6		
8400	8254					CW-7	23116	
8400	8244	78	4000	64033	S355NL/ML	LW-7		
8400	8244					CW-8	27116	
8400	8230	85	3000	52290	S355NL/ML	LW-8		
8400	8230					CW-9	30116	
8400	8204	98	4124	82746	S355NL/ML	LW-9		(Cable hole) -21500
8400	8204					CW-10	34240	
8400	8226	87	4000	71344	S355NL/ML	LW-10		-25000 (SB)
8400	8226					CW-11	38240	
8400	8234	83	4000	68096	S355NL/ML	LW-11		
8400	8234					CW-12	42240	
8400	8236	82	4000	67284	S355NL/ML	LW-12		
8400	8236					CW-13	46240	
8400	8242	79	4000	64846	S355NL/ML	LW-13		
8400	8242					CW-14	50240	
8400	8256	72	4000	59150	S355NL/ML	LW-14		
8400	8256					CW-15	54240	
8400	8268	66	3810	51682	S355NL/ML	LW-15		
8400	8268					CW-16	58050	
8400	8218	91	2400	44753	S355NL/ML	LW-16		
8400	8218						60450	-50450 (BOT)

SEE DETAILED DRAWING: DWG-NAME-AUTO-FLANGE

30136

25450

Orientation of Array Cable Entry Hole(s): [45] degrees clockwise relative to N.

10 m 5 m 1 m 0 m

NOTES:

Drawings are for scheme design and show design intent only. Full detailed design analysis is required prior to fabrication. Secondary steel concept is not shown.

REV	DATE	REVISION DESCRIPTION	PREP.	QA	APPR
A	XXXX.XX.XXX	Issued for Client Review	EMS	XX	XX

DESIGN BY: WOOD THILSTED PARTNERS
APPROVED BY: XX — DATE: 15 Aug 2022
CHECKED BY: XX — DATE: 15 Aug 2022
PREPARED BY: EMS — DATE: 15 Aug 2022
SCALE: NOTED
WT PROJECT NO. 9993

NAN

WOOD THILSTED

GENERIC MORPHEUS MODEL
IEA15MW
MONOPILE: WTG_01

DRAWING NO. WT-9993-NAN-DWG-WTG_01-MP — REV. A

DRAWING NO. WT-9993-nan-DWG-WTG_01-MP
REV. A

Figure D.28: Monopile design drawing of ice case - Archipelago Sea

TP (incl. flanges)

M: 198.9 t

L: 10.0 m

V: 25.2 m^3

D: 8.00 m

A_{ext}: 251.3 m^2

A_{int}: 244.9 m^2

Legend:

Grind: Grind weld flush

Plate tapering (angle 1:4)

Center of gravity

Hole

Longitudinal welds (LW):

Weld ID	No	length	thi	Grinding		IC*	
-	-	mm	mm	in	out	in	out
LW-1	2	2455	91	-	-	II	II
LW-2	2	2565	78	-	-	II	II
LW-3	3	4435	96	-	-	II	II

LW total length: 23.3 m
LW average thickness: 91.0 mm

Circumferential welds (CW):

Weld ID	length	thi	Grinding		IC*	
-	mm	mm	in	out	in	out
CW-1	25133	91-91	-	-	I	I
CW-2	25133	91-78	-	-	II	II
CW-3	25133	78-96	-	-	I	II
CW-4	25133	96-96	-	-	I	I

CW total length: 100.5 m
CW average thickness: 85.7 mm

Steel (TP total excl. flanges)

S355NL/ML:	39.1 t
S355NL/ML+Z35:	126.6 t

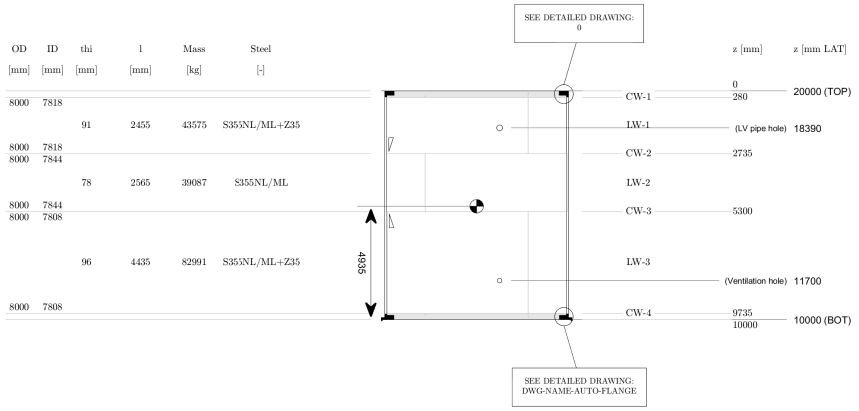

10 m 5 m 1 m 0 m

NOTES:

Drawings are for scheme design and show design intent only. Full detailed design analysis is required prior to fabrication. Secondary steel concept is not shown.

REV	DATE	REVISION DESCRIPTION	PREP.	QA	APPR
A	XXXX.XX.XXX	Issued for Client Review	EMS	XX	XX

DESIGN BY: WOOD THILSTED PARTNERS
APPROVED BY: XX — DATE: 12 Aug 2022
CHECKED BY: XX — DATE: 12 Aug 2022
PREPARED BY: EMS — DATE: 12 Aug 2022
SCALE: NOTED
WT PROJECT NO. 9993

NAN

WOOD THILSTED

GENERIC MORPHEUS MODEL
IEA15MW
TRANSITION PIECE: WTG_01

DRAWING NO. WT-9993-NAN-DWG-WTG_01-TP — REV. A

DRAWING NO. WT-9993-nan-DWG-WTG_01-TP
REV. A

Figure D.29: Transition piece design drawing of reference case - Bothnian Sea South

MP (incl. flange)

M: 1341.3 t

L: 74.6 m

V: 171.0 m^3

D: 8.00 - 9.50 m

A_{ext}: 2122.4 m^2

A_{int}: 2081.6 m^2

Legend:

Grind: Grind weld flush

Plate tapering (angle 1:4)

Center of gravity

Hole

Longitudinal welds (LW):

Weld ID	No	length	thi	Grinding		IC*	
-	-	mm	mm	in	out	in	out
LW-1	3	3783	102	-	-	II	II
LW-2	2	4000	84	-	-	II	II
LW-3	2	4000	76	-	-	II	II
LW-4	2	3199	75	-	-	II	II
LW-5	2	3500	75	-	-	II	II
LW-6	2	3500	73	-	-	II	II
LW-7	2	3500	71	-	-	II	II
LW-8	2	3811	74	-	-	II	II
LW-9	2	4000	74	-	-	II	II
LW-10	2	3500	76	-	-	II	II
LW-11	2	3000	83	-	-	II	II
LW-12	3	4130	95	-	-	II	II
LW-13	3	4000	85	-	-	II	II
LW-14	3	4000	83	-	-	II	II
LW-15	3	4000	82	-	-	II	II
LW-16	3	4000	80	-	-	II	II
LW-17	2	4000	74	-	-	II	II
LW-18	2	4000	74	-	-	II	II
LW-19	2	3599	77	-	-	II	II
LW-20	2	2800	102	-	-	II	II

LW total length: 172.6 m
LW average thickness: 81.6 mm

Circumferential welds (CW):

Weld ID	length	thi	Grinding		IC*	
-	mm	mm	in	out	in	out
CW-1	25133	102-102	yes	-	I	II
CW-2	25133	102-84	-	-	I	II
CW-3	25133	84-76	yes	-	I	II
CW-4	25133	76-75	-	-	I	I
CW-5	25133	75-75	-	yes	II	I
CW-6	26285	75-73	-	-	I	I
CW-7	27438	73-71	-	-	I	II
CW-8	28590	71-74	-	-	I	II
CW-9	29845	74-74	yes	-	I	II
CW-10	29845	74-76	-	-	II	II
CW-11	29845	76-83	-	-	I	II
CW-12	29845	83-95	-	-	I	II
CW-13	29845	95-85	-	-	I	II
CW-14	29845	85-83	-	-	I	II
CW-15	29845	83-82	-	-	I	I
CW-16	29845	82-80	-	-	I	I
CW-17	29845	80-74	-	-	I	II
CW-18	29845	74-74	-	-	II	II
CW-19	29845	74-77	-	-	II	II
CW-20	29845	77-102	-	-	II	II

CW total length: 566.1 m
CW average thickness: 78.1 mm

Steel (MP total excl. flanges)

S355NL/ML:	1325.6 t
Cylindrical:	1101.3 t
Conical:	224.3 t

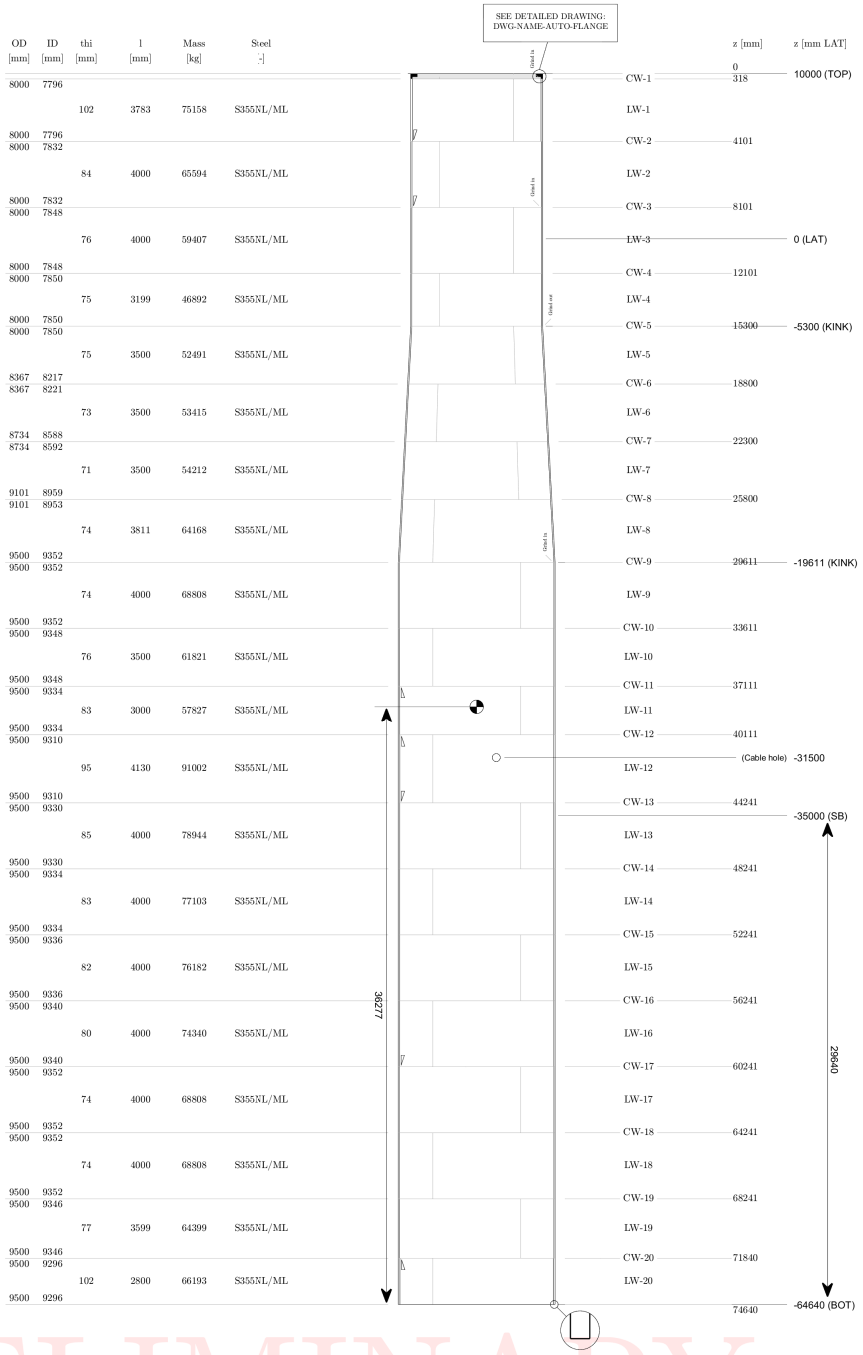

Orientation of Array Cable Entry Hole(s): [45] degrees clockwise relative to N.

10 m 5 m 1 m 0 m

NOTES:

Drawings are for scheme design and show design intent only. Full detailed design analysis is required prior to fabrication. Secondary steel concept is not shown.

REV	DATE	REVISION DESCRIPTION	PREP.	QA	APPR
A	XXXX.XX.XXX	Issued for Client Review	EMS	XX	XX

DESIGN BY: WOOD THILSTED PARTNERS

APPROVED BY: XX	DATE: 12 Aug 2022
CHECKED BY: XX	DATE: 12 Aug 2022
PREPARED BY: EMS	DATE: 12 Aug 2022

SCALE: NOTED

WT PROJECT NO. 9993

NAN

WOOD THILSTED

GENERIC MORPHEUS MODEL
IEA15MW
MONOPILE: WTG_01

DRAWING NO. WT-9993-NAN-DWG-WTG_01-MP

REV. A

DRAWING NO. WT-9993-nan-DWG-WTG_01-MP

REV. A

Figure D.30: Monopile design drawing of reference case - Bothnian Sea South

TP (incl. flanges)

M: 230.8 t

L: 10.0 m

V: 29.3 m^3

D: 8.00 m

A_{ext}: 251.3 m^2

A_{int}: 243.9 m^2

Legend:

Grind: Grind weld flush

Plate tapering (angle 1:4)

Center of gravity

Hole

Longitudinal welds (LW):

Weld ID	No	length	thi	Grinding		IC*	
-	-	mm	mm	in	out	in	out
LW-1	2	2455	113	-	-	II	II
LW-2	2	2565	91	-	-	II	II
LW-3	3	4435	113	-	-	II	II

LW total length: 23.3 m
LW average thickness: 108.2 mm

Circumferential welds (CW):

Weld ID	length	thi	Grinding		IC*	
-	mm	mm	in	out	in	out
CW-1	25133	113-113	-	-	I	I
CW-2	25133	113-91	-	-	I	II
CW-3	25133	91-113	-	-	I	II
CW-4	25133	113-113	-	-	I	I

CW total length: 100.5 m
CW average thickness: 102.0 mm

Steel (TP total excl. flanges)

S355NL/ML:	45.5 t
S355NL/ML+Z35:	151.4 t

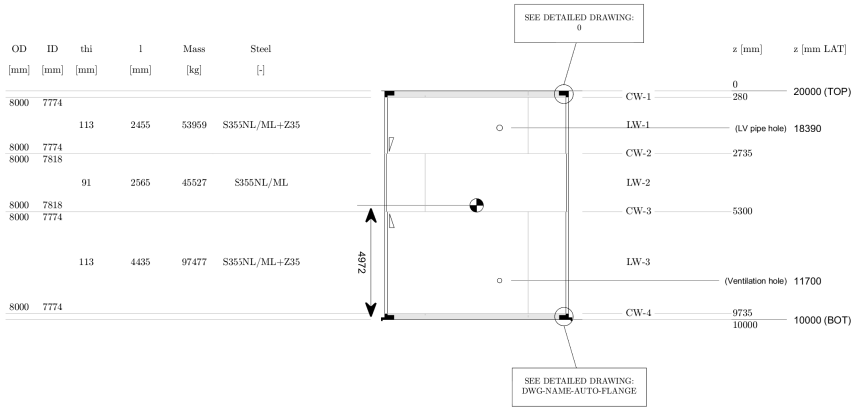

10 m 5 m 1 m 0 m

NOTES:

Drawings are for scheme design and show design intent only. Full detailed design analysis is required prior to fabrication. Secondary steel concept is not shown.

REV	DATE	REVISION DESCRIPTION	PREP.	QA	APPR
A	XXXX.XX.XXX	Issued for Client Review	EMS	XX	XX

DESIGN BY: WOOD THILSTED PARTNERS
APPROVED BY: XX — DATE: 15 Aug 2022
CHECKED BY: XX — DATE: 15 Aug 2022
PREPARED BY: EMS — DATE: 15 Aug 2022
SCALE: NOTED
WT PROJECT NO. 9993

NAN

WOOD THILSTED

GENERIC MORPHEUS MODEL
IEA15MW
TRANSITION PIECE: WTG_01

DRAWING NO. WT-9993-NAN-DWG-WTG_01-TP
REV. A

DRAWING NO. WT-9993-nan-DWG-WTG_01-TP
REV. A

Figure D.31: Transition piece design drawing of ice case - Bothnian Sea South

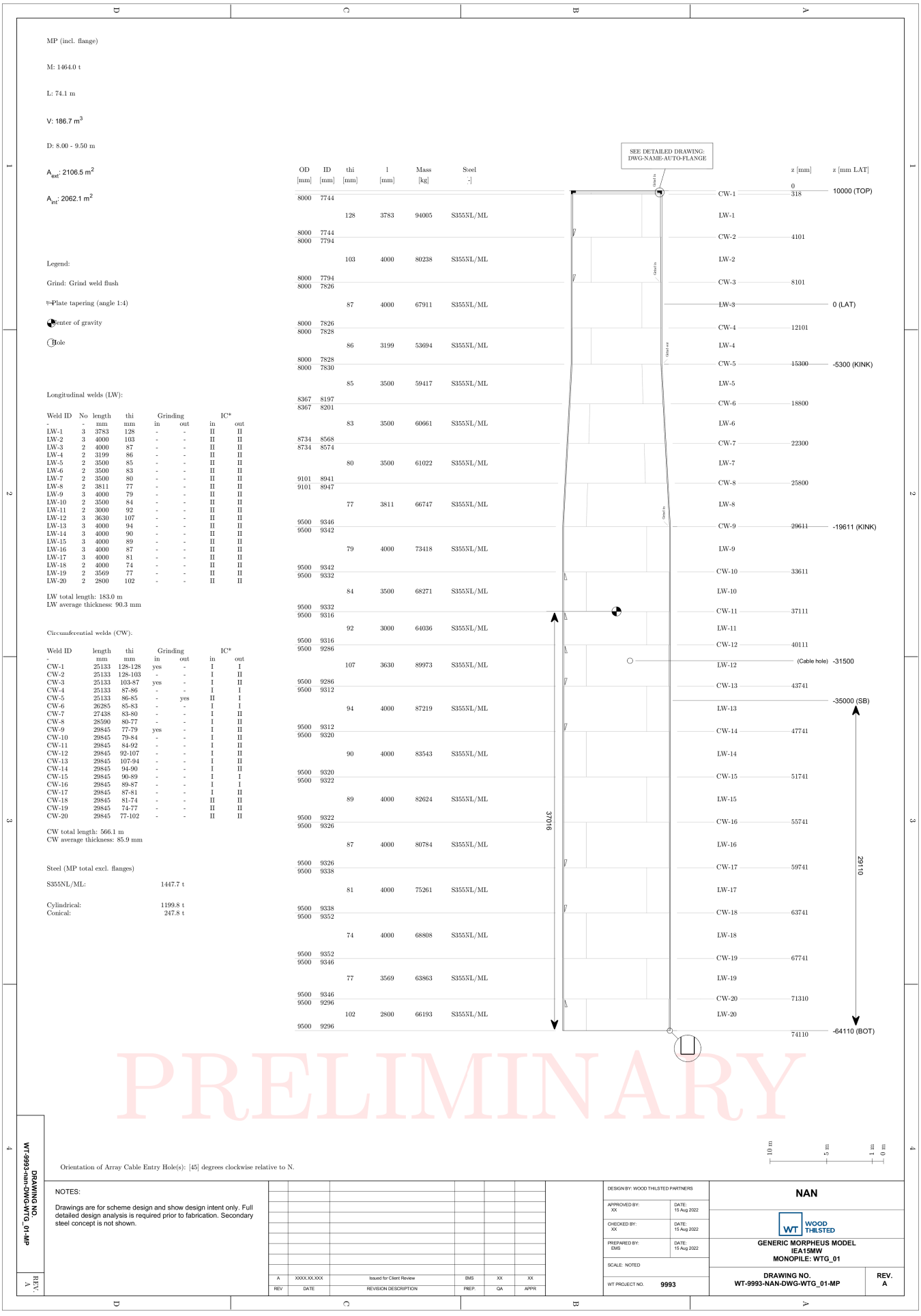

Figure D.32: Monopile design drawing of ice case - Bothnian Sea South

TP (incl. flanges)

M: 240.0 t

L: 10.0 m

V: 30.5 m^3

D: 8.00 m

A_{ext}: 251.3 m^2

A_{int}: 243.6 m^2

Legend:

Grind: Grind weld flush

Plate tapering (angle 1:4)

Center of gravity

Hole

Longitudinal welds (LW):

Weld ID	No	length	thi	Grinding		IC*	
-	-	mm	mm	in	out	in	out
LW-1	2	2455	119	-	-	II	II
LW-2	2	2565	95	-	-	II	II
LW-3	3	4435	118	-	-	II	II

LW total length: 23.3 m
LW average thickness: 113.2 mm

Circumferential welds (CW):

Weld ID	length	thi	Grinding		IC*	
-	mm	mm	in	out	in	out
CW-1	25133	119-119	-	-	I	I
CW-2	25133	119-95	-	-	I	II
CW-3	25133	95-118	-	-	I	II
CW-4	25133	118-118	-	-	I	I

CW total length: 100.5 m
CW average thickness: 106.8 mm

Steel (TP total excl. flanges)

S355NL/ML:	47.5 t
S355NL/ML+Z35:	158.5 t

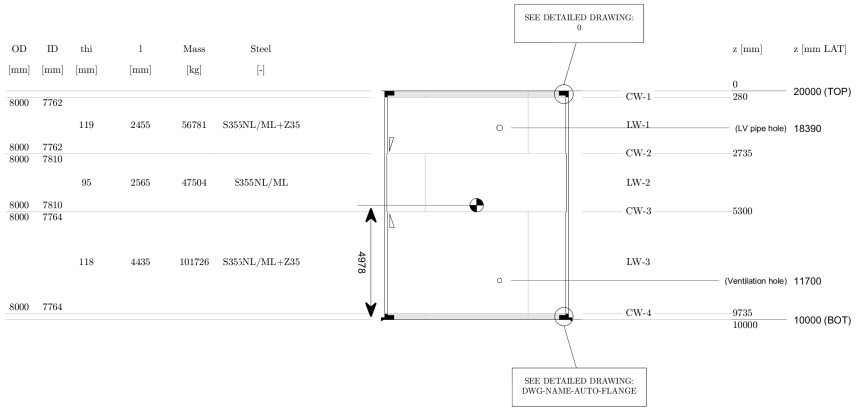

10 m 5 m 1 m 0 m

NOTES:

Drawings are for scheme design and show design intent only. Full detailed design analysis is required prior to fabrication. Secondary steel concept is not shown.

REV	DATE	REVISION DESCRIPTION	PREP.	QA	APPR
A	XXXX.XX.XXX	Issued for Client Review	EMS	XX	XX

DESIGN BY: WOOD THILSTED PARTNERS
APPROVED BY: XX — DATE: 15 Aug 2022
CHECKED BY: XX — DATE: 15 Aug 2022
PREPARED BY: EMS — DATE: 15 Aug 2022
SCALE: NOTED
WT PROJECT NO. 9993

NAN

WOOD THILSTED

GENERIC MORPHEUS MODEL
IEA15MW
TRANSITION PIECE: WTG_01

DRAWING NO. WT-9993-nan-DWG-WTG_01-TP — REV. A

DRAWING NO. WT-9993-nan-DWG-WTG_01-TP
REV. A

Figure D.33: Transition piece design drawing of relaxed case - Bothnian Sea South

MP (incl. flange)

M: 1480.6 t

L: 72.0 m

V: 188.8 m^3

D: 8.00 - 9.50 m

A_{ext}: 2043.9 m^2

A_{int}: 1998.8 m^2

Legend:

Grind: Grind weld flush

Plate tapering (angle 1:4)

Center of gravity

Hole

Longitudinal welds (LW):

Weld ID	No	length	thi	Grinding		IC*	
-	-	mm	mm	in	out	in	out
LW-1	3	3783	135	-	-	II	II
LW-2	3	4000	110	-	-	II	II
LW-3	3	4000	91	-	-	II	II
LW-4	2	3199	89	-	-	II	II
LW-5	2	3500	88	-	-	II	II
LW-6	2	3500	86	-	-	II	II
LW-7	2	3500	83	-	-	II	II
LW-8	2	3811	80	-	-	II	II
LW-9	3	4000	82	-	-	II	II
LW-10	3	3500	88	-	-	II	II
LW-11	2	3000	96	-	-	II	II
LW-12	4	4130	111	-	-	II	II
LW-13	3	4000	98	-	-	II	II
LW-14	3	4000	94	-	-	II	II
LW-15	3	4000	93	-	-	II	II
LW-16	3	4000	90	-	-	II	II
LW-17	2	3000	81	-	-	II	II
LW-18	2	3000	74	-	-	II	II
LW-19	2	2969	77	-	-	II	II
LW-20	2	2800	102	-	-	II	II

LW total length: 186.9 m
LW average thickness: 94.7 mm

Circumferential welds (CW):

Weld ID	length	thi	Grinding		IC*	
-	mm	mm	in	out	in	out
CW-1	25133	135-135	yes	-	I	I
CW-2	25133	135-110	-	-	I	II
CW-3	25133	110-91	yes	-	I	II
CW-4	25133	91-89	-	-	I	I
CW-5	25133	89-88	-	yes	II	I
CW-6	26285	88-86	-	-	I	I
CW-7	27438	86-83	-	-	I	I
CW-8	28590	83-80	-	-	I	II
CW-9	29845	80-82	yes	-	I	II
CW-10	29845	82-88	-	-	I	II
CW-11	29845	88-96	-	-	I	II
CW-12	29845	96-111	-	-	I	II
CW-13	29845	111-98	-	-	I	II
CW-14	29845	98-94	-	-	I	II
CW-15	29845	94-93	-	-	I	I
CW-16	29845	93-90	-	-	I	II
CW-17	29845	90-81	-	-	I	II
CW-18	29845	81-74	-	-	II	II
CW-19	29845	74-77	-	-	II	II
CW-20	29845	77-102	-	-	II	II

CW total length: 566.1 m
CW average thickness: 89.0 mm

Steel (MP total excl. flanges)

S355NL/ML: 1464.1 t

Cylindrical: 1207.2 t
Conical: 256.9 t

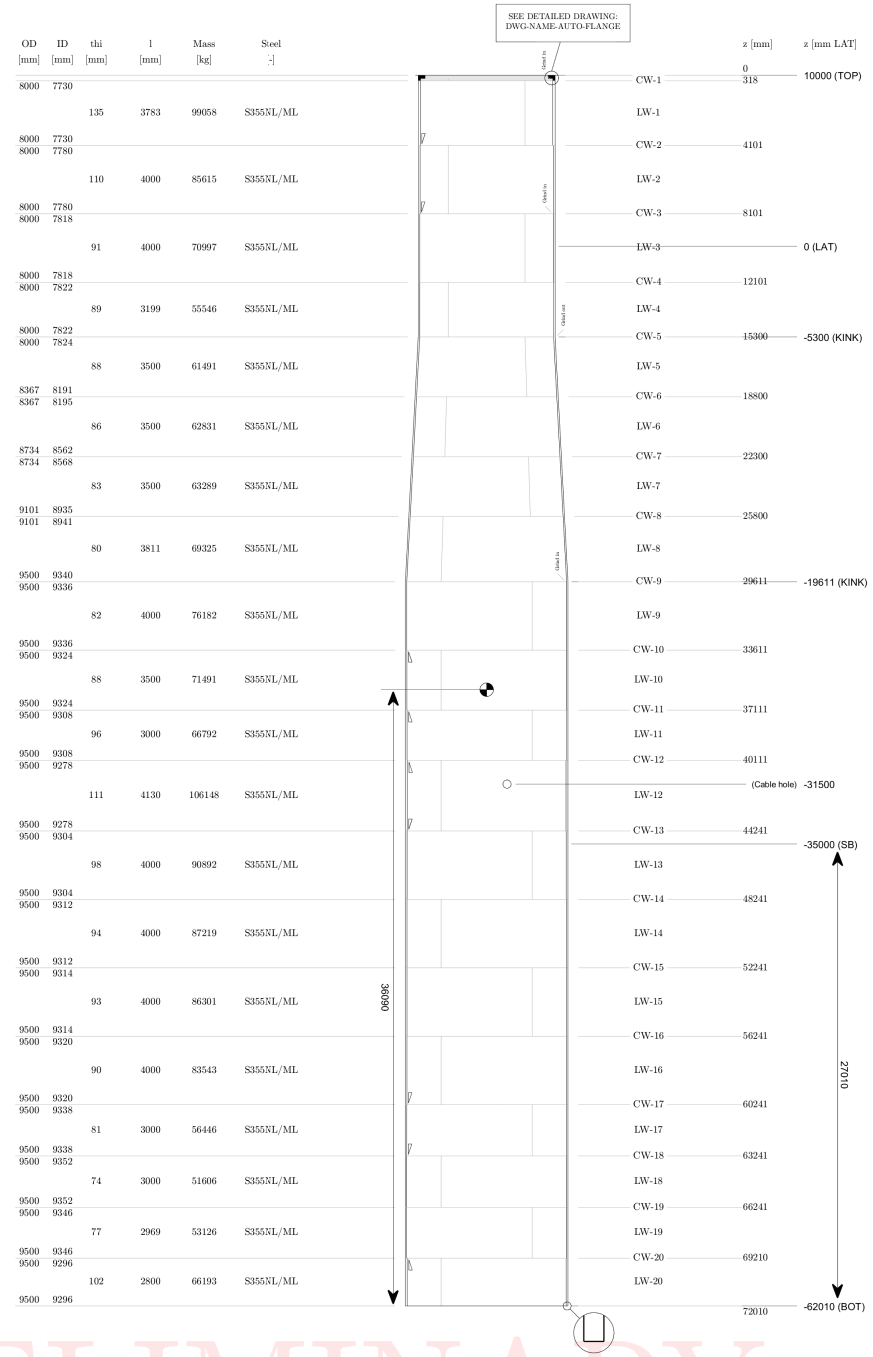

Orientation of Array Cable Entry Hole(s): [45] degrees clockwise relative to N.

10 m 5 m 1 m 0 m

NOTES:

Drawings are for scheme design and show design intent only. Full detailed design analysis is required prior to fabrication. Secondary steel concept is not shown.

REV	DATE	REVISION DESCRIPTION	PREP.	QA	APPR
A	XXXX.XX.XXX	Issued for Client Review	EMS	XX	XX

DESIGN BY: WOOD THILSTED PARTNERS
APPROVED BY: XX DATE: 15 Aug 2022
CHECKED BY: XX DATE: 15 Aug 2022
PREPARED BY: EMS DATE: 15 Aug 2022
SCALE: NOTED
WT PROJECT NO. 9993

NAN

WOOD THILSTED

GENERIC MORPHEUS MODEL
IEA15MW
MONOPILE: WTG_01

DRAWING NO. WT-9993-NAN-DWG-WTG_01-MP
REV. A

Figure D.34: Monopile design drawing of relaxed case - Bothnian Sea South

TP (incl. flanges)

M: 235.0 t

L: 10.0 m

V: 29.8 m^3

D: 8.00 m

A_{ext}: 251.3 m^2

A_{int}: 243.7 m^2

Legend:

Grind: Grind weld flush

Plate tapering (angle 1:4)

Center of gravity

Hole

Longitudinal welds (LW):

Weld ID	No	length	thi	Grinding		IC*	
-	-	mm	mm	in	out	in	out
LW-1	2	2455	116	-	-	II	II
LW-2	2	2565	93	-	-	II	II
LW-3	3	4435	115	-	-	II	II

LW total length: 23.3 m
LW average thickness: 110.4 mm

Circumferential welds (CW):

Weld ID	length	thi	Grinding		IC*	
-	mm	mm	in	out	in	out
CW-1	25133	116-116	-	-	I	I
CW-2	25133	116-93	-	-	I	II
CW-3	25133	93-115	-	-	I	II
CW-4	25133	115-115	-	-	I	I

CW total length: 100.5 m
CW average thickness: 104.3 mm

Steel (TP total excl. flanges)

S355NL/ML:	46.5 t
S355NL/ML+Z35:	154.5 t

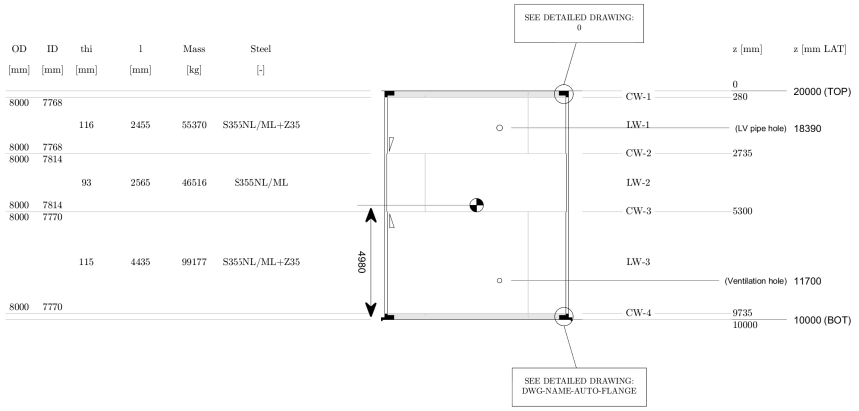

10 m 5 m 1 m 0 m

NOTES:

Drawings are for scheme design and show design intent only. Full detailed design analysis is required prior to fabrication. Secondary steel concept is not shown.

REV	DATE	REVISION DESCRIPTION	PREP.	QA	APPR
A	XXXX.XX.XXX	Issued for Client Review	EMS	XX	XX

DESIGN BY: WOOD THILSTED PARTNERS
APPROVED BY: XX — DATE: 12 Aug 2022
CHECKED BY: XX — DATE: 12 Aug 2022
PREPARED BY: EMS — DATE: 12 Aug 2022
SCALE: NOTED
WT PROJECT NO. 9993

NAN
WOOD THILSTED
GENERIC MORPHEUS MODEL
IEA15MW
TRANSITION PIECE: WTG_01
DRAWING NO. WT-9993-NAN-DWG-WTG_01-TP
REV. A

DRAWING NO. WT-9993-nan-DWG-WTG_01-TP
REV. A

Figure D.35: Transition piece design drawing of reference case - Bothnian Sea North

MP (incl. flange)

M: 1821.3 t

L: 86.4 m

V: 232.2 m^3

D: 8.00 - 10.00 m

A_{ext}: 2559.0 m^2

A_{int}: 2505.6 m^2

Legend:

Grind: Grind weld flush

Plate tapering (angle 1:4)

Center of gravity

Hole

Longitudinal welds (LW):

Weld ID	No	length	thi	Grinding		IC*	
-	-	mm	mm	in	out	in	out
LW-1	3	3783	130	-	-	II	II
LW-2	3	4000	105	-	-	II	II
LW-3	3	4000	92	-	-	II	II
LW-4	2	3199	89	-	-	II	II
LW-5	2	3500	86	-	-	II	II
LW-6	2	3500	85	-	-	II	II
LW-7	2	3000	82	-	-	II	II
LW-8	2	3000	79	-	-	II	II
LW-9	2	3000	76	-	-	II	II
LW-10	2	3081	78	-	-	II	II
LW-11	3	4000	78	-	-	II	II
LW-12	3	4000	83	-	-	II	II
LW-13	3	4000	89	-	-	II	II
LW-14	3	3500	98	-	-	II	II
LW-15	3	3359	114	-	-	II	II
LW-16	3	4000	100	-	-	II	II
LW-17	3	4000	96	-	-	II	II
LW-18	3	4000	95	-	-	II	II
LW-19	3	4000	94	-	-	II	II
LW-20	3	4000	89	-	-	II	II
LW-21	3	4000	79	-	-	II	II
LW-22	2	3000	78	-	-	II	II
LW-23	2	3260	82	-	-	II	II
LW-24	3	2900	107	-	-	II	II

LW total length: 229.7 m
LW average thickness: 92.5 mm

Circumferential welds (CW):

Weld ID	length	thi	Grinding		IC*	
-	mm	mm	in	out	in	out
CW-1	25133	130-130	yes	-	I	I
CW-2	25133	130-105	-	-	I	II
CW-3	25133	105-92	yes	-	I	II
CW-4	25133	92-89	-	-	I	I
CW-5	25133	89-86	-	yes	II	I
CW-6	26285	86-85	-	-	I	I
CW-7	27438	85-82	-	-	I	II
CW-8	28426	82-79	-	-	I	II
CW-9	29414	79-76	-	-	I	II
CW-10	30401	76-78	-	-	I	II
CW-11	31416	78-78	yes	-	I	II
CW-12	31416	78-83	-	-	I	II
CW-13	31416	83-89	-	-	I	II
CW-14	31416	89-98	-	-	I	II
CW-15	31416	98-114	-	-	I	II
CW-16	31416	114-100	-	-	I	II
CW-17	31416	100-96	-	-	I	II
CW-18	31416	96-95	-	-	I	I
CW-19	31416	95-94	-	-	I	I
CW-20	31416	94-89	-	-	I	II
CW-21	31416	89-79	-	-	I	II
CW-22	31416	79-78	-	-	II	II
CW-23	31416	78-82	-	-	II	II
CW-24	31416	82-107	-	-	II	II

CW total length: 707.5 m
CW average thickness: 87.8 mm

Steel (MP total excl. flanges)

S355NL/ML:	1805.0 t
Cylindrical:	1465.0 t
Conical:	339.9 t

OD [mm]	ID [mm]	thi [mm]	l [mm]	Mass [kg]	Steel -]
8000	7740				
		130	3783	95450	S355NL/ML
8000	7740				
8000	7790				
		105	4000	81775	S355NL/ML
8000	7790				
8000	7816				
		92	4000	71769	S355NL/ML
8000	7816				
8000	7822				
		89	3199	55546	S355NL/ML
8000	7822				
8000	7828				
		86	3500	60108	S355NL/ML
8367	8195				
8367	8197				
		85	3500	62108	S355NL/ML
8734	8564				
8734	8570				
		82	3000	53441	S355NL/ML
9048	8884				
9048	8890				
		79	3000	53342	S355NL/ML
9363	9205				
9363	9211				
		76	3000	53101	S355NL/ML
9677	9525				
9677	9521				
		78	3081	57847	S355NL/ML
10000	9844				
10000	9844				
		78	4000	76344	S355NL/ML
10000	9844				
10000	9834				
		83	4000	81197	S355NL/ML
10000	9834				
10000	9822				
		89	4000	87014	S355NL/ML
10000	9822				
10000	9804				
		98	3500	83760	S355NL/ML
10000	9804				
10000	9772				
		114	3359	93359	S355NL/ML
10000	9772				
10000	9800				
		100	4000	97660	S355NL/ML
10000	9800				
10000	9808				
		96	4000	93791	S355NL/ML
10000	9808				
10000	9810				
		95	4000	92823	S355NL/ML
10000	9810				
10000	9812				
		94	4000	91856	S355NL/ML
10000	9812				
10000	9822				
		89	4000	87014	S355NL/ML
10000	9822				
10000	9842				
		79	4000	77315	S355NL/ML
10000	9842				
10000	9844				
		78	3000	57258	S355NL/ML
10000	9844				
10000	9836				
		82	3260	65385	S355NL/ML
10000	9836				
10000	9786				
		107	2900	75706	S355NL/ML
10000	9786				

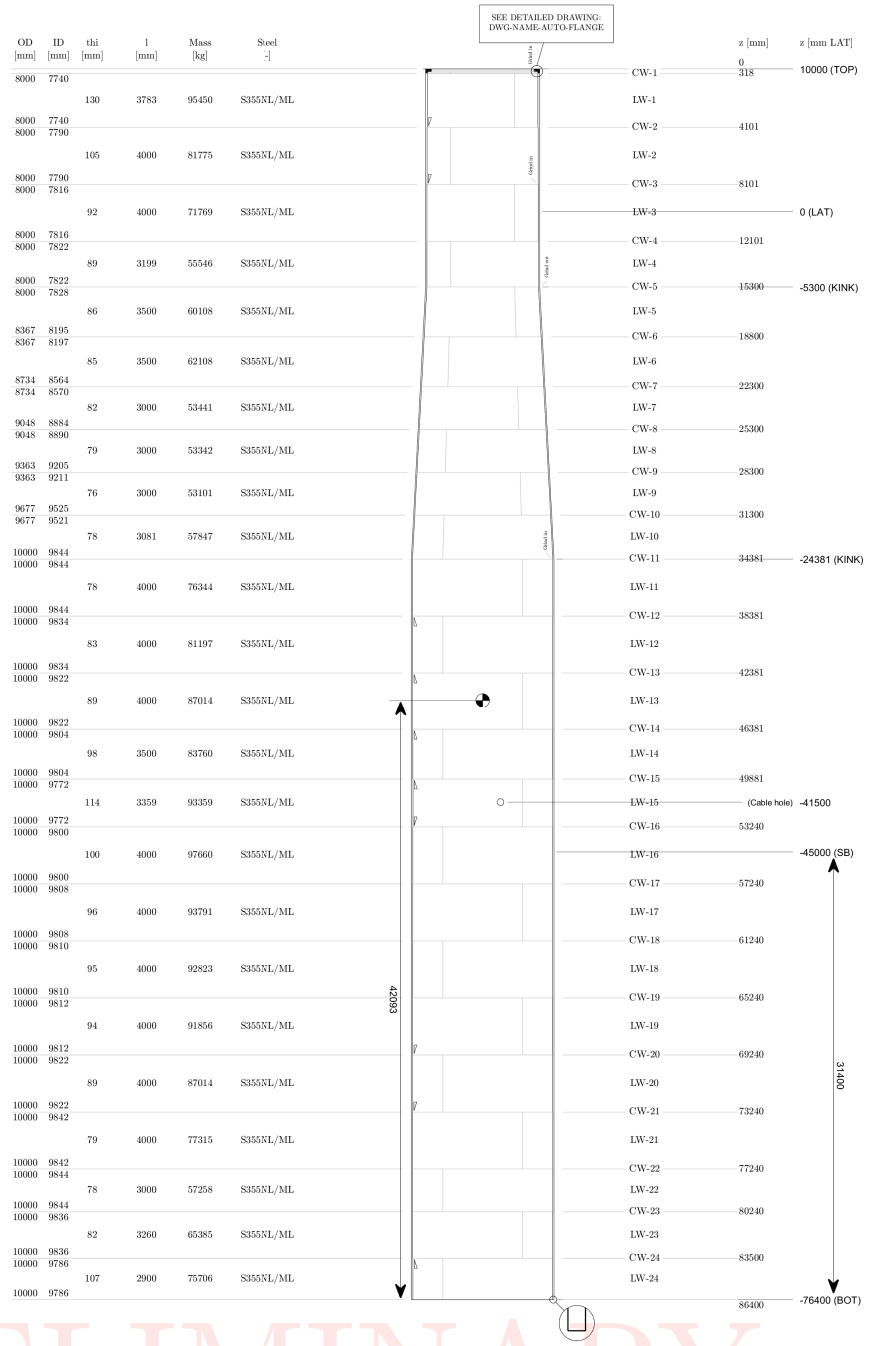

Orientation of Array Cable Entry Hole(s): [45] degrees clockwise relative to N.

10 m 5 m 1 m 0 m

NOTES:

Drawings are for scheme design and show design intent only. Full detailed design analysis is required prior to fabrication. Secondary steel concept is not shown.

REV	DATE	REVISION DESCRIPTION	PREP.	QA	APPR
A	XXXX.XX.XXX	Issued for Client Review	BMS	XX	XX

DESIGN BY: WOOD THILSTED PARTNERS
APPROVED BY: XX — DATE: 12 Aug 2022
CHECKED BY: XX — DATE: 12 Aug 2022
PREPARED BY: EMB — DATE: 12 Aug 2022
SCALE: NOTED
WT PROJECT NO. 9993

NAN

WOOD THILSTED

GENERIC MORPHEUS MODEL
IEA15MW
MONOPILE: WTG_01

DRAWING NO. WT-9993-NAN-DWG-WTG_01-MP
REV. A

DRAWING NO. WT-9993-nan-DWG-WTG_01-MP
REV: A

Figure D.36: Monopile design drawing of reference case - Bothnian Sea North

TP (incl. flanges)

M: 231.7 t

L: 10.0 m

V: 29.4 m^3

D: 8.00 m

A_{ext}: 251.3 m^2

A_{int}: 243.8 m^2

Legend:

Grind: Grind weld flush

Plate tapering (angle 1:4)

Center of gravity

Hole

Longitudinal welds (LW):

Weld ID	No	length	thi	Grinding		IC*	
-	-	mm	mm	in	out	in	out
LW-1	2	2455	112	-	-	II	II
LW-2	2	2565	92	-	-	II	II
LW-3	3	4435	114	-	-	II	II

LW total length: 23.3 m
LW average thickness: 108.7 mm

Circumferential welds (CW):

Weld ID	length	thi	Grinding		IC*	
-	mm	mm	in	out	in	out
CW-1	25133	112-112	-	-	I	I
CW-2	25133	112-92	-	-	I	II
CW-3	25133	92-114	-	-	I	II
CW-4	25133	114-114	-	-	I	I

CW total length: 100.5 m
CW average thickness: 102.5 mm

Steel (TP total excl. flanges)

S355NL/ML:	46.0 t
S355NL/ML+Z35:	151.8 t

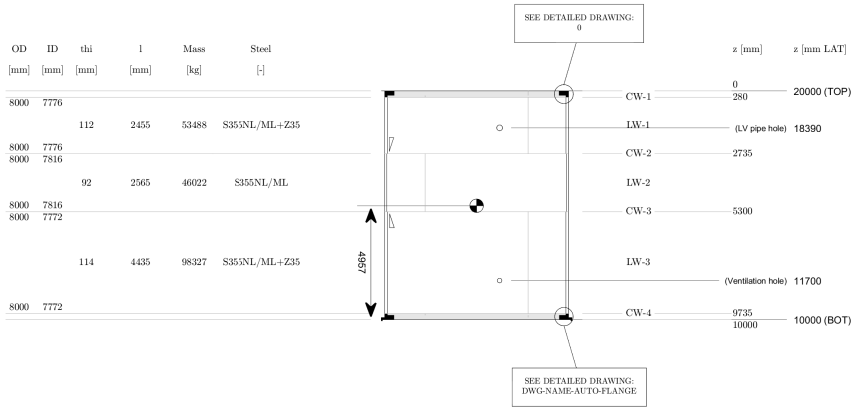

10 m 5 m 1 m 0 m

NOTES:

Drawings are for scheme design and show design intent only. Full detailed design analysis is required prior to fabrication. Secondary steel concept is not shown.

REV	DATE	REVISION DESCRIPTION	PREP.	QA	APPR
A	XXXX.XX.XXX	Issued for Client Review	EMS	XX	XX

DESIGN BY: WOOD THILSTED PARTNERS
APPROVED BY: XX — DATE: 15 Aug 2022
CHECKED BY: XX — DATE: 15 Aug 2022
PREPARED BY: EMS — DATE: 15 Aug 2022
SCALE: NOTED
WT PROJECT NO. 9993

NAN
WOOD THILSTED
GENERIC MORPHEUS MODEL
IEA15MW
TRANSITION PIECE: WTG_01
DRAWING NO. WT-9993-NAN-DWG-WTG_01-TP
REV. A

DRAWING NO. WT-9993-nan-DWG-WTG_01-TP
REV. A

Figure D.37: Transition piece design drawing of ice case - Bothnian Sea North

MP (incl. flange)

M: 2177.7 t

L: 91.0 m

V: 277.6 m^3

D: 8.00 - 10.00 m

A_{ext}: 2704.1 m^2

A_{int}: 2641.5 m^2

Legend:

Grind: Grind weld flush

Plate tapering (angle 1:4)

Center of gravity

Hole

Longitudinal welds (LW):

Weld ID	No	length	thi	Grinding		IC*	
-	-	mm	mm	in	out	in	out
LW-1	3	3783	128	-	-	II	II
LW-2	3	4000	103	-	-	II	II
LW-3	2	4000	87	-	-	II	II
LW-4	2	3199	87	-	-	II	II
LW-5	2	3500	87	-	-	II	II
LW-6	2	3500	86	-	-	II	II
LW-7	2	3000	83	-	-	II	II
LW-8	2	3000	81	-	-	II	II
LW-9	2	3000	81	-	-	II	II
LW-10	2	3081	84	-	-	II	II
LW-11	3	3500	88	-	-	II	II
LW-12	2	3000	95	-	-	II	II
LW-13	3	3000	102	-	-	II	II
LW-14	3	3000	107	-	-	II	II
LW-15	3	3000	112	-	-	II	II
LW-16	3	2860	118	-	-	II	II
LW-17	3	3000	122	-	-	II	II
LW-18	3	3000	129	-	-	II	II
LW-19	3	3000	133	-	-	II	II
LW-20	3	3000	132	-	-	II	II
LW-21	3	3000	132	-	-	II	II
LW-22	3	3000	130	-	-	II	II
LW-23	3	3000	123	-	-	II	II
LW-24	3	3500	110	-	-	II	II
LW-25	3	4000	92	-	-	II	II
LW-26	3	4000	78	-	-	II	II
LW-27	2	2879	82	-	-	II	II
LW-28	3	2900	107	-	-	II	II

LW total length: 239.9 m
LW average thickness: 105.2 mm

Circumferential welds (CW):

Weld ID	length	thi	Grinding		IC*	
-	mm	mm	in	out	in	out
CW-1	25133	128-128	yes	-	I	I
CW-2	25133	128-103	-	-	I	II
CW-3	25133	103-87	yes	-	I	II
CW-4	25133	87-87	-	-	I	I
CW-5	25133	87-87	-	yes	II	I
CW-6	26285	87-86	-	-	I	I
CW-7	27438	86-83	-	-	I	II
CW-8	28426	83-81	-	-	I	II
CW-9	29414	81-81	-	-	II	II
CW-10	30401	81-84	-	-	II	II
CW-11	31416	84-88	yes	-	I	II
CW-12	31416	88-95	-	-	II	II
CW-13	31416	95-102	-	-	II	II
CW-14	31416	102-107	-	-	II	II
CW-15	31416	107-112	-	-	II	II
CW-16	31416	112-118	-	-	II	II
CW-17	31416	118-122	-	-	II	II
CW-18	31416	122-129	-	-	II	II
CW-19	31416	129-133	-	-	II	II
CW-20	31416	133-132	-	-	II	II
CW-21	31416	132-132	-	-	II	II
CW-22	31416	132-130	-	-	II	II
CW-23	31416	130-123	-	-	II	II
CW-24	31416	123-110	-	-	II	II
CW-25	31416	110-92	-	-	II	II
CW-26	31416	92-78	-	-	II	II
CW-27	31416	78-82	-	-	II	II
CW-28	31416	82-107	-	-	II	II

CW total length: 833.1 m
CW average thickness: 101.0 mm

Steel (MP total excl. flanges)

S355NL/ML: 2161.4 t

Cylindrical: 1810.2 t
Conical: 351.2 t

OD [mm]	ID [mm]	thi [mm]	l [mm]	Mass [kg]	Steel -]
8000	7744				
		128	3783	94005	S355NL/ML
8000	7744				
8000	7794				
		103	4000	80238	S355NL/ML
8000	7794				
8000	7826				
		87	4000	67911	S355NL/ML
8000	7826				
8000	7826				
		87	3199	54312	S355NL/ML
8000	7826				
8000	7826				
		87	3500	60800	S355NL/ML
8367	8193				
8367	8195				
		86	3500	62831	S355NL/ML
8734	8562				
8734	8568				
		83	3000	54087	S355NL/ML
9048	8882				
9048	8886				
		81	3000	54680	S355NL/ML
9363	9201				
9363	9201				
		81	3000	56565	S355NL/ML
9677	9515				
9677	9509				
		84	3081	62258	S355NL/ML
10000	9832				
10000	9824				
		88	3500	75289	S355NL/ML
10000	9824				
10000	9810				
		95	3000	69618	S355NL/ML
10000	9810				
10000	9796				
		102	3000	74694	S355NL/ML
10000	9796				
10000	9786				
		107	3000	78316	S355NL/ML
10000	9786				
10000	9776				
		112	3000	81935	S355NL/ML
10000	9776				
10000	9764				
		118	2860	82246	S355NL/ML
10000	9764				
10000	9756				
		122	3000	89160	S355NL/ML
10000	9742				
		129	3000	94209	S355NL/ML
10000	9742				
10000	9734				
		133	3000	97091	S355NL/ML
10000	9734				
10000	9736				
		132	3000	96370	S355NL/ML
10000	9736				
10000	9736				
		132	3000	96370	S355NL/ML
10000	9736				
10000	9740				
		130	3000	94930	S355NL/ML
10000	9740				
10000	9754				
		123	3000	89882	S355NL/ML
10000	9754				
10000	9780				
		110	3500	93902	S355NL/ML
10000	9780				
10000	9816				
		92	4000	89919	S355NL/ML
10000	9816				
10000	9844				
		78	4000	76344	S355NL/ML
10000	9844				
10000	9836				
		82	2879	57743	S355NL/ML
10000	9836				
10000	9786				
		107	2900	75706	S355NL/ML
10000	9786				

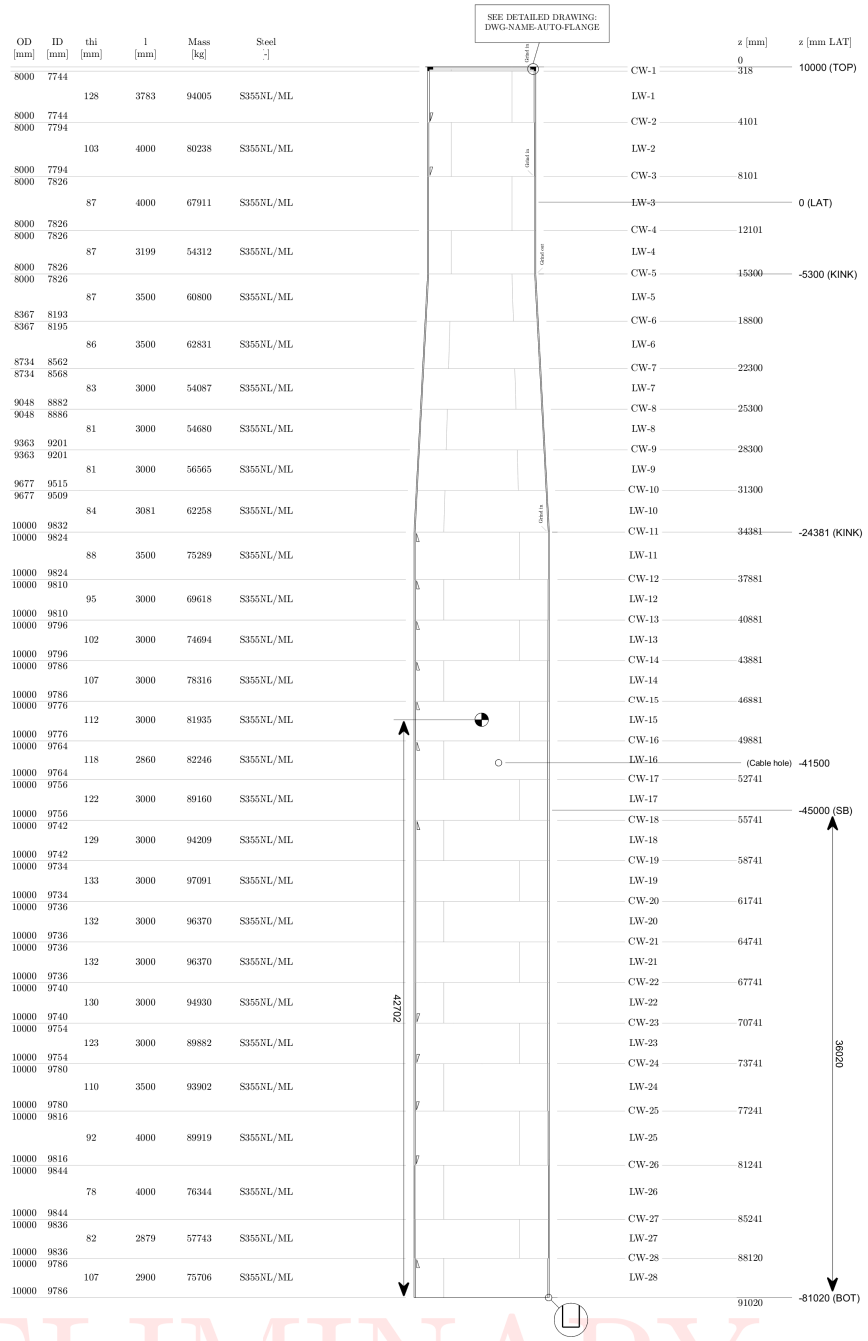

Orientation of Array Cable Entry Hole(s): [45] degrees clockwise relative to N.

10 m 5 m 1 m 0 m

NOTES:

Drawings are for scheme design and show design intent only. Full detailed design analysis is required prior to fabrication. Secondary steel concept is not shown.

REV	DATE	REVISION DESCRIPTION	PREP.	QA	APPR
A	XXXX.XX.XXX	Issued for Client Review	BMS	XX	XX

DESIGN BY: WOOD THILSTED PARTNERS
APPROVED BY: XX — DATE: 15 Aug 2022
CHECKED BY: XX — DATE: 15 Aug 2022
PREPARED BY: EMB — DATE: 15 Aug 2022
SCALE: NOTED
WT PROJECT NO. 9993

NAN

WOOD THILSTED

GENERIC MORPHEUS MODEL
IEA15MW
MONOPILE: WTG_01

DRAWING NO. WT-9993-NAN-DWG-WTG_01-MP — REV. A

DRAWING NO. WT-9993-nan-DWG-WTG_01-MP
REV. A

Figure D.38: Monopile design drawing of ice case - Bothnian Sea North

TP (incl. flanges)

M: 275.6 t

L: 10.0 m

V: 35.0 m^3

D: 8.00 m

A_{ext}: 251.3 m^2

A_{int}: 242.4 m^2

Legend:

Grind: Grind weld flush

Plate tapering (angle 1:4)

Center of gravity

Hole

Longitudinal welds (LW):

Weld ID	No	length	thi	Grinding		IC*	
-	-	mm	mm	in	out	in	out
LW-1	2	2455	141	-	-	II	II
LW-2	2	2565	116	-	-	II	II
LW-3	4	4435	135	-	-	II	II

LW total length: 27.8 m
LW average thickness: 132.6 mm

Circumferential welds (CW):

Weld ID	length	thi	Grinding		IC*	
-	mm	mm	in	out	in	out
CW-1	25133	141-141	-	-	I	I
CW-2	25133	141-116	-	-	II	II
CW-3	25133	116-135	-	-	II	II
CW-4	25133	135-135	-	-	I	I

CW total length: 100.5 m
CW average thickness: 127.0 mm

Steel (TP total excl. flanges)

S355NL/ML:	57.9 t
S355NL/ML+Z35:	183.2 t

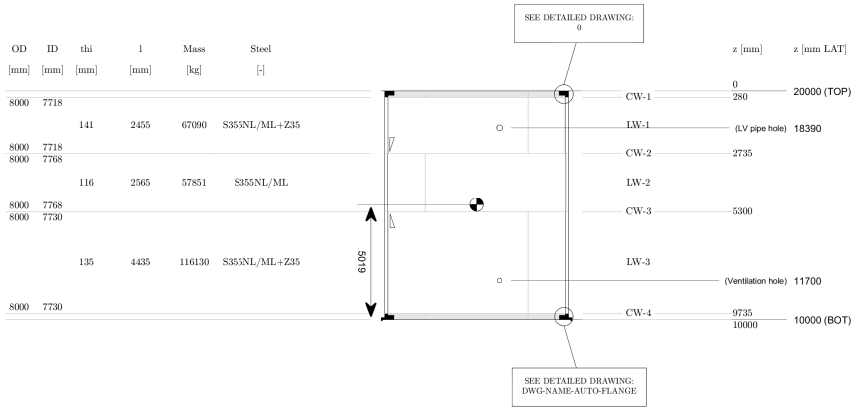

10 m 5 m 1 m 0 m

NOTES:

Drawings are for scheme design and show design intent only. Full detailed design analysis is required prior to fabrication. Secondary steel concept is not shown.

REV	DATE	REVISION DESCRIPTION	PREP.	QA	APPR
A	XXXX.XX.XXX	Issued for Client Review	EMS	XX	XX

DESIGN BY: WOOD THILSTED PARTNERS
APPROVED BY: XX — DATE: 15 Aug 2022
CHECKED BY: XX — DATE: 15 Aug 2022
PREPARED BY: EMS — DATE: 15 Aug 2022
SCALE: NOTED
WT PROJECT NO. 9993

NAN
WOOD THILSTED
GENERIC MORPHEUS MODEL
IEA15MW
TRANSITION PIECE: WTG_01
DRAWING NO. WT-9993-NAN-DWG-WTG_01-TP
REV. A

DRAWING NO. WT-9993-nan-DWG-WTG_01-TP
REV. A

Figure D.39: Transition piece design drawing of relaxed case - Bothnian Sea North

MP (incl. flange)

M: 2018.4 t

L: 82.9 m

V: 257.3 m^3

D: 8.00 - 10.00 m

A_{ext}: 2449.7 m^2

A_{int}: 2390.5 m^2

Legend:

Grind: Grind weld flush

t→t Plate tapering (angle 1:4)

Center of gravity

Hole

Longitudinal welds (LW):

Weld ID	No	length	thi	Grinding		IC*	
-	-	mm	mm	in	out	in	out
LW-1	4	3783	162	-	-	II	II
LW-2	4	4000	137	-	-	II	II
LW-3	3	4000	112	-	-	II	II
LW-4	2	3199	107	-	-	II	II
LW-5	2	3500	98	-	-	II	II
LW-6	3	3500	97	-	-	II	II
LW-7	2	3000	94	-	-	II	II
LW-8	2	3000	91	-	-	II	II
LW-9	2	3000	88	-	-	II	II
LW-10	2	3081	85	-	-	II	II
LW-11	3	4000	89	-	-	II	II
LW-12	3	4000	95	-	-	II	II
LW-13	3	4000	103	-	-	II	II
LW-14	3	3500	114	-	-	II	II
LW-15	4	3859	133	-	-	II	II
LW-16	4	4000	117	-	-	II	II
LW-17	4	4000	112	-	-	II	II
LW-18	4	4000	110	-	-	II	II
LW-19	3	4000	107	-	-	II	II
LW-20	3	4000	99	-	-	II	II
LW-21	2	3000	83	-	-	II	II
LW-22	2	3280	82	-	-	II	II
LW-23	3	2900	107	-	-	II	II

LW total length: 246.4 m
LW average thickness: 110.0 mm

Circumferential welds (CW):

Weld ID	length	thi	Grinding		IC*	
-	mm	mm	in	out	in	out
CW-1	25133	162-162	yes	-	I	I
CW-2	25133	162-137	-	-	II	II
CW-3	25133	137-112	yes	-	I	II
CW-4	25133	112-107	-	-	I	II
CW-5	25133	107-98	-	yes	II	I
CW-6	26285	98-97	-	-	I	I
CW-7	27438	97-94	-	-	I	I
CW-8	28426	94-91	-	-	I	I
CW-9	29414	91-88	-	-	I	II
CW-10	30401	88-85	-	-	I	II
CW-11	31416	85-89	yes	-	I	II
CW-12	31416	89-95	-	-	I	II
CW-13	31416	95-103	-	-	I	II
CW-14	31416	103-114	-	-	I	II
CW-15	31416	114-133	-	-	I	II
CW-16	31416	133-117	-	-	I	II
CW-17	31416	117-112	-	-	I	II
CW-18	31416	112-110	-	-	I	I
CW-19	31416	110-107	-	-	I	I
CW-20	31416	107-99	-	-	I	II
CW-21	31416	99-83	-	-	I	II
CW-22	31416	83-82	-	-	II	II
CW-23	31416	82-107	-	-	II	II

CW total length: 676.0 m
CW average thickness: 101.4 mm

Steel (MP total excl. flanges)

Not Standard Steel:	118.5 t
S355NL/ML:	1882.9 t
Cylindrical:	1615.2 t
Conical:	386.1 t

OD [mm]	ID [mm]	thi [mm]	l [mm]	Mass [kg]	Steel -]
8000	7676				
		162	3783	118461	Not Standard Steel
8000	7676				
8000	7726				
		137	4000	106265	S355NL/ML
8000	7726				
8000	7776				
		112	4000	87149	S355NL/ML
8000	7776				
8000	7786				
		107	3199	66628	S355NL/ML
8000	7786				
8000	7804				
		98	3500	68394	S355NL/ML
8367	8171				
8367	8173				
		97	3500	70776	S355NL/ML
8734	8540				
8734	8546				
		94	3000	61179	S355NL/ML
9048	8860				
9048	8866				
		91	3000	61363	S355NL/ML
9363	9181				
9363	9187				
		88	3000	61407	S355NL/ML
9677	9501				
9677	9507				
		85	3081	62993	S355NL/ML
10000	9830				
10000	9822				
		89	4000	87014	S355NL/ML
10000	9822				
10000	9810				
		95	4000	92823	S355NL/ML
10000	9810				
10000	9794				
		103	4000	100559	S355NL/ML
10000	9794				
10000	9772				
		114	3500	97278	S355NL/ML
10000	9772				
10000	9734				
		133	3859	124891	S355NL/ML
10000	9734				
10000	9766				
		117	4000	114065	S355NL/ML
10000	9766				
10000	9776				
		112	4000	109246	S355NL/ML
10000	9776				
10000	9780				
		110	4000	107317	S355NL/ML
10000	9780				
10000	9786				
		107	4000	104422	S355NL/ML
10000	9786				
10000	9802				
		99	4000	96693	S355NL/ML
10000	9802				
10000	9834				
		83	3000	60897	S355NL/ML
10000	9834				
10000	9836				
		82	3280	65786	S355NL/ML
10000	9836				
10000	9786				
		107	2900	75706	S355NL/ML
10000	9786				

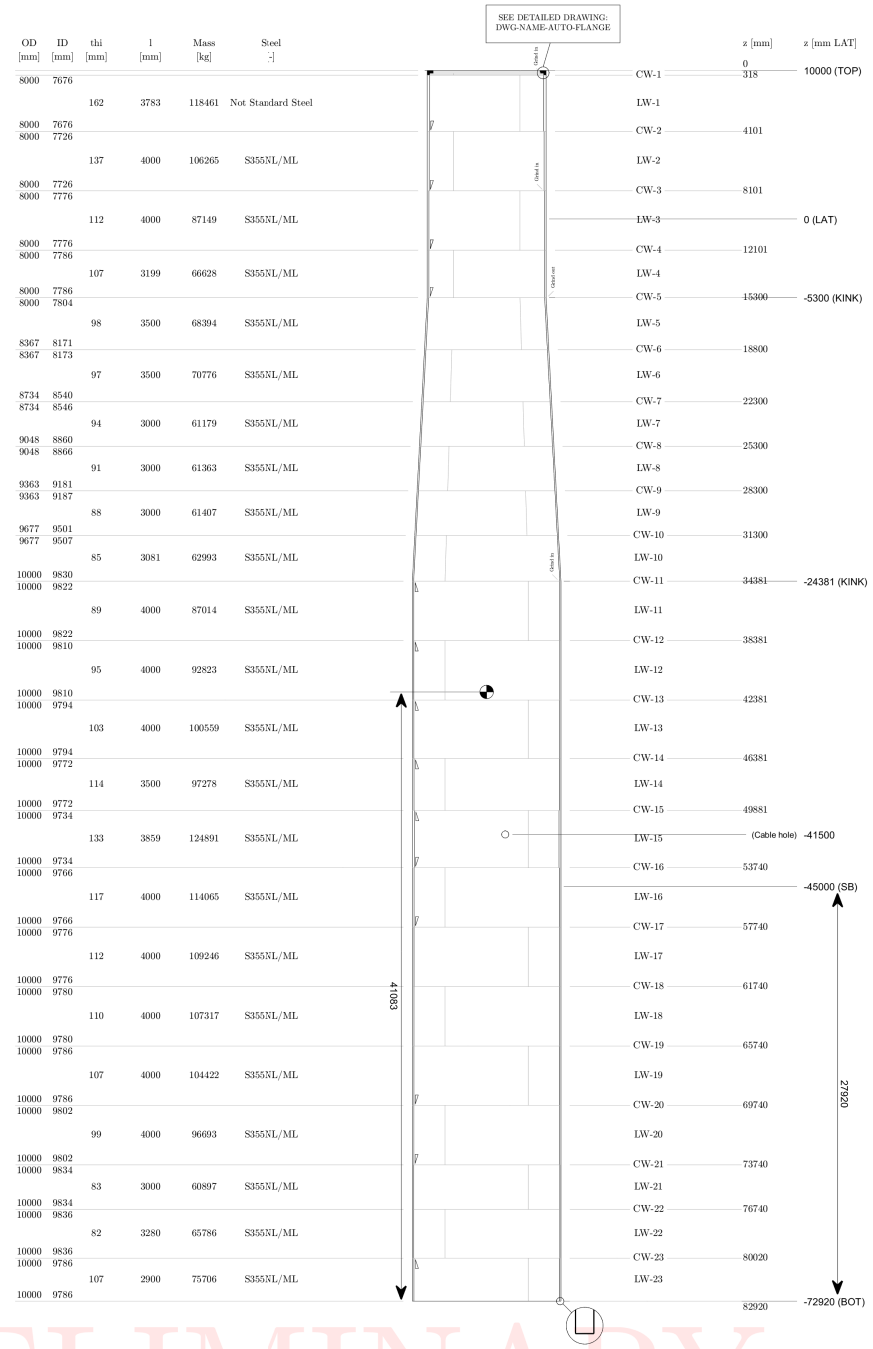

Orientation of Array Cable Entry Hole(s): [45] degrees clockwise relative to N.

10 m 5 m 1 m 0 m

NOTES:

Drawings are for scheme design and show design intent only. Full detailed design analysis is required prior to fabrication. Secondary steel concept is not shown.

REV	DATE	REVISION DESCRIPTION	PREP.	QA	APPR
A	XXXX.XX.XXX	Issued for Client Review	EMS	XX	XX

DESIGN BY: WOOD THILSTED PARTNERS
APPROVED BY: XX — DATE: 15 Aug 2022
CHECKED BY: XX — DATE: 15 Aug 2022
PREPARED BY: EMS — DATE: 15 Aug 2022
SCALE: NOTED
WT PROJECT NO. 9993

NAN

WOOD THILSTED

GENERIC MORPHEUS MODEL
IEA15MW
MONOPILE: WTG_01

DRAWING NO. WT-9993-NAN-DWG-WTG_01-MP — REV. A

DRAWING NO. WT-9993-nan-DWG-WTG_01-MP
REV. A

Figure D.40: Monopile design drawing of relaxed case - Bothnian Sea North

TP (incl. flanges)

M: 193.8 t

L: 10.0 m

V: 24.6 m^3

D: 8.00 m

A_{ext}: 251.3 m^2

A_{int}: 245.1 m^2

Legend:

Grind: Grind weld flush

Plate tapering (angle 1:4)

Center of gravity

Hole

Longitudinal welds (LW):

Weld ID	No	length	thi	Grinding		IC*	
-	-	mm	mm	in	out	in	out
LW-1	2	2455	88	-	-	II	II
LW-2	2	2565	76	-	-	II	II
LW-3	3	4435	93	-	-	II	II

LW total length: 23.3 m
LW average thickness: 88.2 mm

Circumferential welds (CW):

Weld ID	length	thi	Grinding		IC*	
-	mm	mm	in	out	in	out
CW-1	25133	88-88	-	-	I	I
CW-2	25133	88-76	-	-	II	II
CW-3	25133	76-93	-	-	I	II
CW-4	25133	93-93	-	-	I	I

CW total length: 100.5 m
CW average thickness: 83.3 mm

Steel (TP total excl. flanges)

S355NL/ML:	38.1 t
S355NL/ML+Z35:	122.6 t

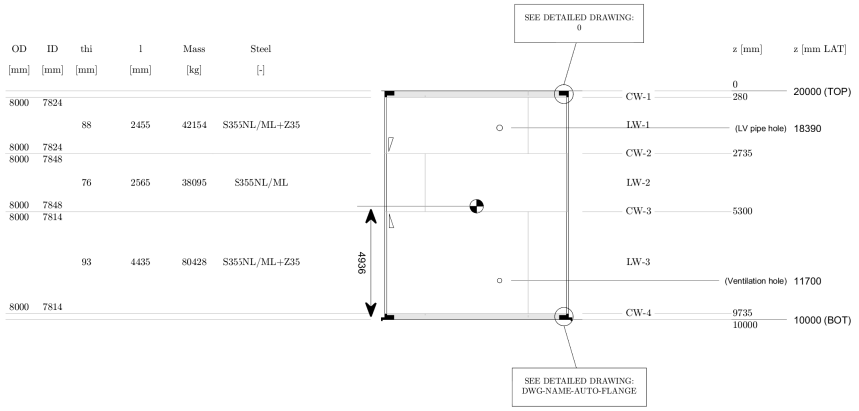

10 m 5 m 1 m 0 m

NOTES:

Drawings are for scheme design and show design intent only. Full detailed design analysis is required prior to fabrication. Secondary steel concept is not shown.

REV	DATE	REVISION DESCRIPTION	PREP.	QA	APPR
A	XXXX.XX.XXX	Issued for Client Review	EMS	XX	XX

DESIGN BY: WOOD THILSTED PARTNERS
APPROVED BY: XX — DATE: 12 Aug 2022
CHECKED BY: XX — DATE: 12 Aug 2022
PREPARED BY: EMS — DATE: 12 Aug 2022
SCALE: NOTED
WT PROJECT NO. 9993

NAN

WOOD THILSTED

GENERIC MORPHEUS MODEL
IEA15MW
TRANSITION PIECE: WTG_01

DRAWING NO. WT-9993-NAN-DWG-WTG_01-TP — REV. A

DRAWING NO. WT-9993-nan-DWG-WTG_01-TP
REV. A

Figure D.41: Transition piece design drawing of reference case - Bay of Bothnia

MP (incl. flange)

M: 1322.7 t

L: 75.3 m

V: 168.7 m^3

D: 8.00 - 9.20 m

A_{ext}: 2097.2 m^2

A_{int}: 2056.9 m^2

Legend:

Grind: Grind weld flush

Plate tapering (angle 1:4)

Center of gravity

Hole

Longitudinal welds (LW):

Weld ID	No	length	thi	Grinding in	Grinding out	IC* in	IC* out
-	-	mm	mm	in	out	in	out
LW-1	3	3783	99	-	-	II	II
LW-2	2	4000	82	-	-	II	II
LW-3	2	4000	75	-	-	II	II
LW-4	2	3199	74	-	-	II	II
LW-5	2	3000	73	-	-	II	II
LW-6	2	2500	73	-	-	II	II
LW-7	2	3000	72	-	-	II	II
LW-8	2	2949	72	-	-	II	II
LW-9	2	4000	72	-	-	II	II
LW-10	2	4000	77	-	-	II	II
LW-11	3	4000	85	-	-	II	II
LW-12	3	3991	98	-	-	II	II
LW-13	3	4000	87	-	-	II	II
LW-14	3	4000	84	-	-	II	II
LW-15	3	4000	83	-	-	II	II
LW-16	3	4000	82	-	-	II	II
LW-17	2	4000	77	-	-	II	II
LW-18	2	4000	72	-	-	II	II
LW-19	2	3000	72	-	-	II	II
LW-20	2	2850	74	-	-	II	II
LW-21	2	2700	99	-	-	II	II

LW total length: 177.7 m
LW average thickness: 81.6 mm

Circumferential welds (CW):

Weld ID	length	thi	Grinding in	Grinding out	IC* in	IC* out
-	mm	mm	in	out	in	out
CW-1	25133	99-99	yes	-	I	I
CW-2	25133	99-82	-	-	I	II
CW-3	25133	82-75	yes	-	I	II
CW-4	25133	75-74	-	-	I	I
CW-5	25133	74-73	-	yes	II	I
CW-6	26121	73-73	-	-	I	I
CW-7	26944	73-72	-	-	I	I
CW-8	27932	72-72	-	-	II	II
CW-9	28903	72-72	yes	-	I	II
CW-10	28903	72-77	-	-	I	II
CW-11	28903	77-85	-	-	I	II
CW-12	28903	85-98	-	-	I	II
CW-13	28903	98-87	-	-	I	II
CW-14	28903	87-84	-	-	I	II
CW-15	28903	84-83	-	-	I	I
CW-16	28903	83-82	-	-	I	I
CW-17	28903	82-77	-	-	I	II
CW-18	28903	77-72	-	-	II	II
CW-19	28903	72-72	-	-	II	II
CW-20	28903	72-74	-	-	II	II
CW-21	28903	74-99	-	-	II	II

CW total length: 582.4 m
CW average thickness: 77.5 mm

Steel (MP total excl. flanges)

S355NL/ML:	1307.1 t
Cylindrical:	1132.6 t
Conical:	174.5 t

OD [mm]	ID [mm]	thi [mm]	l [mm]	Mass [kg]	Steel -]
8000	7802				
		99	3783	72975	S355NL/ML
8000	7802				
8000	7836				
		82	4000	64048	S355NL/ML
8000	7836				
8000	7850				
		75	4000	58633	S355NL/ML
8000	7850				
8000	7852				
		74	3199	46272	S355NL/ML
8000	7852				
8000	7854				
		73	3000	43662	S355NL/ML
8314	8168				
8314	8168				
		73	2500	37682	S355NL/ML
8576	8430				
8576	8432				
		72	3000	46140	S355NL/ML
8891	8747				
8891	8747				
		72	2949	46988	S355NL/ML
9200	9056				
9200	9056				
		72	4000	64832	S355NL/ML
9200	9056				
9200	9046				
		77	4000	69296	S355NL/ML
9200	9046				
9200	9030				
		85	4000	76428	S355NL/ML
9200	9030				
9200	9004				
		98	3991	87794	S355NL/ML
9200	9004				
9200	9026				
		87	4000	78210	S355NL/ML
9200	9026				
9200	9032				
		84	4000	75538	S355NL/ML
9200	9032				
9200	9034				
		83	4000	74647	S355NL/ML
9200	9034				
9200	9036				
		82	4000	73755	S355NL/ML
9200	9036				
9200	9046				
		77	4000	69296	S355NL/ML
9200	9046				
9200	9056				
		72	4000	64832	S355NL/ML
9200	9056				
9200	9056				
		72	3000	48624	S355NL/ML
9200	9056				
9200	9052				
		74	2850	47465	S355NL/ML
9200	9052				
9200	9002				
		99	2700	59994	S355NL/ML
9200	9002				

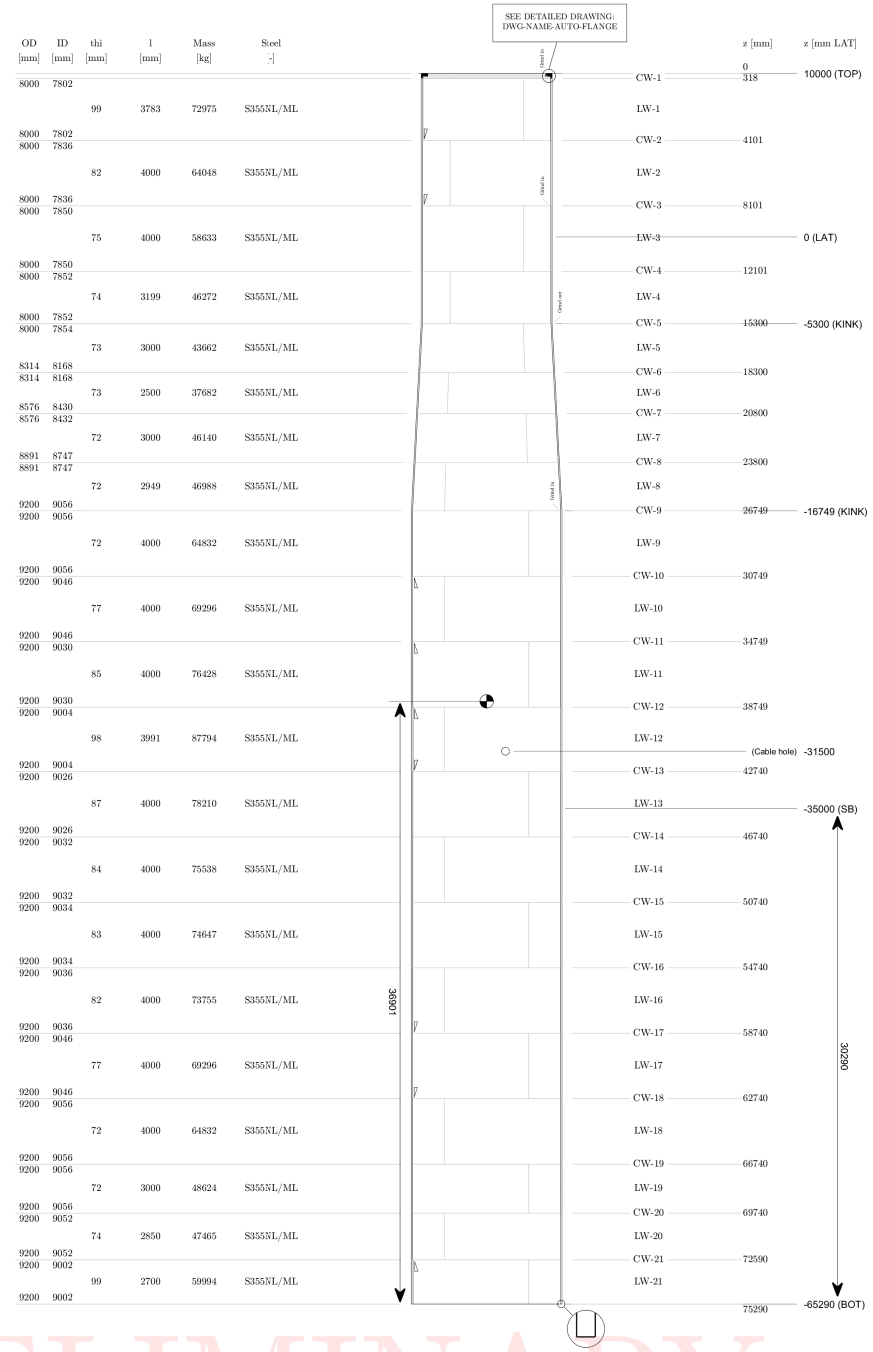

Orientation of Array Cable Entry Hole(s): [45] degrees clockwise relative to N.

10 m 5 m 1 m 0 m

NOTES:

Drawings are for scheme design and show design intent only. Full detailed design analysis is required prior to fabrication. Secondary steel concept is not shown.

REV	DATE	REVISION DESCRIPTION	PREP.	QA	APPR
A	XXXX.XX.XXX	Issued for Client Review	EMS	XX	XX

DESIGN BY: WOOD THILSTED PARTNERS
APPROVED BY: XX — DATE: 12 Aug 2022
CHECKED BY: XX — DATE: 12 Aug 2022
PREPARED BY: EMS — DATE: 12 Aug 2022
SCALE: NOTED
WT PROJECT NO. 9993

NAN

WOOD THILSTED

GENERIC MORPHEUS MODEL
IEA15MW
MONOPILE: WTG_01

DRAWING NO. WT-9993-NAN-DWG-WTG_01-MP
REV. A

Figure D.42: Monopile design drawing of reference case - Bay of Bothnia

TP (incl. flanges)

M: 230.3 t

L: 10.0 m

V: 29.2 m^3

D: 8.00 m

A_{ext}: 251.3 m^2

A_{int}: 243.9 m^2

Legend:

Grind: Grind weld flush

Plate tapering (angle 1:4)

Center of gravity

Hole

Longitudinal welds (LW):

Weld ID	No	length	thi	Grinding		IC*	
-	-	mm	mm	in	out	in	out
LW-1	2	2455	112	-	-	II	II
LW-2	2	2565	91	-	-	II	II
LW-3	3	4435	113	-	-	II	II

LW total length: 23.3 m
LW average thickness: 108.0 mm

Circumferential welds (CW):

Weld ID	length	thi	Grinding		IC*	
-	mm	mm	in	out	in	out
CW-1	25133	112-112	-	-	I	I
CW-2	25133	112-91	-	-	I	II
CW-3	25133	91-113	-	-	I	II
CW-4	25133	113-113	-	-	I	I

CW total length: 100.5 m
CW average thickness: 101.8 mm

Steel (TP total excl. flanges)

S355NL/ML:	45.5 t
S355NL/ML+Z35:	151.0 t

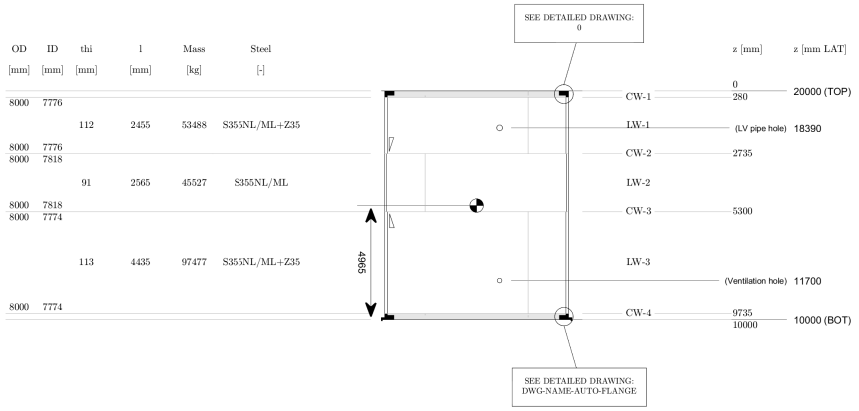

10 m 5 m 1 m 0 m

NOTES:

Drawings are for scheme design and show design intent only. Full detailed design analysis is required prior to fabrication. Secondary steel concept is not shown.

REV	DATE	REVISION DESCRIPTION	PREP.	QA	APPR
A	XXXX.XX.XXX	Issued for Client Review	EMS	XX	XX

DESIGN BY: WOOD THILSTED PARTNERS
APPROVED BY: XX — DATE: 15 Aug 2022
CHECKED BY: XX — DATE: 15 Aug 2022
PREPARED BY: EMS — DATE: 15 Aug 2022
SCALE: NOTED
WT PROJECT NO. 9993

NAN
WOOD THILSTED
GENERIC MORPHEUS MODEL
IEA15MW
TRANSITION PIECE: WTG_01
DRAWING NO. WT-9993-NAN-DWG-WTG_01-TP
REV. A

DRAWING NO. WT-9993-nan-DWG-WTG_01-TP
REV. A

Figure D.43: Transition piece design drawing of ice case - Bay of Bothnia

MP (incl. flange)

M: 1929.5 t

L: 80.9 m

V: 246.0 m^3

D: 8.00 - 9.20 m

A_{ext}: 2260.0 m^2

A_{int}: 2202.2 m^2

Legend:

Grind: Grind weld flush

Plate tapering (angle 1:4)

Center of gravity

Hole

Longitudinal welds (LW):

Weld ID	No	length	thi	Grinding		IC*	
-	-	mm	mm	in	out	in	out
LW-1	3	3783	128	-	-	II	II
LW-2	3	4000	103	-	-	II	II
LW-3	2	4000	85	-	-	II	II
LW-4	2	3199	86	-	-	II	II
LW-5	2	3000	85	-	-	II	II
LW-6	2	2500	84	-	-	II	II
LW-7	2	3000	82	-	-	II	II
LW-8	2	2949	86	-	-	II	II
LW-9	3	4000	93	-	-	II	II
LW-10	3	3500	103	-	-	II	II
LW-11	3	3000	111	-	-	II	II
LW-12	3	3000	120	-	-	II	II
LW-13	3	3491	126	-	-	II	II
LW-14	3	3000	134	-	-	II	II
LW-15	3	3000	141	-	-	II	II
LW-16	3	3000	146	-	-	II	II
LW-17	3	3000	148	-	-	II	II
LW-18	3	3000	146	-	-	II	II
LW-19	3	3000	141	-	-	II	II
LW-20	3	3000	132	-	-	II	II
LW-21	3	3500	118	-	-	II	II
LW-22	3	4000	95	-	-	II	II
LW-23	2	3000	72	-	-	II	II
LW-24	2	2980	74	-	-	II	II
LW-25	2	2700	99	-	-	II	II

LW total length: 214.5 m
LW average thickness: 112.5 mm

Circumferential welds (CW):

Weld ID	length	thi	Grinding		IC*	
-	mm	mm	in	out	in	out
CW-1	25133	128-128	yes	-	I	I
CW-2	25133	128-103	-	-	I	II
CW-3	25133	103-85	yes	-	I	II
CW-4	25133	85-86	-	-	I	I
CW-5	25133	86-85	-	yes	II	I
CW-6	26121	85-84	-	-	I	I
CW-7	26944	84-82	-	-	I	I
CW-8	27932	82-86	-	-	I	II
CW-9	28903	86-93	yes	-	I	II
CW-10	28903	93-103	-	-	II	II
CW-11	28903	103-111	-	-	II	II
CW-12	28903	111-120	-	-	II	II
CW-13	28903	120-126	-	-	II	II
CW-14	28903	126-134	-	-	II	II
CW-15	28903	134-141	-	-	II	II
CW-16	28903	141-146	-	-	II	II
CW-17	28903	146-148	-	-	II	II
CW-18	28903	148-146	-	-	II	II
CW-19	28903	146-141	-	-	II	II
CW-20	28903	141-132	-	-	II	II
CW-21	28903	132-118	-	-	II	II
CW-22	28903	118-95	-	-	II	II
CW-23	28903	95-72	-	-	II	II
CW-24	28903	72-74	-	-	II	II
CW-25	28903	74-99	-	-	II	II

CW total length: 698.0 m
CW average thickness: 106.2 mm

Steel (MP total excl. flanges)

S355NL/ML:	1913.2 t
Cylindrical:	1710.6 t
Conical:	202.6 t

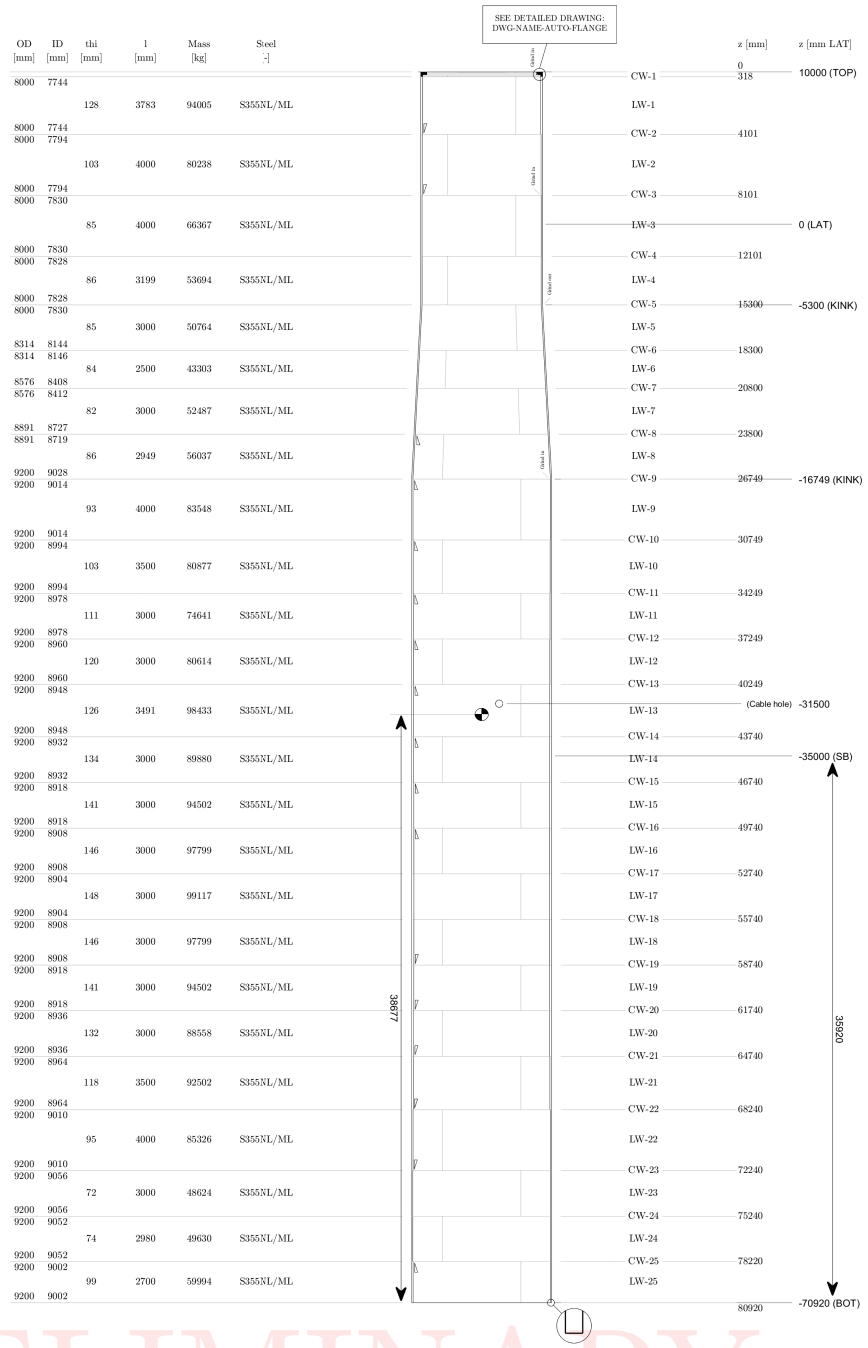

Orientation of Array Cable Entry Hole(s): [45] degrees clockwise relative to N.

NOTES:

Drawings are for scheme design and show design intent only. Full detailed design analysis is required prior to fabrication. Secondary steel concept is not shown.

REV	DATE	REVISION DESCRIPTION	PREP.	QA	APPR
A	XXXX.XX.XXX	Issued for Client Review	EMS	XX	XX

DESIGN BY: WOOD THILSTED PARTNERS
APPROVED BY: XX — DATE: 15 Aug 2022
CHECKED BY: XX — DATE: 15 Aug 2022
PREPARED BY: EMS — DATE: 15 Aug 2022
SCALE: NOTED
WT PROJECT NO. 9993

NAN
WOOD THILSTED
GENERIC MORPHEUS MODEL
IEA15MW
MONOPILE: WTG_01
DRAWING NO. WT-9993-NAN-DWG-WTG_01-MP
REV. A

DRAWING NO. WT-9993-nan-DWG-WTG_01-MP
REV. A

Figure D.44: Monopile design drawing of ice case - Bay of Bothnia

TP (incl. flanges)

M: 289.4 t

L: 10.0 m

V: 36.8 m^3

D: 8.00 m

A_{ext}: 251.3 m^2

A_{int}: 241.9 m^2

Legend:

Grind: Grind weld flush

Plate tapering (angle 1:4)

Center of gravity

Hole

Longitudinal welds (LW):

Weld ID	No	length	thi	Grinding		IC*	
-	-	mm	mm	in	out	in	out
LW-1	3	2455	149	-	-	II	II
LW-2	2	2565	124	-	-	II	II
LW-3	4	4435	142	-	-	II	II

LW total length: 30.2 m
LW average thickness: 140.7 mm

Circumferential welds (CW):

Weld ID	length	thi	Grinding		IC*	
-	mm	mm	in	out	in	out
CW-1	25133	149-149	-	-	I	I
CW-2	25133	149-124	-	-	II	II
CW-3	25133	124-142	-	-	II	II
CW-4	25133	142-142	-	-	I	I

CW total length: 100.5 m
CW average thickness: 134.8 mm

Steel (TP total excl. flanges)

S355NL/ML:	61.8 t
S355NL/ML+Z35:	192.9 t

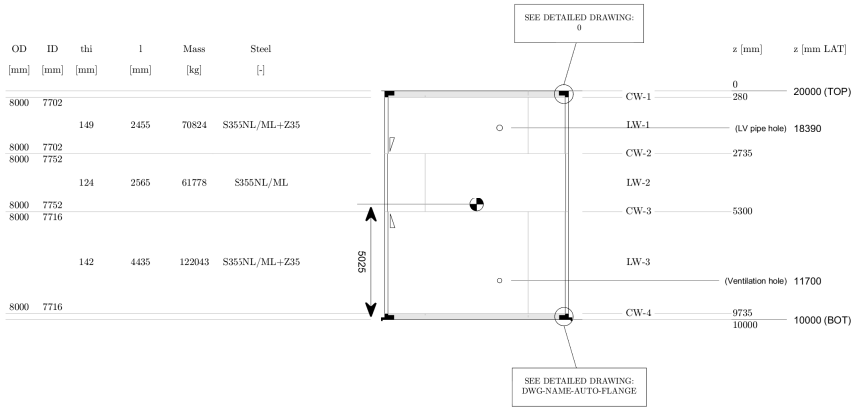

10 m 5 m 1 m 0 m

DRAWING NO. WT-9993-nan-DWG-WTG_01-TP

REV. A

NOTES:

Drawings are for scheme design and show design intent only. Full detailed design analysis is required prior to fabrication. Secondary steel concept is not shown.

REV	DATE	REVISION DESCRIPTION	PREP.	QA	APPR
A	XXXX.XX.XXX	Issued for Client Review	EMS	XX	XX

DESIGN BY: WOOD THILSTED PARTNERS

APPROVED BY: XX — DATE: 15 Aug 2022

CHECKED BY: XX — DATE: 15 Aug 2022

PREPARED BY: EMS — DATE: 15 Aug 2022

SCALE: NOTED

WT PROJECT NO. 9993

NAN

WOOD THILSTED

GENERIC MORPHEUS MODEL
IEA15MW
TRANSITION PIECE: WTG_01

DRAWING NO. WT-9993-NAN-DWG-WTG_01-TP

REV. A

Figure D.45: Transition piece design drawing of relaxed case - Bay of Bothnia

MP (incl. flange)

M: 1832.7 t

L: 74.3 m

V: 233.6 m^3

D: 8.00 - 9.20 m

A_{ext}: 2069.2 m^2

A_{int}: 2013.5 m^2

Legend:

Grind: Grind weld flush

Plate tapering (angle 1:4)

Center of gravity

Hole

Longitudinal welds (LW):

Weld ID	No	length	thi	Grinding		IC*	
-	-	mm	mm	in	out	in	out
LW-1	4	3783	171	-	-	II	II
LW-2	4	4000	146	-	-	II	II
LW-3	3	4000	121	-	-	II	II
LW-4	3	3199	113	-	-	II	II
LW-5	2	3000	102	-	-	II	II
LW-6	2	2500	101	-	-	II	II
LW-7	2	3000	99	-	-	II	II
LW-8	2	2949	96	-	-	II	II
LW-9	3	4000	101	-	-	II	II
LW-10	3	4000	109	-	-	II	II
LW-11	4	4000	122	-	-	II	II
LW-12	4	3992	143	-	-	II	II
LW-13	4	4000	125	-	-	II	II
LW-14	4	4000	119	-	-	II	II
LW-15	3	4000	117	-	-	II	II
LW-16	3	4000	115	-	-	II	II
LW-17	3	4000	109	-	-	II	II
LW-18	2	3000	94	-	-	II	II
LW-19	2	3000	78	-	-	II	II
LW-20	2	2879	76	-	-	II	II
LW-21	2	2700	99	-	-	II	II

LW total length: 222.8 m
LW average thickness: 118.9 mm

Circumferential welds (CW):

Weld ID	length	thi	Grinding		IC*	
-	mm	mm	in	out	in	out
CW-1	25133	171-171	yes	-	I	I
CW-2	25133	171-146	-	-	II	II
CW-3	25133	146-121	yes	-	I	II
CW-4	25133	121-113	-	-	I	II
CW-5	25133	113-102	-	yes	II	I
CW-6	26121	102-101	-	-	I	I
CW-7	26944	101-99	-	-	I	I
CW-8	27932	99-96	-	-	I	I
CW-9	28903	96-101	yes	-	I	II
CW-10	28903	101-109	-	-	I	II
CW-11	28903	109-122	-	-	I	II
CW-12	28903	122-143	-	-	I	II
CW-13	28903	143-125	-	-	I	II
CW-14	28903	125-119	-	-	I	II
CW-15	28903	119-117	-	-	I	I
CW-16	28903	117-115	-	-	I	I
CW-17	28903	115-109	-	-	I	II
CW-18	28903	109-94	-	-	I	II
CW-19	28903	94-78	-	-	I	II
CW-20	28903	78-76	-	-	II	II
CW-21	28903	76-99	-	-	II	II

CW total length: 582.4 m
CW average thickness: 108.2 mm

Steel (MP total excl. flanges)

Not Standard Steel:	124.9 t
S355NL/ML:	1690.5 t
Cylindrical:	1576.9 t
Conical:	238.5 t

OD [mm]	ID [mm]	thi [mm]	l [mm]	Mass [kg]	Steel -]
8000	7658				
		171	3783	124899	Not Standard Steel
8000	7658				
8000	7708				
		146	4000	113116	S355NL/ML
8000	7708				
8000	7758				
		121	4000	94045	S355NL/ML
8000	7758				
8000	7774				
		113	3199	70311	S355NL/ML
8000	7774				
8000	7796				
		102	3000	60788	S355NL/ML
8314	8110				
8314	8112				
		101	2500	51961	S355NL/ML
8576	8374				
8576	8378				
		99	3000	63244	S355NL/ML
8891	8693				
8891	8699				
		96	2949	62483	S355NL/ML
9200	9008				
9200	8998				
		101	4000	90656	S355NL/ML
9200	8998				
9200	8982				
		109	4000	97750	S355NL/ML
9200	8982				
9200	8956				
		122	4000	109252	S355NL/ML
9200	8956				
9200	8914				
		143	3992	127506	S355NL/ML
9200	8914				
9200	8950				
		125	4000	111902	S355NL/ML
9200	8950				
9200	8962				
		119	4000	106601	S355NL/ML
9200	8962				
9200	8966				
		117	4000	104832	S355NL/ML
9200	8966				
9200	8970				
		115	4000	103063	S355NL/ML
9200	8970				
9200	8982				
		109	4000	97750	S355NL/ML
9200	8982				
9200	9012				
		94	3000	63328	S355NL/ML
9200	9012				
9200	9044				
		78	3000	52641	S355NL/ML
9200	9044				
9200	9048				
		76	2879	49233	S355NL/ML
9200	9048				
9200	9002				
		99	2700	59994	S355NL/ML
9200	9002				

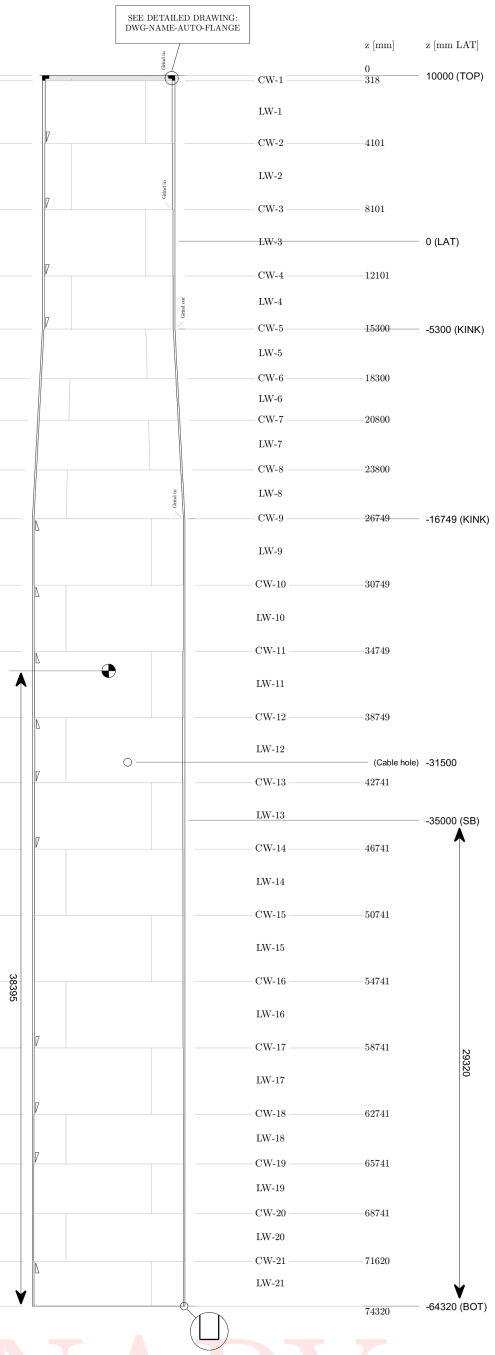

Orientation of Array Cable Entry Hole(s): [45] degrees clockwise relative to N.

NOTES:

Drawings are for scheme design and show design intent only. Full detailed design analysis is required prior to fabrication. Secondary steel concept is not shown.

REV	DATE	REVISION DESCRIPTION	PREP.	QA	APPR
A	XXXX.XX.XXX	Issued for Client Review	EMS	XX	XX

DESIGN BY: WOOD THILSTED PARTNERS
APPROVED BY: XX — DATE: 15 Aug 2022
CHECKED BY: XX — DATE: 15 Aug 2022
PREPARED BY: EMS — DATE: 15 Aug 2022
SCALE: NOTED
WT PROJECT NO. 9993

NAN
WOOD THILSTED
GENERIC MORPHEUS MODEL
IEA15MW
MONOPILE: WTG_01
DRAWING NO. WT-9993-NAN-DWG-WTG_01-MP
REV. A

DRAWING NO. WT-9993-nan-DWG-WTG_01-MP
REV. A

Figure D.46: Monopile design drawing of relaxed case - Bay of Bothnia

E | ACRONYMS

COLOPHON

This document was typeset using LaTeX. The document layout was generated using the `arsclassica` package by Lorenzo Pantieri, which is an adaption of the original `classicthesis` package from André Miede.